NASA-CR-193224

(NASA-CR-193224) RESIDUAL ACCELERATION DATA ON IML-1: DEVELOPMENT OF A DATA REDUCTION AND DISSEMINATION PLAN Final Report, 1 Mar. 1989 - 31 May 1993 (Alabama Univ.) 219 p

N93-30038

Unclas

G3/18 0171491

Center for Microgravity and Materials Research
The University of Alabama in Huntsville

FINAL REPORT

NASA Research Grant NAG8-759

Period of Performance
3/1/89 through 5/31/93

RESIDUAL ACCELERATION DATA ON IML-1: DEVELOPMENT OF A DATA REDUCTION AND DISSEMINATION PLAN

MELISSA J. B. ROGERS

AND

J. IWAN D. ALEXANDER
(Principal Investigator)

Center for Microgravity and Materials Research
The University of Alabama in Huntsville
Huntsville, Alabama 35899

1.0 Introduction

The need to measure and record the low-gravity environment of an orbiting space vehicle was recognized at an early stage of the U.S. Space Program. Such information was considered important for both the assessment of an astronaut's physical condition during and after space missions and the analysis of the fluid physics, materials processing, and biological sciences experiments run in space. Various measurement systems were developed and flown on space platforms beginning in the early 1970s. Similar in concept to land based seismometers that measure vibrations caused by earthquakes and explosions, accelerometers mounted on orbiting space vehicles measure vibrations in and of the vehicle due to internal and external sources, as well as variations in a sensor's relative acceleration with respect to the vehicle it is attached to. The data collected over the years have helped to alter the perception of gravity on-board a space vehicle from the public's early concept of zero-gravity to the science community's evolution of thought from microgravity to milligravity to g-jitter or vibrational environment.

An important feature of the measurement of the acceleration environment is the large amount of data collected per mission. It was recognized by Chassay and Schwaniger [1] that "... *data cannot be stored indefinitely. Thus, prompt analysis and reduction of data to encompass the significant information and storage of that information is essential.*" In the same document, the authors also state "... *low-g users need to strategize their use of low-g data very early in their experiment planning, so that the low-g data can be smoothly integrated into the in-flight and post-flight experiment analyses - not overlooked, as is prevalent today.*" Building on these identified needs, the basic aim of NASA Research Grant NAG8-759 was to lead to significant improvements in the way in which accelerations are recorded, stored, and correlated with particular experiments.

The research performed consisted of three stages.

1. Identification of sensitive IML-1 experiments and sensitivity ranges by order of magnitude estimates, numerical modelling, and investigator input.

2. Research and development towards reduction, supplementation, and dissemination of residual acceleration data.

3. Implementation of the plan on existing acceleration databases.

Stage 1 research was performed in the first two years of the project. The results are presented in section 2. Evaluation of residual acceleration data processing techniques and development of the Acceleration Data Analysis Guide and the Pattern Recognition Data Visualization Database (PRIDE) system occurred over the extent of the project. Implementation of the plans on existing acceleration databases also took place over the duration of the project. Basic background information for the two data processing and analysis systems is given in section 3 and discussions of the implementation of the systems on acceleration databases are given in section 4. More information about the Analysis Guide is given in Appendix A. Section 5 presents areas open for future work and section 6 provides a listing of publications and conferences. Reprints of these publications are provided in Appendix B. A detailed description of the PRIDE system is given in Appendix C, the UAH Thesis Analysis of Large Ill-understood Datasets Using a Combination of Techniques.

2.0 Identification of Sensitive Experiments

The first stage of research was the identification of IML-1 experiments which were likely to be sensitive to residual accelerations, and to characterize the nature of this sensitivity for each experiment. Eight IML-1 experiments were identified as potentially sensitive:

- CAST - Casting and Solidification Technology
- TGS - Triglycine Sulfate Crystal Growth from the Melt
- PCG - Protein Crystal Growth
- MICG - Mercuric Iodide Crystal Growth
- VCGS - Growth of Mercuric Iodide Crystals from Vapor
- GPPF - Plant Growth Physiology Facility
- CPF - Critical Point Facility
- OCGP - Organic Crystal Growth of Proteins.

We contacted the investigator teams for each of these experiments prior to the launch of IML-1. Each team was sent a copy of our Acceleration Data Analysis Guide which we completed to the extent of our knowledge of their experiment. We suggested that completion of the guide questions would be advantageous, if there was interest in analyzing their experiment results in conjunction with accelerometer data. We received positive comments from a few of the investigator teams (CAST, TGS, VCGS). The CAST team provided us with a list of mission times for which they suspected acceleration activity influenced the experiment. Unfortunately, at the close of this project, usable data recorded by the Space Acceleration Measurement System (SAMS) during IML-1 were not available to investigators.

3.0 Residual Acceleration Data Processing

Our initial approach to accelerometer data analysis was to investigate established methods of time series and spectral analysis to see which were most applicable to the large databases resulting from Orbiter missions. Our research eventually led to two related development projects: the Acceleration Data Analysis Guide and the Pattern Recognition Data Visualization Database (PRIDE) system. In general, the former is intended as a pre- and immediate post-flight aid to investigators of low-gravity experiments in assessing their need for accelerometer data and specific data analysis techniques. The latter applies the techniques of pattern recognition, data visualization, database systems, time series and spectral analysis, and expert systems to the problem of characterizing and classifying Orbiter accelerations. The PRIDE system can be used to interpret the acceleration environment during an individual mission, and will ultimately be used to create an overall classification of acceleration signatures for various missions with similar configurations.

3.1 Acceleration Data Analysis Guide

The Acceleration Data Analysis Guide is discussed in detail in several references [2,3] and included in Appendix A. The Guide consists of three main sections of questions meant to prompt investigators into analyzing their data access and data processing needs. Part A pertains to the location and timing of a low-gravity experiment scheduled to fly on an Orbiter mission. Part B identifies times during the mission when an experiment may experience potentially intolerable accelerations and when the experiment may have increased sensitivity to accelerations. The information provided can be used before the mission to identify sections of accelerometer data that may be of interest to an investigator. Post-flight selection of data segments is based on the responses to Part C which addresses the experiment tolerance to quasi-steady accelerations and vibrational excitation (g-jitter).

The motivation behind the Guide was that a gap seemed to exist between some investigators' perceptions that their experiments might be sensitive to accelerations and a more solid understanding of what that sensitivity might be. Use of the Guide should not only help

identify possible acceleration sources that are active during a typical mission and help identify experiment tolerances to resulting accelerations, but should also provide an initial delimiter on the amount of acceleration data an investigator needs to access and analyze.

Upon selection of acceleration data windows to study, detailed analysis should follow an investigator's individual processing plan, either based on the PI team's knowledge of data analysis techniques or prompted by the Acceleration Data Analysis Guide. While such analysis should be confined to limited segments of data, it is also necessary to analyze an entire set of accelerometer data to assess the overall Orbiter low-g environment. The Pattern Recognition Visualization Database (PRIDE) system was developed to provide a means of low-g environment characterization.

3.2 Pattern Recognition Data Visualization Database System

The PRIDE (Pattern Recognition Data Visualization Database) system applies the techniques of pattern recognition, data visualization, database technology, data analysis, and expert systems to the problem of characterizing and classifying the acceleration environment on-board orbital laboratories. See Appendix C for the UAH Thesis resulting from this project.

3.2.1 Introduction to the PRIDE Project

The development of the PRIDE system began as an investigation of large, ill-understood datasets using pattern recognition, data visualization, database systems, frequency analysis, and expert systems. The amount of information describing a given object, process, or event is dependent upon the specific object, process, or event. As a result of recent improvements in hardware (specifically memory capacity), large datasets are becoming more common and sizes are growing rapidly as users attempt to stretch the limits of data collection and storage hardware. Statistical methods provide some aid in analyzing such large amounts of data but do not always provide sufficient analytical capability. It can be expected that, at least for the present and near future, the capacity of the hardware used to collect and store data will often exceed the capacity of the hardware on which the data analysis is performed. The analysis hardware cannot cope with the

original data set, much less the original data set and associated generated data sets. This is a problem that will persist, and effective methods to deal with it must be developed.

Ill-understood datasets exist due to a combination of scarcity of useful information in the data, overabundance of data, and overly complex data. It is possible that a phenomenon being studied is relatively simple but that the available information is incomplete. This situation is similar to attempting to complete a jigsaw puzzle that has pieces missing: it cannot be done. Alternatively, a phenomenon may be simple, but the amount of information describing the problem is excessive and thus overburdens the available cognitive capacity. This situation is similar to attempting to complete a jigsaw puzzle which has an infinite number of pieces: it cannot be done. Finally, it is possible that a phenomenon is complex, is completely described, and is described using a small amount of storage. This situation is similar to having a complete jigsaw puzzle with relatively few pieces, but the pieces are so complex that completion of the puzzle is a function of the raw intellect of the puzzle solver. Acceleration databases are ill-understood; they have all three of these characteristics. Incompleteness arises from the fact that the number of types of physical events which affect acceleration readings is unknown. Some sources are known but their occurrences in time are not recorded. The excessive size of the data is well known - the first three SAMS flights recorded several gigabytes of data. The overly-complex nature of the accelerations arises from the lack of a closed form solution for most vibration problems.

3.2.2 Overview of PRIDE System Components

As mentioned previously, PRIDE combines aspects of pattern recognition, expert systems, data visualization, database systems, and data analysis. The PRIDE system uses both supervised and unsupervised pattern recognition techniques. Supervised pattern recognition uses human knowledge of data to aid in classification while unsupervised pattern recognition does not. In the PRIDE system, the supervised pattern recognition utilizes the application of various data visualization techniques to raw accelerometer data and to transformations of the data, such as vector magnitudes and Fourier transforms. Additional supervision is available through the use of

the CLIPS expert system [4]. CLIPS allows the developing expertise of system users to be stored in the database.

Unsupervised pattern recognition in PRIDE is achieved through the use of the ISODATA algorithm. This algorithm is typically used to classify data for which there is no known prior grouping. This algorithm can be applied directly to the acceleration database by an operator, or can be controlled by a specially written CLIPS shell and run without human intervention. Additionally, an ergodic search technique identifies the location and duration of highest energy events. Notably, this technique offers refined control of the application of Fourier techniques by providing information about when a potentially interesting acceleration event starts and what length data window to select for spectral analysis.

In addition to its supervised pattern recognition applications, data visualization is used in PRIDE for general evaluation of the data character. Analysis of the data character leads to a clearer understanding of possible source type and vibrational effects and should lead to new approaches to acceleration characterization.

A relational database has been installed on the CMMR Stardent computer system and has been fully integrated with all the other functions of PRIDE. Use of this common database form will facilitate the transport of PRIDE to other platforms. Additionally, the use of a database provides several advantages over flat file formats, for example data integrity, maintainability, and large database manipulation.

The manipulation of large databases is achieved through the application of various data reduction techniques. Two main data reduction techniques used are vibration windowing and ergodic windowing. Vibration windowing is used to identify and select windows which fit the definition of a damped high magnitude oscillatory vibration. Ergodic windowing identifies and selects windows based on a measure of the energy attributes of a portion of the acceleration time series. These provide a way to make the processing of huge databases more practical. Additionally, the use of two independent techniques makes the resulting classification more dependable.

3.2.3 System Level Software Configuration

PRIDE was designed to be portable and to take advantage of the capabilities provided by several standard software components. Its portability is derived from its use of the UNIX operating system [5], the X network graphics windowing system, the CDATA relational database, the DORE variant of the PHIGS hierarchical three-dimensional graphics standard, and the CLIPS expert system shell. With the exception of DORE, none of these packages require particular hardware. With the possible exception of DORE, all of these packages are written in the C language [6]. Thus compatibility is preserved at the source code language level. The base source code is available for all of the packages, with the exception of DORE, and thus problems concerning interaction between the packages can be more readily analyzed. Availability of the source code for CDATA and CLIPS was instrumental in the development of PRIDE.

3.2.4 PRIDE Software Components

The software components of PRIDE are UNIX processes. The only exceptions to this are the programs on the VAX which prepare and transmit the raw acceleration data. Usually these processes are linked to a particular X window. Some of these processes are designed so that multiple copies of the same process type may run simultaneously. Some processes are not able to support multiple instantiations of the same process type. Some processes will not "peacefully coexist" with certain other processes. Concurrent processes are problematic in PRIDE because the CDATA database management system does not provide for concurrent usage.

There are eleven PRIDE software components. These components are ***pride***, ***staticcloud***, ***timeseries***, ***fft***, ***query***, ***loadwindow***, ***classify***, ***isodata***, ***expertiso***, ***ergodic***, and ***3dfft***. The ***pride*** component is the X-based main program for PRIDE and allows the user to activate the various functions of PRIDE. The ***loadwindow*** component is an X window used to allow the user to select a given window. The ***staticcloud*** component shows a static drawing of the acceleration vectors of a given event. The ***timeseries*** component provides a dynamic presentation of the time dependent activity of the acceleration vectors of a given event. The ***fft*** component provides a two-dimensional display of various Fourier information for a given

event. The ***3dfft*** component provides a three-dimensional representation of the Fourier information associated with either a single event or a group of events. The ***staticcloud***, ***timeseries***, ***fft***, and ***3dfft*** X-based components may have multiple copies of the same component type running simultaneously. In fact, these components may be freely mixed. None of these component types conflict with the other types or other self-copies.

The ***query*** component is the X-based main query facility for the PRIDE database. The ***query*** component is quite unfriendly in terms of its interaction with the database. No other component may run while ***query*** is running and ***query*** will not run while any other component is running. If another component is activated while ***query*** is active, then the database is corrupted. Recovering from the corruption requires reindexing of the database. The time it takes to reindex is proportional to the size and number of abstract acceleration event windows. If the database contains the events for only a 30 minute period, reindexing takes approximately 10 minutes. A significant sample for the 144 hour SL-3 mission would be in the neighborhood of 30 percent of the data, that is 42 hours. Reindexing time in the event of database corruption would be 840 minutes. The test and development of PRIDE was performed with 30 minutes of data in the database.

The ***classify*** X-based component is based upon the ***query*** component and has a functionality that is simultaneously limited and expanded. The ***classify*** component is limited to modification of the CLASSIFY dataset within the database but it is also capable of X-based interaction with the ***staticcloud***, ***timeseries***, ***fft***, and ***3dfft*** components. The user views different representations of events and then by mouse activity gives commands to ***classify*** to create a classification.

The ***ergodic*** X-based component allows an analyst to analyze the effect of varying the window sizes used to calculate the energy distribution in the raw acceleration data. The ***ergodic*** component does not conflict with other components; multiple instantiations of the ***ergodic*** component would be redundant.

The ***isodata*** non-X-based component applies the ISODATA algorithm to Fourier information. The ***expertiso*** component provides a combination of expert systems and the ISODATA algorithm. The expert system performs many of the same activities that a human analyst would perform.

3.2.5 Overall Assessment of PRIDE Research Results

The PRIDE system is unique in that its development required the merging of many different computer disciplines. Several aspects of this uniqueness and general results are listed below.

- **The Classification:** The acceleration data have a strong vibrational character and it is possible to extract high energy events. These high energy events appear to be weakly clustered. Further analysis is needed to clarify the nature of the classes.

- **Confirmation of the need for disparate disciplines:** Pattern recognition was selected because of the ill-understood nature of the data. Data visualization was selected to provide a wedge to pry open some of the more intractable aspects of the problem so that other methods could be applied. Fourier analysis was selected because of the suspected vibrational characteristics of at least some of the acceleration data. Expert systems were selected because they provide for the inclusion of future expertise into PRIDE and because the discovery mode of expert systems offers a capability that is not represented in the other selected attack technologies. Database technology was selected because it is geared for handling large amounts of data.

- **Display of hyper-dimensional data:** A technique was created that is particularly suited for displaying Fourier information derived from triple series.

- **Expert system control of unsupervised pattern recognition:** Such an approach was created for use in PRIDE.

- **Identification of the optimal window length for acceleration data:** Unfortunately, this was unsuccessful. If it had been successful, then syntactic pattern recognition techniques could have been applied to acceleration data.

4.0 Implementation on Existing Databases

On the 1985 Spacelab 3 (SL-3) mission, a Bell Miniature Electro-Static Accelerometer (MESA) flew as part of the Fluids Experiment System. This data set was collected at a sampling frequency of 300 Hz with a nominal 50 Hz lowpass filter applied. The data were telemetered for ground-based processing and storage. Segments of this data set were provided upon request by the NTI data processing group at MSFC. We used this accelerometer data set for our evaluation of processing and analysis techniques and for the development of the Acceleration Data Analysis Guide and the PRIDE system.

Different time series and spectral analysis techniques were tested on both VAX 11/785 and Stardent Titan computers available at the Center for Microgravity and Materials Research. Processing routines were written in FORTRAN for the VAX, accessing IMSL subroutine libraries. On the Titan, the commercially available mathematical processing software Matlab was used. The use of different computer systems and different analysis structures gave us some indication of the variation in processing time that will be experienced by investigators. Initial work on the PRIDE system was done on the VAX, but, except for initial data transfer, the C-based PRIDE system runs on the Titan, taking advantage of that computer's graphics capabilities, see section 3.2.

During the development of the Acceleration Data Analysis Guide, we obtained an overview of the low-gravity environment of Columbia and the Spacelab during SL-3. In general, we recognized that the dominant frequency components excited during the mission were related to Orbiter and Spacelab structural modes. This was suggested by earlier work by Hamacher and others [7,8] and is supported by more recent analysis of SAMS data [9,10]. We discuss the low-g environment of SL-3 in several publications listed in section 6 and included in Appendix B.

The Acceleration Data Analysis Guide was used to plan our processing of the Honeywell In-Space Accelerometer (HISA) data collected during STS-32 in January 1990. The Guide was used based on CMMR computer modelling of a float-zone indium crystal growth experiment which flew near the HISA. This instrument and the resulting data are discussed in the literature [11,12]. As expected, these data show the familiar pattern of structural mode excitation. STS-32 was not a

Spacelab mission, so modes related to the Spacelab structure and support system are not seen. Of particular interest in this data set is the presence of accelerations induced by treadmill exercise, primary reaction control system jet firings, and Orbiter Maneuvering System operations.

During the recording times, acceleration vector magnitudes ranged from 10^{-4} g to > 10^{-2} g. During periods of crew treadmill exercise, acceleration levels varied with the level of exercise. The most interesting aspect of these data segments is the difference in the amplitude spectra. The frequency of footfalls on the treadmill were evident in the spectra, and tended to enhance Orbiter structural modes when they were of the same frequency or multiples thereof. Acceleration values exceeded time domain tolerance limits, identified while using the Guide, in approximately 35% of the data. Frequency domain limits, however, were not exceeded. Our analysis is presented in reference [13] and included in Appendix B.

Some limited analysis of SAMS data from the SLS-1 mission was also performed. Again, these data show the dominance of structural modes in the frequency domain. There is an expected difference in time history magnitudes among different missions and among different sensor locations on the same mission. This is caused by localized vibration sources, different payloads, and different levels of scheduled crew activity. In general, however, acceleration magnitudes tend to be in the 10^{-4} to 10^{-3} g range during sleep and nominal crew activity periods. Primary thruster firings and OMS burns cause accelerations on the order of 10^{-2} g. Absolute maximum magnitudes of these thruster events are not known because accelerometer saturation levels are exceeded. The structural modes which can be excited by both localized, internal sources and external sources are generally at frequencies between 1 Hz and 50 Hz.

5.0 Future Work

The research conducted under NASA Grant NAG8-759 was highly successful. In particular, the Acceleration Data Analysis Guide is a useful tool that may be used pre- and post-flight by low-gravity principal investigators when evaluating their need for acceleration data analysis. The Pattern Recognition Data Visualization Database (PRIDE) system is useful for single or multiple mission characterization. There is a great potential and need, however, for further development of PRIDE and for further improvements in the acceleration data dissemination process.

There are three main developmental aspects of PRIDE that should be pursued: porting of the system to alternative computer platforms, introduction of ancillary mission data, and syntactic pattern recognition techniques that might lead to automated recognition of acceleration events. PRIDE was designed to be portable to other UNIX based computers. Some modifications to front-end programming and the data visualization aspects would be necessary. Initial plans for PRIDE included the correlation of information about acceleration sources with recorded acceleration signals. This is not considered by the current version of PRIDE because such information was not readily available for the SL-3 mission.

Ancillary data are available for recent SAMS missions and access can be requested pre-flight. While the introduction of data recording the timing of thruster firings, waste water dumps, communication antenna usage, etc. increases the already massive amount of data being analyzed, it would provide opportunities for analysis that would otherwise not be possible. Positive identification of characteristic acceleration signals related to specific activity is the type of learned knowledge that the expert systems part of PRIDE can use to begin to automate the system. Using this ancillary data to identify token time windows for acceleration events, syntactic pattern recognition techniques can also be used for increased analysis capability and for system automation.

One aspect of acceleration data analysis that is still lacking is the dissemination of data to principal investigators. Beginning with the USML-1 mission, SAMS data are being distributed by

the SAMS group at LeRC to PIs, upon request, in a CD-ROM format. Some amount of dissatisfaction has been voiced about this method of data dissemination, and discussions are currently underway between the SAMS project and several European accelerometer designers and users in an attempt to standardize acceleration data formats. Successful resolution of this problem should prompt more experiment investigators to access and analyze acceleration data which will help them to more thoroughly understand the results of their experiments.

6.0 Publications and Conferences Attended

Publications

Rogers, M. J. B., J. I. D. Alexander, and R. S. Snyder, Analysis Techniques for Residual Acceleration Data, **NASA Technical Memorandum 103507**, July 1990.

Rogers, M. J. B. and J. I. D. Alexander, Analysis of Spacelab 3 Residual Acceleration Data, **J. Spacecraft and Rockets 28** (1991) 707-712.

Rogers, M. J. B. and J. I. D. Alexander, A Strategy for Residual Acceleration Data Reduction and Dissemination, **Adv. Space Res. 11** (1991) (7)5-(7)8.

Rogers, M. J. B. and J. I. D. Alexander, Residual Acceleration Data Analysis for Spacelab Missions, **Microgravity Sci. Technol. V/1** (1992) 43-49.

Wolf, R., M. J. B. Rogers, and J. I. D. Alexander, A Residual Acceleration Data Analysis and Management System, Submitted to **Adv. Space Res.** (1992).

Rogers, M. J. B., J. I. D. Alexander, and J. Schoess, Detailed Analysis of Honeywell In-space Accelerometer Data - STS-32, **Microgravity Sci. Technol. VI/1** (1993) 28-33.

Conferences

Alexander, J. I. D., UAH IML Data Analysis, 3rd Microgravity Measurement Group Meeting, Huntsville, AL (invited lecture) August 1989.

Rogers, M. J. B. and J. I. D. Alexander, A Strategy for Residual Acceleration Data Reduction and Dissemination, Paper S.11.1.3, COSPAR 28, The Hague, The Netherlands, June 1990.

Rogers, M. J. B., Fundamental Analysis Techniques and Results from Spacelab 3 Data, 6th Microgravity Measurement Group Meeting, NASA Headquarters, Washington, DC (invited lecture) September 1990.

Rogers, M. J. B. and J. I. D. Alexander, Cross-correlation Analysis of On-orbit Residual Accelerations in Spacelab, AIAA Paper 91-0348, 29th AIAA Aerospace Sciences Meeting, Reno, Nevada, January 1991.

Rogers, M. J. B. and J. I. D. Alexander, Liquid Bridge Model, 7th Microgravity Measurement Group Meeting, NASA Johnson Space Center, Houston, Texas (invited lecture) February 1991.

Rogers, M. J. B., Development of a Residual Acceleration Data Reduction and Dissemination Plan, Invited Lecture, International Workshop on Vibration Isolation Technology for Microgravity Science Applications, NASA Lewis Research Center, April 1991.

Rogers, M. J. B. and J. I. D. Alexander, Experiment Specific Processing of Residual Acceleration Data, AIAA Paper 92-0244, 30th AIAA Aerospace Sciences Meeting, Reno, Nevada, January 1992.

Rogers, M. J. B., J. I. D. Alexander, and J. Schoess, Detailed Analysis of Honeywell In-space Accelerometer Data - STS-32, Paper G.1-S.07, COSPAR 29, Washington, DC, August-September 1992.

Wolf, R., M. J. B. Rogers, and J. I. D. Alexander, A Database Management System for Residual Acceleration Data, Paper G.1-S.08, COSPAR 29, Washington, DC, August-September 1992.

7.0 References

[1] Chassay, R. P. and A. Schwaniger, Low-g Measurements by NASA, Proc. Measurement and Characterization of the Acceleration Environment On Board the Space Station, Guntersville, Alabama, 1986.

[2] Rogers, M. J. B. and J. I. D. Alexander, Residual Acceleration Data Analysis for Spacelab Missions, **Microgravity Sci. Technol. V/1** (1992) 43-49.

[3] Rogers, M. J. B. and J. I. D. Alexander, Experiment Specific Processing of Residual Acceleration Data, AIAA Paper 92-0244, 30th AIAA Aerospace Sciences Meeting, Reno, Nevada, January 1992.

[4] Giarratano, J. C., **CLIPS User's Guide**, JSC-25013, September 1991.

[5] Sobell, M. G., **A Practical Guide to the Unix System**, Benjamin/Cummings Publishing Co., Redwood City, CA, 1989.

[6] Kernighan, B. W. and D. M. Ritchie, **The C Programming Language**, Prentice Hall, Englewood Cliffs, New Jersey, 1988.

[7] Hamacher, H., U. Merbold, and R. Jilg, Analysis of Microgravity Measurements Performed During D1, Proc. Norderney Symposium on Scientific Results of the German Spacelab Mission D1, Norderney, Germany (BMFT, 1986) 48.

[8] Hamacher, H. and U. Merbold, Microgravity Environment of the Material Science Double Rack on Spacelab-1, **J. Spacecraft 24** (1987) 264.

[9] Rogers, M. J. B., C. R. Baugher, R. C. Blanchard, R. DeLombard, W. W. Durgin, D. H. Matthiesen, W. Neupert, P. Roussel, Low Gravity Environment On-board Columbia During STS-40, Paper 93-0833, 31st AIAA Aerospace Sciences Meeting, Reno, Nevada, January 1993.

[10] Rogers, M. J. B., C. R. Baugher, R. C. Blanchard, R. DeLombard, W. W. Durgin, D. H. Matthiesen, W. Neupert, P. Roussel, A Comparison of Low Gravity Measurements On-board Columbia During STS-40, **Microgravity Sci. Technol.** in print (1993).

[11] Dunbar, B. J., D. A. Thomas, and J. N. Schoess, The Microgravity Environment of the Space Shuttle Columbia Middeck During STS-32, **NASA Technical Paper 3140**, November 1991.

[12] Dunbar, B. J., R. L. Giesecke, and D. A. Thomas, The Microgravity Environment of the Space Shuttle Columbia Payload Bay During STS-32, **NASA Technical Paper 3141**, November 1991.

[13] Rogers, M. J. B., J. I. D. Alexander, and J. Schoess, Detailed Analysis of Honeywell In-space Accelerometer Data - STS-32, **Microgravity Sci. Technol. VI/1** (1993) 28-33.

Appendix A.

Acceleration Data Analysis Guide

ACCELERATION DATA ANALYSIS GUIDE

This package is an **Acceleration Data Analysis Guide** to help low-gravity principal investigators assess their need for accelerometer data and form an acceleration data processing plan. The guide consists of three sections. Part A pertains to the location and timing of an experiment. Part B identifies times during the mission when an experiment may experience potentially intolerable accelerations and when the experiment may have increased sensitivity to accelerations. The answers provided can be used before a mission to identify sections of accelerometer data that may be of interest to an investigator. Post-flight selection of data segments is based on the responses to Part C which addresses the experiment tolerance to quasi-steady accelerations and vibrations (g-jitter).

The information needed for **Part A** pertains to the location and timing of an experiment. This information is obtained from various mission documents. Because of the complex orbiter structure, accelerometer data should be obtained from the accelerometer closest to the experiment. Accelerometers on a mission may include:

- Those flown as part of an experiment (it is possible an investigator will share the data)
- MSAD sponsored Space Acceleration Measurement System (SAMS) units
- the Orbiter Experiments Program's High Resolution Accelerometer Package (HiRAP), Aerodynamics Coefficient Identification Package (ACIP), and Orbital Acceleration Research Experiment (OARE) systems.

It is important to know in what form the residual acceleration data are collected and stored and what type of pre-processing and filtering is applied. Different systems save different forms of data, based on experiment sensitivities, computer storage and processing capabilities, and other factors. [1-12] Available data may include acceleration data in g units, counts, or other units such as volts or amps that need to be converted to g. Other possibilities include mean acceleration values, peak acceleration values, or RMS acceleration values for given windowing lengths. Data should also be corrected for any errors related to temperature variations, sensor bias, and other

factors. [13-17] The above information should be available from the accelerometer designer or manufacturer.

The major goal of this processing guide is to allow an investigator to select a minimum amount of accelerometer data to analyze. The data selected should include acceleration information pertinent to an experiment. Some time slices of data can be identified as interesting before and during the mission. Such times are identified in Part B of the data sheet. The responses to Parts B and C depend on the investigator's understanding of the experiment sensitivity to different acceleration levels. The first question of **Part B** addresses the possibility that an experiment will be more sensitive to acceleration variations during certain stages of the experiment. For example, protein crystal growth experiments exhibit increased sensitivity during the nucleation phase. The times that these stages occur should be catalogued by the investigator team during the mission, because experiment activity will not exactly follow the pre-mission timeline.

Question two of Part B addresses the timing of potentially intolerable acceleration sources during the experiment run. Acceleration sources include experiment equipment, Orbiter maintenance equipment (pumps, fans, etc.), crew exercise, and RCS firings for Orbiter attitude adjustments. Again, while this type of activity may be included in pre-mission timelines, it is best to record the times of acceleration sources that may be of interest when they occur. Note that some Orbiter systems activity is recorded in the MSFC Calibrated Ancillary System which may be available for some missions through ACAP. A growing number of references in the literature provide an idea of the acceleration levels related to various sources and the Orbiter structural modes excited during typical mission activity. [1-12,18]

Part C of the data analysis guide allows the investigator to note the quasi-steady acceleration and vibration levels to which an experiment will be sensitive. Particular frequencies at which the experiment has increased sensitivity should also be noted. Experiment tolerance limits can be obtained from previous runs of the experiment in reduced gravity environments, or from computer modelling of the experiment. This information can be used in both time and frequency domain threshold detection routines to further limit the acceleration database.

The use of a threshold detection routine should give some indication of the appropriateness of the sensitivity limits used. If the limits are exceeded the majority of the time, an initial look at the experimental results should indicate whether the acceleration environment was too severe for the experiment or whether the tolerance limits were too strict. Similarly, if the limits are rarely exceeded, analysis of the experimental results should indicate whether the sensitivity limits used were too relaxed or whether the acceleration levels were low enough for a successful experiment run. Based on such information, sensitivity limits should be modified for future flights of the experiment.

ACCELERATION DATA ANALYSIS GUIDE

PART A - General experiment and accelerometer information

(Indicate start and end times of multiple runs, if appropriate)

EXPERIMENT START TIME (MET):

EXPERIMENT END TIME (MET):

EXPERIMENT RUN TIME:

EXPERIMENT LOCATION:

CLOSEST ACCELEROMETER UNIT TO EXPERIMENT, OR ACCELEROMETER UNIT OF INTEREST (LOCATION AND TYPE):

ACCELEROMETER DATA SAMPLING RATE:

NUMBER OF ACCELEROMETER DATA POINTS PER AXIS TO BE COLLECTED DURING EXPERIMENT (To compute the amount of accelerometer data to be collected during the experiment, multiply the accelerometer sampling rate by the length of the experiment. For example, for the extent of a ninety hour experiment, 3.24×10^7 accelerometer data samples would be collected at a sampling frequency of 100 samples per second.):

ORIENTATION OF PRIMARY EXPERIMENT AXES WITH RESPECT TO ORBITER STRUCTURAL AXES (The orientation of the experiment may be important if it has axes of increased or decreased acceleration sensitivity. Accelerometer data can be manipulated to analyze acceleration levels in a particular direction.):

PART B - Identification of specific times of interest

TIMES/REASONS OF KNOWN INCREASED EXPERIMENT SENSITIVITY:

TIMES OF POTENTIAL ACCELERATION SOURCES DURING THE EXPERIMENT (scheduled orbiter attitude adjustment, crew exercise periods):

PART C - Thresholding information for post-flight data selection

FREQUENCY AND MAGNITUDE RANGES OF INTEREST:

MAXIMUM TOLERABLE CONTINUOUS (STEADY) ACCELERATION:

MAXIMUM TOLERABLE (TRANSIENT) ACCELERATION:

EXPERIMENT SENSITIVITY TO CHANGES IN ACCELERATION ORIENTATION:

REFERENCES

[1] Arnett, G., Spacelab-3 low-g accelerometer data from the Fluid Experiments System (FES), in **Proceedings of the Measurement and Characterization of the Acceleration Environment On Board the Space Station**, Guntersville, AL, August 1986, Paper #11.

[2] Blanchard, R. C., M. K. Hendrix, J. C. Fox, D. J. Thomas, and J. Y. Nicholson, Orbital Acceleration Research Experiment, **J. Spacecraft and Rockets 24** (1987) 504-511.

[3] Blanchard, R. C., E. W. Hinson, and J. Y. Nicholson, Shuttle High Resolution Accelerometer Package experiment results: atmospheric density measurements between 60 and 160 km, **J. Spacecraft 26** (1989) 173-180.

[4] Chassay, R. P. and A. Schwaniger, Low-g measurements by NASA, in **Proceedings of the Measurement and Characterization of the Acceleration Environment On Board the Space Station**, Guntersville, AL, August 1986, Paper #9.

[5] Dunbar, B. J., D. A. Thomas, and J. N. Schoess, The Microgravity Environment of the Space Shuttle Columbia Middeck During STS-32, **NASA Technical Paper 3140**, November 1991.

[6] Dunbar, B. J., R. L. Giesecke, and D. A. Thomas, The Microgravity Environment of the Space Shuttle Columbia Payload Bay During STS-32, **NASA Technical Paper 3141**, November 1991.

[7] Hamacher, H. and U. Merbold, Microgravity environment of the Material Science Double Rack on Spacelab-1, **J. Spacecraft 24** (1987) 264-269.

[8] Hamacher, H., U. Merbold, and R. Jilg, Analysis of microgravity measurements performed during D1, in **Proceedings of the Norderney Symposium on Scientific Results of the German Spacelab Mission D1**, Norderney, Germany, 27-29 August 1986, pp. 48-56.

[9] Rogers, M. J. B. and J. I. D. Alexander, A Strategy for Residual Acceleration Data Reduction and Dissemination, **Adv. Space Res. 11** (1991) (7)5-(7)8.

[10] Rogers, M. J. B. and J. I. D. Alexander, Analysis of Spacelab 3 Residual Acceleration Data, **J. Spacecraft and Rockets 28** (1991) 707-712.

[11] Rogers, M. J. B. and J. I. D. Alexander, Residual Acceleration Data Analysis for Spacelab Missions, **Microgravity Sci. Technol. V/1** (1992) 43-49.

[12] Schoess, J. N., D. Thomas, and B. Dunbar, Measuring acceleration in a microgravity environment, **Sensors 7** (1990).

[13] Bendat, J. S., Mathematical theory to determine sensor noise by alternate techniques, Memo to ATA (1986) 27 pp.

[14] Morgan, F. E. and R. O. Goucher, Alternate techniques for determining sensor noise in high signal-to-noise parallel tests, **30th International Instrumentation Symposium**, Denver, CO, May 1984.

[15] Peters, R. B. and S. A. Foote, Computer-automated characterization of a high production volume, inertial grade accelerometer, Sundstrand Data Control, Inc., (1982) 10 pp.

[16] Sebesta, H., Characterizing performance of ultra-sensitive accelerometers, in **Proceedings of the Measurement and Characterization of the Acceleration Environment On Board the Space Station**, Guntersville, AL, August 1986, Paper #20.

[17] Verges, K. R., Acquisition and analysis of accelerometer data, in **Proceedings of the Measurement and Characterization of the Acceleration Environment On Board the Space Station**, Guntersville, AL, August 1986, Paper #19.

[18] Baugher, C. R., Early summary report of mission acceleration measurements from STS-40 (1991).

The following are examples of plots that can be created from the limited database.

1. Acceleration vector magnitude formed from the three axes of accelerometer data:

$$a=(a_1^2 + a_2^2 + a_3^2)^{1/2}.$$

2. The three axes of accelerometer data, a_1, a_2, a_3.

3. Combined amplitude spectrum. Total magnitude of the amplitude spectra of the three axes of data.

4. The amplitude spectra of the three axes of data.

5. Combined power spectral density. Total magnitude of the power spectra of the three axes of data.

6. The power spectral densities of the three axes of data.

6. Direction cosines $\theta_{x,y,z}$ for the time window of interest:

$$\theta_x = \text{acos}(a_1/a).$$

7. Spectra of successive time windows.

8. Percentage of time analyzed that acceleration magnitude was in certain range of values.

Appendix B.

Paper Reprints

N91-10191

NASA
Technical
Memorandum

NASA TM-103507

ANALYSIS TECHNIQUES FOR RESIDUAL ACCELERATION DATA

By Melissa J.B. Rogers, J. Iwan D. Alexander, and Robert S. Snyder

Space Science Laboratory
Science and Engineering Directorate

July 1990

National Aeronautics and
Space Administration

George C. Marshall Space Flight Center

TABLE OF CONTENTS

TECHNICAL MEMORANDUM

ANALYSIS TECHNIQUES FOR RESIDUAL ACCELERATION DATA

I. INTRODUCTION

There are various aspects of observational data that may be of interest to an investigator, e.g., mean, variance, and minimum and maximum values. Observational data such as biomedical data, economic data, seismic data, and accelerometer data are recorded as either continuous time functions or discrete time series. While statistics such as those mentioned above can be obtained from data in this form, additional information can often be obtained by looking at the data from a different perspective, such as can be obtained by transformation of data into a different domain or into different coordinate axes. Of particular interest to us is the analysis of residual acceleration data collected in orbiting space laboratories. A thorough understanding of such data and the ability to manipulate the data will allow the characterization of orbiters so that investigators can better understand the results of low-gravity experiments.

Most time functions can be considered as the sum of sinusoidal and co-sinusoidal terms of various frequencies (all harmonics of some fundamental frequency) and a steady state term. Spectral or Fourier analysis consists of a transformation of data in the time domain into the frequency domain in which the relative strengths of the frequency components of the data can be studied. Although the equations used to perform such transformations were originally applied to continuous, periodic functions, the theory can be adapted to the analysis of discrete, aperiodic time series.

The orientation of recording axes can be an important factor in the collection of observational data. It may be of interest to an investigator to look at data in terms of a set of axes other than that in which the data were collected. Such analysis is performed by means of a transformation of coordinate axes in which data in a given system are referred to in terms of some new set of coordinate axes. A transformation may be useful in the analysis of multiple experiments conducted in different orientations.

Before any such manipulation can be performed on data, the data must be collected. Various details associated with the sampling interval used in the acquisition of data and the window lengths used in the analysis of data are discussed in the next section. The adaptation of Fourier theory to the analysis of discrete, aperiodic time series is discussed in the Spectral Analysis section. Also discussed in that section are the power spectral density function and the application of spectral analysis to residual acceleration data. The transformation of data from one set of coordinate axes to another by means of a transformation matrix and how this can be useful in the analysis of low-gravity data are discussed in the Transformation of Coordinate Axes section. A symbol nomenclature is provided in Appendix A, and detailed derivations are included in Appendix B.

II. SAMPLING CONSIDERATIONS AND FREQUENCY LIMITS

In the analysis of observational data, certain restrictions are imposed by the length of the data window being analyzed and by the sampling rate used when digitizing continuous data, or when collecting discrete data. For a segment of a time series f_λ, of length T (N total points), the fundamental period of the segment is assumed to be T, even though the series is not necessarily periodic, and the lowest frequency represented in spectral analysis of the segment is $1/T = \nu_1$. $1/T$ also represents the highest resolution obtainable in spectral analysis of the time series segment, $1/T=\nu_1=\Delta\nu$.

The sampling interval Δt used in the acquisition of data must be appropriate for the data-two time intervals are needed to define one period. The sampling interval determines the highest obtainable frequency in spectral calculations: $\nu_N = 1/(2\Delta t) = N/(2T)$, the Nyquist frequency. Therefore, for a window of a time series f_λ as described above, the frequency limits $1/T \leq \nu \leq N/(2T)$ exist for spectral analysis of the window.

To avoid aliasing, the contamination of computed spectra by frequencies higher than ν_N (see Bendat and Piersol, 1966, pp. 278-280; Waters, 1981, pp. 121-123), sampling must be frequent enough (i.e., Δt small enough) to have at least two sampling intervals (three sample points) per cycle for the highest frequencies present in a series, not just the highest frequencies of interest. An investigator must, therefore, have some idea of the frequency components that will be present in a series before data are collected. Aliasing problems may also be avoided by appropriate low-pass filtering as part of the data collection process to remove components of frequency higher than the ν_N dictated by the chosen sampling interval.

III. SPECTRAL ANALYSIS OF DISCRETE TIME SERIES

A. Fourier Series and Spectral Analysis - Theory

Spectral analysis consists of the description of a given time function in terms of sinusoidal components present in the function. Such analysis is performed using theory developed in part by Joseph Fourier and is referred to as Fourier analysis. According to Fourier theory, a function f(t), having a fundamental period of 2π and satisfying Dirichlet conditions (see Båth, 1974, p. 26), can be represented by an infinite series (a Fourier series):

$$f(t) = a_0 + \sum_{n=1}^{\infty} (a_n \cos nt + b_n \sin nt), \tag{1}$$

where a_0, a_n, and b_n are constants (the Fourier coefficients) which can be represented by:

$$a_0 = \frac{1}{2\pi}\int_{-\pi}^{\pi} f(t)\, dt, \tag{2a}$$

$$a_n = \frac{1}{\pi}\int_{-\pi}^{\pi} f(t) \cos nt\, dt, \tag{2b}$$

and

$$b_n = \frac{1}{\pi}\int_{-\pi}^{\pi} f(t) \sin nt\, dt. \tag{2c}$$

In general, for a function with fundamental period T, the Fourier series and Fourier coefficients are:

$$f(t) = a_0 + \sum_{n=1}^{\infty} (a_n \cos \frac{2\pi nt}{T} + b_n \sin \frac{2\pi nt}{T}), \tag{3a}$$

$$a_0 = \frac{1}{T}\int_{-T/2}^{T/2} f(t)\, dt, \tag{3b}$$

$$a_n = \frac{2}{T}\int_{-T/2}^{T/2} f(t) \cos \frac{2\pi nt}{T}\, dt, \tag{3c}$$

and

$$b_n = \frac{2}{T}\int_{-T/2}^{T/2} f(t) \sin \frac{2\pi nt}{T}\, dt. \tag{3d}$$

It is the calculation of the Fourier coefficients a_n and b_n which is referred to as Fourier analysis. The value a_0 is often referred to as the d.c. (direct current) or steady state component of f(t), while a_n and b_n are referred to as the a.c. (alternating current) components.

The Fourier transform (a transformation between the time and frequency domains) can be used to calculate the Fourier coefficients of a given time function. The direct Fourier transform is derived in the following (derivation in part from Båth, 1974, pp. 35-37, and Huang, 1966). The Fourier integral is defined as

$$f(t) = \frac{1}{\pi}\int_0^{\infty} d\omega \int_{-\infty}^{\infty} f(\lambda) \cos(\omega(t - \lambda))\, d\lambda, \tag{4}$$

where λ is a dummy integration variable. The cosine and sine transforms of a function $f(\lambda)$ are:

$$a(\omega) = \int_{-\infty}^{\infty} f(\lambda) \cos \omega\lambda\, d\lambda \tag{5a}$$

and

$$b(\omega) = \int_{-\infty}^{\infty} f(\lambda) \sin \omega\lambda\, d\lambda. \tag{5b}$$

Define a function $\Phi(\omega)$ where

$$\sin \Phi(\omega) = - \frac{b(\omega)}{\sqrt{a^2(\omega) + b^2(\omega)}}, \tag{6a}$$

from which it follows that

$$\cos \Phi(\omega) = \frac{a(\omega)}{\sqrt{a^2(\omega) + b^2(\omega)}} \tag{6b}$$

and

$$\tan \Phi(\omega) = - \frac{b(\omega)}{a(\omega)}. \tag{6c}$$

Substituting (5a) and (5b) into the Fourier integral (4), with the cosine term expanded, results in

$$f(t) = \frac{1}{\pi} \int_0^\infty [a(\omega) \cos \omega t + b(\omega) \sin \omega t] \, d\omega; \tag{7}$$

see Appendix B for derivation. Introducing equations (6) involving $\Phi(\omega)$ into equation (7) yields:

$$f(t) = \frac{1}{\pi} \int_0^\infty \left[a^2(\omega) + b^2(\omega)\right]^{1/2} \cos \left[\Phi(\omega) + \omega t\right] d\omega \tag{8}$$

and also

$$f(t) = \frac{1}{2\pi} \int_{-\infty}^\infty \left[a^2(\omega) + b^2(\omega)\right]^{1/2} e^{i\Phi(\omega)} e^{i\omega t} \, d\omega \tag{9}$$

$$= \frac{1}{2\pi} \int_{-\infty}^\infty F(\omega) \, e^{i\omega t} \, d\omega. \tag{10}$$

From equations (5), (6), (9), and (10), we can say that

$$F(\omega) = |F(\omega)| \, e^{i\Phi(\omega)} = \left[a^2(\omega) + b^2(\omega)\right]^{1/2} e^{i\Phi(\omega)} \tag{11}$$

$$= \left[a^2(\omega) + b^2(\omega)\right]^{1/2} \left[\cos \Phi(\omega) + i \sin \Phi(\omega)\right] \tag{12}$$

$$= \left[a^2(\omega) + b^2(\omega)\right]^{1/2} \left[\frac{a(\omega)}{\sqrt{a^2(\omega) + b^2(\omega)}} - i \frac{b(\omega)}{\sqrt{a^2(\omega) + b^2(\omega)}}\right] \tag{13}$$

$$= a(\omega) - i \, b(\omega) \tag{14}$$

$$= \int_{-\infty}^{\infty} f(t) \cos \omega t \, dt - i \int_{-\infty}^{\infty} f(t) \sin \omega t \, dt \tag{15}$$

$$= \int_{-\infty}^{\infty} f(t) \, e^{-i\omega t} \, dt. \tag{16}$$

From the above, the Fourier transform of a time function (direct Fourier transform, Fourier spectrum, complex Fourier transform) is:

$$F(\omega) = \int_{-\infty}^{\infty} f(t) \, e^{-i\omega t} \, dt \tag{17}$$

where

$$F(\omega) = a(\omega) - i \, b(\omega) = |F(\omega)| \, e^{i\Phi(\omega)}. \tag{18}$$

The amplitude spectrum is

$$|F(\omega)| = \left[a^2(\omega) + b^2(\omega)\right]^{1/2} \tag{19}$$

and the phase spectrum is

$$\Phi(\omega) = \tan^{-1}\left[-\frac{b(\omega)}{a(\omega)}\right]. \tag{20}$$

The Fourier spectrum $F(\omega)$ of a time function is basically an average of $f(t)e^{-i\omega t}$ over the length of the function, i.e., an average of the components of $f(t)$ of frequency ω. $F(\omega)$ and $f(t)$ have the same dimensions.

The real and imaginary parts of $F(\omega)$, $a(\omega)$ and $b(\omega)$, respectively, as shown in (14) and (15), are the cosine and sine transforms of $f(t)$ as in equations (5). Comparison of these equations to those for the Fourier coefficients, a_n and b_n (2), shows that the following relations exist:

$$a(\omega) \rightarrow a_n/2 \qquad \text{and} \qquad b(\omega) \rightarrow b_n/2. \tag{21}$$

This can be shown as follows:

$$a(\omega) = \int_{-\infty}^{\infty} f(\lambda) \cos \omega\lambda \, d\lambda = \int_{-\infty}^{\infty} f(t) \cos \frac{2\pi nt}{T} dt$$

$$\rightarrow \lim_{T \rightarrow \infty} \frac{1}{T} \int_{-T/2}^{T/2} f(t) \cos \frac{2\pi nt}{T} \, dt = \frac{a_n}{2}. \tag{22}$$

The inverse Fourier transform is

$$f(t) = \frac{1}{2\pi} \int_{-\infty}^{\infty} F(\omega) \, e^{i\omega t} \, d\omega. \tag{23}$$

This expression can be used to create a time function f(t) from known spectral components F(ω); therefore, (23) is referred to as the Fourier synthesis of f(t).

B. Fourier Series and Spectral Analysis - Discretization

The definitions and derivations given in the previous section are appropriate for continuous functions. The calculation of the Fourier transform F(ω) of a given function f(t) must be approached differently when dealing with a discrete series of observations and when processing data on digital computers. The formulas used must be transformed into discrete form as must data which are recorded in analog form. For data recorded digitally, decisions must be made prior to data acquisition concerning the sampling rate necessary to avoid aliasing problems, as discussed in the previous section. See Båth (1974, Chap. 4) for more details about the equations presented in this section.

In general, a continuous integral may be expressed in discrete form as shown here:

$$\int_0^{N\Delta x} y(x) \, dx \rightarrow \sum_{n=0}^{N-1} y(n\Delta x) \, \Delta x = \sum_{n=0}^{N-1} y_n \, \Delta x, \tag{24}$$

where y(x) is a given curve, Δx is the digitizing interval, and N is the total number of samples.

An integral with infinite integration limits can be approximated using a form of the trapezoidal rule as follows:

$$\int_{-\infty}^{\infty} y(x)\,dx \rightarrow \lim_{X\rightarrow\infty} \frac{1}{X}\int_{-X/2}^{X/2} y(x)\,dx \rightarrow \frac{1}{N\Delta x}\sum_{n=0}^{N} y(n\Delta x)\,\Delta x \tag{25}$$

Assuming y(0) = y(N), the sum of (25) can be represented as:

$$\frac{1}{N}\sum_{n=1}^{N} y(n\Delta x) \quad \text{or} \quad \frac{1}{N}\sum_{n=0}^{N-1} y(n\Delta x). \tag{26}$$

Using the general forms stated above, the Fourier coefficients and Fourier series can be expressed in discrete form as:

$$a_0 = \frac{1}{N}\sum_{\lambda=1}^{N} f_\lambda, \tag{27a}$$

$$a_n = \frac{2}{N}\sum_{\lambda=1}^{N} f_\lambda \cos\frac{2\pi n\lambda}{N}, \tag{27b}$$

$$b_n = \frac{2}{N}\sum_{\lambda=1}^{N} f_\lambda \sin\frac{2\pi n\lambda}{N}, \tag{27c}$$

and

$$f_\lambda = a_0 + \sum_{n=1}^{N/2} a_n \cos\frac{2\pi n\lambda}{N} + \sum_{n=1}^{N/2} b_n \sin\frac{2\pi n\lambda}{N}. \tag{27d}$$

Applying equation (25) to the direct Fourier transform formula yields:

$$F(\omega) = \int_{-\infty}^{\infty} f(t)\, e^{-i\omega t}\,dt \rightarrow \frac{1}{N}\sum_{\lambda=1}^{N} f_\lambda\, e^{-i\omega\lambda}. \tag{28}$$

Equation (28) can be rewritten as follows for ease in computation:

$$F_n = \frac{1}{N}\sum_{\lambda=1}^{N} f_\lambda\, e^{-i(2\pi n\lambda/N)}. \tag{29}$$

Comparison of (29) to the continuous Fourier transform formulas (14-16) and the Fourier coefficient equations stated above (27) results in:

$$F_n = \frac{1}{2}(a_n - ib_n), \tag{30}$$

i.e., the real and imaginary parts of a Fourier transform are one-half the values of the Fourier coefficients, a_n and b_n, respectively. The inverse Fourier transform is also easily represented in discrete form:

$$f_\lambda = \sum_{n=1}^{N} F_n \, e^{i(2\pi n\lambda/N)}. \tag{31}$$

C. Power Spectral Density Function - Definition

The power spectral density is a frequency domain function which is often used to indicate the dominant frequency components present in data (see Bendat and Piersol, 1966, Chap. 3). Before we can define the power spectral density function, we must first introduce the autocorrelation function (Robinson and Treitel, 1980, Chapters 3 and 6). The autocorrelation function for random data gives some indication of the relative amount of power at different frequencies in the data. The autocorrelation function is the expected value of the product of a time series and a time shifted version of that series

$$R(\tau) = E\{f_\lambda f_{\lambda+\tau}\}, \tag{32}$$

which can also be written as

$$R(\tau) = \lim_{T\to\infty} \frac{1}{T} \int_0^T f(t)\, f(t+\tau)\, dt. \tag{33}$$

The autocorrelation function is a real and positive valued even function with the maximum value occurring at $\tau=0$. This maximum value corresponds to the mean square value of f(t), and represents the energy or power of the time function.

The power spectral density S(v), associated with the time function f(t), with frequencies defined over the interval $(-\infty,\infty)$, is related to the autocorrelation function:

$$R(0) = E\left\{f^2(t)\right\} = \int_{-\infty}^{\infty} S(v)\, dv. \tag{34}$$

The power spectral density function represents how the mean square value of a time function is distributed over the infinite frequency range. S(v) is called the two-sided power spectral density function of f(t) because of the frequency interval $(-\infty,\infty)$ over which it is

defined. It can be shown that the two functions in equation (34) form a Fourier transform pair:

$$R(\tau) = \int_{-\infty}^{\infty} S(\nu)\, e^{i2\pi\nu\tau}\, d\nu \;\leftrightarrow\; S(\nu) = \int_{-\infty}^{\infty} R(\tau)\, e^{-i2\pi\nu\tau}\, d\tau. \tag{35}$$

Because of the nature of the autocorrelation function and properties of the Fourier transform, the power spectral density function is a real and positive valued even function of frequency. The above transforms may therefore be simplified to:

$$S(\nu) = \int_{-\infty}^{\infty} R(\tau) \cos 2\pi\nu\tau\, d\tau = 2\int_{0}^{\infty} R(\tau) \cos 2\pi\nu\tau\, d\tau \tag{36}$$

and

$$R(\tau) = 2\int_{0}^{\infty} S(\nu) \cos 2\pi\nu\tau\, d\nu. \tag{37}$$

Assuming that $R(\tau)$ exists, and that it has the Fourier transform $S(\nu)$, the power spectral density function can be defined as the direct Fourier transform of the autocorrelation function:

$$S(\nu) = \int_{-\infty}^{\infty} R(\tau)\, e^{-i2\pi\nu\tau}\, d\tau. \tag{38}$$

The physically realizable one-sided power spectral density function $G(\nu)$ for the frequency interval $(0,\infty)$ is defined as:

$$G(\nu) = 2S(\nu), \qquad 0 \le \nu < \infty. \tag{39}$$

The correspondence between the one-sided power spectral density function and the autocorrelation function is:

$$G(\nu) = 4\int_{0}^{\infty} R(\tau) \cos 2\pi\nu\tau\, d\tau \tag{40}$$

and

$$R(\tau) = \int_0^{\infty} G(\nu) \cos 2\pi\nu\tau \, d\nu. \tag{41}$$

D. Power Spectral Density Function - Estimation

To get the power spectral density function into a form that can be computed directly from observational data, without calculation of the autocorrelation function, we must consider the estimation of sample parameters (Bendat and Piersol, 1966, Chap. 5). The estimation of a previously defined parameter will be indicated by a hat (^) symbol over the parameter symbol. For example, $\hat{e}$ is an estimate of e, where e is any parameter, such as the mean value or power spectral density of f_λ, a sample time series existing for the finite time interval T. Estimators are often defined arbitrarily and may not clearly give a correct estimation of a given parameter.

Consider the time function f(t); the autocorrelation function $R(\tau)$ can be estimated by the sample autocorrelation function $\hat{R}(\tau)$, for f(t) existing over the time interval T by

$$\hat{R}(\tau) = \frac{1}{T-\tau} \int_0^{T-\tau} f(t)\, f(t+\tau)\, dt, \qquad 0 \le \tau < T. \tag{42}$$

Assuming that the data exist for time $T+\tau$, the sample autocorrelation function can be estimated by

$$\hat{R}(\tau) = \frac{1}{T} \int_0^{T} f(t)\, f(t+\tau)\, dt, \qquad 0 \le \tau < T. \tag{43}$$

The formula for the estimation of the power spectral density function is not defined directly in terms of the autocorrelation function, but takes into account the fact that the autocorrelation function is related to the mean square value of a time function. For a time function f(t) with zero mean, existing over a time interval T, the estimate of the one-sided power spectral density function $\hat{G}(\nu)$ describes the time average of $f^2(t)$ in terms of its frequency components, in the frequency interval $(\nu-(B_e/2), \nu+(B_e/2))$, where B_e is the frequency bandwidth.

The mean square value of f(t) within the bandwidth B_e centered at ν is estimated by

$$\widehat{\Psi^2}(\nu, B_e) = \frac{1}{T} \int_0^{T} f^2(t, \nu, B_e)\, dt. \tag{44}$$

The power spectral density is defined as

$$G(\nu) = \lim_{B_e \to 0} \frac{\Psi^2(\nu,B_e)}{B_e} = \lim_{\substack{T \to \infty \\ B_e \to 0}} \frac{1}{B_e T} \int_0^T f^2(t,\nu,B_e)\, dt$$

$$= \lim_{\substack{T \to \infty \\ B_e \to 0}} \hat{G}(\nu). \tag{45}$$

From equations (44) and (45), the sample estimate for the one-sided power spectral density function $\hat{G}(\nu)$ is:

$$\hat{G}(\nu) = \frac{\hat{\Psi}^2(\nu,B_e)}{B_e} = \frac{1}{B_e T} \int_0^T f^2(t,\nu,B_e)\, dt. \tag{46}$$

The limits in equation (45) must be evaluated to obtain the true function $G(\nu)$; $\hat{G}(\nu)$ is generally a biased estimate of $G(\nu)$. The power spectral density function estimate $\hat{G}(\nu)$ is one-sided and is related to the mathematical two-sided power spectral density function estimate defined for positive and negative frequencies as shown here:

$$\hat{S}(\nu) = \hat{S}(-\nu) = \frac{\hat{G}(\nu)}{2}. \tag{47}$$

The above formula (46) for the estimate of the power spectral density function can be discretized as follows, taking into account that the bandwidth B_e is equivalent to the Nyquist frequency ν_N:

$$\hat{G}(\nu) = \frac{1}{B_e T} \int_0^T f^2(t,\nu,B_e)\, dt \tag{48a}$$

$$\rightarrow \frac{1}{B_e T} \sum_{\lambda=0}^{N-1} f_\lambda^2 \Delta\lambda = \frac{1}{B_e T} \sum_{\lambda=0}^{N-1} f_\lambda^2 \frac{T}{N} \tag{48b}$$

$$= \frac{1}{\nu_N N} \sum_{\lambda=0}^{N-1} f_\lambda^2 = \frac{1}{(N/2T)N} \sum_{\lambda=0}^{N-1} f_\lambda^2 \tag{48c}$$

$$= \frac{2T}{N^2} \sum_{\lambda=0}^{N-1} f_\lambda^2. \tag{49}$$

The estimate of the one-sided power spectral density function as defined above is related to the Fourier spectrum of a time series. Working from the formula for the discrete Fourier transform of f_λ, $F_n=(a_n-ib_n)/2$, where a_n and b_n are the Fourier coefficients of f_λ, the relation can be shown as follows:

$$F_n = \frac{1}{2}(a_n - i\, b_n) \tag{50}$$

$$F_n^2 = \frac{1}{4}(a_n - i\, b_n)(a_n + i\, b_n) = \frac{1}{4}(a_n^2 + b_n^2) \tag{51a}$$

$$= \frac{1}{4}\left[\left(\frac{2}{N}\sum_{\lambda=1}^{N} f_\lambda \cos\frac{2\pi n\lambda}{N}\right)^2 + \left(\frac{2}{N}\sum_{\lambda=1}^{N} f_\lambda \sin\frac{2\pi n\lambda}{N}\right)^2\right] \tag{51b}$$

$$= \frac{1}{4}\left(\frac{4}{N^2}\sum_{\lambda=1}^{N} f_\lambda \cos\frac{2\pi n\lambda}{N}\sum_{\lambda=1}^{N} f_\lambda \cos\frac{2\pi n\lambda}{N}\right)$$

$$+ \frac{1}{4}\left(\frac{4}{N^2}\sum_{\lambda=1}^{N} f_\lambda \sin\frac{2\pi n\lambda}{N}\sum_{\lambda=1}^{N} f_\lambda \sin\frac{2\pi n\lambda}{N}\right) \tag{51c}$$

$$= \frac{1}{N^2}\left[\sum_{\lambda=1}^{N}\sum_{\lambda=1}^{N} f_\lambda^2 \cos^2\left(\frac{2\pi n\lambda}{N}\right) + \sum_{\lambda=1}^{N}\sum_{\lambda=1}^{N} f_\lambda^2 \sin^2\left(\frac{2\pi n\lambda}{N}\right)\right] \tag{51d}$$

$$= \frac{1}{N^2}\left[\sum_{\lambda=1}^{N}\sum_{\lambda=1}^{N} f_\lambda^2\left(\cos^2\left(\frac{2\pi n\lambda}{N}\right) + \sin^2\left(\frac{2\pi n\lambda}{N}\right)\right)\right] \tag{51e}$$

$$= \frac{1}{N^2}\sum_{\lambda=1}^{N} f_\lambda^2. \tag{52}$$

Comparing equation (52) with the discrete equation for the estimate of the power spectral density (49) yields the following relation:

$$\widehat{G_n} = 2TF_n^2. \tag{53}$$

This can be rewritten, to ease comparison to the Fourier transform of a time series of interest:

$$PSD_n = \widehat{G_n} = \frac{2T}{N^2}\left|\sum_{\lambda=1}^{N} f_\lambda \, e^{-i2\pi n\lambda/N}\right|^2 . \qquad (54)$$

The units of the power spectral density function are (units of Fourier transform)^2/Hz.

E. Application to Residual Acceleration Data

Residual acceleration data have been collected in orbiting space laboratories with a variety of instruments. The data are typically recorded and distributed to investigators in discrete form. Sampling rates vary considerably from one experiment to the next, depending on the specific goal of the experiment. Typical sampling rates range from 12.5 to 500 samples per second. Sampling is often done at higher rates than required to obtain a particular maximum frequency. For example, if the highest frequency of interest to an investigator is 100 Hz, data may be collected at 500 samples per second and then lowpass filtered down to 100 Hz. Such a procedure is useful when investigators are not sure of the maximum frequencies that compose the process being sampled. This also allows for higher resolution of frequency domain data than would be available if a sampling rate of only 200 Hz was used.

Before any specific Fourier analysis can be done on accelerometer data, some pre-processing is usually required. Pre-processing is performed so that the output represents as closely as possible the actual residual accelerations experienced at the recording site. Artificial signals, or noise, can be introduced from a multitude of sources. Manufacturers of recording devices typically furnish users with specific corrections for deviations from pure signal caused by temperature variations, instrumental bias, and other factors. Filtering can also be applied to data to minimize the effects of aliasing, instrumental noise, and other known noise sources. Specific filtering techniques will not be discussed here, but discussions of filtering can be found in most signal processing texts, see Båth (1974), Bendat and Piersol (1980), and Cadzow (1987).

Once such pre-processing has been applied to residual acceleration data, Fourier analysis can be applied in order to determine what frequency components are significantly present. Windows must be chosen of a length appropriate to what minimum frequencies one wants to see, as discussed in the Sampling Considerations section. Many Fourier transform algorithms are most efficient when the number of samples is highly composite, e.g., a power of two, which places further restrictions on the window length. After pre-processing, the data are assumed free of artificial signals. The results of inadequate correction for instrumental bias can often be seen in Fourier transformed data. An artificial bias from the zero point will cause a significant steady state component. Other incorrect processing, however, is not as easy to identify, but may be manifested as a simple bias, or as long-term variations or trends.

Most standard Fourier transform computer programs use algorithms based on the discrete Fourier transform formula

$$F_n = \frac{1}{N}\sum_{\lambda=1}^{N} f_\lambda \, e^{-i(2\pi n\lambda/N)}, \tag{29}$$

and may give as output the cosine and sine transforms, $a(\omega)$ and $b(\omega)$, respectively, or the amplitude and phase spectra:

$$F_n = \sqrt{a^2(\omega) + b^2(\omega)} \qquad \Phi_n = \tan^{-1}\left[-\frac{b(\omega)}{a(\omega)}\right]. \tag{55}$$

The Fourier coefficients a_n and b_n which differ from the cosine and sine transforms by a factor of 2 may also be output, so it is important to completely understand the transform routine being used. See, for example, Bloomfield (1976, Chap. 4), Elliott and Rao (1982), and Cadzow (1987, Chap. 4) for information on Fourier transform algorithms.

Given the Fourier transform F_n, the original series may be recreated using the discrete inverse Fourier transform (31) or it may be synthesized using the relation between F_n and the Fourier coefficients (30) and the discrete Fourier series equation (27d). Using equation (54), output from Fourier transform programs can be used to form the power spectral density function of the time series considered which can be investigated in addition to, or as an alternative to, the Fourier spectrum.

IV. TRANSFORMATION OF COORDINATE AXES

A. Transformation of Coordinate Axes - Theory

Observational time series data are usually recorded in a stationary set of coordinate axes, which may be located and oriented arbitrarily. Such data can be analyzed in terms of alternative axes by a relatively simple transformation operation, as long as the transformation parameters between the axes of interest and the recording axes are known.

One common form of coordinate axes transformation is that which transforms axes that share a common origin and differ by an angle of rotation θ about a common axis; see Figure 1. In the transformation of axes, a known vector g, such as a residual acceleration measurement, is written in terms of some (primed) coordinate axes which are related to the original (unprimed) coordinate axes by a known rotation angle. That is, g has some coordinates in the unprimed axes (g_1,g_2,g_3), and some other coordinates in the new, primed axes (g_1',g_2',g_3').

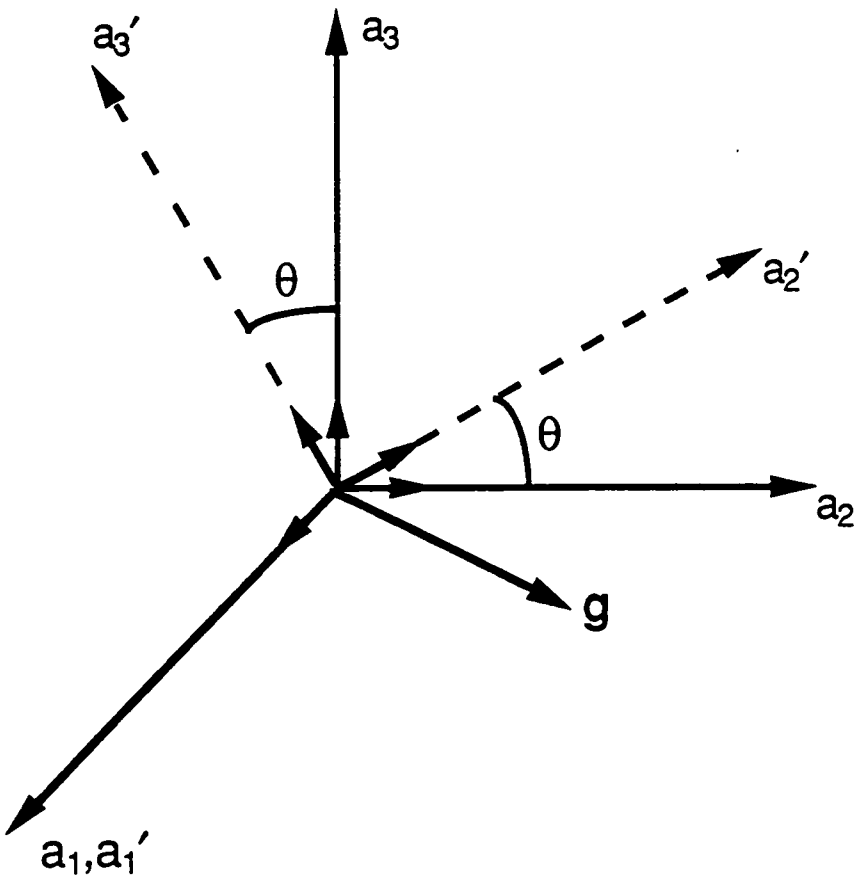

Figure 1. Axes a_2' and a_3' are rotated by an angle of θ about the a_1 axis. g is some vector with coordinates (g_1, g_2, g_3) in the unprimed axes and (g_1', g_2', g_3') in the primed axes. Unit vectors e and e′ are marked by short vectors along the coordinate axes.

Referring to the vector $\mathbf{g}$ in terms of some new coordinate axes is equivalent to a change in basis of a vector space from an original basis to a new basis (Anton, 1981, Chap. 4). The vector $\mathbf{g}$ is rewritten as $\mathbf{g}'$ in terms of the new coordinate axes. $\mathbf{g}'$ is obtained by the application of a transition matrix to $\mathbf{g}$:

$$\mathbf{g}' = \mathbf{R}\mathbf{g}. \tag{56}$$

$\mathbf{R}$ is called the transformation matrix (or rotation matrix). The columns of $\mathbf{R}$ are the components of the old basis vectors relative to the new basis. Consider, for example, the unit vectors $\mathbf{e}_1$, $\mathbf{e}_2$, $\mathbf{e}_1'$, and $\mathbf{e}_2'$ of two coordinate axes rotated with respect to one another by an angle θ. The transition matrix can be constructed by writing $\mathbf{e}_1$ and $\mathbf{e}_2$ in terms of the primed axes:

$$\begin{aligned} \mathbf{e}_1 &= \mathbf{e}_1' \cos\theta - \mathbf{e}_2' \sin\theta \\ \mathbf{e}_2 &= \mathbf{e}_1' \sin\theta + \mathbf{e}_2' \cos\theta \end{aligned} \tag{57}$$

which yields the transition matrix:

$$\mathbf{R} = \begin{bmatrix} \cos\theta & \sin\theta \\ -\sin\theta & \cos\theta \end{bmatrix}. \tag{58}$$

This is the transition matrix from unprimed to primed coordinate axes:

$$\mathbf{g}' = \mathbf{R}\mathbf{g}. \tag{59}$$

This can be checked by writing out the elements of $\mathbf{g}'$:

$$\begin{aligned} g_1' &= g_1 \cos\theta + g_2 \sin\theta \\ g_2' &= -g_1 \sin\theta + g_2 \cos\theta \end{aligned} \tag{60}$$

and comparing them to the equations for $\mathbf{e}_1'$ and $\mathbf{e}_2'$ in terms of the unprimed axes:

$$\begin{aligned} \mathbf{e}_1' &= \mathbf{e}_1 \cos\theta + \mathbf{e}_2 \sin\theta \\ \mathbf{e}_2' &= -\mathbf{e}_1 \sin\theta + \mathbf{e}_2 \cos\theta. \end{aligned} \tag{61}$$

Equations (60) and (61) are equivalent. Equations (61) could be used to create the transition matrix for primed to unprimed coordinate axes, which would be equal to the inverse ($\mathbf{R}^{-1}=\mathbf{R}^t$) of the transition matrix from unprimed to primed coordinate axes. The process is easily extended to three dimensions (Anton, 1981, Chap. 4).

In general, for a coordinate system defined by three mutually perpendicular axes, the transition matrix can be constructed from the direction cosines of the primed axes with respect to the unprimed axes:

$$\mathbf{R} = \begin{bmatrix} R_{11} & R_{12} & R_{13} \\ R_{21} & R_{22} & R_{23} \\ R_{31} & R_{32} & R_{33} \end{bmatrix} = R_{ij} \tag{62}$$

where the first subscript denotes a primed axis and the second an unprimed axis (Frederick and Chang, 1972, Chap. 1). For example, R_{12} is the cosine of the angle between the a_1'-axis and the a_2-axis. Hence, the transition of a vector from an unprimed system to a primed system can be obtained by

$$g_i' = R_{ij}\, g_j. \tag{63}$$

The use of equation (62) is preferred over that of equation (58) because (62) is more general and can be used for cases where the rotation is around any line through the origin, not only around a shared axis.

B. Application to Residual Acceleration Data

The transformation of coordinate axes can be a very useful operation in the analysis of data. In the case of the analysis of residual acceleration data in conjunction with experimental data, the ability to consider data in terms of different coordinate axes is a necessity. Experiments run in orbiting space laboratories, including accelerometer systems, are often oriented in a manner convenient to space restrictions. This results in a plethora of experimental coordinate systems for one mission.

While the total acceleration vector has the same magnitude in any coordinate system, the disturbance level in some particular direction may be of interest to investigators. Some experiments may be more sensitive to disturbances in one direction than in another direction. In the analysis of the results of such experiments, it is beneficial to transform the accelerometer data into a set of axes coincident with the direction of interest. The magnitude of disturbances in the direction of interest can then be obtained. If the sources of disruptive disturbances can be identified, and if these disturbances tend to be uni-directional, such knowledge could be used in the future when positioning experiments in orbiters.

V. CONCLUSIONS

Various aspects of residual acceleration data are of interest to investigators. The mean, variance, and minimum and maximum values can be obtained from the data as collected in the time domain. Additional information can be obtained by looking at data from a different perspective. Dominant frequency components can be identified following a transformation of data into the frequency domain (amplitude spectrum or power spectral density) using Fourier transform methods. Information obtained in both the time and frequency domains can be used by investigators to determine what magnitude disturbances and what frequency modes are disruptive to their experiments.

The orientation of accelerometer recording axes and of recorded accelerations is important in the analysis of low-gravity experiments. The ability to refer to acceleration data in terms of different coordinate axes (such as those of a separate experiment) is useful in the post-flight analysis of experiments.

Methods such as those discussed here can be implemented in the analysis of residual acceleration data collected in orbiting space laboratories and used to support analysis of experiments run under low-gravity conditions.

REFERENCES

Anton, H., Elementary Linear Algebra, John Wiley & Sons, 1981.

Båth, M., Spectral Analysis in Geophysics, Elsevier Scientific Publishing, Amsterdam, 1974.

Bendat, J. S. and A. G. Piersol, Measurement and Analysis of Random Data, John Wiley & Sons, 1966.

Bendat, J. S. and A. G. Piersol, Engineering Applications of Correlation and Spectral Analysis, John Wiley & Sons, 1980.

Bloomfield, P., Fourier Analysis of Time Series: An Introduction, John Wiley & Sons, 1976.

Cadzow, J. A., Foundations of Digital Signal Processing and Data Analysis, Macmillan Publishing Company, 1987.

Elliott, D. F. and K. R. Rao, Fast Transforms: Algorithms, Analyses, Applications, Academic Press, 1982.

Frederick, D. and T. S. Chang, Continuum Mechanics, Scientific Publishers, Inc., 1972.

Huang, Y. T., "Spectral Analysis of Digitized Seismic Data," Bull. Seis. Soc. Amer. 56 (2), 425-440, 1966.

Robinson, E. A. and S. Treitel, Geophysical Signal Processing, Prentice-Hall, 1980.

Waters, K. H., Reflection Seismology, John Wiley & Sons, 1981.

APPENDIX A - NOMENCLATURE

a_n, b_n	Fourier coefficients
$a(\omega)$	cosine transform of time function
$b(\omega)$	sine transform of time function
e_1, e_2	unit vectors
$f(t)$	function of time, t
f_λ	time series with increment λ, digitized version of f(t)
$F(\omega)$	Fourier transform of f(t)
F_n	Fourier transform of f_λ
$\mathbf{g}$	vector with coordinates (g_1, g_2, g_3)
$G(\nu)$	one-sided power spectral density function
i	$\sqrt{-1}$
N	length of time series in number of samples
R_{ij}	transformation matrix = **R**
$R(\tau)$	autocorrelation function of a time series
$S(\nu)$	two-sided power spectral density function
T	length of time series or function in seconds, also fundamental period of time series or function
Δt	sampling interval
$\Phi(\omega)$	phase spectrum of f(t)
θ	angle of rotation between coordinate axes
τ	time shift
ν	cyclic frequency
ν_N	Nyquist frequency
ω	angular frequency, $\omega=2\pi\nu$

^ over a symbol in the text represents an estimate of the parameter.

APPENDIX B - DETAILED DERIVATIONS

The derivation of equations (9) and (10) in the main text from the Fourier integral (4) can be done as follows. Given the Fourier integral

$$f(t) = \frac{1}{\pi}\int_0^\infty d\omega \int_{-\infty}^\infty f(\lambda)\cos(\omega(t-\lambda))\,d\lambda, \tag{B1}$$

the cosine term can be expanded, yielding:

$$f(t) = \frac{1}{\pi}\int_0^\infty d\omega \int_{-\infty}^\infty f(\lambda)\left[\cos\omega t\cos\omega\lambda + \sin\omega t\sin\omega\lambda\right] d\lambda \tag{B2}$$

$$= \frac{1}{\pi}\int_0^\infty d\omega \left[\int_{-\infty}^\infty \left[f(\lambda)\cos\omega t\cos\omega\lambda + f(\lambda)\sin\omega t\sin\omega\lambda\right] d\lambda\right] \tag{B3}$$

$$= \frac{1}{\pi}\int_0^\infty d\omega \left[\int_{-\infty}^\infty f(\lambda)\cos\omega\lambda\cos\omega t\,d\lambda + \int_{-\infty}^\infty f(\lambda)\sin\omega\lambda\sin\omega t\,d\lambda\right] \tag{B4}$$

$$= \frac{1}{\pi}\int_0^\infty \left[a(\omega)\cos\omega t + b(\omega)\sin\omega t\right] d\omega. \tag{B5}$$

Equation (B5) is the same as equation (7) in the main text. Introducing equations (6) from the main text for $\Phi(\omega)$, $a(\omega)$, and $b(\omega)$ yields:

$$f(t) = \frac{1}{\pi}\int_0^\infty \left[a^2(\omega) + b^2(\omega)\right]^{1/2}\cos\Phi(\omega)\cos\omega t$$

$$-\left[a^2(\omega) + b^2(\omega)\right]^{1/2}\sin\Phi(\omega)\sin\omega t\,d\omega \tag{B6}$$

$$= \frac{1}{\pi}\int_0^\infty \left[a^2(\omega) + b^2(\omega)\right]^{1/2}\left[\cos\Phi(\omega)\cos\omega t - \sin\Phi(\omega)\sin\omega t\right] d\omega \tag{B7}$$

$$= \frac{1}{\pi} \int_0^{\infty} \left[a^2(\omega) + b^2(\omega)\right]^{1/2} \left[\cos\left(\Phi(\omega) + \omega t\right)\right] d\omega. \qquad \text{(B8)}$$

Equation (B8), which is equation (8) in the main text, can be rewritten as follows:

$$f(t) = \frac{1}{2\pi} \int_0^{\infty} \left[a^2(\omega) + b^2(\omega)\right]^{1/2} \left[e^{i(\Phi(\omega) + \omega t)} + e^{-i(\Phi(\omega) + \omega t)}\right] d\omega \qquad \text{(B9)}$$

$$= \frac{1}{2\pi} \int_0^{\infty} \left[a^2(\omega) + b^2(\omega)\right]^{1/2} \left[e^{i(\Phi(\omega) + \omega t)}\right] d\omega$$

$$+ \frac{1}{2\pi} \int_{-\infty}^{0} \left[a^2(\omega) + b^2(\omega)\right]^{1/2} \left[e^{i(\Phi(\omega) + \omega t)}\right] d\omega, \qquad \text{(B10)}$$

by reversal of the limits of integration. Manipulation of the exponential terms yields:

$$f(t) = \frac{1}{2\pi} \int_0^{\infty} \left[a^2(\omega) + b^2(\omega)\right]^{1/2} \left[e^{i\omega t}\, e^{i\Phi(\omega)}\right] d\omega$$

$$+ \frac{1}{2\pi} \int_{-\infty}^{0} \left[a^2(\omega) + b^2(\omega)\right]^{1/2} \left[e^{i\omega t}\, e^{i\Phi(\omega)}\right] d\omega. \qquad \text{(B11)}$$

Addition of the two integrals results in equations (9) and (10) of the main text, the inverse Fourier transform:

$$f(t) = \frac{1}{2\pi} \int_{-\infty}^{\infty} \left[a^2(\omega) + b^2(\omega)\right]^{1/2} \left[e^{i\omega t}\, e^{i\Phi(\omega)}\right] d\omega \qquad \text{(B12)}$$

$$= \frac{1}{2\pi} \int_{-\infty}^{\infty} F(\omega)\, e^{i\omega t}\, d\omega. \qquad \text{(B13)}$$

APPROVAL

ANALYSIS TECHNIQUES FOR RESIDUAL ACCELERATION DATA

By Melissa J.B. Rogers, J. Iwan D. Alexander, and Robert S. Snyder

The information in this report has been reviewed for technical content. Review of any information concerning Department of Defense or nuclear energy activities or programs has been made by the MSFC Security Classification Officer. This report, in its entirety, has been determined to be unclassified.

E. Tandberg-Hanssen

E. TANDBERG-HANSSEN
Director
Space Science Laboratory

☆ U.S. GOVERNMENT PRINTING OFFICE 1990—731—061/20187

NASA—MSFC

Analysis of Spacelab 3 Residual Acceleration Data

M. J. B. Rogers and J. I. D. Alexander

Reprinted from

Journal of Spacecraft and Rockets

Volume 28, Number 6, November–December 1991, Pages 707–712

AIAA

A publication of the
American Institute of Aeronautics and Astronautics, Inc.
The Aerospace Center, 370 L'Enfant Promenade, SW
Washington, DC 20024-2518

Analysis of Spacelab 3 Residual Acceleration Data

Melissa J. B. Rogers* and J. Iwan D. Alexander†
University of Alabama in Huntsville, Huntsville, Alabama 35899

A data reduction plan is being developed to efficiently process residual acceleration data, making such data more accessible to principal investigators of low-gravity experiments. Accelerometer data collected during the Spacelab 3 mission is being processed using a prototype version of this plan. The plan addresses various aspects of acceleration data analysis: the identification of disturbances that are intolerable to experiments, the investigation of acceleration orientations, the definition and characterization of the background acceleration corresponding to a given experiment time line, the isolation and examination of particular significant disturbances, and the identification of disturbance sources. Acceleration magnitude, frequency, and orientation are discussed: transient accelerations can have magnitudes as large as $10^{-2}g$ with frequency components (from 4.5×10^{-3} to 150 Hz) no greater than $10^{-3}g$. These accelerations fluctuate rapidly in orientation. The occurrence of disturbance sources in an orbiter is tentatively identified as a random process, whereas the response of the orbiter to given accelerations is considered deterministic. The need to continue monitoring of residual accelerations in orbiting space laboratories is stressed: future measurements are needed to establish acceleration characterizations of specific orbiters and to establish appropriate acceleration tolerance limits for specific experiment classes in low-gravity conditions.

Nomenclature

A_i = amplitude spectra of three components of a_i, g
a = magnitude of residual acceleration vector
a_i = residual acceleration vector, g
$f_{\min}$ = minimum frequency investigated, $1/T_w$
g = gravitational acceleration at the earth's surface, 9.81 ms^{-2}
R_{ij} = transformation matrix
T_w = window length, s (or number of points)

Introduction

THE low-gravity environment of space has been a subject of interest since the early days of manned spaceflight. Early references to zero gravity were based on the fact that at the center of mass of a freely orbiting spacecraft the gravitational force is balanced by the centrifugal force. This ideal situation cannot be realized in an actual spacecraft because of a variety of internal and external disturbing forces causing low-amplitude residual accelerations in orbiters over a broad range of frequencies. Sources of residual accelerations are classified as quasisteady, having magnitudes in the $10^{-6}g$ range and frequencies on the order of the orbital frequency (the Earth's gravity gradient, spacecraft attitude motions, atmospheric drag), and transient or oscillatory, having high magnitudes (up to $10^{-2}g$) and frequencies up to 100 Hz (machinery vibrations and rotations, spacecraft vibrations, thruster firings, crew activity).[1,2]

The gravitational environment of an orbiter is continuously changing because of these residual accelerations. Investigators are interested in the effects of such an environment on man, spacecraft, and the variety of experiments being run under low-g conditions. To analyze the effects and evaluate the experiments, a complete description of the environment is required. To define the environment quantitatively, various accelerometer systems designed to measure residual accelerations in the $10^{-6}g$ range at frequencies from 10^{-4} to 150 Hz have been flown on several different spacecraft. These projects have resulted in a plethora of accelerometer data that has been subjected to only limited analysis. Discussions of various accelerometer measurements and low-gravity experiments since the mid-1970s can be found in the literature.[1,3-9]

We are developing a data reduction plan to efficiently process residual acceleration data, making such data more accessible to principal investigators. Using a prototype version of this plan, we have begun to process accelerometer data collected during the Space Transportation System (STS) 51-B Spacelab 3 (SL3) mission in April-May 1985. Some typical disturbances have been identified and cataloged and a general description of background accelerations has been made. This work complements previous descriptive studies of the low-g environment of the orbiter.[1,7,8]

In the Data and Data Processing sections, we give some details about the collection of the SL3 accelerometer data and introduce the data reduction plan used to process the data. In the Results section, we present some examples of typical disturbances that are seen in the SL3 data, compare these accelerations to ones discussed in other references,[4,8] and discuss the magnitude and orientation of certain disturbances measured by the accelerometer system. In the Discussion section, we consider the question of whether the data are random or deterministic and comment on the need to monitor residual accelerations in orbiting space laboratories to aid in the planning and development of future low-gravity experiments.

Data

The residual acceleration data from Spacelab 3 were collected with a Bell Aerospace Miniature Electrostatic Accelerometer (MESA) package. The data were recorded at 300 samples/s with a bandwidth of 50 Hz. The system was a part of the Fluids Experiment System, which was mounted on a double rack in the Spacelab module. The accelerometer's x and z axes were rotated 112.5 deg clockwise about the orbiter y axis (orbiter structural coordinate system). The origin of the accelerometer coordinate system was a little more than 1 m radially off from the orbiter center of gravity.[3]

We obtained the SL3 data from the Marshall Space Flight Center (MSFC) in the form shown in Table 1. Experiment x-, y-, and z-axis data are given for each time mark in units of $10^{-6}g$. The total amount of acceleration data expected from the experiment was approximately 1.5×10^8 data points per

Received April 9, 1990; revision received Nov. 2, 1990; accepted for publication Nov. 5, 1990.

*Research Associate, Center for Microgravity and Materials Research.

†Associate Director, Center for Microgravity and Materials Research.

Table 1 Data as received from the Marshall Space Flight Center

Time, h:min:s.ms	L20Q6002A[a], μg	L20Q6005A[a], μg	L20Q6008A[a], μg
123:10:00.000	−0.760000E+02	0.110000E+04	0.480000E+03
123:10:00.003	−0.200000E+03	0.120000E+04	−0.510000E+03
123:10:00.007	0.960000E+03	0.800000E+03	−0.200000E+04
123:10:00.010	0.120000E+04	0.620000E+03	−0.120000E+04
123:10:00.013	0.100000E+04	0.360000E+03	−0.130000E+04
123:10:00.017	0.560000E+03	0.220000E+03	0.200000E+04
123:20:00:020	−0.690000E+02	−0.680000E+02	0.760000E+03
.	.	.	.
.	.	.	.
.	.	.	.

[a] Accelerometer axes x, y, and z correspond to L20Q6002A, L20Q6005A, and L20Q6008A, respectively; acceleration is in $10^{-6}g$.

axis, which represents 140 h and would comprise about 9 Gbytes of data as stored at MSFC.[3] Because of telemetry and instrument problems, however, blocks of data up to 1 h in length are missing. For the SL3 data base, this makes the task of data processing time intensive because windows of missing data must be identified and avoided.

Data Processing

We are developing a multistep data reduction plan for the analysis of residual acceleration data. The plan addresses various aspects of acceleration data analysis: the identification of disturbances which are potentially disruptive to experiments, the investigation of acceleration orientations, the definition and characterization of the background acceleration corresponding to a given experiment time line, the isolation and examination of particular significant disturbances, and the identification of disturbance sources. All of these aspects are important for the analysis of experimental results. Standard digital signal processing techniques were used[10-12]; specifics of the application of these techniques to residual acceleration data are discussed elsewhere.[13] The first two topics mentioned above are specifically addressed in this section.

Identification of Intolerable Accelerations

The initial concern of the plan is the identification of potentially disruptive disturbances. A disturbance is deemed potentially disruptive when certain acceleration limits are surpassed. Ideally, these limits should be specified by investigators who know what levels of acceleration, in reference to both time and frequency, their experiments can tolerate. However, for most experiments, such tolerance limits have not yet been established. Nonetheless, it can be expected that as we obtain a better knowledge of the low-g environment of specific orbiters and the sensitivity levels of experiments run in space, the a priori establishment of realistic disturbance limits will be easier to achieve. In working with the SL3 data, test limits were chosen based on our current understanding of the sensitivity of crystal growth from solution.[14] These limits were used because such an experiment was flown on SL3 in conjunction with the accelerometer system.

The identification of potentially disruptive disturbances consists of two equally important parts: a peak detection routine applied in the time domain to identify accelerations exceeding designated limits and a spectral analysis technique to identify significant frequency components and to test these components against frequency limits. The importance of both time and frequency domain analyses for the identification of potentially disruptive accelerations will be discussed later in this section.

Segments of the SL3 accelerometer data were processed as follows. The data from all three axes were used to calculate the magnitude of the residual acceleration vector a_i for each sample time:

$$a = \sqrt{a_1^2 + a_2^2 + a_3^2} \tag{1}$$

The resulting total acceleration array was used as input to a peak detection routine that identifies times when test limits are exceeded in the time domain. From the list of times produced by the detection routine, windows containing occurrences of high acceleration values were identified and plotted. Windows of length $T_w = 6.8$ s (2048 points) were used for further analysis; this window length provides good detail and is long enough to include most types of transient disturbances. Unfortunately, this window length imposes a 0.15-Hz lower limit on frequencies that can be studied using spectral analysis because $f_{\min} = 1/T_w$.[13] To test the lower frequency limits (<0.15 Hz), windows of length $T_w = 3.6$ min (65,536 points) containing several disturbances were chosen and processed as mentioned earlier. This length window contains information on frequencies as low as 4.5×10^{-3} Hz.

Table 2 Maximum tolerable acceleration levels for given frequencies, determined from numerical modeling of crystal growth from solution[14]

Frequency, Hz	Magnitude of component, g
$<10^{-2}$	10^{-4}
10^{-2}–1.0	10^{-3}
>1.0	10^{-2}

The second part of the identification process involves the spectral analysis of the data windows. The frequency domain tolerance limits used with the SL3 data are shown in Table 2. To test these for a given window, the three axes of residual acceleration data are individually transformed into the frequency domain using a fast Fourier transform algorithm ($a_1 \leftrightarrow A_1$, $a_2 \leftrightarrow A_2$, $a_3 \leftrightarrow A_3$). The three resulting amplitude spectra (A_1, A_2, A_3) are used to form a combined amplitude spectrum array: $A = (A_1^2 + A_2^2 + A_3^2)^{1/2}$. The values of this combined spectrum are tested against the frequency limits. If any of the limits are exceeded, the window is identified as potentially intolerable.

As stated earlier, the time and frequency domain analyses of residual acceleration data are equally important. The effect of an acceleration on a given experiment depends on the response of that experiment to the amplitude, frequency, and orientation of the acceleration.[2,14,15] It is, therefore, necessary to establish both time and frequency tolerance limits for different classes of experiments. The two domains provide different perspectives on the data from which it is possible to obtain important information. The time history gives an indication of the instantaneous acceleration experienced at the sensor location for each time sample and is especially important in the analysis of experiments sensitive to transient disturbances. The representation of data in the frequency domain gives an indication of the frequency components that sum together to produce the time domain record. Because of this, the amplitude at any given frequency can only be a fraction of the highest magnitude represented in the time window. The use of amplitude spectra, as opposed to power spectral densities, gives the magnitude of a particular frequency component over the time period considered in the same units as the original time series.[10-13] This frequency domain representation is the most practical when comparing acceleration components to thresh-

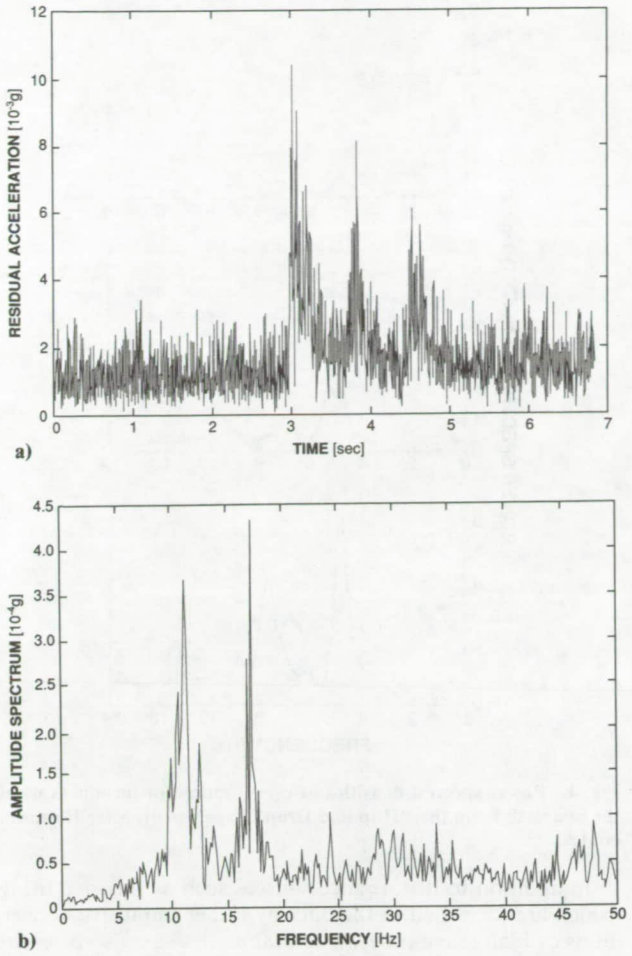

Fig. 1 Window containing three large magnitude pulses surrounded by quiet data: a) total acceleration array, maximum magnitude $\sim 1 \times 10^{-2} g$; b) combined amplitude spectrum, dominant frequency components 11 and 17 Hz.

old limits typically stated as units of g at a particular frequency.

Investigation of Acceleration Orientation

In the process of identifying potentially disruptive accelerations, we are not concerned with the orientation of the disturbing acceleration, only the magnitude and frequency. Information on the orientation of disturbing forces can aid in the analysis of experiment results, and so two options are included in the processing plan involving the orientation of the data: 1) data can be transformed into coordinate axes other than those in which they were recorded, and 2) the direction cosines of the three axes of acceleration can be computed, giving an indication of the continuously changing orientation of the recorded accelerations. Such manipulation of data will be useful in the postflight analysis of experimental results for cases when the orientation of accelerations, as well as magnitude and frequency, is important to experiment sensitivity.[2,14,15]

The orientation of experiments flown on orbiters varies greatly. Transformation of accelerometer data into other experiment axes will aid in the analysis of results of experiments sensitive to impulses in specific directions. The transformation of data is obtained by the application of a transition matrix to the original data

$$a_i' = R_{ij} a_j \tag{2}$$

where a_i' denotes the acceleration components in the transformed coordinates, and a repeated index indicates a summation.[13] The transformation matrix R_{ij} is constructed from the direction cosines of the primed axes with respect to the unprimed axes. This procedure has been used to transform the SL3 accelerometer data into the orbiter structural coordinate axes so that data plots may be compared more directly to results from other papers.

An additional processing technique in the data reduction plan provides an indication of the orientation of the recorded accelerations. As with the ability to transform data into different coordinate axes, a knowledge of the direction of measured accelerations will aid in the analysis of experimental results. Direction cosines are used to determine the orientation of measured accelerations with respect to the recording axes. Tests have been run on the SL3 data using this method to determine whether certain transient disturbances act in characteristic directions or whether acceleration orientations vary with time.

Results

Residual acceleration data collected during the SL3 mission were processed using the prototype data reduction plan discussed earlier. Acceleration events were declared potentially intolerable when the time domain tolerance limit of $4 \times 10^{-3} g$ and/or the frequency domain limits given in Table 2 were exceeded. In addition to events identified as intolerable, windows with no apparent high-magnitude disturbances were also studied in an attempt to definitively characterize the background acceleration level. This is important because the steady accelerations contained in the background have just as great a potential to adversely affect some experiments as high-magnitude transient disturbances have to affect other experiments.[2,14,15] It must be emphasized that the measurement of steady accelerations is currently restricted in part by instru-

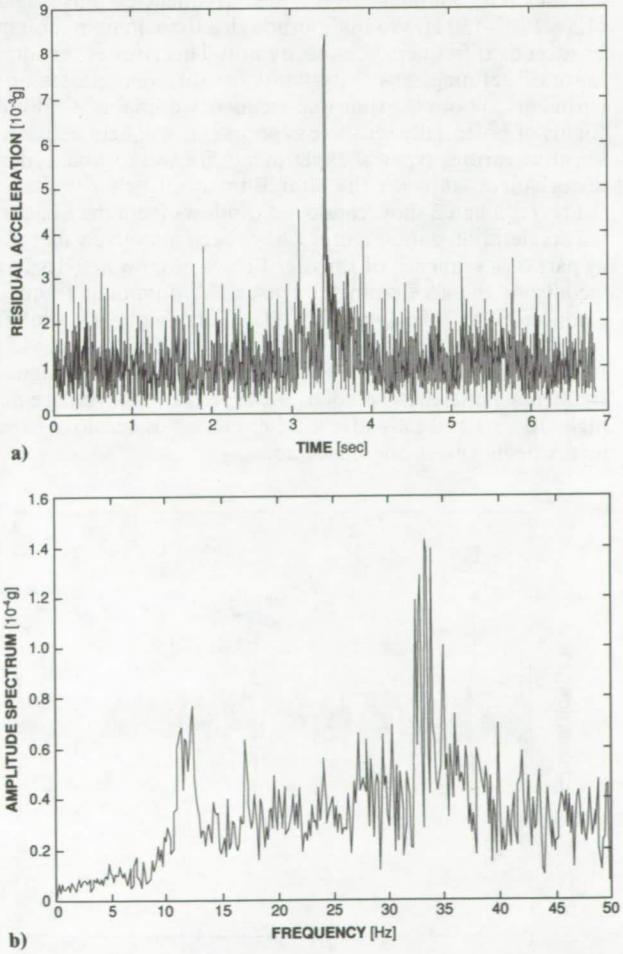

Fig. 2 Window containing crew induced disturbance: a) total acceleration array, maximum magnitude $\sim 8.5 \times 10^{-3} g$; b) combined amplitude spectrum, dominant frequency component 33 Hz.

ment limitations, but also largely by the presence of low-magnitude background accelerations and instrument noise. However, steady accelerations can be predicted to some extent from a knowledge of the orbiter altitude and attitude and solar activity during a mission.

On the order of 4×10^6 samples of SL3 residual acceleration data have been processed to date, representing approximately 3 noncontinuous hours of data. Windows of interest ($T_w = 6.8$ s) from the SL3 data identified as intolerable or background have been cataloged. Cataloging consists of the notation of identification codes and occurrence times and the plotting of time histories and amplitude spectra for each window (Figs. 1 and 2). Although we have no way of correlating these disturbances with specific sources, we are comparing them to signals with known sources presented in other papers.[1,4,7,8] As a result of these comparisons, the sources of the cataloged signals have been tentatively identified and the signals are considered to be representative of certain classes of disturbances: those caused by thruster firings; those stemming from mechanical sources such as motors, fans, etc.; those induced by crew activity; and those of unknown origin, but nonetheless interesting. Comparisons of windows of quiet data ($a \le 4\times10^{-3}g$) reveal that a characteristic background acceleration level does not exist for the SL3 data. Amplitude spectra vary among windows, indicating the presence of low-magnitude accelerations and instrument noise, which masks any information on quasi-steady accelerations we might wish to gain directly from the data.

Despite the fact that the $4\times10^{-3}g$ time domain tolerance limit was often exceeded, the frequency domain limits (obtained from the same modeling) were never surpassed. This indicates that the power contained in the windows studied is spread out enough over the frequencies investigated (4.5×10^{-3}–150 Hz) so that, although a time domain limit may be exceeded, frequency limits are not. This stresses the importance of defining sensitivity limits for different classes of experiments in both the time and frequency domains. Continued flights of potentially sensitive experiments will help define how sensitive various types of experiments are and to what types of disturbances, allowing the establishment of better limits.

Figures 1 and 2 show cataloged windows from the SL3 residual acceleration data. Figures 1 have been tentatively identified as part of a sequence of thruster firings or crew activity in the vicinity of the accelerometer sensors. A dominant frequency component of this data is 11 Hz. This frequency probably reflects the excitation of orbiter structural modes as well as localized modes within the Spacelab.[16] Although no designated frequency limits are exceeded, the acceleration levels are quite high ($10^{-2}g$) and may affect other classes of sensitive experiments being run in the Spacelab.

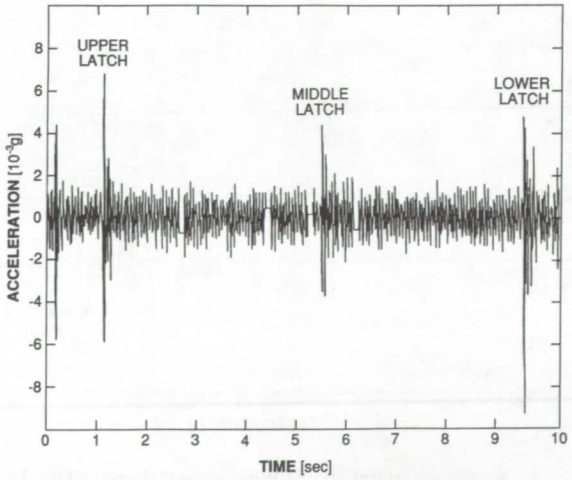

Fig. 3 Crew induced disturbances related to FES latch openings during Spacelab 3, experiment x axis, after Chassay and Schwaniger.[4]

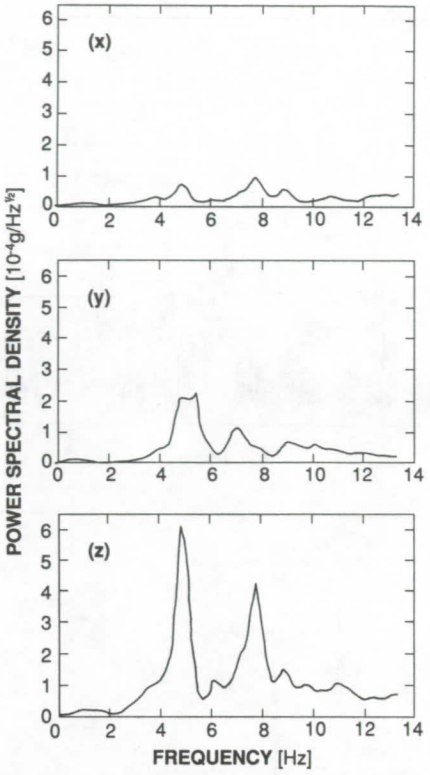

Fig. 4 Power spectral densities of crew induced disturbances within the Spacelab from the "Hop and Drop" experiment, after Hamacher et al.[8]

In addition to disturbance sources such as thruster firings, which are identified in the data by rather impulsive accelerations of high magnitude, structural modes can also be excited by mechanical sources. Accelerations caused by such sources may be no greater in magnitude than the background level and can often be identified only by the presence of related frequency components. One 30-min block of SL3 data that we analyzed was dominated by a 17-Hz component. No impulsive start for this oscillatory event could be identified in the data and the source was therefore attributed to some mechanical device. Previous study of the SL3 data has identified the driving motor of the KU band antenna as a probable source of this disturbance.[17] Although this type of disturbance has no associated high-magnitude impulses, experiments that are sensitive to oscillations in a particular frequency range could be affected by such accelerations. The 17-Hz disturbance can also be seen superimposed on transient disturbances, as in Figs. 1.

Figures 2 show one other typical high-magnitude acceleration disturbance from the SL3 data. The disturbance shown in the time window appears to be of a higher frequency than the previously discussed accelerations. This is confirmed by the amplitude spectrum, which indicates that the dominant frequency present is 33 Hz. This disturbance is very similar to accelerations caused by the opening of latches on the Fluids Experiment System (FES) optical bench doors[4] and to other accelerations originating within the Spacelab[8] (Fig. 3). Although we are not able to correlate this disturbance with any specific event, we believe it is typical of disturbances caused by general crew activity, especially within the Spacelab module.

The comparison of the signal shown in Figs. 2 to the latch opening plot of Fig. 3 was made only in the time domain. No amplitude or power spectra were provided for this identified source.[4] Previous studies have identified several common frequency components that are excited by transient sources.[4,7,8] Frequencies of approximately 5 and 7 Hz are known to be excited by activity within the Spacelab. Hamacher et al.[8] state that the 5-Hz signal represents the eigenfrequency of the suspended Spacelab module and that the 7-Hz component represents the eigenfrequency of the Spacelab rack row. In addition

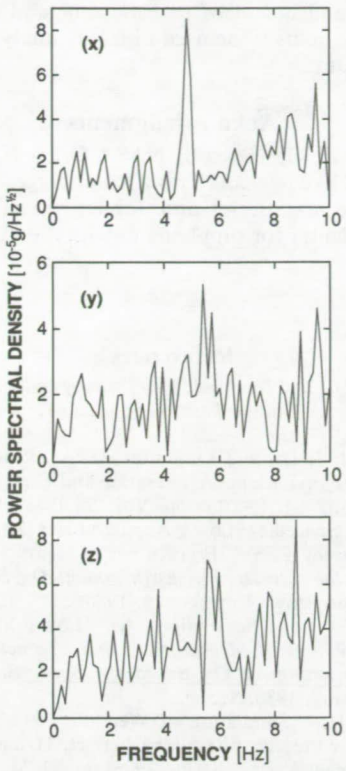

Fig. 5 Power spectral densities from the three individual accelerometer axes representing a crew induced disturbance. Data are rotated into orbiter structural axes and Butterworth filtered at 13 Hz. Note presence of components of various strengths in the 4.5–5.5 and 7–8 Hz ranges.

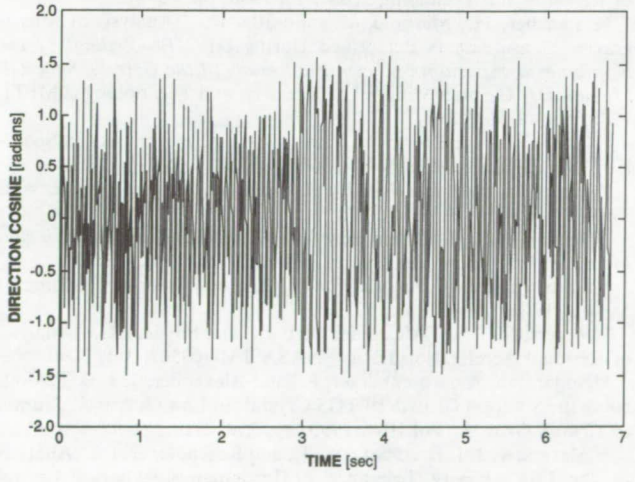

Fig. 6 Orientation of measured acceleration shown in Fig. 1 with respect to recording axis, $\alpha = \cos^{-1}(a_1/a)$. Note rapidly fluctuating behavior with marked change in character approximately three seconds into the window, representing large disturbance.

to these Spacelab modes, there are orbiter modes related to similar frequencies. A frequency of 5.2 Hz represents the fuselage first normal bending mode and 7.4 Hz represents the fuselage first lateral bending mode.[16]

In the analysis of SL3 residual acceleration data, 5- and 7-Hz frequency components were identified in the amplitude spectra of several windows we investigated. We compared examples of filtered SL3 data to power spectral densities from Hamacher et al.[8] (Fig. 4). Their data were collected at 107 samples/s with a bandwidth of 10 Hz. We identified several windows ($T_w = 6.8$ s) in the SL3 data that had fairly significant components present at frequencies < 10 Hz, and applied a 13-Hz Butterworth filter[12,16] to the data to aid in the comparison. The data were also rotated into coincidence with the recording axes of the D1 accelerometer system (orbiter structural axes) (Fig. 5). The various components do not line up exactly, but this is not surprising due to the different data collection and analysis techniques used. In addition, we do not know whether the sources of these two disturbances were at all similar. It is notable, however, that, even with the higher sampling and cutoff frequencies used for the SL3 data, these components are discernible above the background.

The final phase of processing the data windows discussed earlier is the calculation of direction cosines to determine acceleration orientation. For all windows tested and for all axes of data, the orientation of accelerations fluctuates rapidly between the positive and negative recording axes (Fig. 6). This is as expected for a system such as the orbiter where there are potential sources of disturbances at almost every point. Even barring sources of large accelerations, such as thruster firings and crew activity in the vicinity of accelerometers, other factors such as mechanical devices, general crew motion, and the steady acceleration sources contribute to a continuously fluctuating background level. When specific high-magnitude and/or oscillatory disturbances occur, a change in the character of the acceleration orientation can be seen. If a characteristic orientation of certain acceleration types can be determined, such information will aid in the analysis of experiments that are sensitive to disturbances in a particular direction. At this stage, however, it appears as if the accelerations recorded during SL3 fluctuate rapidly in orientation for most types of disturbances.

Discussion

Several general comments can be made about the low-gravity environment of the orbiter during the SL3 mission and about the future of residual acceleration measurements and low-g experimentation in orbiting space laboratories. The SL3 residual acceleration data are very noisy; background levels are consistently above limiting values deemed potentially intolerable to experiments. The general background level is $\leq 4 \times 10^{-3} g$ and consists of a broad range of frequencies, with rapid fluctuations in orientation.

Several characteristic signals have been identified in the SL3 residual acceleration data and grouped into four general categories: those caused by thruster firings, those mechanically induced, those induced by crew activity, and those of unknown origin. Most of these disturbances are transient and can have magnitudes as large as $10^{-2} g$ (Figs. 1). In the frequency domain, the amplitudes of the individual components associated with these disturbances are rarely greater in magnitude than $10^{-3} g$ and do not surpass any frequency limits used in this study (Figs. 1 and 2, Table 2). Further modeling of potentially sensitive experiments and further experimentation in orbiters should indicate whether such limits are realistic and what levels of disturbances may be detrimental to sensitive experiments.

Specific frequency components, 5 and 7 Hz, were discussed. Examples of such frequencies in the SL3 data were compared to examples from Hamacher et al.[8] Both crew activity within the Spacelab module and the firing of thrusters have been identified as sources that excite sets of modes at these frequencies. One set of modes is related to the Spacelab, whereas another set is related to the orbiter. For a given transient source, either or both sets of modes can be excited. Comparisons of acceleration magnitudes from individual axes may allow the identification of which specific modes are excited (Figs. 4 and 5).

To establish an acceleration characterization of a given orbiter, specific tests to distinguish between sets of modes will be necessary. Data from an array of accelerometers within the Spacelab module and throughout the orbiter, in conjunction with a well-documented time line of flight events, would aid in the assessment of what types of disturbances cause what levels of accelerations and how far the effects of such disturbances

propagate throughout the craft. Tests involving known sources, for example, the opening and closing of specific doors in the Spacelab and the use of specific equipment by crew members, will also further the characterization of the orbiter environment.

Residual acceleration data collected in orbiting space laboratories have been described as random.[9] We raise some objections to this description and advocate care when not qualifying such comments. The basic question involved here is what aspect of the data is being described. The distribution of disturbance sources affecting the orbiter may best be described as temporally and spatially random. For example, during any given mission, disturbance sources such as the opening of latches and doors, the manipulation of equipment, and general crew motion, as well as thruster firings, water dumps, and other operational activities, occur in a random fashion, despite preflight scheduling of some operations. The likelihood of these disturbances occurring can be described by some probability distribution based on our knowledge of past missions.

The response of the orbiter at a given location (e.g., at the sensor site) to given disturbances, such as those stated earlier, however, can be predicted based on past experiments on the orbiter and modeling of the orbiter system. Such a response is considered deterministic. For example, as discussed previously, we know that certain activities within the Spacelab (hop and drop experiments, equipment manipulation) have associated characteristic frequency components, 5 and 7 Hz.[8] Among the identifiable orbiter modes, thruster firings appear to excite components in the 11-Hz range as well as orbiter structural modes around 5 and 7 Hz.[16] Future analysis of specific disturbance-acceleration-frequency response relations will result in a better understanding of the orbiter response to specific accelerations.

Conclusions

A prototype data reduction plan is being applied to SL3 residual acceleration data. The plan can be used to identify potentially intolerable acceleration events, to investigate acceleration orientation, to isolate and examine particular acceleration windows, and to identify probable acceleration sources. For the SL3 mission, a $4 \times 10^{-3}g$ time domain threshold limit was often exceeded and transient accelerations with magnitudes as large as $10^{-2}g$ were identified. Such acceleration events have frequency components (over 6.8-s to 3.6-min windows) no greater than $10^{-3}g$ and fluctuate rapidly in orientation. Although the occurrence of such accelerations in an orbiter is identified as both temporally and spatially random, the response of the orbiter is considered deterministic; it is this response, and the response of experiments, that we are ultimately interested in.

Continued monitoring of residual accelerations in orbiting space laboratories is important for several reasons. Such monitoring will help to better define the response of an orbiting system to typical disturbances and will also improve the accuracy of probability distributions used to define the occurrence of disturbance sources. These two factors are integral parts of the desired characterization of the low-gravity environment of orbiting space laboratories. Characterization of an orbiter's low-g environment, however, is not an easy task. Attempts made to date have only scratched the surface and additional data are needed to complete such a characterization.[1,3-9,16] A knowledge of experiment and orbiter responses will also help in the planning and development of future experiments and in the establishment of realistic time and frequency domain tolerance limits to be used in future analyses of residual acceleration data.

Acknowledgments

This work was supported by NASA Grant NAG8-759. The authors would like to thank Franz Rosenberger for his careful reading of the manuscript and John Scott at the Marshall Space Flight Center for supplying us with the SL3 accelerometer data.

References

[1]Hamacher, H., and Merbold, U., "Microgravity Environment of the Material Science Double Rack on Spacelab-1," *Journal of Spacecraft,* Vol. 24, 1987, pp. 264–269.

[2]Alexander, J. I. D., and Lundquist, C. A., "Motions in Fluids Caused by Microgravitational Acceleration and Their Modification by Relative Rotation," *AIAA Journal,* Vol. 26, 1988, pp. 34–39.

[3]Arnett, G., "Spacelab-3 Low-g Accelerometer Data from the Fluid Experiments System (FES)," *Proceedings of Measurement and Characterization of the Acceleration Environment On Board the Space Station,* Teledyne Brown Engineering, 1986, Sec. 11.

[4]Chassay, R. P., and Schwaniger, A., "Low-g Measurements by NASA," *Proceedings of Measurement and Characterization of the Acceleration Environment On Board the Space Station,* Teledyne Brown Engineering, 1986, Sec. 9.

[5]Hamacher, H., "Simulation of Weightlessness," *Materials Sciences in Space,* edited by B. Feuerbacher, H. Hamacher, and R. J. Naumann, Springer-Verlag, Berlin, 1986, pp. 31–51.

[6]Naumann, R. J., "Historical Development," *Materials Sciences in Space,* edited by B. Feuerbacher, H. Hamacher, and R. J. Naumann, Springer-Verlag, Berlin, 1986, pp. 11–30.

[7]Trappen, N., and Demond, F. J., "Post Flight Accelerometer Data Evaluation," *Proceedings of the Norderney Symposium on Scientific Results of the German Spacelab Mission D1,* German Ministry of Research and Technology (BMFT), 1986, pp. 43–47.

[8]Hamacher, H., Merbold, U., and Jilg, R., "Analysis of Microgravity Measurements Performed During D1," *Proceedings of the Norderney Symposium on Scientific Results of the German Spacelab Mission D1,* German Ministry of Research and Technology (BMFT), 1986, pp. 48–56.

[9]Knabe, W., and Eilers, D., "Low-Gravity Environment in Spacelab," *Acta Astronautica,* Vol. 9, 1982, pp. 187–198.

[10]Båth, M., *Spectral Analysis in Geophysics,* Elsevier, Amsterdam, The Netherlands, 1974.

[11]Bendat, J. S., and Piersol, A. G., *Random Data: Analysis and Measurement Procedures,* 2nd ed., Wiley, New York, 1986.

[12]Lynn, P. A., *An Introduction to the Analysis and Processing of Signals,* Wiley, New York, 1973.

[13]Rogers, M. J. B., Alexander, J. I. D., and Snyder, R., "Analysis of Residual Acceleration Data," NASA TM-103507, July 1990.

[14]Nadarajah, A., Rosenberger, F., and Alexander, J. I. D., "Modelling the Solution Growth of TGS Crystals in Low Gravity," *Journal of Crystal Growth,* Vol. 104, 1990, pp. 218–232.

[15]Alexander, J. I. D., Ouazzani, J., and Rosenberger, F., "Analysis of the Low Gravity Tolerance of Bridgman-Stockbarger Crystal Growth I. Steady and Impulse Accelerations," *Journal of Crystal Growth,* Vol. 97, 1989, pp. 285–302.

[16]Cooke, C., Koenig, M., Lepanto, J., Levine, G., Miller, J., Sargent, D., and Schlundt, R., "SDI Space Shuttle Based Experiments for Acquisition, Tracking, and Pointing—Definition of Space Shuttle Operational Environment," Charles Stark Draper Laboratory, Cambridge, MA, R-1868, April 1986.

[17]Bergmann, E., private communication, 1989.

Paul F. Mizera
Associate Editor

Adv. Space Res. Vol. 11, No.7 pp. (7)5–(7)8, 1991
Printed in Great Britain.

0273–1177/91 $0.00 + .50

A91-53402

A STRATEGY FOR RESIDUAL ACCELERATION DATA REDUCTION AND DISSEMINATION

Melissa J. B. Rogers and J. Iwan D. Alexander

Center for Microgravity and Materials Research, University of Alabama in Huntsville, Huntsville, AL 35899, U.S.A.

ABSTRACT

A data reduction plan is being developed to efficiently process residual acceleration data from orbiting space laboratories. Implementation of the reduction plan will result in a useful, manageable accelerometer data base which can be readily employed by principal investigators during post-flight analysis of experimental results. The data reduction plan will also assist in the characterization of the acceleration environment of orbiters, which is important for the planning of future experimental missions.

Prototype versions of the reduction plan are being tested using accelerometer data recorded during the Spacelab 3 (SL3) mission. Transient disturbances caused by shuttle and experiment operations and crew activities are being catalogued. The magnitudes of such disturbances can be as much as 10^{-2}g, but are rarely sustained for more than a fraction of a second and tend to vary greatly in orientation. We have found that the recorded frequency components of the SL3 disturbances do not exceed tolerance limits determined from modelling for a selected experiment set.

INTRODUCTION

A data reduction plan is being developed at the Center for Microgravity and Materials Research (CMMR) to efficiently process residual acceleration data recorded in orbiting space laboratories. Implementation of the plan will enable principal investigators to create a user specific accelerometer data base that can be readily employed during post-flight analysis of their experimental results. Another important use of the data reduction plan is the characterization of the acceleration environment of orbiters. Knowledge of the low-gravity environment of an orbiter and of the effects of that environment on experiments will help investigators plan future experiments to best exploit the low-gravity conditions of space.

Various aspects of orbiter characterization are discussed in the next section. The creation of a limited residual acceleration data base and analysis of low-gravity experimental results are discussed in the section on Post-flight Analysis of Experiments. Results of analysis of accelerometer data collected during the Spacelab 3 (SL3) mission are presented in the Analysis of Residual Acceleration Data section.

ORBITER CHARACTERIZATION

A data reduction plan such as that being developed at the CMMR can be used for general orbiter characterization purposes. Features of residual acceleration data that can be utilized for the characterization of an orbiter are the time history of the data (maximum values, mean values, and particular disturbance patterns), the frequency components present in a given window of data, and the orientation of the acceleration vector during some given time period.

There are numerous other pieces of information that are needed to complete the residual acceleration characterization of an orbiter. An important aspect of the characterization process is a thorough understanding of the recording system and data collection scheme being used. Initial processing of accelerometer data requires information on the noise floor of the instruments, instrument biases, and

some insight from investigators into what data format is acceptable. Standardized output format from various systems and cataloging of recorded accelerometer data is ideal, but has not been seen to date.

Specific characterization missions should be planned during which various equipment and experiments are activated and the start and end times noted for comparison to accelerometer data records. Standardized timing of experiments and operational activities is required for such testing as well as for general missions. For both characterization missions and experiment payload missions, complete "as-flown" timelines are a necessity. Without consistent notation of operations, correlation of possible sources with recorded accelerations is difficult.

A potentially useful step in the characterization process is the use of accelerometer arrays on orbiter missions. Past missions have included several different accelerometer systems, designed to span the broad amplitude-frequency range of expected residual accelerations. While the data obtained from these systems are useful, an array of identical systems located throughout an orbiter during a mission would enhance the characterization process considerably and result in more data which can be used in the planning of future experiment-oriented missions.

POST-FLIGHT ANALYSIS OF EXPERIMENTS

In addition to orbiter characterization, an important aspect of the data reduction plan is the ability of investigators to create useful, manageable data bases that can be used in the post-flight analysis of experimental results. In general, the three main features of an acceleration disturbance (magnitude, frequency, and orientation) are of interest to investigators. The acceleration magnitude, in particular, can be used to limit the amount of data an investigator needs to access for analysis of a specific experiment. For investigators who have prior knowledge of the acceleration tolerance of their experiments, a relatively simple peak detection routine can be used to identify accelerations to which their experiments are sensitive. Windows containing such disturbances can be cut from the surrounding data to form a new data base for further investigations. A limited data base can also be created by selecting windows of data during times corresponding to unexpected experimental results. Subsequent analysis may involve the computation of various acceleration statistics, investigation of the variation of acceleration vector orientation, and evaluation of the frequency components present in the record.

After potentially intolerable accelerations have been identified, or after obvious deviations from expected experiment results are seen, an attempt can be made to correlate acceleration events with experimental observations. Cross-correlation or group delay schemes can be used to identify time lags between acceleration events and experiment perturbations /1/, /2/. Such tests, and subsidiary modelling of experiments, can be used to identify whether transient or oscillatory accelerations, or both, tend to affect experiments. Results can be used to determine whether some reorientation or relocation of an experiment within the orbiter and/or changes in the experiment parameters would make it less susceptible to expected accelerations on future missions or whether certain experiment classes are too sensitive to residual accelerations to be flown in a specific orbiter.

ANALYSIS OF RESIDUAL ACCELERATION DATA

The goal of the accelerometer data reduction project at the CMMR is to determine what useful information can be obtained from the massive data bases resulting from typical missions. Up to 2 Gbytes of raw accelerometer data are expected per mission from the NASA Space Acceleration Measurement System (SAMS). If investigators are able to readily identify limited data windows of interest to them, they will be more apt to work with residual acceleration data in the analysis of their experiments. Our reduction scheme has been developed while working with accelerometer data collected during the SL3 mission /3/. To date, approximately 3.5×10^6 samples of SL3 data have been accessed for testing of the data reduction plan. In addition, the ensuing analysis of the SL3 data is a much needed step towards the characterization of the orbiter Columbia. Early work towards this goal has been reported in the literature /4/, /5/, /6/.

The initial step of our data reduction plan is the identification of accelerations that exceed specified tolerance limits. A peak detection routine tests the magnitude of the residual acceleration vector at each time mark against limits obtained from modelling of crystal growth from solution /7/. Windows containing excessively large acceleration events as well as windows of "background" signals are

processed further. Fourier analysis is used to identify the frequency components of the accelerations and direction cosines are calculated to obtain information about the variation of the residual acceleration vector with time. A secondary peak detection routine is used to test the magnitude of the frequency components of acceleration windows against frequency domain tolerance limits. See /3/ for more detail about the analysis procedure.

The results of our research to date can be summarized as follows. Transient accelerations can be caused by activities as diverse as thruster firings and the opening of cabinets. Such accelerations can have magnitudes as large as 2.5×10^{-2}g with frequency components (from 4.5×10^{-3} to 50 Hz) no greater than 1×10^{-3}g, see Figures 1 and 2 /3/. These disturbances are rarely sustained for more than a fraction of a second and fluctuate rapidly in orientation. While recorded SL3 acceleration values often exceed a tolerance limit of 4×10^{-3}g, frequency domain tolerance limits for frequencies up to 150 Hz are never exceeded. The identification of steady state and very low frequency ($<10^{-3}$ Hz) components of acceleration was impossible for the SL3 accelerometer data because of the presence of low magnitude accelerations and instrument noise. Even with a thorough knowledge of the accelerometer noise basement, the dynamic environment of an active orbiting space laboratory and limitations of recording systems may preclude the identification of very low frequency components.

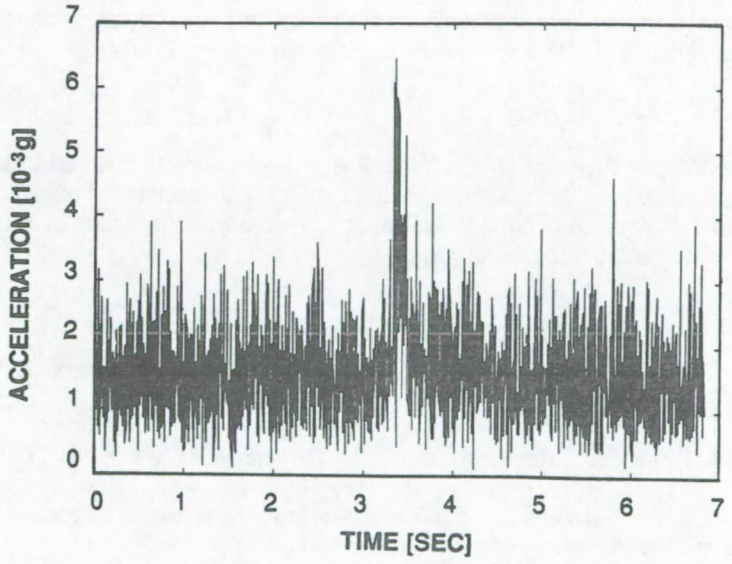

Fig. 1. Transient acceleration recorded on Spacelab 3. Source is identified as crew activity within the spacelab /3/.

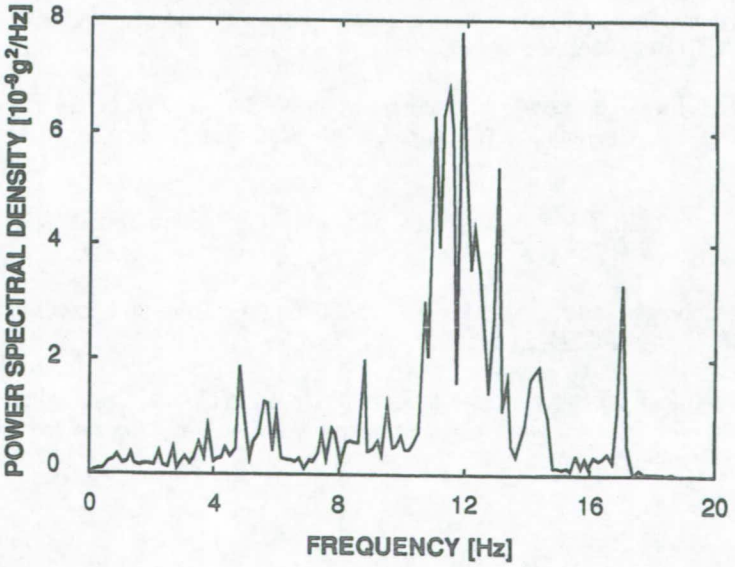

Fig. 2. Power spectral density of acceleration window in Figure 1. Note frequency components around 4-5 Hz and 7-9 Hz related to spacelab and orbiter structural modes, 11-12 Hz components possibly related to structural vibration after thruster firing, and 17 Hz component related to the KU band antenna dither /3/, /6/.

Characteristic frequency components and acceleration patterns related to some specific operational and crew activities have been identified, see Figure 2 /3/, /6/. Frequency modes at about 5 and 7 Hz are related to the spacelab structure and the orbiter structure. Both external (thrusters) and internal (crew activity, manipulation of experiments) forces excite these modes. A strong 17 Hz component appearing frequently in the data is related to the driving motor of the KU band antenna. Work with accelerometer data collected during missions in the near future (such as that to be collected with SAMS) is necessary before a more complete orbiter characterization can be obtained.

We are performing preliminary work towards the correlation of acceleration events to specific experimental results. Some qualitative correlation attempts are discussed in /4/ and /8/. We are currently evaluating several correlation techniques and anticipate testing these routines on synthetic data and SAMS data later this year. The results of such analyses in conjunction with experiment modelling will help determine the suitability of experiments for the low-gravity conditions in an orbiter.

CONCLUSIONS

A general data reduction plan is being developed to allow efficient processing of residual acceleration data. Implementation of the plan will enable investigators to create user specific data bases that can be employed during post-flight analysis of experimental results. The plan will also be useful in the characterization of the low-gravity environment of orbiting space laboratories. The results of characterizations as well as correlation and experimental analyses should provide information on preferred locations and orientations of experiments within orbiting laboratories and information on whether certain experiments are too sensitive to residual accelerations to be flown in specific orbiters.

ACKNOWLEDGEMENTS

This work was supported by NASA grant NAG8-759. The authors would like to thank Gary Martin of NASA for his encouragement during this project. Our interpretation of acceleration signals has benefited from discussions with Ed Bergmann of the C. S. Draper Laboratory. We would like to thank Franz Rosenberger for his careful reading of the manuscript.

REFERENCES

1. J. S. Bendat and A. G. Piersol, *Measurement and Analysis of Random Data*, John Wiley and Sons, New York, 1966.

2. E. J. Hannan and P. J. Thomson, Estimating group delay, *Biometrika* 60, # 2, 241 (1973).

3. M. J. B. Rogers and J. I. D. Alexander, Analysis of Spacelab-3 Residual Acceleration Data Using a Prototype Data Reduction Plan, *J. Spacecraft and Rockets*, submitted (1990).

4. G. Arnett, Spacelab-3 Low-g Accelerometer Data from the Fluid Experiments System (FES), in: *Proceedings of Measurement and Characterization of the Acceleration Environment On Board the Space Station*, Guntersville, Alabama 1986, Section 11.

5. R. P. Chassay and A. Schwaniger, Low-g Measurements by NASA, in: *Proceedings of Measurement and Characterization of the Acceleration Environment On Board the Space Station*, Guntersville, Alabama 1986, Section 9.

6. H. Hamacher and U. Merbold, Microgravity Environment of the Material Science Double Rack on Spacelab-1, *J. Spacecraft* 24, # 3, 264 (1987).

7. A. Nadarajah, F. Rosenberger and J. I. D. Alexander, Modeling the Solution Growth of TGS Crystals in Low Gravity, *J. Crystal Growth* 104, 218 (1990).

8. J. Trolinger, R. Lal and R. Ruff, Acceleration Effects Observed in Optical Data Taken in Spacelab 3 FES, in: *Proceedings of Measurement and Characterization of the Acceleration Environment On Board the Space Station*, Guntersville, Alabama 1986, Section 6.

Authors run-on-prints of the journal

MICRO GRAVITY SCIENCE AND TECHNOLOGY

International Journal for Microgravity Research and Applications

M. J. B. Rogers and J. I. D. Alexander

Residual Acceleration Data Analysis for Spacelab Missions

Materials processing and life sciences experiments are being conducted in earth orbiting laboratories to take advantage of the reduced gravity environment of space. Accelerometer data are collected during low-g missions to describe the acceleration environment, but the amount collected per mission is overwhelming (on the order of gigabytes). Different research goals, sensor types, and processing techniques make it difficult to compare acceleration data plots from different missions. In particular, spectral representations of data differ widely. Specific structural modes are known for the orbiter and Spacelab from engineering models and ground tests, but a complete characterization of primary and secondary acceleration sources has not yet been compiled.

We have developed a two level reduction plan that will allow investigators to create limited, user specific accelerometer data bases that can be used in post-flight experiment analysis and orbiter characterization. First level processing uses our knowledge of experiment sensitivity to identify times when tolerable acceleration levels are exceeded. Together with a preliminary analysis of experiment results, this enables the experimenter to identify particular time intervals which require more detailed processing. Second level analysis centers on acceleration time histories (magnitude and orientation) and frequency components. Data decimation is introduced as a means for reducing the amount of data that must be processed while analyzing a given time window. Cross-correlation analysis is discussed; it is useful in post-flight experiment analysis for assessing causal relationships between residual accelerations and experimental responses. The ability to identify and process limited windows of acceleration data will further the acceleration environment characterization process and will be essential in revising the design, location, and use of low-gravity experiment equipment for future missions.

1 Introduction

In recent years, low-gravity experimenters have shown increased interest in obtaining residual acceleration data to use in pre-flight modelling and post-flight processing of their experiments. The object of many low-gravity materials processing and life sciences experiments is to study physical and biological phenomena in space under drastically reduced acceleration conditions relative to the steady 9.8 ms^{-2} (1 g) acceleration experienced on the earth's surface. Because some of these experiments are sensitive to even small magnitude accelerations [1–5], it is necessary to characterize the time-dependent acceleration environment in order to properly interpret the experimental results. To date, one of the major factors that have prevented investigators from accessing residual acceleration data for post-flight experiment analysis and orbiter characterization is the vast amount of data that results from a typical orbiter mission. Even for a sampling rate as low as 12.5 Hz, on the order of 10^6 samples per axis can be expected from a seven day low-gravity mission.

In the following section, we discuss residual acceleration measurements that have been reported in the literature and suggest reasons for the differences in magnitude among the various data bases. In sect. 3, we introduce various aspects of the orbiter characterization process and in sect. 4 we present several specific techniques that investigators can use in the post-flight processing of residual acceleration data and experimental results.

2 Residual Acceleration Data

Measurements of residual acceleration have been collected during several orbiter missions with a variety of instruments [6–13]. The resulting data, supplemented by the simulation of orbiter attitude motion accelerations, have provided us with a general idea of the low-gravity environment aboard an orbiter during a typical mission. Specific acceleration sources, however, are still difficult to characterize. In general, three categories of residual accelerations are experienced in orbiting space laboratories: quasi-steady, transient, and oscillatory [9, 14]. The quasi-steady accelerations are related to the earth's gravity gradient, spacecraft attitude and altitude, and atmospheric drag. They have frequencies on the order of the orbital frequency (10^{-4} Hz) and magnitudes in the 10^{-9}–$10^{-6}\,g$ range [9, 12, 14]. $10^{-6}\,g$ accelerations have been recorded using specialized accelerometer systems such as HiRAP [13], but these quasi-steady accelerations have yet to be successfully identified in data recorded with conventional systems because of instrument limitations and the relative strength of higher magnitude and higher frequency accelerations [15].

These higher magnitude, higher frequency accelerations constitute the other categories of residual accelerations. Transient accelerations can have magnitudes as large as $10^{-2}\,g$ and tend to vary considerably in orientation, but such disturbances are rarely sustained for more than a fraction of a second [11]. These accelerations can be caused

Mail address: Melissa J. B. Rogers, Center for Microgravity and Materials Research, University of Alabama in Huntsville, Huntsville, Alabama 35899, USA.

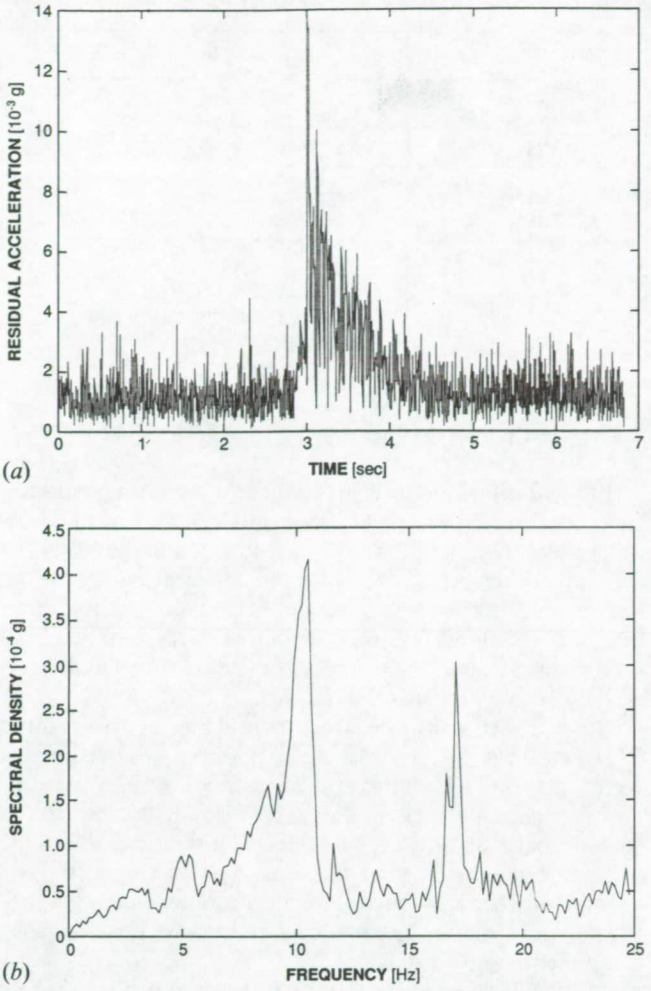

Fig. 1. Window of accelerometer data collected during the SL3 mission (Bell Miniature Electro-Static Accelerometer, $f_s = 300$ Hz, nominal 50 Hz lowpass filter). The disturbance was probably caused by a thruster firing or a local acceleration source within the Spacelab; (a) acceleration vector magnitude; (b) combined spectral density for the three recording axes. Note frequency components at 5, 12, and 17 Hz

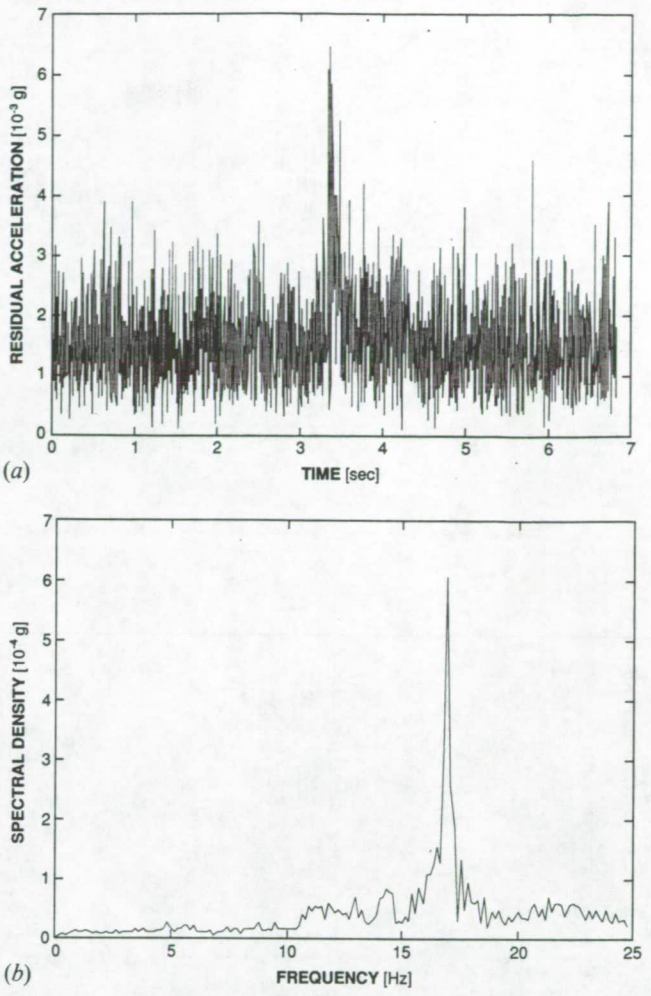

Fig. 2. Window of accelerometer data from SL3 probably caused by crew activity within the Spacelab; (a) acceleration vector magnitude; (b) combined spectral density for the three recording axes. Note the dominant 17 Hz component

by both crew related and operational activities (figs. 1 and 2). Oscillatory accelerations have magnitudes comparable to transient accelerations (10^{-5}–10^{-3} g), fluctuate rapidly in orientation, and are experienced over a broad range of frequencies for longer times. Recorded oscillatory accelerations are generally related to machinery vibrations and rotations and to structural modes of the orbiter excited by both transient and oscillatory sources. Frequency domain analysis of one second to fifteen minute long windows of *S*pace*l*ab *3* (SL3) acceleration data indicates that, from $5 \cdot 10^{-3}$–50 Hz, transient and oscillatory accelerations have amplitude spectra with maximum magnitudes no greater than 10^{-3} g, figs. 1b and 2b [11, 15].

When comparing acceleration measurements from different missions, it is important to note that few accelerometer systems have the same characteristics. Because of different research goals, sensor types, electronics, sampling rates, processing techniques, instrument locations, and other factors, comparisons among residual acceleration data plots presented in the literature are often difficult. The sampling rate, especially, can cause an appreciable magnitude difference among various sets of data [12]. Higher frequency data are constructively added to lower frequency data when high sampling rates are used. This results in overall higher magnitude readings than obtained with lower sampling rates. Similarly, analog filtering performed as part of the data collection scheme, as well as post-flight digital filtering, can result in different magnitude levels for different data sets (see fig. 3).

The use of different processing techniques results in a variety of data presentation styles that may initially appear comparable. Time history plots vary considerably, however, and may include plots of individual axes of data, acceleration vector magnitude, RMS values, and integrated data. In addition, the data presented may be regularly sampled data, peak value data, or some specialized form of data [6–12]. Representations of residual acceleration data as a function of frequency can also take a variety of forms [15–18]. Most

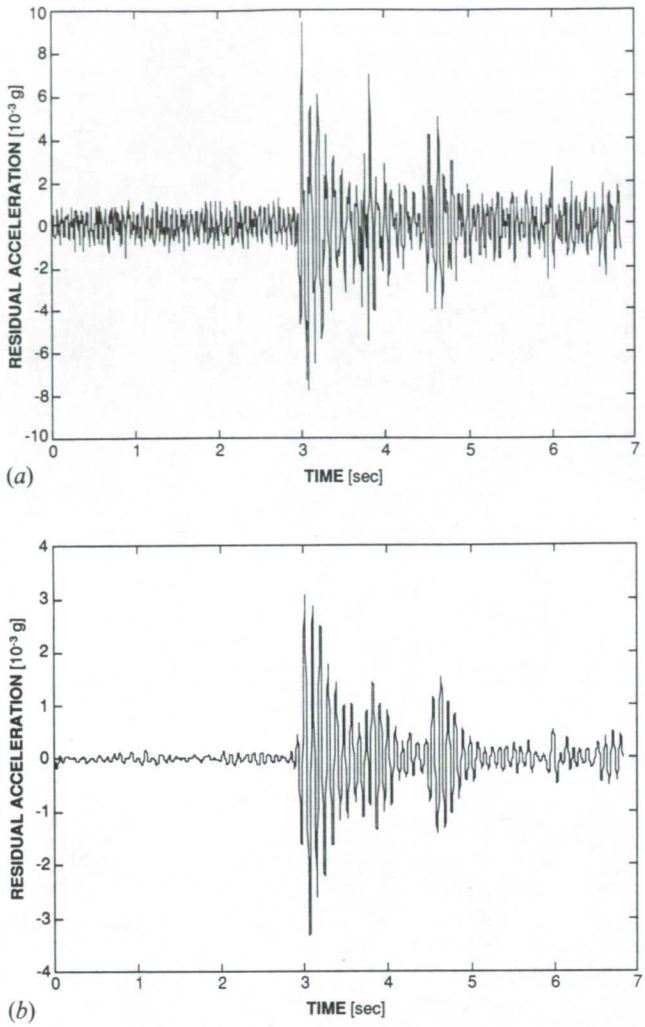

Fig. 3. Differences in magnitude level result from the use of different sampling rates and/or filter cut-offs; (a) window of SL3 accelerometer data (y-axis of fig. 1); (b) same data window with 13 Hz lowpass filter applied. Note difference in magnitude between two plots

common are the amplitude and power spectral densities (see sect. 4.2). If an investigator is only interested in the identification of dominant frequency components, then any type of spectrum is adequate. Meaningful comparisons of component magnitudes among various plots or between spectra and sensitivity plots, however, require a standardized spectral density format.

Instrument location is another important factor involved in comparative data analysis. Data collected near a dominant acceleration source (motors, fans, areas of high crew activity) will show higher overall acceleration levels than data collected with an equivalent system located at a distance from such sources. Some interest has been expressed by low-*g* investigators in evaluating the propagation of accelerations from known sources through various structures of an orbiter [19]. This is an important factor in orbiter characterization, and in the identification of especially noisy systems and appropriate sites for low-gravity experiments.

Table 1. Orbiter natural frequencies, after Cooke et al. [12]

natural frequency	*structure*
0.43 Hz	cargo bay doors
0.57 Hz	cargo bay doors
0.86 Hz	cargo bay doors
1.2 Hz	cargo bay doors
1.5 Hz	cargo bay doors
2.1 Hz	radiators
2.4 Hz	radiators
3.5 Hz	fuselage torsion wing and fin bending
5.2 Hz	fuselage first normal bending
7.4 Hz	fuselage first lateral bending

3 Orbiter Characterization

Limited attempts have been made to date to construct a characterization of the low-gravity environment of the shuttle orbiters [6–11, 15]. Specific structural modes are known for the orbiter and Spacelab from engineering modelling and ground testing (see table 1) [9, 12, 19, 20]. The excitation of these modes has been identified in residual acceleration data as associated with thruster firings and crew activity within the Spacelab [7, 9, 11, 12, 15].

Both orbiter and Spacelab structural modes exist around 5 Hz and 7 Hz [9, 12]. A 12 Hz component observed in the data represents an orbiter structural mode excited by shuttle operations [12]. A ubiquitous 17 Hz signal, present in accelerometer data recorded by different systems, represents another orbiter structural mode as well as the dither frequency of the KU band communications antenna [11]. Figs. 1 and 2 show the presence of these specific frequency components in SL3 data.

A difficulty that will continue to hamper orbiter characterization attempts is that no acceleration source acts alone. Orbiter maneuvers involve the firing of multiple thrusters in a sequence of pulses, and experiment manipulation involves the handling of various pieces of equipment. These transient acceleration sources occur in addition to the back-

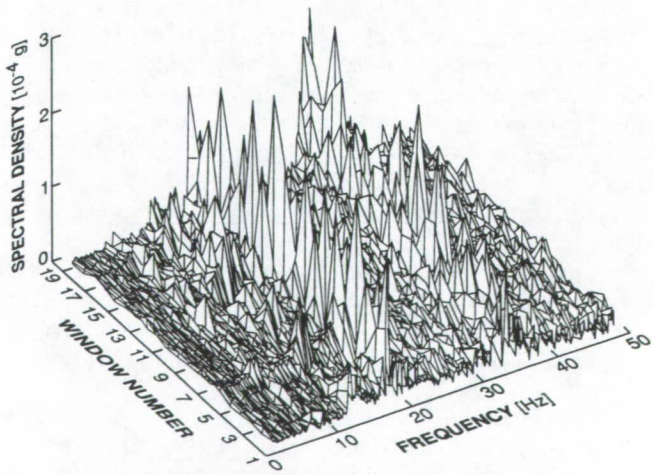

Fig. 4. Spectral densities of twenty successive SL3 time windows. Note varying strengths of 5 Hz, 12 Hz, 17 Hz, and 34 Hz components

ground accelerations related to numerous mechanical systems active during a mission. Fig. 4 shows the dynamic nature of the Spacelab environment. The spectral densities of twenty successive time windows are shown. It can be seen that, while there are dominant frequency components consistently present, the relative strengths of specific components vary over time.

The active environment of the orbiting laboratory does not mean, however, that the task of orbiter characterization is impossible. Through a sequence of ground-based and in-space tests of the response of specific structures to known acceleration sources, we can eventually construct a catalogue of characteristic accelerations and acceleration levels in particular areas of the space laboratory [19, 20]. A knowledge of the acceleration environment to be expected during a mission and of the acceleration levels expected in specific locations in an orbiter will allow the development and siting of future experiments to best utilize or avoid specific aspects of the low-gravity environment.

4 Post-flight Data Analysis

As stated earlier, one of the major obstacles encountered in the analysis of residual acceleration data is the amount of data resulting from a single mission. Gigabytes of accelerometer data are expected from most flights of the NASA *S*pace *A*cceleration *M*easurement *S*ystem (SAMS). In an attempt to effectively manage these data, we have developed an analysis plan that will allow principal investigators of low-gravity experiments to create limited, user specific data bases. The limited data base can be efficiently used in post-flight processing of experimental results. We are also analyzing various processing techniques that may be useful for more detailed residual acceleration data analysis. Two of these techniques, data decimation and cross-correlation analysis, are discussed later in this section.

4.1 Creation of Limited, User Specific Data Bases

In order to create user specific data bases, investigators must have some knowledge of the sensitivity of their experiments to the residual accelerations expected during flight. Such knowledge can be gained from pre-flight modelling of the experiment or from preliminary runs of the experiment in low-gravity conditions (drop-towers, sounding rockets, parabolic flights, orbital flights). Post-flight analysis of experimental results in conjunction with residual acceleration data will also be easier if appropriate experiment parameters are recorded during the experiment.

Our suggested approach to the reduction of residual acceleration data invokes a two level plan that uses sensitivity limits and preliminary experimental results. The plan is outlined in table 2. Pre-flight identification of acceleration sensitivity of a particular experiment will determine acceleration frequency and magnitude ranges of interest and experiment tolerance limits [1]. Particular times when the experiment is most likely to be affected by residual accelerations can also be identified prior to the mission. This includes increased experiment sensitivity during certain stages (e.g., protein crystal growth during the nucleation stage) and expected experiment response to certain timelined mission operations (e.g., thruster firings and crew exercise periods). Preliminary post-flight analysis of experimental results will allow the investigator to identify times when unexpected results occurred that may be related to perturbations in the residual acceleration environment of the laboratory.

Table 2. Outline of data reduction plan

Level One
1. Pre-flight identification of acceleration sensitivity to determine frequency and magnitude ranges of interest and experiment tolerance limits.
2. Pre-flight identification of times at which the experiment is liable to be most vulnerable, i.e., some experiments may be most sensitive at specific stages (e.g. protein crystal growth during the nucleation stage).
3. Preliminary post-flight analysis of experimental results to identify times when unexpected results occurred that may be related to perturbations in the residual acceleration environment of the laboratory.
Level Two
1. Selection of time windows of interest using a threshold detection routine based on sensitivities identified in Level One, Step 1 above.
2. Use of data decimation techniques, when appropriate, to reduce the number of data points needed to evaluate lengthy windows of data.
3. Specific analysis of windows of data identified in Level One and first step of Level Two, including estimation of mean and mean squared values, determination of the acceleration vector orientation, and spectral analysis to investigate the magnitude of the frequency components for the specific time window of interest.
4. Evaluation of accelerometer data in conjunction with experimental results to identify causal relationships and revise sensitivity limits.

The second level of the data reduction plan involves the actual limitation and processing of the residual acceleration data base using the results of level one. A simple threshold detection routine can be used to identify times when the acceleration magnitude is greater than defined sensitivity limits. Windows of interest can also be selected based on the experiment and mission timelines and preliminary post-flight analysis. Timelines will indicate when sensitive stages of an experiment are scheduled and when potentially intolerable mission events such as orbiter maneuvers are to occur.

4.2 General Processing Techniques

We have found that three main features of residual acceleration data can be used to characterize the acceleration environment of an orbiting space laboratory: the magnitude, direction, and frequency components of the residual accelerations in a given window. Time history information can be used to identify maximum and mean accelerations recorded per axis as well as various other statistics. The

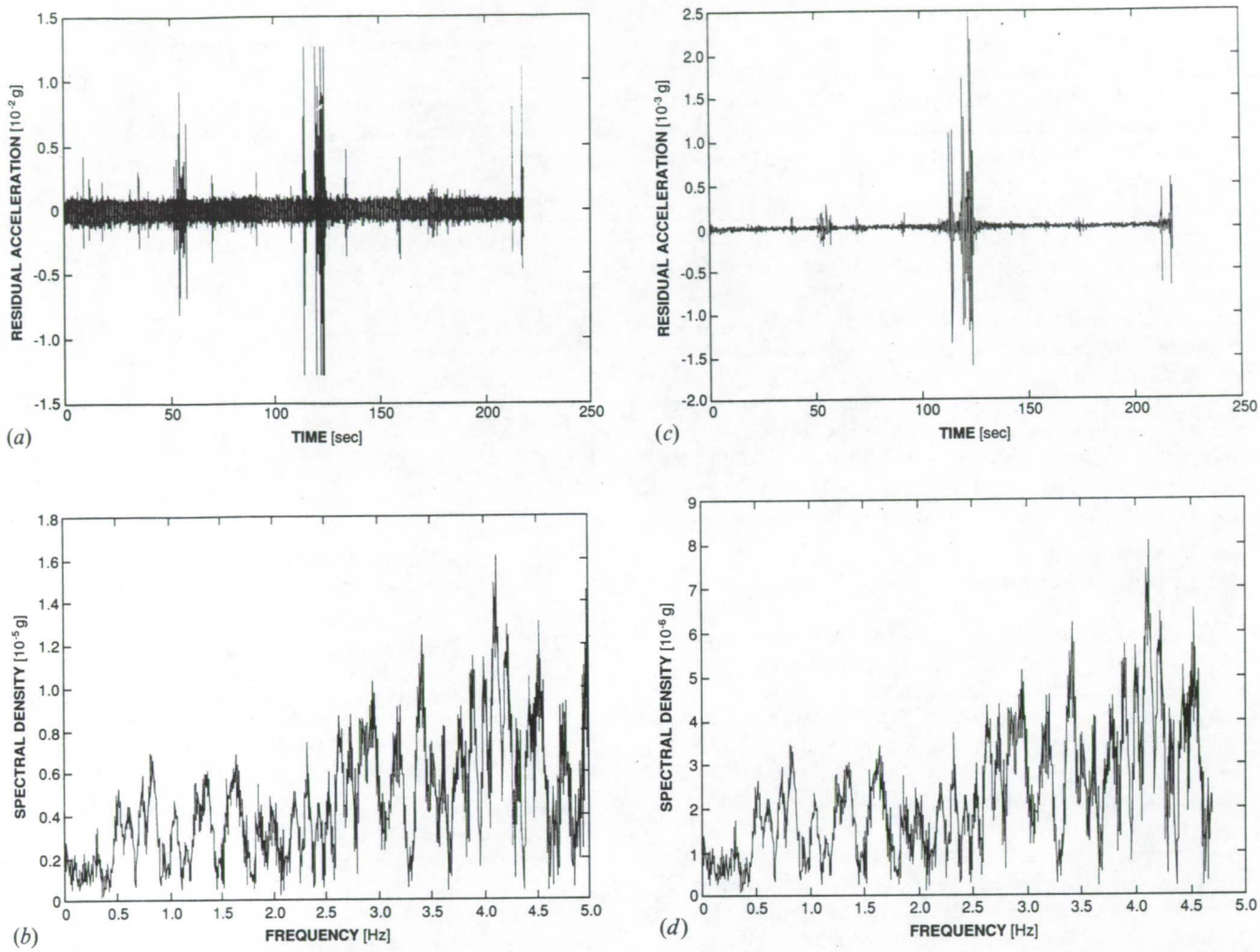

Fig. 5. Example of data decimation; (a) original SL3 time series of 65,536 points (218 s); (b) spectral density of (a); (c) time series decimated 16 times – 5 Hz lowpass filter applied; (d) spectral density of (c). Note decrease in magnitude from original series to decimated series

orientation of a residual acceleration vector can be estimated using direction cosines which give an indication of the angle between a measured acceleration and the recording axis. Because of the number of acceleration sources present in the orbiter and the nature of oscillatory accelerations, the orientation of the residual acceleration vector tends to fluctuate with time [11]. See [16] for more details about evaluating residual acceleration magnitudes, orientations, and frequency components.

The frequency components of a window of residual acceleration data are computed using the Fourier transform. The spectral density obtained for a time series using Fourier analysis indicates the frequencies of the sine and cosine terms that make up the signal being studied. The spectral density of an axis of residual acceleration data a_λ is:

$$A_n = \frac{1}{N} \sum_{\lambda=1}^{N} a_\lambda \, e^{-i2\pi n\lambda/N} \qquad (1)$$

where N is the number of points in the data window.

For the time period considered, the spectral density at a given frequency is an average of the components of a_λ that have that frequency and has the dimensions of an acceleration [16–18].

The power spectral density of a window of data can be computed by:

$$P_n = 2TA_n^2 \qquad (2)$$

where T is the length of the data window in time units.

The power spectral density has dimensions of [(units of original data)^2/Hz] and indicates the power or energy present in the series per unit frequency interval. The square root of the area under the power spectral density plot for a given frequency interval represents the RMS value of the input time series in that frequency range [12, 16, 17].

Comparisons of spectral plots in the literature may be difficult because of differences in software involving scaling factors and definitions of spectra [17, 18]. The two spectra discussed above are generally referred to as densities because they refer to a unit frequency interval. The use of a particular spectral representation often depends on the type of numerical analysis an investigator has planned. Because of the rather straightforward representation provided by eq.

(1), we advocate the use of this form. This spectrum gives frequency component magnitudes in units of acceleration. Most experiment sensitivity curves published to date are in the form of acceleration versus frequency, allowing ease of the comparison for the time periods concerned [1]. In addition, the spectral density of eq. (1) can be mathematically converted to a power spectral density by eq. (2).

4.3 Data Decimation

Because of the high sampling rates used in the collection of residual acceleration data, detailed analysis is often limited to a minute or less of data. If an investigator is interested in processing long blocks of data (more than several minutes for sampling frequencies on the order of 100 Hz), an additional tool that can be used to limit data is data decimation, which reduces the sampling rate [18, 21–23]. Like any other data processing technique, some amount of caution must be practiced when decimating data, especially so that higher frequency data are not aliased into the lower frequency region of interest.

Fig. 5 gives an example of data decimation applied to a window of SL3 accelerometer data. The original time series (fig. 5a) is 65,536 points long and has a maximum value of $1.28 \cdot 10^{-2}\,g$. The spectral density of this series out to 5 Hz is shown in fig. 5b. Fig. 5c shows the same window after the data were decimated 16 times; a 5 Hz lowpass filter was applied. This process reduced the number of points to 4,096, while maintaining the temporal coverage of 218 s. Note, however, that the maximum acceleration level represented has decreased to $2.5 \cdot 10^{-3}\,g$. This occurs because the user has no control over data point selection – the sampling is periodic and the original extrema are not necessarily selected. The values of the spectral density of the decimated data are also decreased compared to the original spectrum. The general character of the data is maintained in both the time and frequency domains, so the impact of the decreased magnitudes on the post-flight analysis of accelerometer data depends on the specific needs of the investigator.

4.4 Cross-correlation Analysis

We are interested in analyzing the results of experiments run in a low-g environment. Cross-correlation techniques are generally used to determine the equivalence of time histories and to determine temporal relationships among time series. This appears to be, for specific experiment classes, a viable means of assessing causal relationships between residual accelerations and experimental responses to these accelerations. This analysis method is useful not only in situations where experiments are sensitive to high magnitude, transient accelerations, but also when experiments are most sensitive to oscillatory disturbances [24].

The cross-correlation of two time series can be written as:

$$\phi_{12}(\tau) = \int_{-\tau}^{\tau} f_1(t) f_2(t+\tau)\,\mathrm{d}t \qquad (3)$$

where f_1 and f_2 are two zero-mean series and τ is a time lag.

A normalized cross-correlation function is used when the time series considered are of different dimensions and/or comparisons are to be made among different sets of results. The normalized cross-correlation function is [17]:

$$\varrho_{12}(\tau) = \frac{\phi_{12}(\tau)}{[\phi_{11}(0)\phi_{22}(0)]^{1/2}}. \qquad (4)$$

The maximum value of the normalized cross-correlation function is unity, which indicates that the two time series considered are identical at the given lag; values close to zero indicate that there is very little similarity between the two series. Positive normalized cross-correlation values close to unity indicate good correlation and negative values with magnitudes close to unity indicate good correlation but with the series out of phase.

While the cross-correlation function between two time series can be estimated directly using eqs. (3) and (4), it can be estimated more efficiently by calculation of the cross-power spectrum:

$$\Phi_{12}(\omega) = F_1^*(\omega) F_2(\omega) \qquad (5)$$

where F_1 and F_2 are the spectral densities of f_1 and f_2 and a superscript * denotes complex conjugation.

The cross-power spectrum and cross-correlation function form a Fourier transform pair, so one can be easily obtained from the other. Estimation of the cross-correlation function of two series using the cross-power spectrum affords a factor of $N/4p$ savings of computation time where $N = 2^p$ is the length of the time series considered [22].

The application of cross-correlation techniques to the analysis of low-gravity experiments requires an experiment time history which represents parameters affected by variations of the low-gravity environment. Pre-flight modelling of experiments will enable the investigator to identify appropriate parameters to record. In the case that such a parameter cannot be recorded quantitatively, modelling may also be used to determine typical experiment responses to be used in the creation of experiment time series for cross-correlation analysis [1–5, 24].

5 Summary

Investigators running experiments in the reduced gravity conditions of space need to be able to characterize the time-dependent acceleration environment in order to properly interpret their results. Characterization of the orbiter acceleration environment to date has identified some orbiter and Spacelab structural modes (table 1 and figs. 1–4) [9, 12, 19, 20].

Because the amount of accelerometer data resulting from a typical Spacelab mission is on the order of gigabytes, we have introduced a data reduction and analysis plan with which investigators can merge pertinent segments of residual acceleration data into the post-flight analysis of their experiments. The two level data reduction plan is easily tailored to an investigator's needs based on mission and experiment timelines and information about the experiment sensitivity to accelerations. The first level of the plan involves identification of pertinent experiment time windows to study and the second level involves analysis of these windows. General data processing techniques that can be

used include the analysis of time history statistics, acceleration vector magnitudes, and the orientation of the acceleration vector with respect to a set of coordinate axes. Analysis of frequency components can be achieved through spectral analysis, but we urge that caution should be practiced when comparing different spectral representations (figs. 1–4).

Data decimation can be used to limit the amount of data an investigator should process for post-flight experiment analysis. The reduced acceleration levels resulting from decimation may restrict the usefulness of this technique, depending on the specific needs of the investigator. Cross-correlation analysis is a viable means of assessing causal relationships between residual accelerations and experimental response to accelerations. This method is useful for experiments sensitive to transient accelerations and to oscillatory disturbances.

As we increase our understanding of the acceleration environment of orbiting space laboratories, we will be better able to design and locate low-g experiments to obtain the best results possible. Most experiment sensitivity limits used at present are derived from numerical modelling or order of magnitude estimates. With a knowledge of low-g experiment results and the environment in which these results were obtained, we can revise tolerance limits, identify "normal" acceleration levels, and decrease further the amount of accelerometer data that must be accessed by investigators after future missions.

Acknowledgements

This work was supported by the National Aeronautics and Space Administration through grant NAG8-759. We would like to thank G. Martin, R. Snyder, and C. Baugher for their interest in and support of this project. We would also like to thank L. Carver for graphics support and two anonymous reviewers for their valuable comments.

References

1 *Alexander, J. I. D.:* Low-gravity Experiment Sensitivity to Residual Acceleration: A Review, Microgravity Sci. Technol. 3 (1990), 52.
2 *Alexander, J. I. D., Ouazzani, J., Rosenberger, F.:* Analysis of the Low Gravity Tolerance of Bridgman-Stockbarger Crystal Growth. I. Steady and Impulse Accelerations, J. Crystal Growth 97 (1989), 285.
3 *Alexander, J. I. D., Amiroudine, S., Ouazzani, J., Rosenberger, F.:* Analysis of the Low Gravity Tolerance of the Bridgman-Stockbarger Crystal Growth. II. Transient and Periodic Accelerations, to appear J. Crystal Growth 113 (1991), 21.
4 *Monti, R., Favier, J. J., Langbein, D.:* Influence of Residual Accelerations on Fluid Physics and Materials Science Experiments, in Fluid Sciences and Materials Science in Space, A European Perspective, ed. H. U. Walter (Springer, Berlin, 1987), p. 637.
5 *Nadarajah, A., Rosenberger, F., Alexander, J. I. D.:* Modelling the Solution Growth of Triglycine Sulfate in Low Gravity, J. Crystal Growth 104 (1990), 218.
6 *Chassay, R. P., Schwaniger, A.:* Low-g Measurements by NASA, Proc. Measurement and Characterization of the Acceleration Environment On Board the Space Station, Guntersville, Alabama (Teledyne Brown Engineering, 1986), Section 9.
7 *Hamacher, H., Merbold, U., Jilg, R.:* Analysis of Microgravity Measurements Performed During D1, Proc. Norderney Symposium on Scientific Results of the German Spacelab Mission D1, Norderney, Germany (BMFT, 1986), 48.
8 *Trappen, N., Demond, F. J.:* Post Flight Accelerometer Data Evaluation, Proc. Norderney Symposium on Scientific Results of the German Spacelab Mission D1, Norderney, Germany (BMFT, 1986), 43.
9 *Hamacher, H., Merbold, U.:* Microgravity Environment of the Material Science Double Rack on Spacelab-1, J. Spacecraft 24 (1987), 264.
10 *Schoess, J.:* Honeywell In-Space Accelerometer STS-32 Final Report, Honeywell, 1990.
11 *Rogers, M. J. B., Alexander, J. I. D.:* Analysis of Spacelab-3 Residual Acceleration Data, J. Spacecraft and Rockets, in print.
12 *Cooke, C., Koenig, M., Lepanto, J., Levine, G., Miller, J., Sargent, D., Schlundt, R.:* SDI Space Shuttle Based Experiments for Acquisition, Tracking, and Pointing – Definition of Space Shuttle Operational Environment, The Charles Stark Draper Laboratory, Cambridge, Massachusetts, R-1868, 1986.
13 *Blanchard, R. C., Hinson, E. W., Nicholson, J. Y.:* Shuttle High Resolution Accelerometer Package Experiment Results: Atmospheric Density Measurements Between 60 and 160 km, J. Spacecraft 26 (1989), 173.
14 *Alexander, J. I. D., Lundquist, C. A.:* Motions in Fluids Caused by Microgravitational Acceleration and Their Modification by Relative Rotation, AIAA Journal 26 (1988), 34.
15 *Rogers, M. J. B., Alexander, J. I. D.:* A Strategy for Residual Acceleration Data Reduction and Dissemination, COSPAR Paper S.11.1.3, to appear Advances in Space Research 11 (1991), (7) 5.
16 *Rogers, M. J. B., Alexander, J. I. D., Synder, R. S.:* Analysis Techniques for Residual Acceleration Data, NASA TM-103507, July 1990.
17 *Båth, M.:* Spectral Analysis in Geophysics (Elsevier, Amsterdam, 1974).
18 *Karl, J. H.:* An Introduction to Digital Signal Processing (Academic Press, San Diego, 1989).
19 *Stavrinidis, C., Stark, H., Eilers, D., Hornung, E.:* Microgravity Quality Provided by Different Flight Opportunities, Microgravity Sci. Technol. 3 (1991), 191.
20 *Knabe, W., Eilers, D.:* Low-gravity Environment in Spacelab, Acta Astronautica 9 (1982), 187.
21 *Crochiere, R. E.:* Interpolation and Decimation, in: Programs for Digital Signal Processing, Digital Signal Processing Committee (ed.), IEEE Press (1979), Section 8.
22 *Bendat, J. S., Piersol, A. G.:* Random Data: Analysis and Measurement Procedures, 2nd ed. (John Wiley, New York, 1986).
23 *Otnes, R. K., Enochson, L.:* Applied Time Series Analysis, Volume 1: Basic Techniques (John Wiley, New York, 1978).
24 *Rogers, M. J. B., Alexander, J. I. D.:* Cross-correlation Analysis of On-orbit Residual Accelerations in Spacelab, Proc. 29th Aerospace Science Meeting, Reno, Nevada, 1991, AIAA Paper No. 91-0348.

Authors run-on-prints of the journal

MICRO GRAVITY SCIENCE AND TECHNOLOGY

International Journal for Microgravity Research and Applications

21 *Velten, R., Schwabe, D., Scharmann A.:* The periodic instability of thermocapillary convection in cylindrical liquid bridges, Phys. Fluids A, 3, 267–279 (1991)
22 *Smith, M. K.:* Instability mechanisms in dynamic thermocapillary liquid layers, Phys. Fluids, 29, 3182–3186 (1986)
23 *Rupp, R. Müller, G., Neumann, G.:* Three-dimensional time dependent modelling of the Marangoni convection in zone melting configurations for GaAs, J. Crystal Growth, 97, 34–41 (1989)

A93-32070

M. J. B. Rogers, J. I. D. Alexander, and J. Schoess

Detailed Analysis of Honeywell In-space Accelerometer Data – STS-32

The Honeywell In-Space Accelerometer system (HISA) collected data in the mid-deck area of the Shuttle Columbia during the flight of STS-32, January 1990. The resulting data were to be used to investigate the response of crystal microstructure to different types of residual acceleration. The HISA, using Sundstrand QA-2000 sensors, is designed to detect and record transient and oscillatory accelerations. The sampling and electronics package stored averaged accelerations over two sampling periods; two sampling rates were available: 1 Hz and 50 Hz. Analysis of the HISA data followed the CMMR Acceleration Data Processing Guide, considering in-house computer modelling of a float-zone indium crystal growth experiment. Characteristic examples of HISA data showing the response to the primary reaction control system (PRCS), Orbiter Maneuvering System (OMS) operations and crew treadmill activity are presented. Various orbiter structural modes are excited by these and other activities. Such modes are in the 1 Hz to 20 Hz range. Of particular note is the distinct frequency of crew footfalls during exercise periods and the resultant excitation of orbiter frequencies. Acceleration vector magnitudes ranged from 10^{-4} g to $>10^{-2}$ g. Acceleration values recorded at the crystal growth site exceeded time domain tolerance limits in approximately 35% of the data, especially during PRCS firings, OMS burns, and treadmill exercise. Frequency domain limits, however, were not exceeded.

1 Introduction

The *Honeywell In-Space Accelerometer* system (HISA) collected data on the mid-deck of the Space Shuttle *Columbia* during the flight of STS-32, January 1990. The HISA was part of the *Microgravity Disturbances Experiment* (MDE) which also included the *Rockwell Fluids Experiment Apparatus* (FEA). The FEA is a float-zone materials processing furnace; for this flight, it was used to grow single crystals of metallic indium. At various times during growth, acceleration sources were activated in order to investigate the response of crystal microstructure to different types of residual acceleration. The HISA acceleration measurements are presented and discussed herein.

In sect. 2 we outline the MDE location and HISA operation in the orbiter mid-deck. Sect. 3 discusses our processing plan, based on estimated acceleration sensitivities. In sect. 4 we present and discuss time history and frequency domain plots of segments of the HISA data. These data are compared to data from other missions in sect. 5 and suggestions are made for revisions of the HISA system before its further use in low-gravity environments.

2 Experiment Set-up

We present here a brief overview of the MDE; more detailed discussions can be found in *Schoess* [1] and *Dunbar* et al. [2]. During operation the MDE was mounted at locker MA9F in the aft mid-deck of *Columbia*. Crew members observed and videotaped the shape changes of the liquid indium zone. Post flight crystal characterization was planned to investigate crystallographic defects and impurity content; the experiment was designed to investigate the relationships between crystal quality and variations in acceleration level, growth rate, and zone stability [1].

The HISA, composed of three *Sundstrand QA-2000* sensors and an electronics package, is designed to detect and record transient and oscillatory accelerations. Table 1 lists HISA performance specifications. Data were recorded at both 1 Hz and 50 Hz sampling frequencies as averages of acceleration impulses over two sampling periods. They do not, therefore, represent instantaneous acceleration. The electronics package is such that positive and negative aver-

Table 1. HISA performance specifications, after Schoess [1]

parameter	performance
orientation	three-axis orthogonal
range	10^{-6} to 10^{-2} g at 1 Hz 10^{-5} to 10^{-2} g at 50 Hz
accuracy	$\pm(1\,\%\,\lvert\text{reading}\rvert + 0.00002)$ g
resolution	$<1.0 \times 10^{-6}$ g at 1 Hz 8.7×10^{-6} g at 50 Hz
frequency response ($\pm 5\,\%$)	0.025 to 19.500 Hz
DC bias	none (AC output)
sample data rate	50 Hz, 1 Hz
communications	RS-422/ASCII format
size	$20.3 \times 9.7 \times 5.3$ cm (1,046 cm^3)
mass	1.8 kg
power	5.6 W (28 V)

Mail address: Melissa J. B. Rogers, J. Iwan D. Alexander, Center for Microgravity and Materials Research, University of Alabama in Huntsville, Huntsville AL 35899, USA; Jeff Schoess, Honeywell Inc., Bloomington MN 55420, USA.

ages were recorded separately. This recording technique resulted in twelve data files for each time period studied: $\pm x$, $\pm y$, and $\pm z$ data for both the 1 Hz and 50 Hz sampling rates.

3 Data Analysis

The HISA data files were provided by the NASA *A*ccerleration *C*haracterization and *A*nalysis *P*roject (ACAP). The data were in tabular form with the averaged acceleration values and sensor temperatures listed for each time mark. The temperature variation recorded by the system was not enough to warrant temperature corrections to the data [3]. A problem with the recording hardware responsible for the switch between the two sampling rates caused spurious values to be recorded approximately once a second in the 50 Hz data. We tested three methods to resolve this problem: replacing the spurious points with zero, with a "not-a-number" marker, and with the same value as the preceding data point. The three techniques showed similar results, and we chose to use the zero replacement method.

Our approach to the analysis of the HISA data follows the Acceleration Data Processing Guide developed at the Center for Microgravity and Materials Research. This guide was developed to assist low-g experimenters interested in accelerometer data in determining their data access and processing needs based on their knowledge of experiment and acceleration sensor location and of experiment sensitivity to acceleration [4]. We assessed the sensitivity of the float-zone indium crystal growth experiment based on computer modelling of the experiment [5–6]. Table 2 lists the sensitivity limits used in our analysis.

Table 2. Sensitivity limits used in analysis, after Alexander and Zhang [6]

frequency and magnitude ranges of interest	$10^{-4}\,g$ for 10^{-2} to 0.1 Hz $10^{-3}\,g$ for 0.1 to 10 Hz
maximum tolerable acceleration (steady)	$10^{-6}\,g$
maximum tolerable acceleration (transient)	$10^{-3}\,g$

Typically, sensitivity limits are used to determine what segments of an acceleration data base to analyze in conjunction with experimental results. Sections of accelerometer data in which the sensitivity limits are exceeded are selected using a threshold detection routine. A relatively limited amount of accelerometer data was recorded by the HISA during STS-32 ($\sim$10 megabytes representing $\sim$5 discontinuous hours). Because of this, the entire data base was analyzed, with increased attention given to segments where the sensitivity limits were exceeded and where known acceleration sources were active.

A typical processing routine for residual acceleration data uses the basic techniques of time series and spectral analysis. These include calculating series statistics (mean, minimum, maximum, variance), plotting time histories of individual axes of data and vector magnitudes, and evaluating and plotting amplitude and power spectral densities to investigate the frequency components present and their relative strengths [4, 7–9].

As mentioned in sect. 2, the HISA data were digitized so that positive and negative averages were recorded separately. This recording technique necessitated some specialized analysis. Because we are generally more interested in the magnitude of the acceleration vector at a location than in the individual axial acceleration readings, we used the six data files from each sampling frequency to form the vector magnitude, that is $|\boldsymbol{a}| = \sqrt{(\pm a_x^2 + \pm a_y^2 + \pm a_z^2)}$, where $\boldsymbol{a} = (\pm a_x, \pm a_y, \pm a_z)$ represents the positive and negative averages of the accleration vector.

We transformed the HISA time histories into the frequency domain in a similar manner. Each of the six data files for each sampling rate was Fourier transformed to create the corresponding amplitude spectrum. To demonstrate that this technique is appropriate, we made a visual comparison of the spectra with spectra resulting from more standard data bases. For a more quantitative test, we processed data from the STS-40 flight of the *S*pace *A*cceleration *M*easurement *S*ystem (SAMS) to simulate the HISA sampling and averaging technique. The time and frequency domain magnitudes obtained with the resampled SAMS data were comparable to those obtained through our standard SAMS processing techniques.

The visual comparisons of the HISA results to other data bases and the SAMS simulated data show that the typical structural modes seen in orbiter accelerometer data were present in the HISA data. The lowest frequencies, unfortunately, are obscured to some extent by a remnant effect of the "$\pm$" digitization. The lowest frequency component resulting from a Fourier transformation of a time series is a representation of the mean value of the series. The "$\pm$" digitization of the HISA data creates an artificial non-zero mean that corrupts the mean represented in the corresponding spectrum. Because of this effect, we generally disregard the lowest spectral components calculated. For the shortest HISA data files (the various thruster firings), this results in a lower frequency limit of about 0.1 Hz.

4 HISA Data Plots

We present several characteristic examples from the HISA data base. Fig. 1 shows a time history and amplitude spectrum for 50 Hz data collected during a primary reaction control system firing. A high thrust pulse occurs about 5 s into the record, with possible lower magnitude thrusts occuring at about 45 and 90 s. The amplitude spectrum indicates that several orbiter structural modes are excited during this period, most notably in the 3, 5, 7, 10, and 13 Hz regions. The 17 Hz component, which is related to the Ku band antenna dither and a nearby orbiter structural mode, is excited. The lower magnitude, narrow band signals at 16 and 20 Hz are unusual, and at present their origin is uncertain. Early analysis of SAMS mid-deck data from STS-43, August 1991, suggests that the 20 Hz frequency may be a local, mid-deck structural or equipment-related excitation. Fig. 2 shows comparable plots for the 1 Hz data. Note that the amplitude spectrum plot can be used to

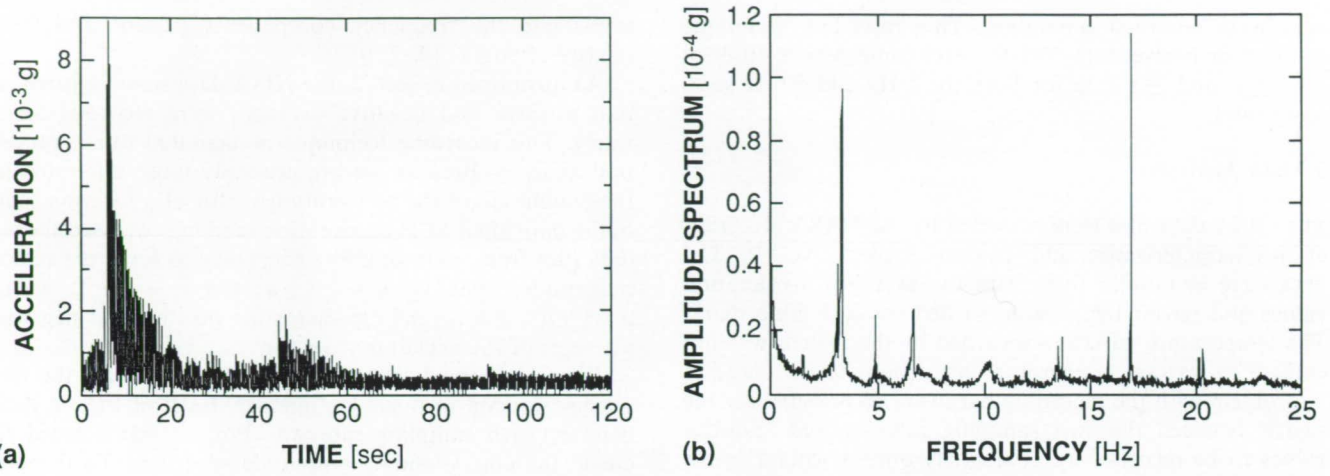

Fig. 1. Example of a primary reaction control system firing recorded by the HISA in the mid-deck of Columbia on STS-32, 50 Hz data, (a) acceleration vector magnitude, (b) combined amplitude spectrum

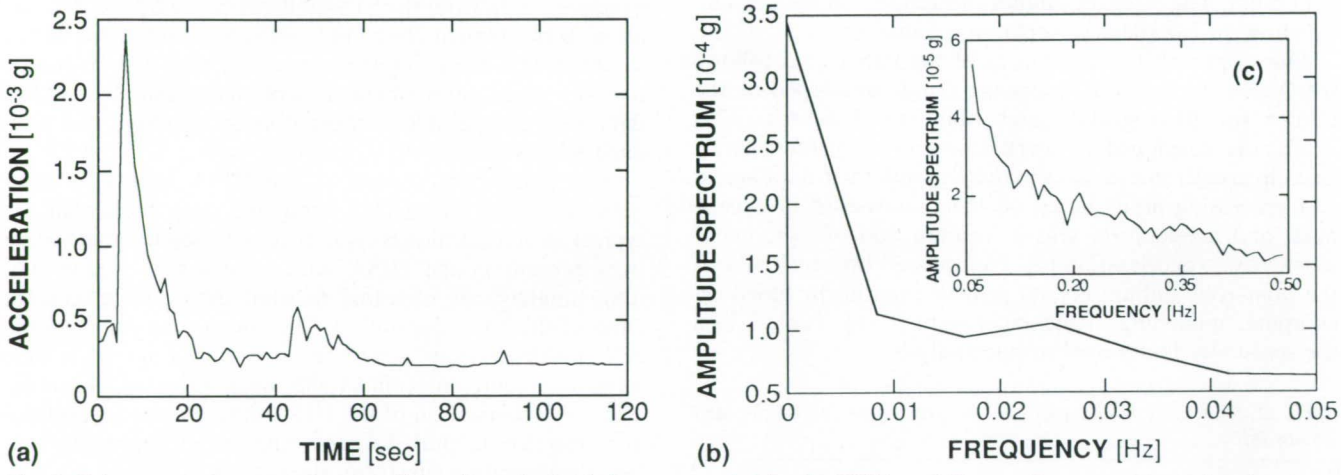

Fig. 2. Primary reaction control system firing shown in fig. 1, but as recorded by the HISA at 1 Hz sampling rate, (a) acceleration vector magnitude, (b) combined amplitude spectrum

supplement the lower frequency information obscured in fig. 1. Data recorded during an *O*rbiter *M*aneuvering *S*ystem (OMS) burn are shown in fig. 3. The burn produces a short pulse-like acceleration response at the mid-deck location of the HISA. Structural modes in the 3.5 and 7 Hz range are excited.

Figs. 4–6 show HISA data collected during a period of crew exercise on the mid-deck treadmill. The treadmill was located approximately 2 m from the HISA. Fig. 4 shows a 1 Hz data window, and corresponding amplitude spectrum, collected during a crew treadmill exercise period. Note the high and low magnitude segments related to different exercise intensities. Fig. 5 shows 50 Hz data collected during a running or jogging (high intensity) exercise phase. Fig. 6 shows a segment from a less intense exercise stage, such as a walking or cool down period. Note that the overall acceleration level of fig. 6 is lower in magnitude than that of fig. 5. The most interesting aspect of these plots is the difference in the amplitude spectra. The spectra alone could be used to identify that the crew member was exercising at different levels of intensity.

This is explained as follows. The higher magnitude (running) segments of the treadmill data are dominated by a 2.7 Hz component, fig. 5. This frequecy is related to an orbiter structural mode and is being driven by the footfalls of the crew member. In fig. 6, a slower exercise rate is represented (walking) and has a correspondingly lower frequency of footfalls. The 1.8 Hz component may be a higher harmonic of the 0.9 Hz component, or the two components may represent the crew member's upward and downward movements which differ in magnitude due to the treadmill restraint system. In this case, the 3.5 Hz structural mode is excited, possibly related to a doubling of the 1.8 Hz mode.

Because of the relatively small amount of data collected with the HISA during STS-32, we analyzed the entire data set, rather than limit the analysis based on sensitivity values given in table 2. Comparison of the HISA time histories to the limits in table 2 indicates that the transient time domain limit of $10^{-3}\,g$ was exceeded about 35 % of the time as recorded at 50 Hz and 39 % of the time at 1 Hz. The transient limit typically was exceeded during periods of

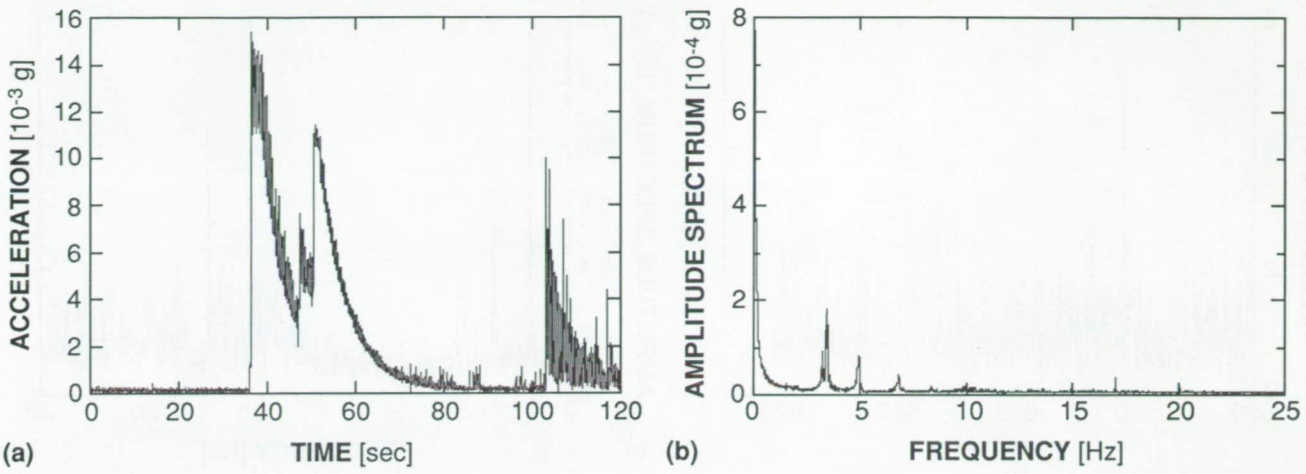

Fig. 3. Example of an orbiter maneuvering system firing recorded by the HISA in the mid-deck of Columbia on STS-32, 50 Hz data, (a) acceleration magnitude, (b) combined amplitude spectrum

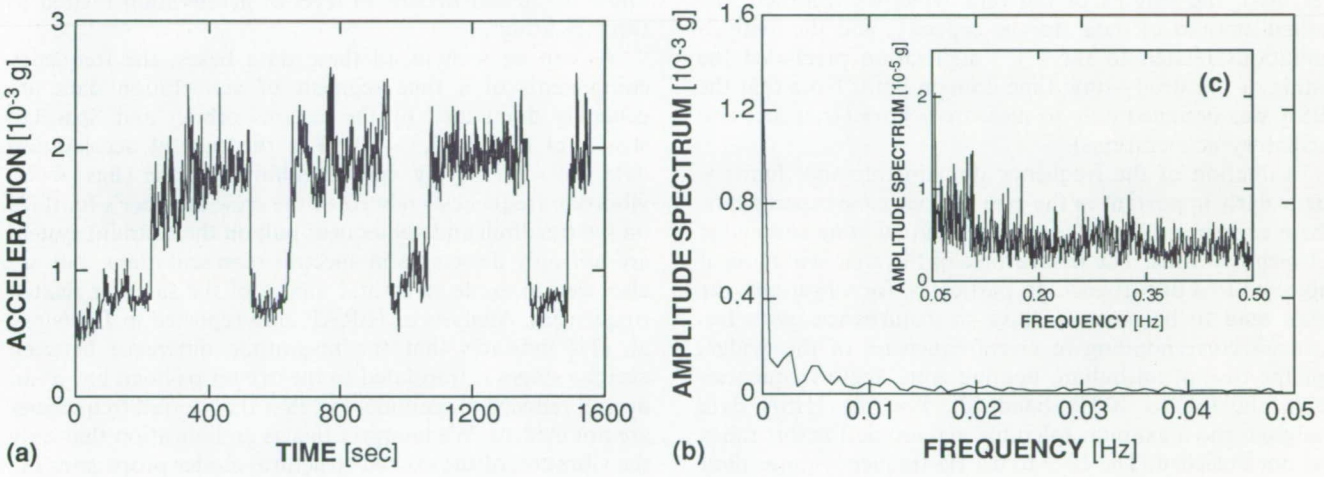

Fig. 4. Example of acceleration level during crew treadmill exercise period recorded by the HISA in the mid-deck of Columbia on STS-32, 1 Hz data. Note the different acceleration levels corresponding to different stages of the treadmill exercise protocol

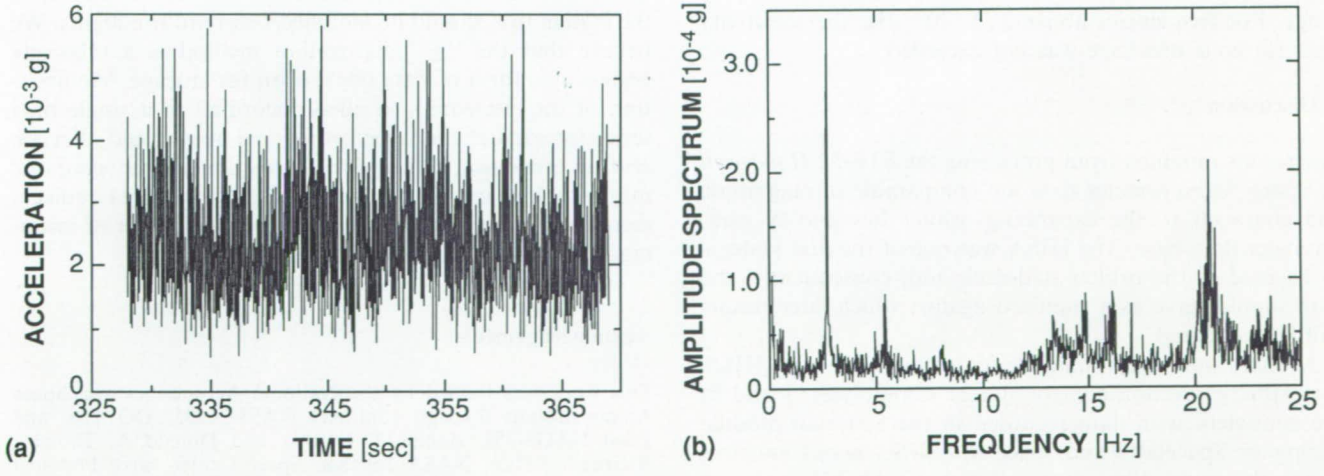

Fig. 5. Segment of 50 Hz data from higher magnitude section of fig. 3, (a) acceleration vector magnitude, (b) combined amplitude spectrum. Note the 2.7 Hz structural mode excited by footfall frequency

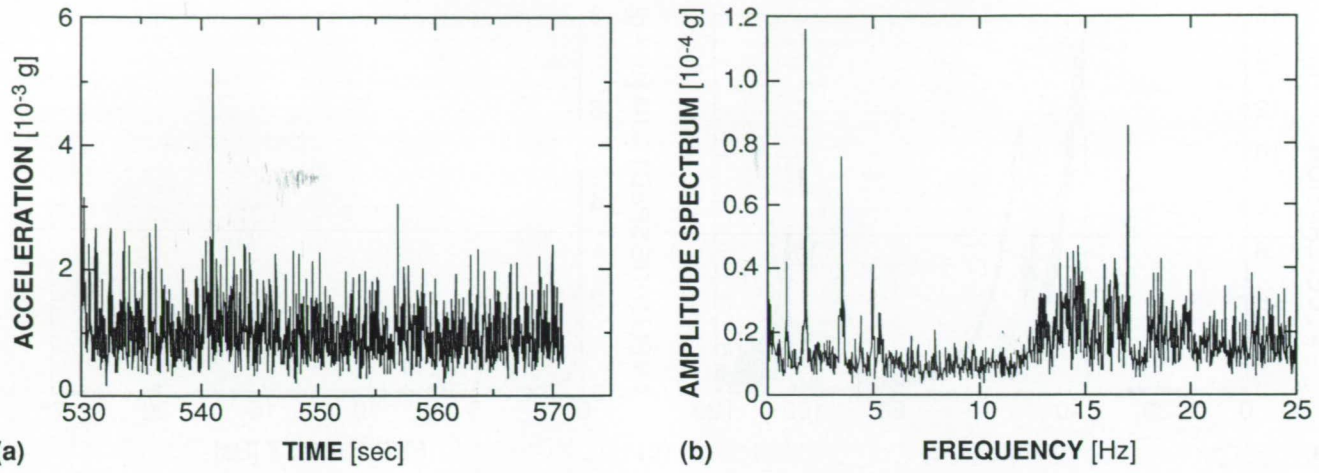

Fig. 6. Segment of 50 Hz lower magnitude section of fig. 3, (a) acceleration vector magnitude, (b) combined amplitude spectrum. Note the lower footfall frequency

crew exercise and orbiter maneuvers. The sampling frequencies used, the lengths of the time windows recorded, the limited amount of data storage capacity, and the analysis limitations related to the "$\pm$" digitization precluded the testing of the steady-state time domain limit. Note that the HISA was designed only to measure g-jitter (transient and oscillatory accelerations).

Evaluation of the frequency domain tolerance limits is particularly important in the case of float-zone experiments. These experiments involve a molten liquid zone suspended between two rods. The free surface of the zone will move if subjected to a disturbance. In particular, for vibrations, the zones tend to be most sensitive to disturbances with frequencies corresponding to eigenfrequencies of the bridge. For the case of an indium floating zone, these frequencies lie in the 0.1 to 10 Hz band [6]. For the HISA data analyzed, the maximum tolerable magnitude for this range was not exceeded. The 10^{-2} to 0.1 Hz frequency range limit in table 2 was not exceeded for segments of data during treadmill activity and quiet periods. The lowest frequencies of this range cannot be evaluated for the segments of thruster firings because the short time windows recorded impose a lower frequency analysis limit in the 10^{-2} Hz range. For frequencies above $2-3 \cdot 10^{-2}$ Hz, the sensitivity limit for zone breakage was not exceeded.

5 Discussion

The results obtained from processing the STS-32 *Honeywell* In-Space Accelerometer data are comparable in magnitude and character to the expanding orbiter low-gravity measurement data base. The HISA was one of the first systems to be used in the orbiter mid-deck and, consequently, the data should serve as a standard against which later results will be compared.

Acceleration vector magnitudes recorded by the HISA for primary reaction control system firings (figs. 1 and 2) are consistent with data recorded in the Spacelab module during the Spacelab 3 and Spacelab Life Sciences 1 missions and in the payload bay during STS-32 [7, 11, 12]. It should be noted, however, that in some cases the accelerations exceed the accelerometer maximum range, so we do not know the actual maximum level of acceleration related to thruster firings.

As can be seen in all these data bases, the frequency components of a time segment of acceleration data are generally dominated by the various orbiter and Spacelab structural modes [4, 7–10]. For the case of acceleration data collected during crew treadmill exercise (figs. 4–6), vibration frequencies related to the crew member's footfalls on the treadmill and subsequent pull on the restraint system are not only detectable in spectral representations, but are also seen to excite structural modes of the same or related frequencies. Analysis of HiRAP data reported in *Dunbar* et al. [11] indicates that the magnitude difference between exercise stages is translated to the orbiter payload bay at an overall reduced magnitude, but that the footfall frequencies are not evident. We interpret this as an indication that only the vibration of the excited structural modes propagates the distance 18 m between the treadmill and payload bay. The footfall source excites structures local to the mid-deck treadmill and HISA sensors.

Despite the fact that the HISA data are consistent with other data bases, we think that there are several aspects of the system that should be modified before future flights. We believe that the "$\pm$" digitization method is a relatively undesirable form of data conversion for storage. Modification of the electronics to allow recording of a single time series for each of the three orthogonal axes would alleviate several processing difficulties. Correction of the sampling rate switching problem would also obviate data replacement or filtering schemes and increase the number of meaningful data points available to the experimenter.

Acknowledgements

This work was funded by the National Aeronautics and Space Administration through contracts NAS8-36995, DO 126, and grant NAG8-759. Bonnie J. Dunbar and Donald A. Thomas, Astronaut Office, NASA Johnson Space Center, were Principal Investigators of the MDE. Dr. Dunbar was also Mission Specialist on STS-32 and was responsible for most of the MDE operations.

We would like to thank Charles R. Baugher, Marshall Space Flight Center, for providing us with the HISA data and funding for the processing and experiment modelling.

References

1 *Schoess, J. N.:* Honeywell In-Space Accelerometer STS-32 Final Report, Honeywell Technical Report, 1990
2 *Dunbar, B. J., Thomas, D. A., Schoess, J. N.:* The Microgravity Environment of the Space Shuttle Columbia Middeck During STS-32, NASA Technical Paper 3140, November 1991
3 *Schoess, J. N.:* Personal Communication
4 *Rogers, M. J. B., Alexander, J. I. D.:* Experimental Specific Processing of Residual Acceleration Data, 30th Aerospace Sciences Meeting, January 1992, AIAA Paper No. 92-0244
5 *Zhang, Y. Q., Alexander, J. I. D.:* Sensitivity of Liquid Bridges Subject to Axial Residual Acceleration, Phys. Fluids A 2 (1990) 1966–1974
6 *Alexander, J. I. D., Zhang, Y. Q.:* The Sensitivity of a Non-Isothermal Liquid Bridge to Residual Acceleration, in: Microgravity Fluid Mechanics, K. J. Rath (ed.), Springer Verlag, Berlin, 1992, 167–174.
7 *Rogers, M. J. B., Alexander, J. I. D.:* Analysis of Spacelab 3 Residual Acceleration Data, J. Spacecraft and Rockets 28 (1991) 707–712
8 *Rogers, M. J. B., Alexander, J. I. D., Snyder, R. S.:* Analysis Techniques for Residual Acceleration Data, NASA Technical Memorandum, NASA TM-103507, July 1990
9 *Rogers, M. J. B., Alexander, J. I. D.:* Cross-correlation Analysis of On-orbit Residual Accelerations in Spacelab, Proceedings of the 29th Aerospace Sciences Meeting, January 1991, AIAA Paper 91-0348
10 *Baugher, C. R.:* Early Summary Report of Acceleration Measurements for STS-40, October 1991
11 *Dunbar, B. J., Giesecke, R. L., Thomas, D. A.:* The Microgravity Environment of the Space Shuttle Columbia Payload Bay During STS-32, NASA Technical Paper 3141, November 1991
12 *Arnett, G.:* Spacelab-3 Low-*g* Accelerometer Data from the Fluid Experiments System (FES). In: Proceedings of the Measurement and Characterization of the Acceleration Environment On Board the Space Station, Guntersville, AL, August 1986, Paper 11

G. Lorenzi, F. K. Gmünder, and A. Cogoli

Cultivation of Hamster Kidney Cells in a Dynamic Cell Culture System in Space (Spacelab IML-1 Mission)

Cell proliferation, tissue plasminogen activator (t-PA) production and metabolic changes of Hamster Kidney cells (HaK) grown on microcarriers in an automatic Dynamic Cell Culture System (DCCS) were determined on the first International Microgravity Mission (IML-1) Spacelab (22–30 January 1992). The DCCS was designed for two cell culture chambers (volume: 200 µl each), one operating as a batch system, the other as a perfusion system. Medium exchange was achieved with an osmotic pump (flow rate 1 µl h^{-1}). Two major items were investigated: the biological performance of the DCCS in space and the effect of microgravity on HaK cells. The results obtained demonstrated that (1) the DCCS can be used for biological experiments on long term Spacelab missions. In fact, higher cell densities and higher concentration of glucose but lower concentration of lactate in the perfusion chambers than in the batch chambers were measured. The concentration of t-PA, glutamine and ammonia was similar in all chambers. (2) Microgravity had no effect on cell growth and metabolism of HaK cells.

1 Introduction

A considerable amount of important experiments with single cells (bacteria, protozoa, slime molds, plant and animal cells) suggest that important cellular functions like proliferation, differentiation and biosynthesis might be affected in microgravity. In particular from the Biorack results on the *Spacelab* D-1 mission a broad spectrum of information on several different monocellular systems were obtained. (Naturwissenschaften [1], special issue). Most of the equipment used for cell cultivation consisted of culture chambers allowing batch experiments only and consequently short incubation times (3 to 6 days). This was due to the exhaustion of nutrients and accumulation of waste products in the culture medium.

A very interesting experiment with mammalian cells was performed in *Skylab* in 1973 [2]. In a fully automated instrument outfitted with microscope, time-lapse camera, medium refurbishing and chemical fixation devices, human embryonic lung cells WI-38 were cultured for 28 days. The authors reported that no effect of microgravity was detected on the cells investigated. However, there was a marked reduction of glucose consumption, indicating that metabolism of the cell was changed in microgravity.

Other experiments performed in space reported that microgravity had no effect on the morphology of human kidney cells [3] and on the growth rate of hybridoma cells, but that their viability was slightly reduced by 15% [4] in microgravity. Some effects of microgravity were observed on the cellular ultrastructure of chinese hamster cells [5]. A slight increase in cell size and a trend to higher viability of HeLa cells exposed to microgravity was reported by *Zhukov-Verezhnikov* et al. [6]. *Schnettler* et al. described a tenfold increase in hybridoma cell yield by electrofusion technique in a sounding rocket flight (TEXUS) [7]. A review of the most important experiments on single cells has recently been published by *Cogoli* and *Gmünder* [8]. However, differentiating cells seem to be much more sensitive to changes in the *g*-environment that non-differentiating cells. The proliferative response of human lymphocytes following mitogen-induced activation was negligible in microgravity [9–11]. Recently we reported that the observed depression of lymphocyte activation in microgravity was due to an inhibition of interleukin-1 synthesis by macrophages [12]. Based on the results of experiments performed on two different space flights, *Talas* and her co-workers [13, 14] reported an approximately five times increase of in-vitro biosynthesis of interferon by human lymphocytes in space. On the other hand, *Limouse* et al. [15] found a dramatic inhibition of phorbol-ester induced interleukin-1 and -2 production in Jurkat cells in microgravity.

A miniaturized automatic cell cultivation instrument (*D*ynamic *C*ell *C*ulture *S*ystem: DCCS) for animal cell experiments aboard *Spacelab* has been developed. The DCCS has already been tested in a 14 days flight onboard the Soviet *Biokosmos 9* satellite, where the growth and development of plant protoplasts was studied [16].

The purpose of this study was to test the biological performance of the DCCS during the IML-1 mission. Cell growth after an 8 day mission in the batch should be

Mail address: Dr. Giovanna Lorenzi, Dr. Felix K. Gmünder, Dr. Augusto Cogoli, Space Biology Group, ETH-Technopark, Pfingstweidstr. 30, CH-8005 Zürich, Switzerland, fax: 41-1-445 1271

Submitted to Advances in Space Research, September 1992/ Paper No. G.1-S.9.08X

A RESIDUAL ACCELERATION DATA ANALYSIS AND MANAGEMENT SYSTEM

R. Wolf, M.J.B. Rogers, and J.I.D. Alexander
Center for Microgravity and Materials Research,
University of Alabama in Huntsville, Huntsville, AL 35899 USA

ABSTRACT

Efficient analysis, management, and dissemination of large, complex, and sometimes poorly understood residual acceleration datasets obtained from low earth orbit space laboratories is necessary in order to maximize the scientific return from microgravity experiments. In view of the large amounts of data that will be collected in future missions, the need for an organized approach to the reduction, analysis, and dissemination is anticipated. Thus, the development of an acceleration data processing plan was started at the Center for Microgravity and Materials Research. Toward that goal we are developing a data analysis and management system that employs a variety of pattern recognition, database management, Fourier analysis, and vibration and ergodic windowing techniques.

INTRODUCTION

It has been recognized for some time that the low-gravity environment of a low-earth-orbit spacecraft can be used as a laboratory for the study of a variety of physical phenomena under reduced (equivalent) gravity conditions. It has also been recognized that the residual accelerations arising from gravity gradient tides, atmospheric drag, thruster firings, crew motions, etc. are sufficient to cause measurable deviations from "zero-gravity" conditions. The need to measure and record the ever-changing low-gravity environment in order to provide important "environmental" data for the post-flight assessment of low-gravity experiments and the physical condition of astronauts has led to the development of several acceleration measurement systems since the early 1970's. Lately, particularly since dedicated spacelab missions began, the interest in residual acceleration data has increased. Indeed with the now regular use of NASA's Space Acceleration Measurement System

(SAMS), the amount of acceleration data being collected is increasing rapidly. The first three flights of SAMS (SLS-1, STS-43, and IML-1) yielded several gigabytes of data. In response to the need for an organized approach to the reduction, analysis and dissemination of data, an acceleration data processing plan was developed at the Center for Microgravity and Materials Research /1,2/.

We have developed a data base management system to handle the large quantity of residual acceleration data that results from a typical low-gravity Orbiter mission. The system will manage a large, graphic data base in support of supervised and unsupervised pattern recognition /3,4/. Use of pattern recognition techniques allows identification of specific classes of accelerations so that these classes can be easily recognized in any set of acceleration data retrieved from spacecraft accelerometer systems. The data will be partitioned following the ANSI/SPARC model /5/. The entire mission time history will form the internal layer of the model. Data reduction techniques will identify limited time windows of interest. Time and frequency domain representations of these windows will compose the conceptual level of the model. The graphics aspect of the management system includes several data visualization techniques that help the user better understand the nature of the acceleration signal being studied. The data base management system was developed on a UNIX-based Stardent Titan computer and is being tested on Spacelab 3 (SL-3) residual acceleration data. When fully developed, it will be suitable for use with other residual acceleration data bases and will be portable to other UNIX-based workstations.

PATTERN RECOGNITION AND DATA VISUALIZATION SYSTEM

An acceleration data analysis and management system has been developed to serve as the core of future residual acceleration data analysis. The PRIDE (Pattern Recognition Visualization Database system applies the techniques of pattern recognition, data visualization, database systems, data reduction, and expert systems to the problem of characterizing acceleration activity from orbital laboratories.

Both supervised and unsupervised pattern recognition techniques are incorporated into the PRIDE system. Supervised pattern recognition uses human knowledge of data to aid in classification while unsupervised pattern recognition does not. In the PRIDE system,

supervised pattern recognition is primarily achieved through the application of various data visualization techniques to raw acceleration data. In addition, these techniques are applied to various transformations of the raw data, such as vector magnitudes and Fourier transforms. Additional supervision will be possible through use of the CLIPS expert system /6/. This allows the increasing expertise of the system users to be stored in the data base through CLIPS.

Unsupervised pattern recognition in PRIDE is achieved through the use of the ISODATA algorithm /4/. This algorithm is typically used to classify data for which there is no known classification. This algorithm will be applicable to the acceleration data base directly by an operator, and will also be available for controlled use by a specially written CLIPS shell. This will make it possible to run ISODATA without human intervention. In addition, an ergodic search technique has been developed which identifies the location and duration of high energy acceleration events. Note that this technique offers refined control of the application of Fourier techniques. For example, information such as the start of a potentially interesting acceleration event, or the optimum length of the data window for spectral analysis, can be readily provided.

Data visualization is used not only in supervised pattern recognition as discussed above, but it is also used for general evaluation of the data character. Analysis of the data character leads to a clearer understanding of the nature of the problem and should lead to the development of new approaches to acceleration analysis. Note that this use of data visualization is independent of the supervised pattern recognition support function.

A relational data base has been installed on the CMMR Stardent computer system and has been fully integrated with all the functions of PRIDE. Use of this common data base form will enhance the transport of PRIDE to other platforms. Additionally, the use of a data base provides several advantages over flat file formats, for example data integrity, maintainability, and large data base manipulation.

The manipulation of large data bases is achieved through the application of various data reduction techniques. Two main data reduction techniques used are vibration windowing and ergodic windowing. Vibration windowing is used to identify and select windows that fit

the definition of a damped high magnitude oscillatory vibration. Ergodic windowing identifies and selects windows based on a measure of the energy attributes of a portion of the accelerometer time series. These provide a way to make the processing of such huge data bases more practical. Additionally, the use of two independent techniques makes the resulting classification more dependable.

Expert systems technology is used to provide two basic capabilities. First of all, it is used to make the use of ISODATA more practical. Normal use of ISODATA requires a human operator and, even with data reduction, the data sizes that must be handled in a finite time are still enormous. The use of a CLIPS shell to control the ISODATA algorithm is useful. Second, and more important, the availability of an expert system built into the system with a database form of access to the data will provide in the future (when a complete understanding of the processes involved has been achieved) a way to store this knowledge and use this knowledge to drive the characterization process.

Figures 1-3 give examples of typical screen images that can be obtained using PRIDE. Figure 1 is an example of the 3D-FFT technique applied to a 30 minute acceleration time-series from SL-3. The sample time-series contains 420, 000 datapoints per axis. Visual display of this many data-points, even for this relatively short duration, tends to mask the character of the acceleration and is often not very useful. The 3D-FFT, combined with vibration or ergodic windowing, enables identification and display of acceleration events that fit predetermined specifications (either thresholds or particular patterns). This reduces the amount of data that is actually displayed, while supplying more information than visualization of the time series itself. Fig. 1 displays 3D-FFT information for windows which exceeded specified acceleration thresholds. Each axis represents the acceleration component for each of the x-, y-, and z-directions. For each window, the discrete Fourier transform of the acceleration data for each axis produces a discrete set of frequencies separated by a fixed interval, Δf. Each frequency f_i is connected by a straight line segment to the $f_{i-1} = f_i - \Delta f$ and $f_{i+1} = f_i + \Delta f$. Note that the events in this figure are dominated by accelerations associated with the z-direction. Figure 2 is the standard FFT for one of the event (windows) used to produce Figure 1. Figure 3 is an overlap graph drawn from an ergodic analysis. This graph is

produced by using the best window size produced by ergodic analysis to focus attention of a given set of window energy values. Subsequently, an acceleration threshold histogram is selected. The temporal location of all windows with associated energy greater than or equal to the characteristic energy of the threshold are recorded. The time segments associated with these high energy events within the overall time interval are used to determine the number of high energy events occurring at any given time.

SUMMARY

PRIDE is in its initial stages of development. Preliminary results suggest that it will be a useful basis for future acceleration processing strategies. It is currently being used to examine recently obtained SAMS /7/ data as well as Spacelab-3 accelerometer data. Correlation of experiment events with acceleration events as well as general characterization of space laboratory environments can readily be accomplished using organized approaches such as PRIDE. The development of such data processing and dissemination packages combined with NASA's program of acceleration measurements planned under the ACAP /8/ program will enable future low-gravity experiment investigators to obtain a clear description of the residual acceleration conditions prevailing during their experiment.

Acknowledgements

This project is supported by the National Aeronautics and Space Administration through grant NAG8-759. The authors would like to thank Dr. Robert Snyder and Charles Baugher for their encouragement and continuing interest in this work.

REFERENCES

1. M.J.B. Rogers and J.I.D. Alexander, Residual acceleration data analysis for spacelab-3 missions, *Microgravity Sci. Technol.* V, 43 (1992).
2. M.J.B. Rogers and J.I.D. Alexander, A strategy for residual acceleration data reduction and dissemination, *Adv. Space Res.* 11, #7, (7)5 (1991).
3. A. Stevens, *C Database Development*, MIS Press, Portland, Oregon,1991.

4. J. T. Tou and R. C. Gonzales, *Pattern Recognition Principles*, Addison-Wesley, Reading, Massachusetts, 1974.

5. C.J. Date, *An Introduction to Database Systems*, Addison-Wesley, Reading, Massachusetts,1990.

6. J.C. Giarrantano, *CLIPS User's Guide, Version* 5.1 , Artificial Intelligence Section, Lyndon B. Johnson Space Flight Center, JSC-25013, 1991.

7. R. DeLombard, R.B. Finley and C. Baugher, Development of and flight results from the Space Acceleration Measurement System (SAMS), AIAA paper 92-0354, 30th Aerospace Sciences Meeting, Reno, January 1992.

8. *Acceleration Characterization and Analysis Project*, C. Baugher, Marshall Space Flight Center, personal communication, 1992.

FIGURE CAPTIONS

Fig. 1. 3D-FFT representation showing a projection from a 4-tuple ($A_x(f)$, $A_y(f)$, $A_z(f)$, f) to 3-tuples ($A_x(f)$, $A_y(f)$, $A_z(f)$) plotted in 3-D space and linked by lines. Data from a 30 minute high energy event during SL-3.

Fig. 2. Amplitude spectrum for each of the three acceleration components. Data is taken from one of the event windows shown in Fig. 1.

Fig. 3. "Overlap" plot indicates the temporal location of high energy events within the best window length.

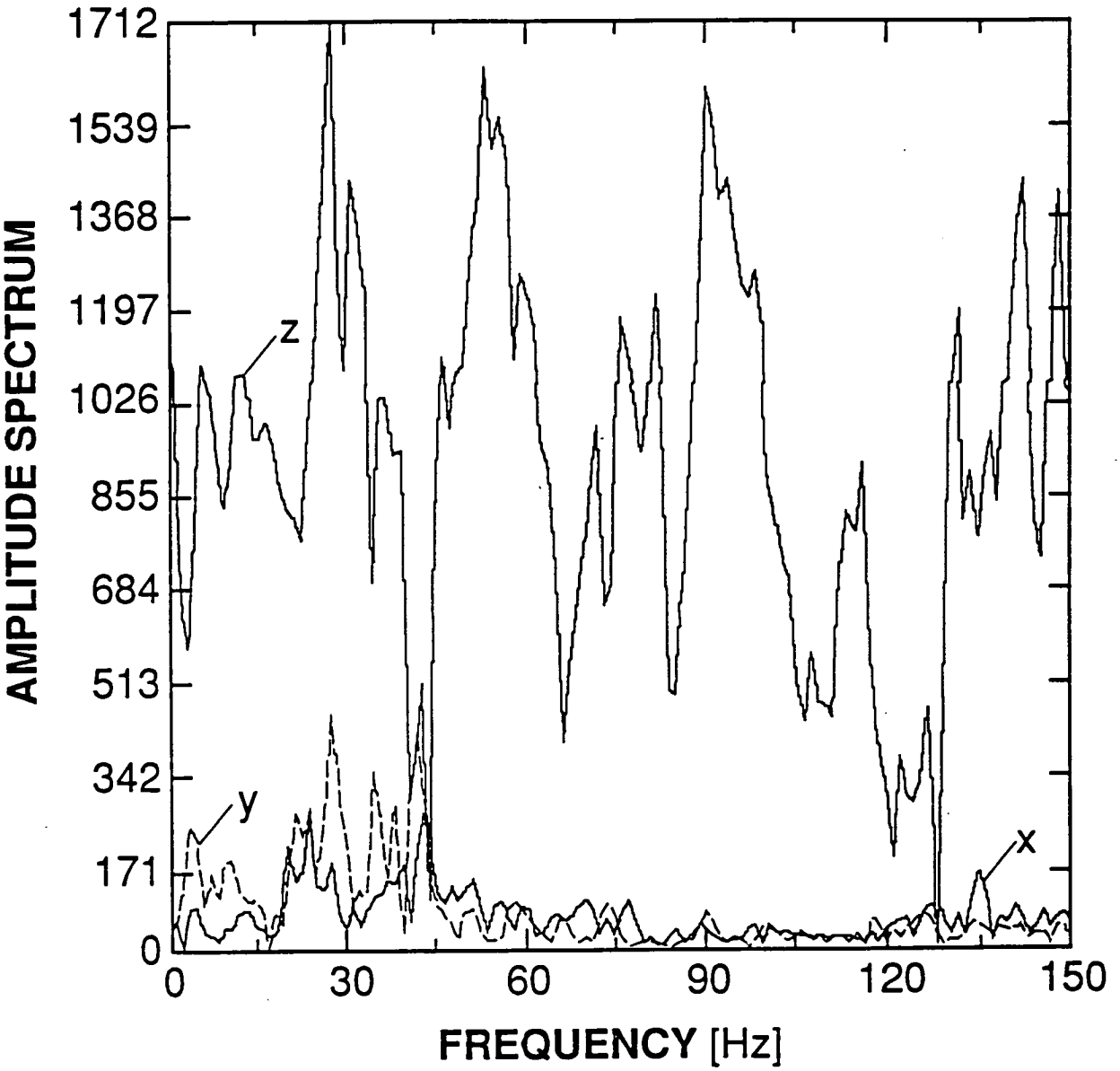
AMPLITUDE SPECTRUM
1712
1539
1368
1197
1026
855
684
513
342
171
0
z
y
x
0
30
60
90
120
150
FREQUENCY [Hz]

FIG. 1

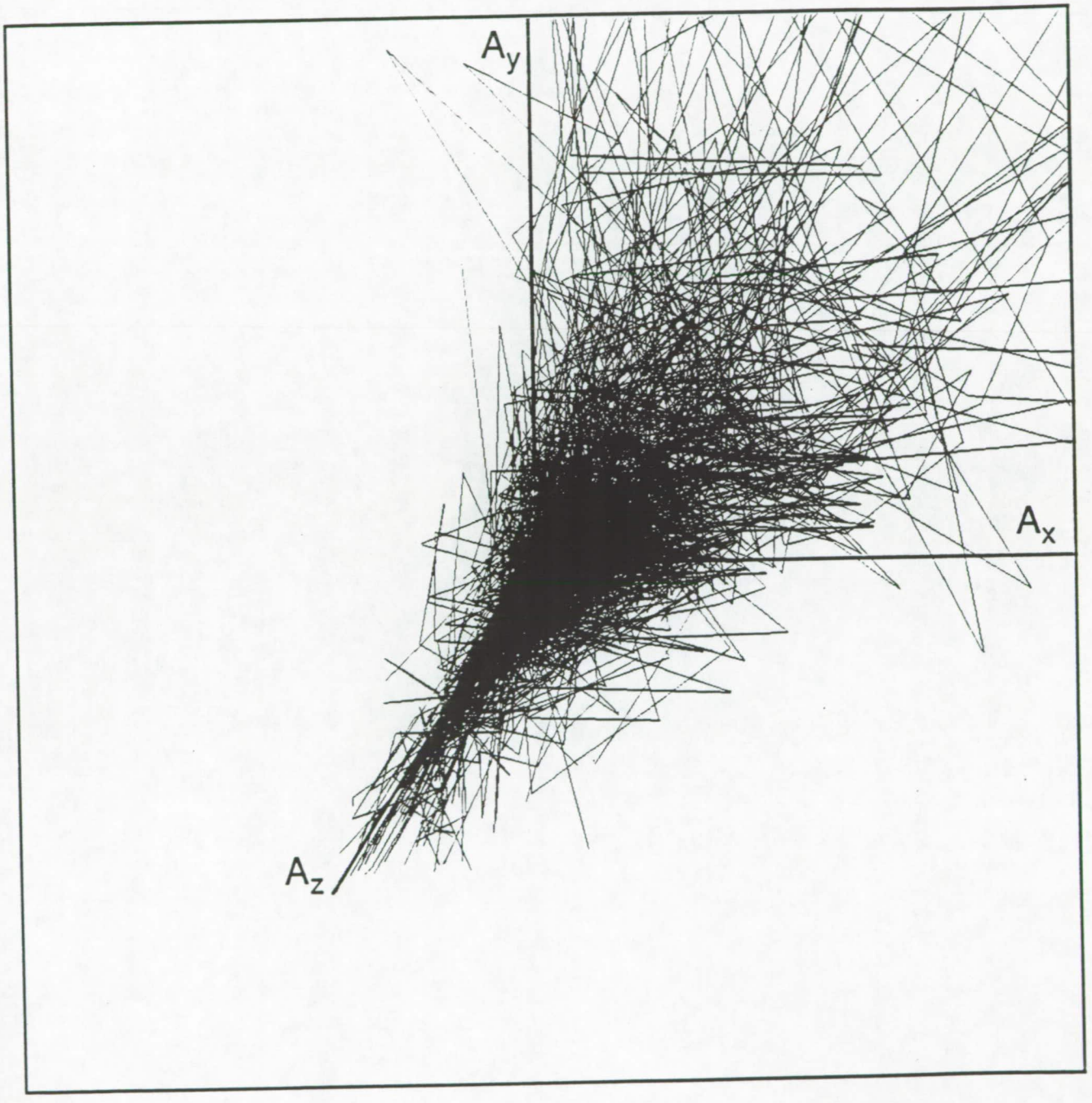

FIG. 2

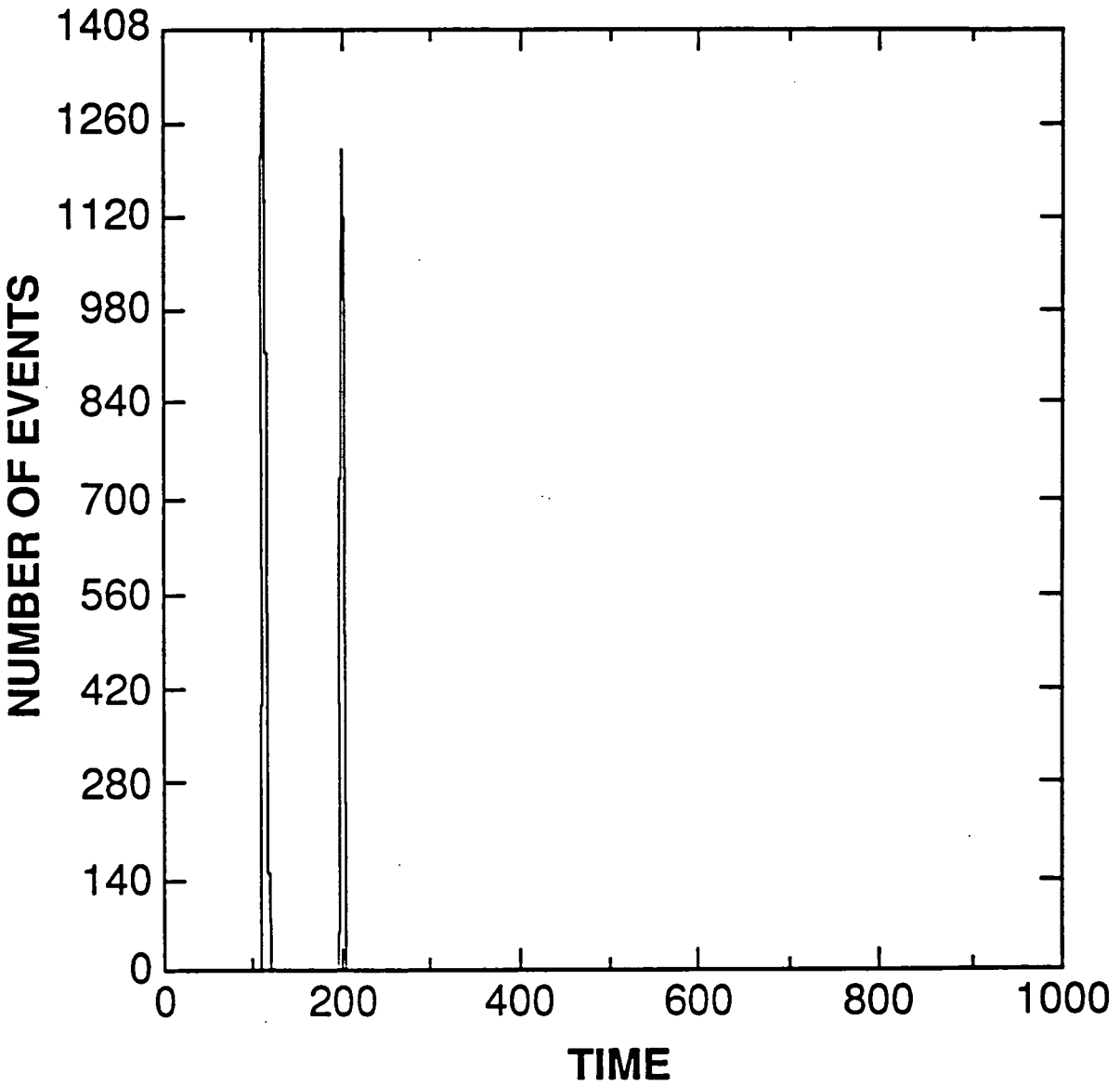
1408
1260
1120
980
840
700
560
420
280
140
0
NUMBER OF EVENTS
0
200
400
600
800
1000
TIME

FIG. 3

AIAA 91-0348

Cross-correlation Analysis of On-orbit Residual Accelerations in Spacelab

M.J.B. Rogers and J.I.D. Alexander
Center for Microgravity and Materials Research
The University of Alabama in Huntsville
Huntsville, Alabama 35899

29th Aerospace Sciences Meeting
January 7–10, 1991/Reno, Nevada

CROSS-CORRELATION ANALYSIS OF ON-ORBIT RESIDUAL ACCELERATIONS IN SPACELAB

Melissa J. B. Rogers and J. Iwan D. Alexander

Center for Microgravity and Materials Research
University of Alabama in Huntsville
Huntsville, Alabama 35899

Abstract

To characterize the low-gravity environment within orbiting space laboratories, researchers are operating sensitive accelerometer systems. Transient accelerations recorded in spacecraft can have magnitudes up to 10^{-2} g over a wide range of frequencies. These, and oscillatory, accelerations have components in the 10^{-3} Hz to 100 Hz range no greater in magnitude than 10^{-3} g. Some experiments can be sensitive to such accelerations, so investigators are interested in identifying causal relationships between accelerations and experimental results. Cross-correlation analysis is suggested as a means for analyzing such relationships. The basics of cross-correlation analysis are introduced and problems with obtaining experimental time series are discussed. The use of experiment models is advocated to identify appropriate experiment parameters to monitor and to identify experiment response patterns to use in the creation of representative experiment time series from qualitative output. Two forms of synthetic experiment data created using Spacelab 3 accelerometer data are evaluated using cross-correlation analysis. From the results of this analysis, the use of cross-correlation techniques is deemed appropriate, for specific experiment classes, for assessing relationships between both transient and oscillatory residual accelerations and experimental results recorded in a low-gravity environment.

Nomenclature

$f_1(t)$	zero-mean time series
m	maximum lag
t	time
$F_1(\omega)$	Fourier transform of time series f_1
$F_1^*(\omega)$	complex conjugate of F_1
N	total number of points in time series
Δt	sampling interval
$\rho_{12}(\tau)$	normalized cross-correlation function
$\phi_{11}(\tau)$	auto-correlation function
$\phi_{12}(\tau)$	cross-correlation function
τ	lag time
τ_{max}	maximum lag time
ω	angular frequency
$\Phi_{12}(\omega)$	cross-power spectrum

1. Introduction

In order to characterize the reduced gravity environment within orbiting spacecraft, researchers are operating sensitive accelerometer systems. The object of many low-gravity fluid physics and materials science experiments is to study physical phenomena in the absence of the steady 9.8 ms^{-2} (1 g) acceleration experienced under terrestrial conditions. Because some of these experiments are sensitive to even small magnitude accelerations,[1-5] it is necessary to characterize the time-dependent acceleration environment in order to properly interpret the experimental results. Both quasi-steady and higher frequency transient and oscillatory accelerations are expected during a typical mission. The quasi-steady accelerations are related to the Earth's gravity gradient, spacecraft attitude and motions, and atmospheric drag. Analysis to date of accelerometer data collected during the STS 51-B Spacelab 3 mission (SL3) flown in April-May 1985 indicates that the transient accelerations that contribute to the higher frequency g-jitter can cause accelerations as large as 10^{-2} g. Such accelerations, caused by diverse operational and crew related activities, have a wide range of frequencies, but components in the 10^{-3} Hz to 100 Hz range are typically no greater in magnitude than 10^{-3} g.[6]

Model studies of low-gravity experiments and analysis of experiments already run in low-earth orbit indicate that certain experiments are sensitive to acceleration magnitudes such as indicated above.[1-5] In situations where it is impossible to avoid causing intolerable accelerations and where experiments are not successfully isolated from the acceleration effects, it is of interest to investigators to identify causal relationships between accelerations and experimental results.

Cross-correlation techniques are generally used to determine the equivalence of time histories and to determine time delays between related time series. Such a technique should be useful in identifying relationships between acceleration events and experimental results. We present in section 2 a brief introduction to cross-correlation theory; more detailed explanations can be found in most time series analysis texts.[7,8] In section 3 we discuss the application of cross-correlation analysis to synthetic data that represent low-gravity experimental results. The results of this analysis and an assessment of the use of cross-correlation analysis in this context are discussed in sections 4 and 5.

2. Cross-correlation Analysis

2.1 Theory

Correlation techniques are applied in statistical analysis and in signal processing to determine the amount of parallelism between two time series of interest.[9,10] For residual acceleration data analysis, such techniques may be useful in identifying causal relationships between specific acceleration events and experimental results. The cross-correlation ϕ_{12} of two series is written as:

$$\phi_{12}(\tau) = \int_{-\infty}^{\infty} f_1(t)\, f_2(t+\tau)\, dt \qquad (1)$$

where f_1 and f_2 are two zero-mean time series and τ represents a time lag. In discrete form, the cross-correlation function can be written as:

$$\phi_{12}(\tau) = \frac{1}{N} \sum_{t=1}^{N} f_1(t)\, f_2(t+\tau) \qquad (2)$$

for f_1, f_2 both of length N and $\tau = 0,1,...,m$. Here the time series considered must be collected or digitized with the same sampling interval Δt. Different length time windows can be analyzed by placing a sequence of zeroes at the end of the shorter series so that the two series have the same number of points.[8,11] In order to avoid errors owing to "circular" correlation, padding of time series files with zeroes is particularly important.[8]

While it is possible to compute cross-correlation values out to the length of the time series, it is generally preferable to consider lags out to a maximum lag of $m \leq N/10$. For sampling interval Δt, $\tau_{max} = m\Delta t$ is the maximum lag time or delay time considered in the analysis.[8,11] Some *a priori* information about the time series considered is usually required so that appropriate length time windows and maximum lags are used.

The magnitude of the cross-correlation function ϕ_{12} depends on the relative magnitudes of the series f_1 and f_2. To simplify the interpretation of cross-correlation analyses, a normalized cross-correlation function can be computed so that the maximum possible cross-correlation value is unity. This indicates that the two time series are identical at the given lag. Values close to zero indicate that there is very little similarity between the two series, while positive values close to unity indicate good correlation. Negative values with magnitude near unity indicate the degree of correlation is high, but the series are out of phase. The normalized cross-correlation function is:

$$\rho_{12}(\tau) = \frac{\phi_{12}(\tau)}{[\phi_{11}(0)\, \phi_{22}(0)]^{1/2}} \qquad (3)$$

where $\phi_{11}(0)$ and $\phi_{22}(0)$ are the auto-correlation functions of f_1 and f_2 at zero lag.[9]

The cross-correlation between two time series can be estimated using both time domain and frequency domain analysis techniques. Analysis in the time domain involves relatively straightforward programming of equations (2) and (3). A potentially faster method, depending on the series lengths considered, is to compute the cross-power spectrum,

$$\Phi_{12}(\omega) = F_1^*(\omega)\, F_2(\omega), \qquad (4)$$

where F_1 and F_2 are the Fourier transforms of f_1 and f_2 and a superscript * denotes the complex conjugate. The cross-power spectrum $\Phi_{12}(\omega)$ forms a Fourier transform pair with the cross-correlation function, i.e.,

$$\phi_{12}(\tau) \leftrightarrow \Phi_{12}(\omega). \qquad (5)$$

The savings of computation speed achieved by computing the cross-correlation function via the cross-power spectrum rather than using the direct method is approximately a factor of $N/4p$ where $N=2^P$ is the file length considered.[11]

2.2 Application to Residual Acceleration Data

The application of cross-correlation techniques to the analysis of low-gravity experiments requires both accelerometer data and a time history representation of the experiment of interest. Various forms of experiment output may be used in post-flight analysis, but output data that track some key parameter in the experiment are probably the most useful type of experiment time series. The parameter monitored must be one that will be affected by variations of the low-gravity environment. Unfortunately, such parameters are not always numerical and, therefore, experiment time series must be created from visual and qualitative experiment output such as interferograms, photographs, and video. We must denote visually identified experiment perturbations by defined response patterns and get cross-correlation results using this time series and the accelerometer data. A problem here is the determination of the relative magnitudes and specific response patterns to use in the creation of the time series.

Modelling will enable the investigator to identify appropriate experiment parameters to record as a time series. In the case that such a parameter cannot be recorded quantitatively, modelling may also be used to determine typical experiment responses.[1-5] This information can be used to create experiment time series by convolution of the response pattern with a series of spikes, the timing of which would be identified from qualitative experiment output. Modelling results should also give an indication of typical response times, suggesting time lags to expect in experimental results and lengths of acceleration windows to investigate.

When threshold tolerance limits are known from experiments and/or modelling, then an investigator should be able to correlate experimental output with accelerations whenever these thresholds are exceeded. Windows of accelerometer data can be selected based on the occurrence of poor experimental results and time lags predicted by modelling. These windows can be scanned for the occurrence of accelerations in excess of a pre-defined threshold value and cross-correlation methods can be applied specifically to these windows. Such a method will considerably limit the amount of residual acceleration data an investigator need access.

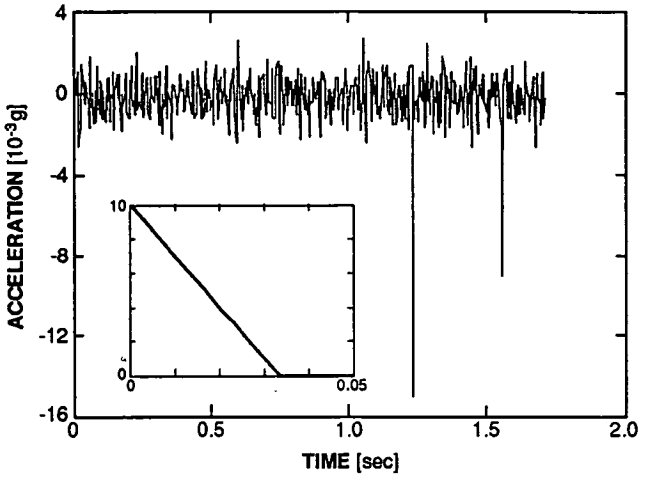

Fig. 1. Sample time series from SL3 accelerometer data and 0.05 second long seed function (inset) that are convolved together to form synthetic test series, see Fig. 2.

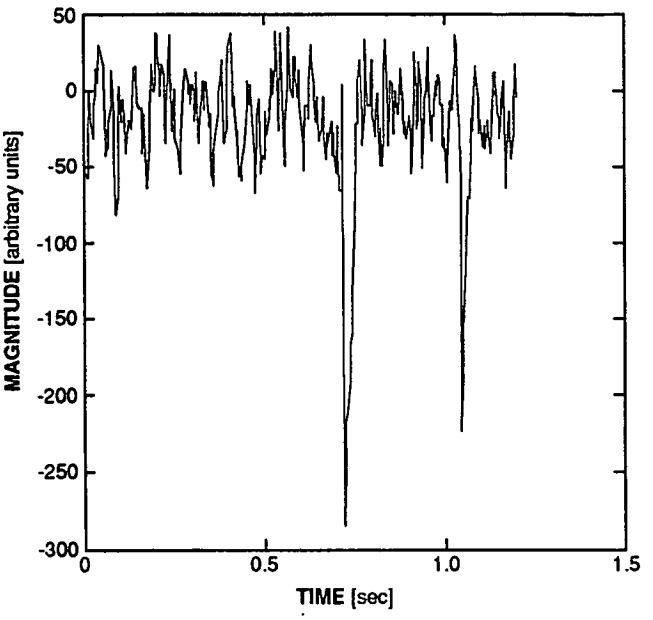

Fig. 2. Convolved synthetic data, 150 Points removed from beginning of file to simulate time lag.

3. Data Analysis

We have performed cross-correlation tests using two types of synthetic data constructed with SL3 data: one created by the convolution of a simple seed file with SL3 data windows and one taken from the results of modelling a directional solidification/melt convection experiment.[3] The cross-power spectrum method discussed in section 2.1 was used. Maximum lags in the range $0.1N \leq m \leq 0.25N$ were used in the analysis, depending on the lengths of the files considered. The routines used for the analysis allow the accelerometer and synthetic time series to be of different lengths; the ends of both series are padded with zeroes to a specified length.

3.1 Synthetic Data - Convolution

The first type of synthetic data files examined were created by convolving relatively simple functions with windows of SL3 accelerometer data. Convolution of a seed function with accelerometer data creates a synthetic time series that is similar to the acceleration series without a time lag. Figure 1 shows a time series of accelerometer data used to create synthetic data by convolution with the inset ramp function. Figure 2 shows the resulting convolved data with 150 points (0.5 sec) deleted from the beginning of the file to simulate a time lag.

The synthetic data were used to test the performance of the cross-correlation routine. Various tests were done with this data. The accuracy of the program was tested using the auto-correlation of the time series. At zero lag, the normalized auto-correlation of the series should, and did, equal unity. Cross-correlations of the synthetic data and associated accelerometer data were computed. The maximum possible normalized cross-correlation value is unity. In each test performed, the maximum values were all less than unity and occurred at zero lag. This result was expected for the synthetic time series used.

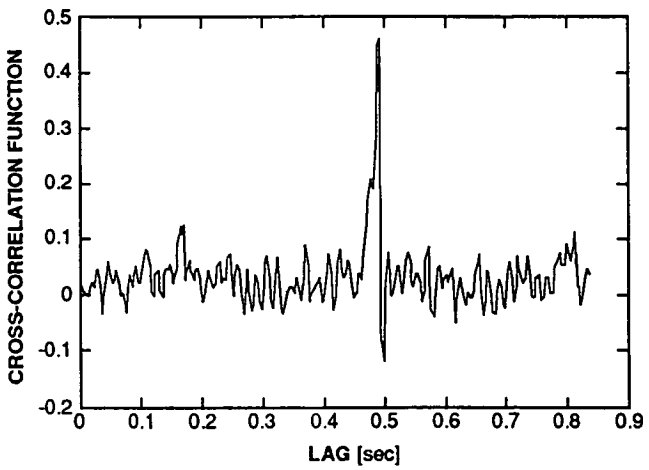

Fig. 3. Cross-correlation of series in Fig. 2 and Fig. 1. Peak value at 0.5 seconds indicates lag simulated by removal of points (150 points at 300 samples per second).

In addition to these tests, the convolved data were used to identify the presence of simulated time lags between two series. Time lags are simulated in synthetic data by the addition or deletion of data points at the beginning of one of the time series. The evaluation of the cross-correlation function can be thought of as the shifting of time series with respect to one another in search of similar patterns. The relative direction of shift indicates which time series lags behind or leads the other. For example, cross-correlations of synthetic data padded in front with zeroes and the associated accelerometer data were performed. No obvious maxima occur in these cross-correlation functions because, for the relative shift directions of the time series, the zero padding by-passed the similarity that would have normally occurred at zero lag. If the series are shifted in the opposite sense, a maximum occurs after a shift corresponding to the number of zeroes added, but this would indicate that the experiment response caused the accelerations, which is not an appropriate conclusion.

On the other hand, cross-correlations of the synthetic data, with a series of points removed in the beginning, Fig. 2, and the associated accelerometer data, Fig. 1, were done. The resulting cross-correlation function indicates the appropriate lag time, Fig. 3. After successful completion of these tests, the routine was used on modelled data to assess the viability of cross-correlation techniques in post-flight analysis of low-gravity experiments.

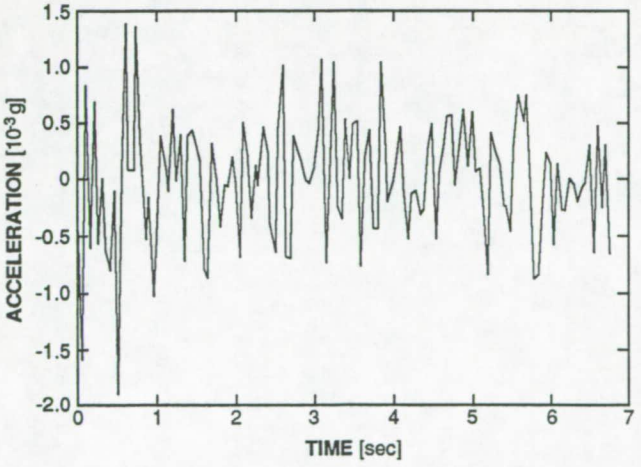

Fig. 4. SL3 accelerometer data used in experiment model. Data sampled at 300 Hz; 10 Hz lowpass filter applied.

3.2 Synthetic Data - Modelling Results

While the tests discussed in section 3.1 involve SL3 accelerometer data, they do not represent the expected response of a low-gravity experiment to the acceleration environment represented in the SL3 time series. To better assess how useful cross-correlation techniques are in the post-flight analysis of experiments, we obtained results from numerical modelling of the response of a directional solidification/melt convection experiment to windows of SL3 accelerometer data.[3] The two measures of experiment response considered were melt velocity and lateral compositional non-uniformity in the crystal.

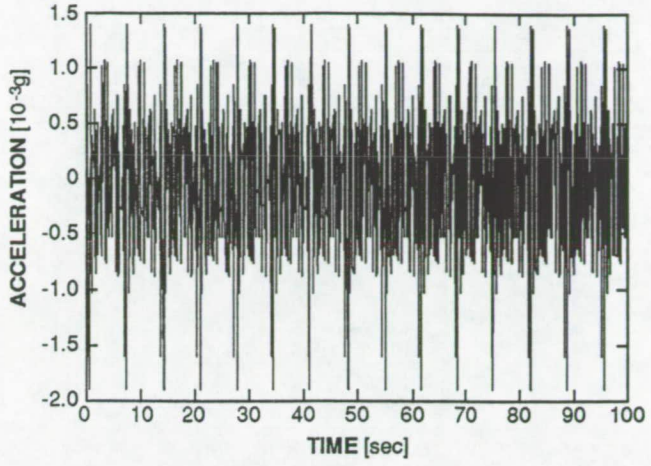

Fig. 5. SL3 data from Fig. 4 as input to experiment model. The data window was repeated out to 100 seconds.

The modelling was performed using the SL3 data shown in Fig. 4. This window contains accelerations typical of a relatively quiet period during the SL3 mission. Frequency components higher than 10 Hz are filtered out to avoid saturation of the modelling algorithm and the window is repeated out to 100 seconds for input to the model, Fig. 5. Generally, the transient accelerations recorded by the SL3 accelerometer system have a wide range of frequencies, with a limited number of characteristic components. Particular frequency components are associated with the response of structures to specific acceleration sources such as thruster

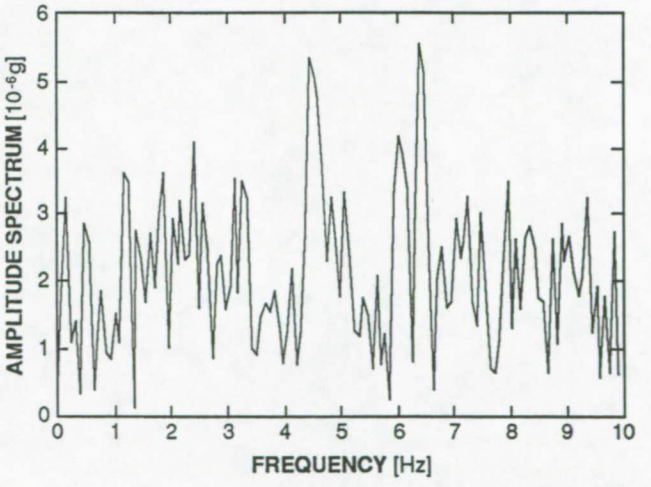

Fig. 6. Amplitude spectrum of filtered SL3 data shown in Fig. 4.

firings and crew activity within the spacelab. Figure 6 shows the amplitude spectrum of the filtered window. The components in the 4 Hz to 7 Hz range represent the excitation of structural modes of both the orbiter system and spacelab.[6] Cross-correlation analysis was performed on the accelerometer data time series shown in Fig. 5 and various series of model results. For example, Fig. 7 shows the velocity parallel to the growth direction at a point in the melt as a function of time; note the 6.8 second periodicity. The cross-correlation between the data shown in Figs. 5 and 7 was calculated and the results are shown in Fig. 8.

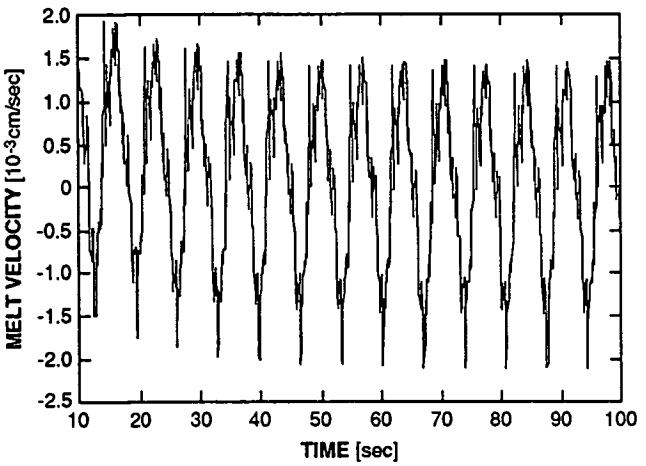

Fig. 7. Velocity parallel to growth direction at a point in the melt, as a function of time, for directional solidification/melt convection experiment model.[3] Note the 6.8 second periodicity.

4. Results of Testing

The cross-correlation results outlined in section 3.1 indicate that the routine used is appropriate for the evaluation of time series relationships between experimental results and accelerometer time histories. For the series tested here, relatively good correlation (~0.4) was found at appropriate lag times, Fig. 3.

For the modelled data, maximum cross-correlation values are relatively low (0.15), indicating a low magnitude response of the system to the acceleration input, Fig. 8. In this example, however, the cross-correlation function provides additional information about the two series considered. While the correlation is low, it has a periodic nature that reflects the lowest period of the acceleration input. The corresponding periodicity of the melt velocity series is so strong that higher frequency components similar to those of the SL3 data that might contribute to higher cross-correlation values are drowned out. Obviously, the fact that the melt responds to lower frequencies indicates that these are the most important frequencies for this experiment. Therefore, some *a priori* information on experiment sensitivity can be used for the

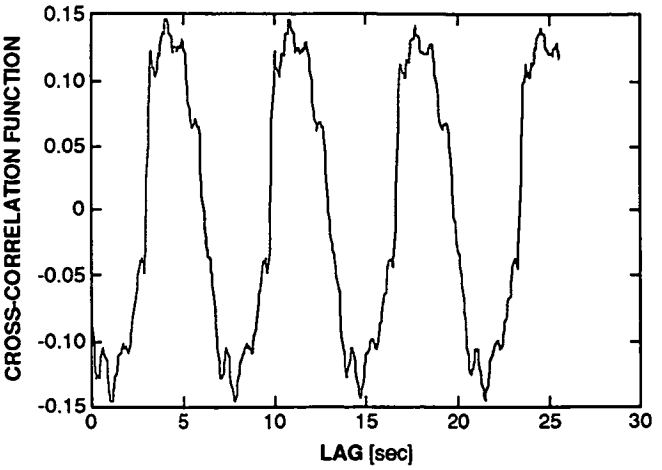

Fig. 8. Cross-correlation of Fig. 7 and Fig. 4, note periodicity of the result.

identification of similar frequency components in experiment and accelerometer time series. This suggests that cross-correlation techniques may be useful in the analysis of experiments sensitive to oscillatory, as well as transient, accelerations.

Owing to the short windows considered in these tests (6.8 seconds, 300 samples per second), the minimum frequency represented in the analysis is 0.15 Hz. Lower frequency components present in the modelled data are an artifact of the modelling process, and do not necessarily represent frequencies present in the accelerometer data. Ongoing analysis of the SL3 accelerometer data will indicate whether or not cross-correlation analysis is appropriate for experiments sensitive only to very low frequency disturbances.

5. Conclusions

Based on the results of the testing presented here, cross-correlation techniques appear to be, for specific experiment classes, a viable means of assessing causal relationships between residual accelerations and experimental responses in a low-gravity environment. Such analysis should be useful not only in situations where experiments are sensitive to high magnitude, transient accelerations, but also when experiments are sensitive to oscillatory disturbances.

Unfortunately, the experiment parameters recorded by investigators are not always ones that are affected by variations of the low-gravity environment of the space laboratory. In addition, experiment output may be qualitative, and not readily converted to a numerical time series that can be used in cross-correlation analyses. Modelling of experiments prior to flight should indicate appropriate experiment parameters to record, and should also give some indication of how appropriate cross-correlation would be in the post-flight analysis of a particular experiment. Modelling results will also indicate what type of experiment response pattern is

appropriate for generating experiment time series, if necessary, from qualitative output, and how extensive a time window around experiment perturbations is needed for correlation analysis. The ability to identify windows of data to analyze based on known experiment threshold values and a brief look at experimental results will considerably limit the amount of recorded residual acceleration data an investigator need access in post-flight processing of an experiment.

Acknowledgements

This work was supported by NASA Grant NAG8-759. Sakir Amiroudine of the CMMR provided the directional solidification/melt convection modelling results.

References

[1]Alexander, J. I. D., Low-Gravity Experiment Sensitivity of Residual Acceleration: A Review, **Microgravity Science and Technology 3** (1990) 52.

[2]Alexander, J. I. D., Ouazzani, J., and Rosenberger, F., Analysis of the Low Gravity Tolerance of Bridgman-Stockbarger Crystal Growth. I. Steady and Impulse Accelerations, **J. Crystal Growth 97** (1989) 285.

[3]Alexander, J. I. D., Amiroudine, S., Ouazzani, J., and Rosenberger, F., Analysis of the Low Gravity Tolerance of the Bridgman-Stockbarger Technique. II. Transient and Periodic Accelerations, to be submitted to **J. Crystal Growth** (1990).

[4]Monti, R., Favier, J. J., and Langbein, D., Influence of Residual Accelerations on Fluid Physics and Materials Science Experiments, in **Fluid Sciences and Materials Science in Space, A European Perspective**, ed. H. U. Walter (Springer, Berlin 1987) p. 637.

[5]Nadarajah, A., Rosenberger, F., and Alexander, J. I. D., Modelling the Solution Growth of Triglycine Sulfate in Low Gravity, **J. Crystal Growth 104** (1990) 218.

[6]Rogers, M. J. B. and Alexander, J. I. D., Analysis of Spacelab 3 Residual Acceleration Data, submitted to **J. Spacecraft and Rockets** (1990).

[7]Chatfield,C., **The Analysis of Time Series: An Introduction**, 2nd ed. (Chapman and Hall, London 1980).

[8]Otnes, R. K. and Enochson, L., **Applied Time Series Analysis, Volume 1: Basic Techniques** (John Wiley, New York 1978).

[9]Båth, M., **Spectral Analysis in Geophysics** (Elsevier, Amsterdam 1974).

[10]Camina, A. R. and Janacek, G. J., **Mathematics for Seismic Data Processing and Interpretation** (IHRDC, Boston 1984).

[11]Bendat, J. S. and Piersol, A. G., **Random Data: Analysis and Measurement Procedures**, 2nd ed. (John Wiley, New York 1986).

N92-28453

Presented at the International Workshop on Vibration Isolation Technology for Microgravity Science Applications, NASA Lewis Research Center, April 1991.

DEVELOPMENT OF A RESIDUAL ACCELERATION DATA REDUCTION AND DISSEMINATION PLAN

Melissa J. B. Rogers
Center for Microgravity and Materials Research
University of Alabama in Huntsville
Huntsville, Alabama 35899

ABSTRACT

A major obstacle in evaluating the residual acceleration environment in an orbiting space laboratory is the amount of data collected during a given mission: gigabytes of data will be available as SAMS units begin to fly regularly. Investigators taking advantage of the reduced gravity conditions of space should not be overwhelmed by the accelerometer data which describe these conditions. We are therefore developing a data reduction and analysis plan that will allow principal investigators of low-g experiments to create experiment specific residual acceleration data bases for post-flight analysis. The basic aspects of the plan can also be used to characterize the acceleration environment of earth orbiting laboratories.

Our development of the reduction plan is based on the following program of research:

- The identification of experiment sensitivities by order of magnitude estimates and numerical modelling [1],
- Evaluation of various signal processing techniques appropriate for the reduction, supplementation, and dissemination of residual acceleration data, and
- Testing and implementation of the plan on existing acceleration data bases.

Discussions of the basic analysis techniques we are using and of the results of our analysis of the Spacelab 3 data base can be found in references [2-5]. Three initial aspects of residual acceleration data that can be analyzed are the acceleration vector magnitude and orientation and the relative strengths of the frequency components that make up the data window of interest. The acceleration time history can be subjected to a variety of statistical analyses and can be manipulated into a range of data presentation styles aimed at the identification of potentially intolerable acceleration events while reducing the number of data points plotted.

The orientation of the residual acceleration vector with respect to some set of coordinate axes is important for experiments with known directional sensitivity. Orientation information can be obtained from the evaluation of direction cosines.

Fourier analysis is commonly used to transform time history data into the frequency domain. Common spectral representations are the amplitude spectrum which gives the average of the components of the time series at each frequency and the power spectral density which indicates the power or energy present in the series per unit frequency interval.

The data reduction and analysis scheme developed involves a two tiered structure to 1) identify experiment characteristics and mission events that can be used to limit the amount of accelerometer data an investigator should be interested in and 2) process the data in a way that will be meaningful to the experiment objectives. A general outline of the plan follows:

LEVEL ONE

1. Pre-flight identification of acceleration sensitivity to determine frequency and magnitude ranges of interest and experiment tolerance limits.

2. Pre-flight identification of times at which the experiment is liable to be vulnerable, i.e., some experiments may be more sensitive at specific stages (e.g. protein crystal growth during the nucleation stage).

3. Preliminary post-flight analysis of experimental results to identify times when unexpected results occurred that may be related to perturbations in the residual acceleration environment of the laboratory.

LEVEL TWO

1. Selection of time windows of interest using a threshold detection routine based on sensitivities identified in Level One, Step 1 above.

2. Use of data decimation techniques, when appropriate, to reduce the number of data points needed to evaluate lengthy windows of data.

3. Specific analysis of windows of data identified in Level One and the first step of Level Two, including estimation of mean and mean squared values, determination of the acceleration vector orientation, and spectral analysis to investigate the magnitude of the frequency components for the specific time window of interest.

4. Evaluation of accelerometer data in conjunction with experimental results to identify causal relationships and revise sensitivity limits.

Cross-correlation analysis of accelerometer data and experimental output is suggested as a viable means of identifying causal relationships between specific acceleration events and noticeable experiment perturbations [4].

We have devised a contact sheet for IML1 principal investigators that gives an overview of the basic types of residual acceleration data processing that can be useful, including example plots. In order to make this more meaningful to the investigators, we have suggested specific data windows that should be of interest to them, based on the current mission timeline and our evaluation of their experiment sensitivity to acceleration. The use of such a plan will make the evaluation of the residual acceleration environment during a particular experiment considerably less time consuming than processing the entire accelerometer data base.

REFERENCES

[1] Alexander, J. I. D., Low-gravity Experiment Sensitivity to Residual Acceleration: A Review, **Microgravity Sci. Technol. III** (1990) 52.

[2] Rogers, M. J. B. and Alexander, J. I. D., Analysis of Spacelab 3 Residual Acceleration Data, **J. Spacecraft and Rockets** (1991), to be published May/June 1991.

[3] Rogers, M. J. B. and Alexander, J. I. D., A Strategy for Residual Acceleration Data Reduction and Dissemination, **Proceedings of the 28th COSPAR Plenary Meeting, Advances in Space Research** (1991) to be published.

[4] Rogers, M. J. B. and Alexander, J. I. D., Cross-correlation Analysis of On-orbit Residual Accelerations in Spacelab, **AIAA Paper 91-0348**, presented at the AIAA 29th Aerospace Sciences Meeting, 7-10 January 1991, Reno, Nevada.

[5] Rogers, M. J. B., Alexander, J. I. D., and Snyder, R. S., Analysis Techniques for Residual Acceleration Data, **NASA TM-103507**, July 1990.

AIAA 92-0244

Experiment Specific Processing of Residual Acceleration Data

M.J.B. Rogers and J.I.D. Alexander
Center for Microgravity and Materials Research
The University of Alabama in Huntsville
Huntsville, Alabama 35899

30th Aerospace Sciences Meeting & Exhibit
January 6-9, 1992 / Reno, NV

AIAA-92-0244

EXPERIMENT SPECIFIC PROCESSING OF RESIDUAL ACCELERATION DATA

Melissa J. B. Rogers and J. Iwan D. Alexander
Center for Microgravity and Materials Research
University of Alabama in Huntsville
Huntsville, Alabama 35899 USA

Abstract

A synthesis of experimental output and correlated accelerometer data is necessary for investigators to fully understand the results of low-gravity experiments. Both quantitative and visual correlation techniques can be used to determine the effects of quasi-steady and higher frequency accelerations on these experiments. In addition to improving our quantitative understanding of experiment sensitivity, the results of experiment and accelerometer data processing will lead to the systematic characterization of the Spacelab acceleration environment. This will enable investigators to plan their experiments so as to minimize residual acceleration effects and, therefore, take advantage of limited flight opportunities.

Modelling of low-gravity experiments has indicated that different classes of experiments are sensitive to different types of residual accelerations. Current space accelerometer systems measure high magnitude, high frequency, transient and oscillatory residual accelerations ($\leq 10^{-2}$ g, 0.1 - 100 Hz). Lower amplitude, low frequency ($< 10^{-4}$ g, < 0.1 Hz) accelerations due to atmospheric drag and gravity gradient effects are also present. These quasi-steady accelerations are generally overwhelmed in recorded data by transient and oscillatory accelerations. We will introduce a simple, passive accelerometer system developed to measure low frequency accelerations. The results of this experiment will improve our understanding of the quasi-steady accelerations experienced in the Spacelab with respect to both the general low-g environment and the effects on low-g experiments.

To test the idea that recorded acceleration data and experimental responses can be usefully correlated, we have produced model responses for experiments using actual acceleration data and made correlations between experiment response and the accelerometer time history. We have used Spacelab 3 accelerometer data as input to a variety of experiment models and have obtained sensitivity limits for particular experiment classes. These modelling results differ from earlier sensitivity estimates because the models use actual acceleration data in addition to simple sinusoidal and transient/pulse accelerations. The results of this type of modelling, order of magnitude estimates, and investigator input are being used to create experiment specific residual acceleration data processing schemes for interested IML-1 investigators. The detailed plan will help identify data windows to study, based on experiment sensitivity to accelerations and preliminary analysis of experiment results.

1. Introduction

A synthesis of experimental output and correlated accelerometer data is necessary for investigators to fully understand the results of low-gravity experiments. Both quantitative and visual correlation techniques can be used to determine the effects of quasi-steady and higher frequency accelerations on these experiments. The results of such correlations improve our understanding of experiment sensitivities to accelerations and allow us to develop a characterization of specific acceleration sources on orbiting laboratories.

Investigation of low-gravity experiments indicates that all types of residual accelerations can affect experimental results.[1-5] Unfortunately, low frequency data that may be collected with conventional accelerometer systems are overwhelmed by higher-frequency, higher magnitude g-jitter. We have, therefore, only been able to make numerical estimates of the magnitudes of quasi-steady accelerations. A simple, passive accelerometer has been developed, based on the concept of Stokes drag, that will be used to measure atmospheric drag and gravity gradient accelerations on Columbia during USML-1. The data collected will be used in conjunction with higher frequency acceleration data to map the low-g environment and for experiment - acceleration correlation.

The amount of residual acceleration data collected during a low-gravity mission is excessive. This makes the identification of interesting data windows and the processing of these windows difficult. We have, therefore, developed a residual acceleration data processing scheme that can be easily tailored for the analysis of a given space experiment. The plan will be used to select acceleration events from the data base that have the greatest potential for affecting the experiment being analyzed, and to process these data windows to best assess and characterize the acceleration environment. The resulting limited data base will be used to correlate acceleration events with experimental results.

An assessment of the use of the quantitative cross-correlation technique for experiment - acceleration data processing was presented at the 29th AIAA Aerospace Sciences Meeting[6] and is discussed briefly in section 2. The passive accelerometer is introduced in section 3. Section 4 includes an overview of the experiment specific data analysis plan and details of the processing techniques that can be used in experiment - acceleration data analysis.

2. Cross-correlation Analysis

Cross-correlation analysis has been identified as a viable means of assessing causal relationships between particular acceleration events and experiment results. This analysis technique is appropriate both for experiments sensitive to transient accelerations and for those sensitive to oscillatory accelerations.[6] It is a numerical process requiring both accelerometer and experiment data collected at the same sampling rate. In the case that regularly sampled data are not available, qualitative or unevenly sampled numerical data can be used to create a quantitative experiment data base using known characteristics of experiment-acceleration interaction.

We tested this technique on synthetic data representing the response of a directional solidification/melt convection experiment to acceleration data collected during the Spacelab 3 (SL3) mission. The experiment response was driven by a periodic acceleration imposed by the modelling process. A phase lag existed between the acceleration series and the experiment response, related to a "sloshing" effect of the melt. Cross-correlation analysis readily identified this periodic experiment response. The correlation between synthetic experiment and acceleration data including transient disturbances was also identified in our analysis.

3. Passive Accelerometer

A passive accelerometer has been developed to measure residual acceleration in an orbiting space laboratory caused by the atmospheric drag on an Orbiter and the gravity gradient effect related to the position of the accelerometer.[7] We expect these quasi-steady accelerations to have magnitudes in the micro-g range ($1\ g = 9.81\ ms^{-2}$) and frequencies on the order of the orbital frequency ($\leq 10^{-4}$ Hz). They cannot be extracted from the acceleration data collected with conventional accelerometer systems because of the relatively high magnitude and frequency background signals recorded.

The passive accelerometer is based on the concept of Stokes drag.[8] It consists of a fluid-filled glass tube containing a steel ball, Fig. 1. The system is attached to the Orbiter structure. When in use, the length of the tube is aligned with the Orbiter flight direction and the ball moved with a magnet to the distal tube end (relative to the flight direction). The ball is released and allowed to "fall" to the other end of the tube in response to the residual gravitational forces. The time required for the ball to travel a distance marked on the tube is measured. From this, and the fluid viscosity and ball size and density, the Stokes velocity and the residual acceleration experienced by the ball are calculated.

This measurement of the quasi-steady acceleration experienced in low-earth orbit will allow us to better assess the effects of residual acceleration on sensitive space experiments. These low frequency accelerations do not vary considerably between orbits at one location for a given mission. It is not necessary therefore, to take more than a few measurements at an experiment site during a mission. The use of this simple accelerometer will eliminate the difficult task of processing other recorded accelerometer data in an attempt to extract these accelerations from noisy, high magnitude, high frequency data.

4. Data Processing Plan

We propose a two level plan for the processing of residual acceleration data, to deal with the excessive amount of accelerometer data that results from typical low-gravity missions. This plan is outlined below.

Level One

1. Pre-flight identification of acceleration sensitivity to determine frequency and magnitude ranges of interest and experiment tolerance limits.
2. Pre-flight identification of times at which the experiment is liable to be most vulnerable. Some experiments may be most sensitive at specific stages, for example, protein crystal growth during the nucleation stage.
3. Preliminary post-flight analysis of experimental results to identify times when unexpected results occurred that may be related to perturbations in the residual acceleration environment of the laboratory.

Level Two

1. Selection of time windows of interest using a threshold detection routine based on sensitivities identified in Level One, Step 1 above.
2. Use of data decimation techniques, when appropriate, to reduce the number of data points needed to evaluate lengthy windows of data.
3. Specific analysis of windows of data identified in Level One and the first step of Level Two, including estimation

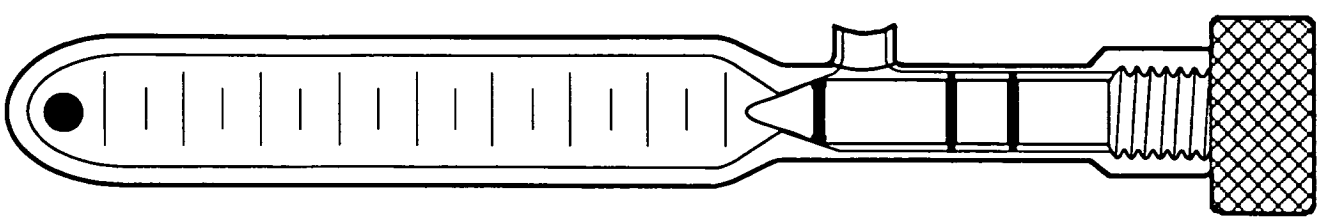

Fig. 1. Passive accelerometer.

of mean and mean squared values, determination of the acceleration vector orientation, and spectral analysis to investigate the magnitude of the frequency components for the specific time window of interest.

4. Evaluation of accelerometer data in conjunction with experimental results to identify causal relationships and revise sensitivity limits.

We addressed Level One processing in Rogers and Alexander (1991a & b).[9-10] Details of processing routines for Level Two analysis are discussed in this section.

4.1 Threshold Detection and Data Formatting

Segments of residual acceleration data which may be of interest to investigators can be identified by the use of a threshold detection routine. This is used to identify times when the magnitude of the recorded residual acceleration vector exceeds the sensitivity limits of a given experiment. It is assumed that the data represent, as accurately as possible, the residual acceleration environment that exists at the sensor location. This means that all temperature, instrument, and other biases should be properly removed from the data before analysis.

Specifics of this stage of processing include general data formatting, the calculation of various statistics, the formation of zero-mean series from the accelerometer data, the calculation of the acceleration vector magnitude, and the testing of the acceleration magnitude against sensitivity limits.

4.2 Fourier Transformation - Calculation of Amplitude Spectrum and Power Spectral Density

Fourier analysis is used to investigate the relative strengths of the frequency components of a given time series. Amplitude and power spectral densities give an indication of the dominant frequencies that compose the accelerations experienced at the sensor site. Specific frequencies are related to machinery vibration and rotation and structural modes of the Orbiter and Spacelab which are excited by a variety of internal and external sources.[9-12] A general outline of this stage of processing is:

- Read in three axes of zero-mean accelerometer data and transform each series into the frequency domain.
- Compute amplitude spectrum of each axis of data and normalize.
- Compute total magnitude of "amplitude spectrum vector" with a root-sum-square method.
- Compute power spectral density for each axis and total power spectral magnitude with a RSS method.
- Identify maximum valued frequency component from total magnitude information.
- Test total magnitude information against frequency domain limits, identify frequency and magnitude of occurrences over limits, and keep progressive count of these occurrences.

4.3 Rotation and Orientation

Rotation of residual acceleration data is necessary if the sensor heads are not aligned in the orientation of interest. It is necessary to know the angle of rotation between the existing and desired coordinate systems. Because we do not have detailed information about the acceleration sources, the structure of the vehicle and laboratory, and the nature of wave propagation through the structure, it is important to use acceleration data from the sensors closest to the region of interest.

The rotation convention that we use is as follows. When looking down a positive axis of rotation towards the origin, a counterclockwise rotation around that axis is considered positive. For both right- and left-handed coordinate systems, the following holds for positive rotations.

Rotation Axis	Direction of Positive Rotation
x	y into z
y	z into x
z	x into y

The acceleration components along the axes of a coordinate system of interest can be obtained from the original, recording axes by means of a transition matrix:

$$g_o = R_{oa}\, g_a .$$

The transition matrix R_{oa} is composed of direction cosines. R_{12} is the cosine of the angle between the x_o-axis and the y_a-axis in Fig. 2. The transition matrix can also be obtained through a change of vector basis. For a counterclockwise rotation:

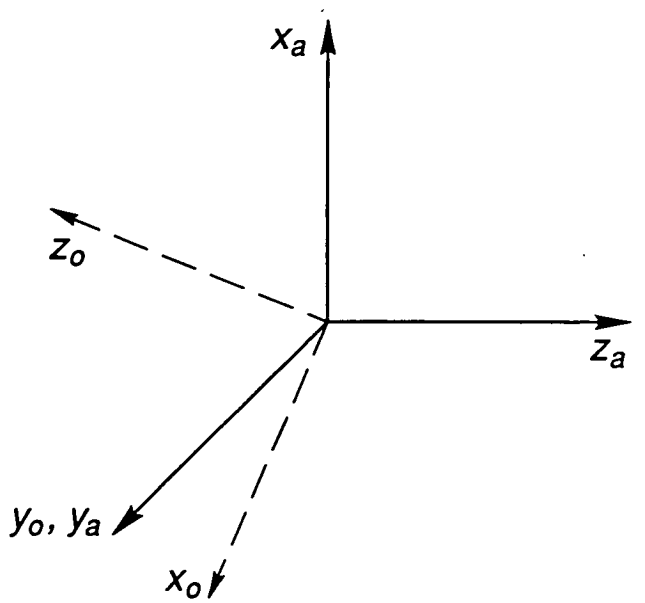

Fig. 2. Positive rotation of data from accelerometer coordinate system into Orbiter coordinate system. Rotation is about the y_a-axis.

$$R_{os} \rightarrow \begin{bmatrix} \cos\theta & 0.0 & -\sin\theta \\ 0.0 & 1.0 & 0.0 \\ \sin\theta & 0.0 & \cos\theta \end{bmatrix}$$

where θ is the angle of rotation.[13-14]

The change of vector rotation matrix is generally easier to program and is therefore used in our processing. The rotation angle about a coordinate axis is the only information input to the program. For situations where rotation is about some axis other than a coordinate axis, the direction cosine rotation matrix must be used.

The orientation of the residual acceleration vector with respect to some set of coordinate axes is important for experiments with known directional sensitivity. The orientation of a vector in rectangular coordinates cannot be represented by a single value. Direction cosines are computed to denote the orientation of a recorded acceleration vector with respect to a set of coordinate axes. This stage of processing involves the input of the three axes of zero-mean accelerometer data, calculation of direction cosines of the acceleration vector with respect to coordinate axes, and calculation of amplitude spectra of direction cosine arrays if desired.

4.4 Filtering

Digital filtering is applied to data to investigate the time series patterns and magnitudes related to particular bands of frequencies. We give an example of a Butterworth filter as used for lowpass filtering. The Butterworth lowpass filter can be represented as:

$$|H(i\omega)|^2 = \frac{1}{\left[1 + \left(\frac{\omega}{\omega_0}\right)^{2m}\right]}$$

where m is the order of the filter, see Fig. 3. A general rule of thumb is that the attenuation outside the filter passband (defined by ω_0) in dB per octave is approximately 6m.[15-16] This stage of the processing routine is:

- Read in the three axes of zero-mean accelerometer data and transform into the frequency domain using an FFT, normalizing if necessary.
- Form the Butterworth filter, programming the above equation. The length of the filter should be the same as the number of points in the amplitude spectrum.
- Apply the filter to the data by multiplication of the filter with the amplitude spectrum of the data window.
- Return to the time domain with an inverse FFT (with appropriate normalization) to get filtered time series.
- Compute the magnitude of the filtered acceleration vector with a root-sum-square method.

5. Summary

To date, most Spacelab residual acceleration data collection projects have resulted in data bases that are overwhelming to the investigator of low-gravity experiments. We have proposed several techniques that will help an investigator limit the amount of acceleration data needed for the analysis of

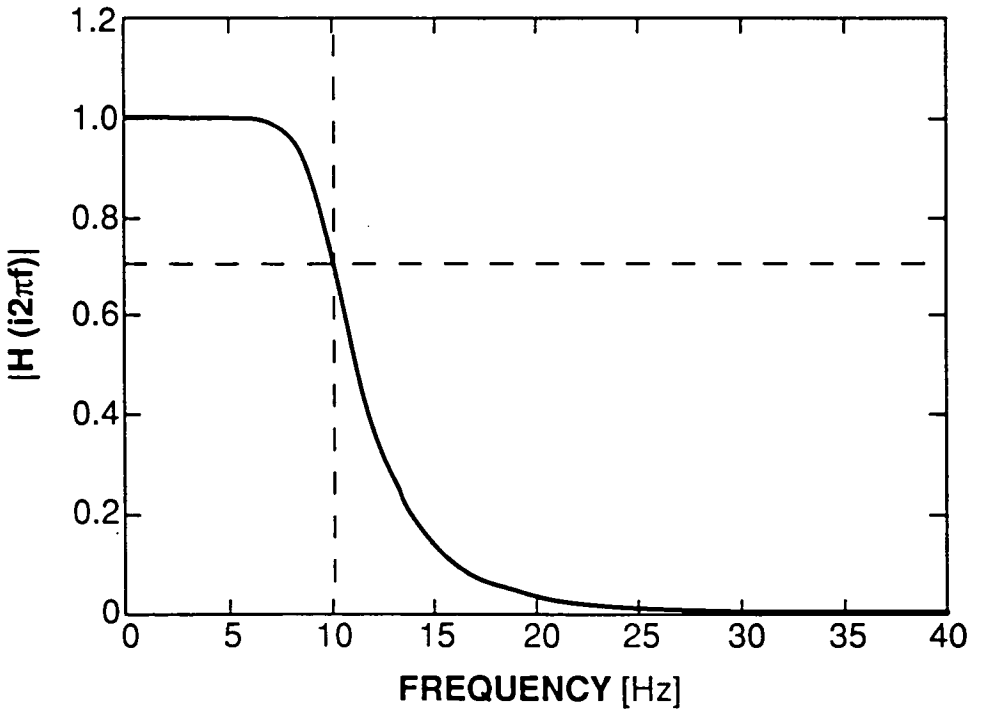

Fig. 3. Order m=5, 10 Hz lowpass Butterworth filter. Note that filter curve has value of $1/\sqrt{2}$ at the cut-off frequency.

experimental results. A general processing plan is being used to assess the data needs of principal investigators of selected experiments on the IML-1 mission. Cross-correlation analysis is useful for the analysis of experiment response to both transient and oscillatory accelerations.

A simple, passive accelerometer will be flown in mid-1992 to examine the quasi-steady acceleration level that is overpowered in data recorded with more conventional accelerometer systems. Because these accelerations do not vary much at a given location from one orbit to the next, this system will be able to map the quasi-steady acceleration environment of an orbiting space laboratory with a limited amount of data collection.

Acknowledgements

This work was funded by NASA through grant NAG8-759. We would like to thank Gary Martin, Bob Snyder, and Charlie Baugher for their continued support of our research and Lynne Carver for graphics support.

6. References

[1]Alexander, J. I. D. , Low-Gravity Experiment Sensitivity of Residual Acceleration: A Review, **Microgravity Sci. and Technol. 3** (1990) 52.

[2]Alexander, J. I. D., Ouazzani, J., and Rosenberger, F., Analysis of the Low Gravity Tolerance of Bridgman-Stockbarger Crystal Growth. I. Steady and Impulse Accelerations, **J. Crystal Growth 97** (1989) 285.

[3]Alexander, J. I. D., Amiroudine, S., Ouazzani, J., and Rosenberger, F., Analysis of the Low Gravity Tolerance of Bridgman-Stockbarger Crystal Growth. II. Transient and Periodic Accelerations, **J. Crystal Growth 113** (1991) 21.

[4]Monti, R., Favier, J. J., and Langbein, D., Influence of Residual Accelerations on Fluid Physics and Materials Science Experiments, in **Fluid Sciences and Materials Science in Space, A European Perspective**, ed. H. U. Walter (Springer, Berlin 1987).

[5]Nadarajah, A., Rosenberger, F., and Alexander, J. I. D., Modelling the Solution Growth of Triglycine Sulfate in Low Gravity, **J. Crystal Growth 104** (1990) 218.

[6]Rogers, M. J. B. and Alexander, J. I. D., Cross-correlation Analysis of On-orbit Residual Accelerations in Spacelab, **Proc. 29th Aerospace Science Meeting**, Reno, Nevada, 1991, AIAA Paper No. 91-0348.

[7]Alexander, J. I. D., Unpublished research, 1991.

[8]Alexander, J. I. D. and Lundquist, C., Motions in Fluids Caused by Microgravitational Acceleration and Their Modification by Relative Rotation, **AIAA Journal 26** (1988) 34.

[9]Rogers, M. J. B. and Alexander, J. I. D., Residual Acceleration Data Analysis for Spacelab Missions, **Microgravity Sci. and Technol.** (1991a), in print.

[10]Rogers, M. J. B. and Alexander, J. I. D., Analysis of Spacelab-3 Residual Acceleration Data, **J. Spacecraft and Rockets** (1991b), in print.

[11]Hamacher, H. and Merbold, U., Microgravity Environment of the Material Science Double Rack on Spacelab-1, **J. Spacecraft 24** (1987) 264.

[12]Chassay, R. P. and Schwaniger, A., Low-g Measurements by NASA, **Proceedings of Measurement and Characterization of the Acceleration Environment On Board the Space Station**, NASA / Teledyne Brown Engineering, 1986, Section 9.

[13]Anton, H., **Elementary Linear Algebra** (John Wiley, New York 1981).

[14]Frederick, D. and Chang, T. S., **Continuum Mechanics** (Scientific Publishers, Cambridge 1972).

[15]Båth, M., **Spectral Analysis in Geophysics** (Elsevier Scientific Publishing, Amsterdam 1974).

[16]Karl, J. H., **An Introduction to Digital Signal Processing**

Appendix C.

Analysis of Large Ill-understood Datasets Using a Combination of Techniques

Analysis of Large Ill-understood Datasets Using a Combination of Techniques

by

RANDALL PHIPPS WOLF

A THESIS

Submitted in partial fulfillment of the requirements
for the Degree of Master of Science
in
The Department of Computer Science
of
The School of Graduate Studies
of
The University of Alabama in Huntsville

Huntsville, Alabama

1993

ACKNOWLEDGEMENTS

The author would like to thank Dr. Hooper for the knowledge and effort he applied toward making this research possible. Similary, the author would like to thank Dr. Alexander for the opportunity to perform this research and his invaluable help during the effort. The author would like to thank Dr. Ranganath for his suggestions during the development of this thesis. Finally, the author would like to thank all the personnel at CMMR for their support during this research effort.

ABSTRACT

This research effort demonstrates the feasibility and necessity of a multidisciplinary approach to solving problems which involve large amounts of ill-understood data. A specific problem of this type which is concerned with acceleration information from orbital laboratories is analyzed using the disciplines of pattern recognition, data visualization, databases, Fourier analysis, and expert systems.

TABLE OF CONTENTS

LIST OF FIGURES

CHAPTER I
BACKGROUND AND INTRODUCTION

The purpose of this thesis is to investigate large, ill-understood datasets using pattern recognition, data visualization, database techniques, frequency analysis, and expert systems. The work is motivated by the need to analyze specific large residual acceleration datasets. Understanding of such ill-understood datasets is important because of the need to properly characterize the residual acceleration environment of a spacecraft in which low-gravity experiments are being conducted [1]. Since the purpose of many experiments is to minimize or eliminate buoyancy or weight effects, it is essential that the residual acceleration (or equivalent low gravity) be monitored and well-documented. Figure 1 is a simple illustration of the basic intent of the project.

In the rest of this chapter, the important attributes of the raw data to be analyzed is described. It is explained why large, ill-understood datasets will become more common; and, some of the problems associated with their handling are outlined.

1.1. Large Datasets

The amount of information describing a given object, process, or event is dependent, of course, upon the specific object, process, or event; but, as a result of recent improvements in hardware (specifically memory capacity), large datasets are becoming more common and sizes are growing rapidly as users attempt to stretch the limits of data collection and storage hardware [2]. Statistical methods provide some aid in analyzing such large amounts of data but do not always provide sufficient analytical capability. It can be expected that, at least for the present and near future, the capacity of the hardware used to collect and store data will often exceed the capacity of the hardware on which the data analysis is performed; i.e. the analysis hardware cannot cope with the original data set, much less the original data set and associated generated data sets. This is a problem that will persist, and effective methods to deal with it must be developed.

1.2. Ill-understood Datasets

Ill-understood datasets exist due to a combination of scarcity of useful information in the data, overabundance of data, and overly complex data. It is possible that the phenomenon in question is relatively simple but that the available information is incomplete. This situation is similar to attempting to complete a jigsaw puzzle that has pieces missing: it cannot be done. Alternatively, the phenomena may be simple, but the amount of information describing the problem is excessive and thus overburdens the

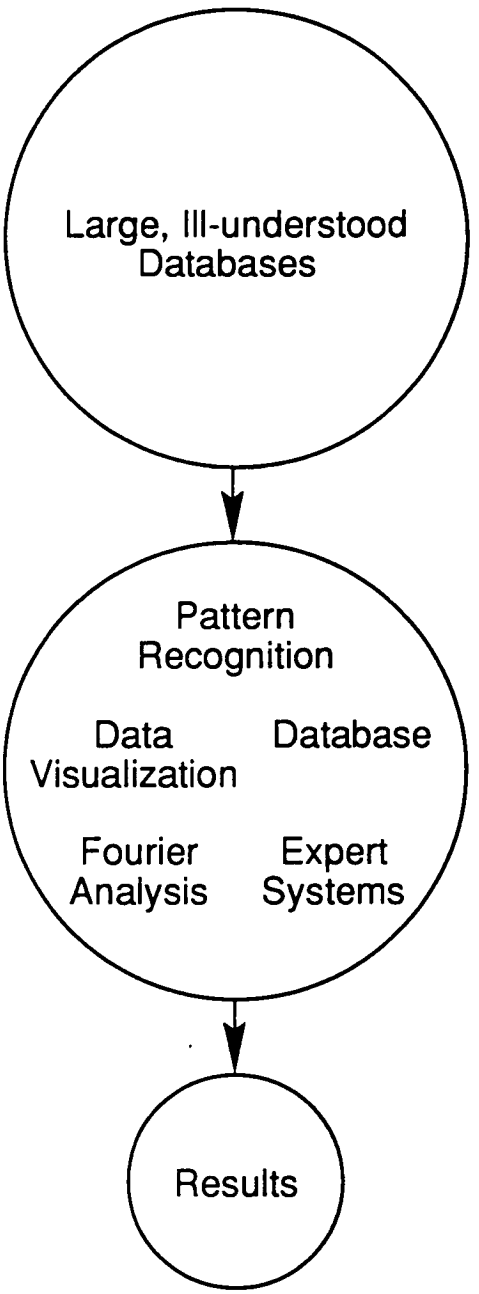

Figure 1. General concept.

available cognitive capacity. This situation is similar to attempting to complete a jigsaw puzzle which has an infinite number of pieces: it cannot be done. Finally, it is possible that the phenomena is complex, is completely described, and is described using a small amount of storage. This situation is similar to having a complete jigsaw puzzle with relatively few pieces, but the pieces are so complex that completion of the puzzle is a function of the raw intellect of the puzzle solver. Acceleration databases are ill-understood because they partake of all three of these characteristics. Incompleteness arises from the fact that the number of types of physical events which affect acceleration readings is unknown. Some are known but are not recorded. The excessive size of the data has been mentioned previously. The overly-complex nature of the accelerations arises from the lack of a closed form solution for most vibration problems.

1.3. Orbital Acceleration Characterization

Orbital laboratories provide a low gravity mission environment because the spacecraft is in a state of continuous "free fall". In the past, this low gravity environment was referred to as zero-gravity, microgravity, or even "milli"-gravity. This evolution in terminology reflects a growing awareness of the fact that the residual acceleration environment which arises in an orbiting craft is anything but zero-gravity. These accelerations arise from a number of sources which include atmospheric drag, spacecraft attitude , solar pressure, gravity gradient, tidal forces, crew activity, and experiment activity. Experiments in such a laboratory are designed to be conducted under a reduced "effective" gravity and thus are able to explore physical, chemical, and biological processes that were inaccessible on Earth. To accurately interpret experimental results it is important to measure and analyze the associated acceleration environment [1]. Figure 2 depicts some of these forces in relation to an orbiter.

The three classes of accelerations that an orbital laboratory can expect to encounter are quasi-steady, transient, and oscillatory. Quasi-steady accelerations are mainly attributed to the gravity gradient and atmospheric drag. Transient accelerations are typically abrupt, brief, high magnitude accelerations which stem from crew and spacecraft activity. Oscillatory accelerations are the vibrations of the spacecraft after it has been excited by transient, rotary, and quasi-steady accelerations.

All three types of accelerations can affect experiments. Some experiments may be susceptible to high magnitude transient acceleration. Others may be susceptible to acceleration in a certain direction. Still others may be adversely affected by a vibration at a certain frequency. Since space processing is extremely expensive, it would be advantageous to avoid compromising experiments due to unwanted accelerations, or at

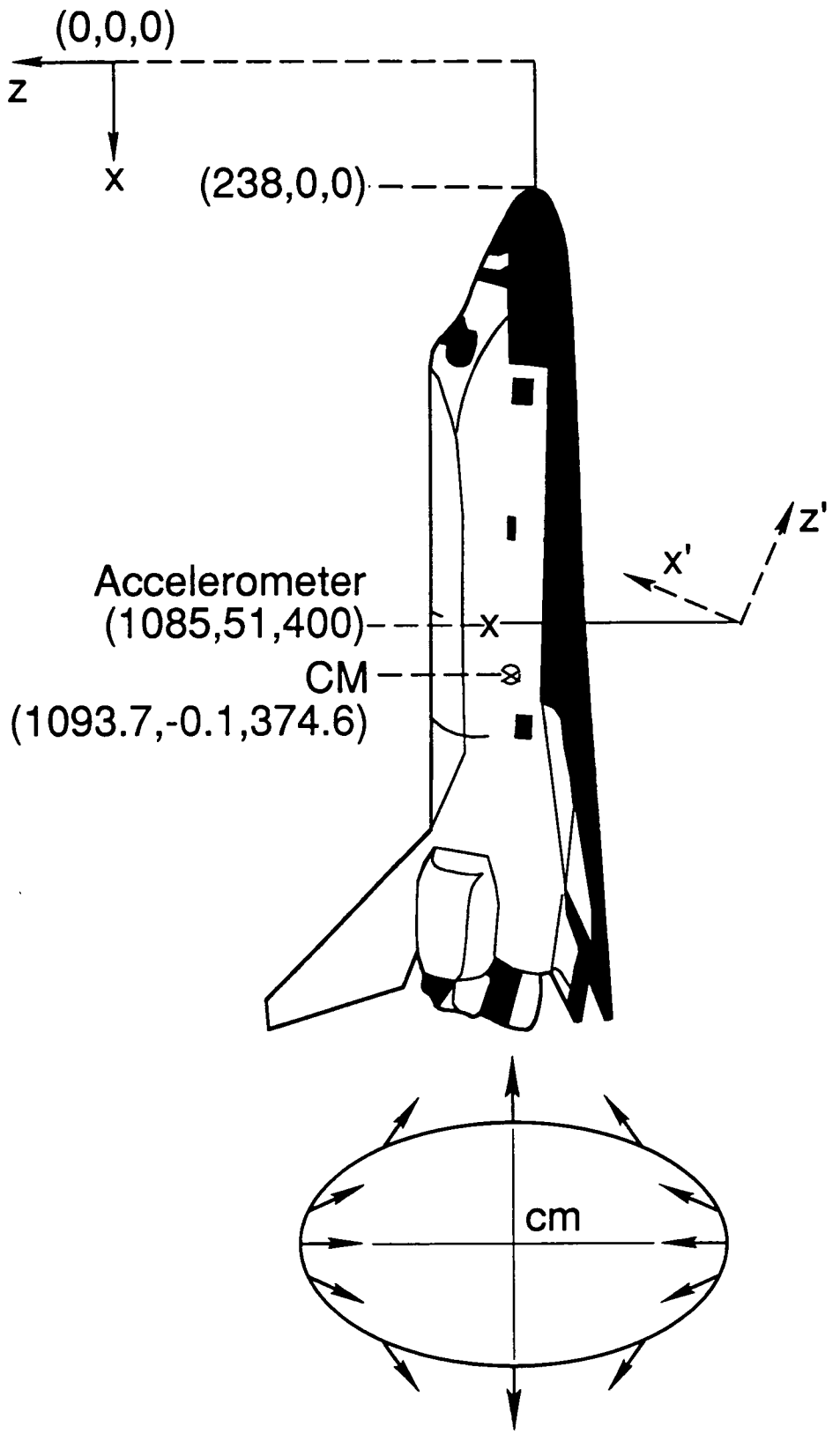

Figure 2. Orbital Acceleration Forces

least to be able to determine the time periods when a susceptible experiment was subjected to (possibly detrimental) acceleration and to determine the acceleration source. The latter would fall under post-flight analysis, while the former would fall under in-flight or pre-flight analysis.

1.4. SL-3 Acceleration Dataset

The Spacelab 3(SL-3) data set covers a 144 hour mission. Since each second produced 300 4-tuples of data, there are approximately 25 megabytes of data per half hour of the mission. This produces a total of approximately 4 gigabytes of raw acceleration information. Potentially there were other sources of information but in fact these sources were not available(thruster firing times, crew activity schedules, multiple acceleration sensors, etc.). These additional sources of information would be useful because they provide opportunities for analysis that would otherwise not be possible, but they would be detrimental in that they would increase the storage and computation load. The most important point here is that the analysis of such information must be able to proceed under non-optimal conditions with respect to computation and storage facilities.

The following chapters describe various aspects of the research effort. Chapter 2 describes the various techniques being combined in this work. Pattern recognition will be described in general, as will some of the more applicable techniques of pattern recognition. Data visualization is discussed in general terms and the specific forms of data visualization that are used in this work are introduced in detail. The various effects of database technology upon the processing of persistent data is investigated. Special emphasis is given to the impact of database technology upon the storage and processing strategies of the supporting software for this project. The utility of Fourier analysis for residual acceleration data analysis will be discussed in detail. Finally, the way in which expert system technology is used to assist the project will be covered.

An analysis of pattern recognition as it applies to acceleration databases is provided by Chapter 3. The unusual mapping of events to event information is described. The hardware and software configuration of PRIDE is detailed in Chapter 4. PRIDE is the name of the software package developed to aid in the analysis of the SL-3 data. PRIDE stands for "Pattern Recognition data vIsualization DatabasE". PRIDE is implemented upon the Ardent graphics mini-supercomputer utilizing the UNIX operating system and the X windowing system. A brief discussion of the practical details of using PRIDE is contained in Chapter 5. Chapter 6 discusses the results of applying the capabilities of PRIDE to SL-3 data and outlines improvements that need to be made to PRIDE in order to provide greater capabilities.

CHAPTER II
MAJOR TECHNIQUES

2.1. Pattern Recognition

Pattern recognition involves the determination of the basic characteristics of structures or patterns implicit in a dataset without depending upon knowledge concerning the source of the data. Since one of the two overriding characteristics of the datasets defined to be of interest here is "ill-understood" data , pattern recognition will play a critical role in data analysis.

Pattern recognition has been used in many disciplines in order to achieve useful classification. One example is the technique used to perform optical character recognition of bank checks. In this case there is a known, finite number of patterns that produce unique responses when subjected to the recognition technique. This automatic process provides a vastly more reliable and efficient means of checks processing than previous manual methods. The fingerprint matching process used by the FBI also relies on pattern recognition. Fingerprints obtained at a crime scene are subjected to a reduction process which removes all extraneous information-i.e. information superfluous to the identification process. Then a search is undertaken for a match between the unknown fingerprint and search candidates which are taken from previously reduced fingerprint datasets. This ability to utilize fingerprint information is vital to modern law enforcement [3].

The above two examples of pattern recognition are fairly simple. For the first example, feasibility is dependent upon the fact that there is a very small number of possible patterns and that each pattern is known. The second example is dependent upon the fact that the number of possible patterns is finite (although large) and that search candidates are known. The other characteristic of the second technique is the use of dimensional reduction upon the input data. Dimensional reduction uses only significant portions of the pattern vectors which describe events.

Unfortunately, there is not always a known number of patterns, a known number of classes of patterns, or a known technique for matching example patterns to their classes. Three ways in which this more difficult problem may be tackled involve supervised pattern recognition, unsupervised pattern recognition, and syntactic pattern

recognition. It should be noted that these categories are by no means exhaustive or mutually exclusive.

2.1.1. Supervised Pattern Recognition

Supervised pattern recognition is the use of a "teacher" to guide pattern recognition. This "teacher" may take the form of a human being interacting with the computer in order to link pattern to class or it may take the form of a set of matchings between patterns and their respective classes. The assumption in this case is that there exists a certain amount of knowledge concerning the relation of the patterns to the classes of patterns. If there is a priori comprehensive knowledge concerning the classification process then the more difficult part of the pattern recognition problem is solved. The creation of an efficient procedure for extracting events from the database would still need to be developed.

Supervised pattern recognition may be based upon several different types of knowledge concerning the sample set. For example, the number of classes may be known but the linkage of patterns to particular classes may not be known. The likelihood of events falling within certain classes may be known in advance. We may know the similarity between patterns in the dataset but not the relationship between patterns and classes. It is this final form of knowledge that is used by PRIDE to aid in the classification of acceleration samples.

PRIDE supervised pattern recognition is provided by a combination of visualization and database techniques. Since absolutely no knowledge about the characteristics of acceleration samples is known by PRIDE, all supervisory linkage information is provided via human operator through a process of viewing graphics of the samples and entering opinions into the database by a specialized database query X interface. The types of graphics available are both animated and static two-dimensional and three-dimensional color representations of the samples. This form of recognition is not meant to be deterministic but rather to be heuristic. The capability for several different and possibly contradictory classifications is available.

2.1.2. Unsupervised Pattern Recognition

Unsupervised pattern recognition is applicable when very little is known about the data samples. The specific form of unsupervised pattern recognition provided by PRIDE is the ISODATA algorithm. ISODATA is a well-known algorithm which, when provided with a completely unknown dataset, not only determines the number of classes, but also determines the mapping between patterns and their respective classes [4,5,6]. The

standard ISODATA algorithm assumes the presence of a human operator in order to guide the classification process. Despite this, ISODATA is normally considered to be an unsupervised pattern recognition technique [3].

PRIDE also provides a variant of ISODATA which consists of ISODATA being controlled by a CLIPS expert shell which acts as a surrogate human and helps to alleviate the disadvantages of the ISODATA algorithm. CLIPS (C Language Production System) is a rule-based forward inferencing expert system shell produced by the Artificial Intelligence Section at NASA/Johnson Space Center.

The CLASS algorithm which is a variant of ISODATA was tested during the development process of PRIDE and was found to have both advantages and disadvantages [7]. The advantage was the technique for making an initial guess concerning the number and location of patterns. This initial guess allowed CLASS to start from a more reasonable starting state than ISODATA. CLASS assumed $2^n + 1$ clusters. One cluster center was located at the center of all data points. The other 2^n centers were located at the 2^n points created by adding the positive and negative standard deviations for each dimension to the center point. The literature on ISODATA does not define a technique for assigning initial cluster centers. The disadvantage was the forcing of the algorithm to converge. This was achieved by continually modifying the split and merged parameters. The modification was used to make cluster modification impossible after a given number of iterations. The convergence that was forced was not of sufficient quality and thus it was decided that the disadvantages of CLASS outweighed the advantages of CLASS. Thus, CLASS was not included in the final version of PRIDE.

2.1.3. Syntactic Pattern Recognition

Syntactic pattern recognition is applicable when the raw data, or some set of attributes generated from the raw data, are definable as elements of a language [3,8,9]. When this is possible, the classes of the raw data are equivalent to the possible sentences of the language. Unfortunately, time constraints during the development of PRIDE have precluded the presence of syntactic pattern recognition within the present version. It is felt that syntactic pattern recognition has the potential to provide a more finely honed characterization of the behavior of acceleration activity.

2.2. Data Visualization

Data visualization is the utilization of recently developed graphics capabilities to better display images of data sets [10]. Such visualization has been used in many disciplines such as physics, chemistry, biology, and management in order to allow users

to comprehend data that otherwise would merely serve to confuse. These recently developed graphics capabilities arise from advances in the basic understanding of the process of visual image generation and from constantly-improving display technologies.

PRIDE uses data visualization in order to gain basic understanding of the structure of acceleration events. PRIDE applies visualization to individual events and to groups of events to create graphic displays containing information solely about one given event and displays containing information concerning several events. PRIDE presently depends on the capabilities of the Ardent 1500 graphics mini-supercomputer to produce these displays. These capabilities consist of the rapid drawing speed inherent in the system, the X11R3 network graphics windowing system, and the DORE graphics package[11,12].

2.2.1. Photorealistic Three-Dimensional Graphics

Recently, the speed and cost of three-dimensional graphics has become such that its use is practical and widespread. Human beings see the world in three dimensions with a large variety of supportive information such as shading, color, texture, and transparency. Displays which provide this kind of information are inherently more capable of expressing the range of visual information to which the human eye is accustomed than older, less-capable displays. When the information of interest is inherently three-dimensional the match of the display data, the display technique, and the human eye is particularly strong. The raw orbital acceleration data is inherently three dimensional, as is at least one representation of the Fourier information of acceleration events. This capability for photorealistic three-dimensional graphics is provided by the Ardent hardware in conjunction with the DORE graphics package. PRIDE presently uses the three-dimensionality, shading, color, and transparency capabilities of DORE.

2.2.2. Animation

Animation is the use of graphics to display a sequence of related frames of a scene. Animation provides the ability to see the interrelation of visual structures over the range of the independent variable. Normally, this sequence of frames represents the evolution of the event with time. When the process of interest can be expressed as a function of one or more independent variables, then animation is of use. The raw acceleration signal recorded at a given location x will vary in magnitude and orientation, or $a(x,t)=(a_x(t),a_y(t),a_z(t)$. The ergodic analysis technique produces information concerning window energy values that is a function of window size. Animation using window size as the independent variable can be used to display ergodic analysis results.

The capability for animation is provided by the base graphics capabilities of the Ardent in conjunction with DORE and X [13-17]. Three-dimensional animations are produced using DORE while two-dimensional animations are produced using X graphics. PRIDE does not presently use an animation language to produce its associated animations.

2.2.3. Hierarchical Graphics

Hierarchical graphics use database techniques to aid in the creation and maintenance of a given image [18]. Each object that affects the display--whether it is a visual object, a light, a camera or some other more primitive or more complex object--is placed within a graph structure. This graph structure contains all the information needed to produce a full drawing. Typically such graphs contain a light source, a camera, and at least one object(see figure 3). An ordered visitation (traversal) of the nodes of the graph at drawing time provides the drawing algorithm with the necessary information to create the desired visual image. These graphs must not contain cycles in the traversal path and are thus hierarchical.

In database terms, the graph structure is the database. As opposed to normal databases, the information store is kept in random access memory rather than disk. The structure comparable to a dataset is a subgraph of the overall graph.

Only some of the characteristics of a database are met by a hierarchical graphics system. Reduced redundancy of information is provided by the approach that whenever a given object is required in the image a link to that object is inserted rather than a copy of the object. Timely generation of information is provided in that an object in the image graph may be a procedure. Thus during the traversal process for building the image, when that node is "hit", a user-defined procedure is executed which may modify the graph dynamically. Since the database is so fluid, the ability to react to changes is strong. Concomitantly there does not exist a formal definition of the datasets, nor does there exist keyed access to graphics information. Concurrent access to an image is provided under PRIDE. This is possible since DORE provides the hierarchical graphics capability for PRIDE and DORE is built on top of X. X allows multiple processes to access the same window. Thus, concurrent, multi-user access is possible.

2.2.4. Graphical User Interface

Graphical user interfaces (GUIs) are a technique combining text and graphical output with input devices such as locator, keyboard, choice, and 3D interaction devices in order to provide the user with a more intuitive and rapid means of controlling activity

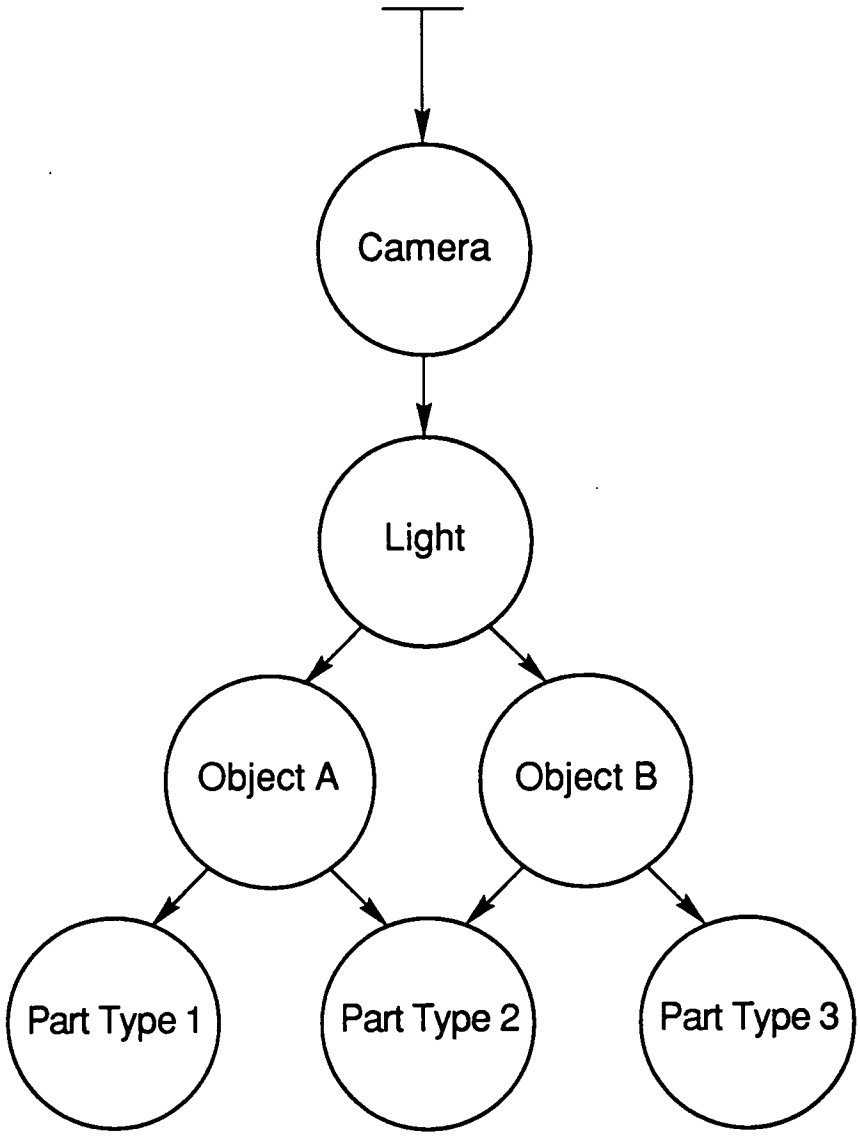

Figure 3. DORE graphic database.

[19]. Figure 4 shows an example of a screen for a GUI. Locator devices include mice, data tablets, and trackballs. An example of a choice device is a set of function keys. 3Dinteraction devices include the Polhemus 3D sensor, spaceball, and Dataglove. A dataglove is a glove fitted with sensors in order to sense hand and finger movements. Typically, GUIs function in a multi-window environment. GUIs increase productivity because the system is easier to use and easier to learn. Selection activities are facilitated using a mouse rather than a keyboard and are thus more rapidly performed and put less demand on the user's memory. A keyboard is used for some operations that are easier to control in that fashion. Operations concerning spatial relations are more accurately and rapidly controlled by analog devices than by a keyboard.

A User Interface Manager (UIM) is a tool used by the developer of systems to provide graphic user interfaces. UIMs provide a formal definition of the normal activity of the interface. UIMs allow for the rapid creation and modification of user interfaces.

PRIDE uses the Athena widget set on top of the X11R3 network graphics windowing system to provide these GUI capabilities [20-22]. A number of new widget types have been created to provide greater functionality to PRIDE. Specifically, a mouse is used to perform selection and spatial activities. Keyboard input is used whenever alphanumeric input is more appropriate. DORE provides a pick capability to allow a user to use a mouse to pick a specific object, but PRIDE does not presently take advantage of this capability. PRIDE does not presently have an available UIM.

2.3. Database

Database technology provides for the efficient and dependable use of stored information [23]. Both of these characteristics are important for analyzing any database, but are particularly critical for large, ill-understood databases. Efficiency is relatively more important for large, ill-understood databases than for more normal sized databases. A relatively slow method of accessing this large data size may make it impossible to complete the analysis. Dependability is relatively more important for large, ill-understood databases than for normal databases due to the relatively larger amount of time it takes to load raw data into the large, ill-understood database.

The database management system used by PRIDE is CDATA [24], which is a relatively simple relational database written in C for which the source code is available. Availability of the souce code provided the critical ability to tune and modify the database management system's functionality while the fact that the source code was written in C yielded improved compatibility with the rest of PRIDE.

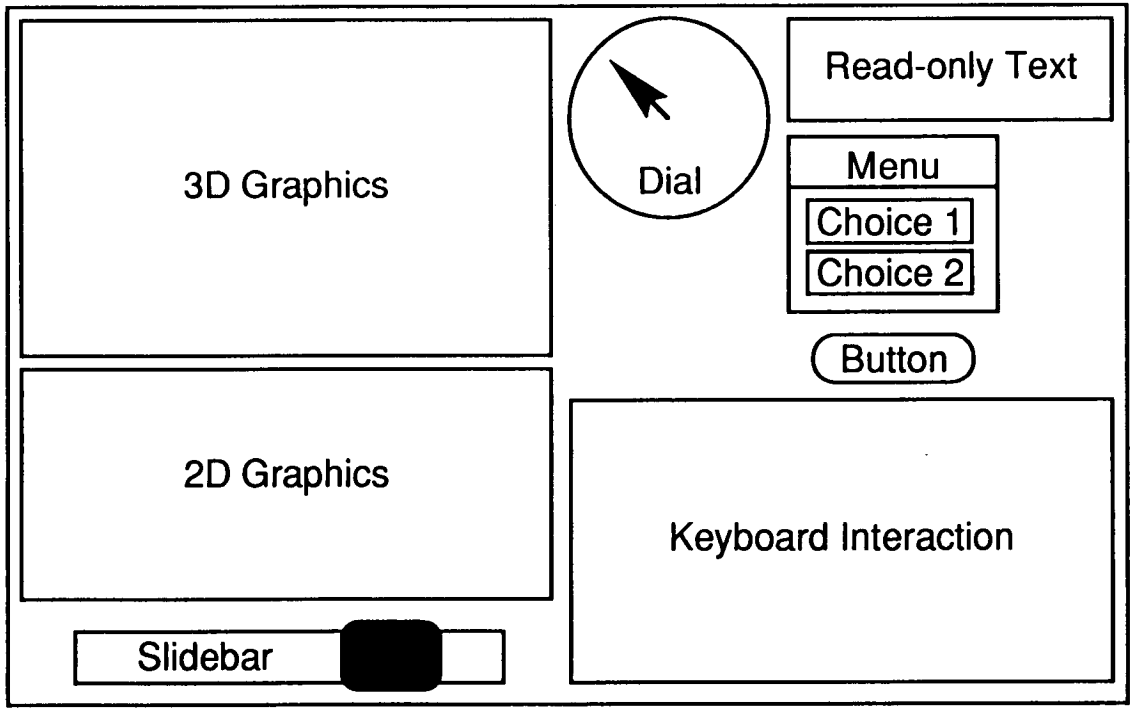

Figure 4. GUI example.

2.3.1. Efficiency

Database management systems (DBMSs) provide efficiency in the storage and processing of data. Storage efficiency stems partly from the fact that one of the precepts of database technology is that a given item of information appears in only one place. Compare this philosophy of non-redundant storage of information to a set of programs which all have their own copies of the same raw information. If the size of a single copy is significant, then the storage requirements for the non-database form may be excessive.

Storage efficiency is also enhanced by the practice of not storing information which is not basic or is easily generated. The classic example of this type of efficiency is the storage of the age of a given object. The age of an object changes from day to day and year to year. The database conceivably could periodically update this age tag on an object, but this would not only require the disk space into which to put the age, but it would also require the CPU time to perform the updates. The alternative is to produce the age of an object on demand, which is done by retaining a creation time for the object and then using that to calculate the age of the object when the age is requested. Note that this timely generation of non-basic information may imply the generation of much more complex temporary structures. This occurs during user interaction with external views in the ANSI/SPARC model[23]. ANSI/SPARC stands for American National Standards Institute/System Planning and Requirements Committee. Another form of storage efficiency commonly provided by databases is data compression.

The final form of storage efficiency listed here is the ability of a database to react to changing requirements and changing available resources. Since the data structures of the datasets making up the database are formally defined, they may be readily changed. This capability is critical for PRIDE since the available disk space is limited, it can be expected that the number and types of datasets will change, and it is simply impossible to completely reload the database every time a change is made. Reloading is impossible since it takes a full day to transfer 30 minutes of SL-3 information from tape to the VAX to the Ardent. There are approximately 144 hours of information for SL-3 and thus a significant sample would be around 40 hours. This takes 80 days or approximately 3 months to load. Practically speaking, this can only be done once. The CDATA database system, after appropriate modification, is used to store the acceleration data and associated data.

Efficiency of processing is aided by the efficient storage of information. The fact that an item of information occurs in a single location means that an update of that item requires only one search-write operation. The fact that certain information is generated

on demand does imply a processing time penalty for such requests, but also implies processing and storage savings for information that is never requested. The indexing capability of databases provides for decreased search times for constrained information. The data description and data manipulation facilities of databases, in conjunction with indexing, allows for the rapid generation of new datasets based upon the old datasets.

CDATA provides some but not all of these forms of efficiency. Reduced redundancy storage is provided, but demand-generated data is not. CDATA does provide a data definition language but it does not provide a data manipulation language. There are C functions that are part of the database code which provide data manipulation capabilities. Processing efficiency is provided by reduced redundancy, by data definition, and by data manipulation capabilities.

2.3.2. Dependability

Database management systems provide dependable usage of stored information under several situations. One situation is when certain datasets are being used by several users. If every user has a personal copy, there is an increased probability of error occurring during the update of information in the subject datasets. Dependability can also be increased by the use of the formal definition of the structure of the datasets. Dependability is also increased because more constraints are required to access and modify database information. Since databases generally maintain compliance with the entity integrity and referential integrity rules, the incorporation of inaccurate information into the database is further reduced. The entity integrity rule states that "No component of the primary key of a base relation is allowed to accept nulls". In simpler terms, this specifies that every object in the database must be unique. The referential integrity rule states that "The database must not contain any unmatched foreign key values". This rule means that no object in the database may refer to an object that does not exist and/or is not unique.

Security procedures and backup facilities also enhance the dependability of databases. Finally, the data definition and data manipulation languages of the database provide modification and recovery capabilities. CDATA provides dependability via reduced redundancy, its data definition language, and its adherence to the entity integrity and referential integrity rules.

2.3.3. ANSI/SPARC Model

The ANSI/SPARC model is a general definition of the structure and capabilities of a database. It can be used as a base definition against which database management

system implementations may be compared. The ANSI/SPARC model defines a database to consist of three levels. The lowest level is the internal level, which defines the physical layout of the database. The middle level is the conceptual level, where the data takes it's most natural form in the eyes of the average user of the database. The top level is the external layer with which the majority of users of the database interact. This external layer consists of a number of views each of which is associated with a specific user. In the same sense that the conceptual layer restructures the internal layer, the external layer restructures the conceptual layer. Specifically, each external view has been tailored to a given user. Figure 5 displays the interrelationships of the components of the ANSI/SPARC model.

In terms of the ANSI/SPARC model, CDATA only implements the external layer. However, PRIDE can be viewed in three different ways in terms of ANSI/SPARC. The raw acceleration data could be viewed to be wholly outside the database, and the extracted windows, FFT spectra, and classifications viewed as the internal layer. Alternatively, the raw acceleration data could be viewed as an offline part of the internal layer. The other datasets would be viewed as being internal. The final way to match PRIDE to ANSI/SPARC is for the raw acceleration data to be considered to be offline-internal and the other datasets to be online-conceptual.

2.3.4. Relational Databases

An intuitive definition of a relational database is that a relational database is a set of tables. Each table has a fixed number of columns and each column within a table contains information different from every other column within that table. Each individual table may or may not have one or more associated orderings of the rows of the table. An ordering is accomplished by designating certain columns to be used as a key. That is, by concatenating certain fields within the rows in a given order, a lexical ordering is imposed upon the entries in the table. Other orderings may be achieved by changing the order of the key fields or the selected fields. Figure 6 produces an example of a simplified relational database.

New tables may be generated from the existing tables of a relational database using the concepts of either relational algebra or relational calculus. Relational algebra applies set operations to the existing tables to generate the new tables. There are many relational algebra operations, but the minimal set consists of restriction, projection, product, union, and difference. Figure 7 gives example of each of these operations. Restriction consists of creating a new table by restricting the new values to consist of only certain rows of the original table. Projection consists of creating a new table by including

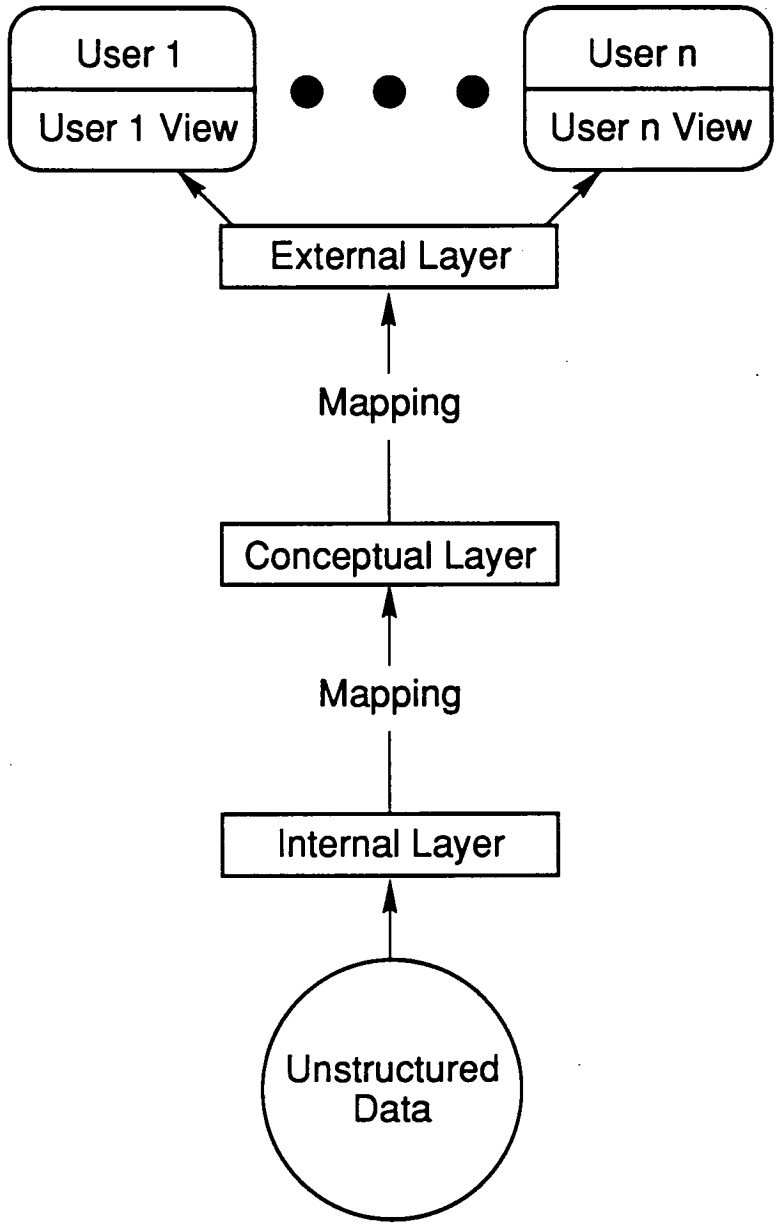

Figure 5. ANSI/SPARC model.

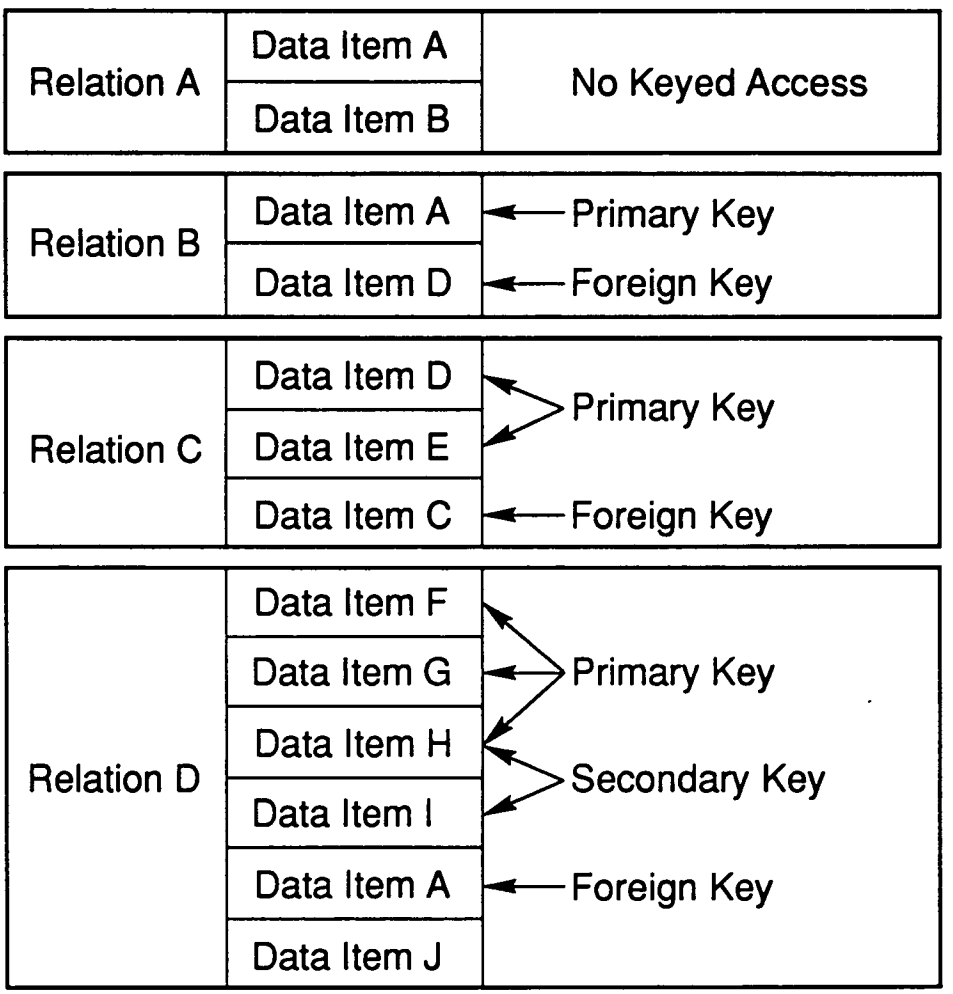

Figure 6. Example of relations.

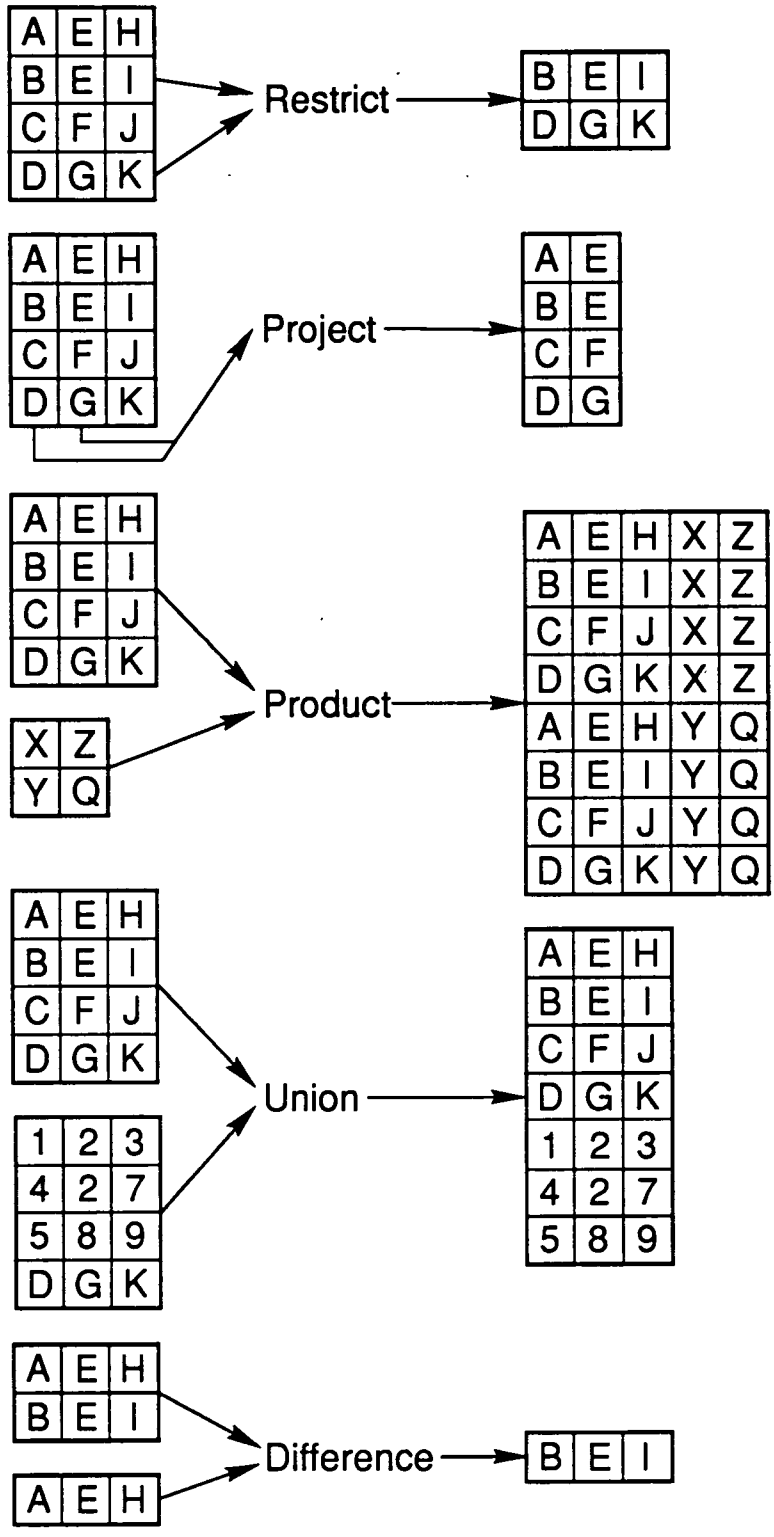

Figure 7. Relational database operations.

all the rows of the old table while retaining only certain columns. Product produces a new table using the Cartesian product operation. Union makes a new table by adding all tuples from two beginning tables to create the target table. Difference makes a new table by taking tables A and B and creating a table C which contains all entries in A that are not also in B. Note that all of these new tables are also relations. Relational calculus is the application of predicate calculus to the generation of new tables. It has the same power as relational algebra. It allows the application of formal logic to manipulation of relations.

The CDATA DBMS is relational but does not generally provide the operations of relational algebra or relational calculus. A primitive form of restrict and project are available at the source code level. Note that, in a certain sense, the goal of PRIDE is to provide a restrict operation to locate the tuples of high energy events.

2.3.5. Multi-User Concurrent Access

One of the advantages of databases is the potential sharing of common information. More than one individual may work on the same information without experiencing inefficiency of access and processing or experiencing data integrity problems. Additionally, the way in which any given user perceives and interacts with the database may be tuned to the requirements of that user. This tuning provides convenience to the user because the environment is arranged so that the user obtains the needed information yet it provides security to the database as a whole because the user is prevented from performing actions detrimental to the users of the database.

Another advantage of databases is access to the same information at the same time. Concurrent access allows many individuals to perform useful database activity simultaneously, which is necessary when the work to be done is more than one person can do in the allotted time, and is often convenient in any case.

CDATA provides neither a multi-user capability nor a concurrent access capability. The normal operation of PRIDE is such that a marginal amount of apparent concurrent access is provided. In general, database activity in PRIDE must be performed sequentially .

2.4. Fourier analysis

Fourier analysis is a technique for analyzing functions [8], and is based upon the use of the Fourier transform. The following is the one-dimensional Fourier transform:

$$F(u)=\int_{-\infty}^{\infty} f(x)e^{-j2\pi ux}dx \qquad (1)$$

Well-behaved functions may be analyzed using this continuous form while less well-behaved or unknown functions are typically analyzed using the discrete Fourier transform [25]. The following is the discrete one-dimensional Fourier transform:

$$F(u)=\frac{1}{N}\sum_{x=0}^{N-1} f(x)e^{-j2\pi ux} \qquad (2)$$

Note that x is the independent variable and f(x) is the dependent variable of the original function. The symbol j is $\sqrt{-1}$ and thus this integral is a complex function of u. For analysis purposes, |F(u)| is normally treated as the dependent variable with u being the independent variable. The variable u is the frequency and |F(u)| is the magnitude of the frequency. Thus, the Fourier transform is said to convert a function in the spatial domain to an equivalent function in the frequency domain.

There are many ways in which Fourier analysis is useful. Two of these uses will be described here. The first general category of utility arises from the fact that any operation that may be performed in one of the domains has an associated operation in the other domain. A Fourier transform pair is indicated by the following equation:

$$f(x)*g(x)=F(x)+G(x)$$

where F and G are given by (1) and (2). The operations * and + are not meant to indicate multiplication and addition, but rather two unique variable operations. This is useful because if the goal is to perform f(x)*g(x) then it may be more efficient computationally to transform f(x) to F(x) and g(x) to G(x), perform the + operation, and transform F(x)+G(x) back to the spatial domain than to directly perform f(x)*g(x). For example, the correlation between two functions in the spatial domain has an associated operation in the frequency domain. For large data sizes, it is more efficient to work in the frequency domain representation than it is to work in the spatial domain.

Fourier analysis is also useful is when the interest of the investigator is focused upon the frequency behavior of the function. One situation where this may occur is when the digital data describing the function is noisy. When this happens, it is sometimes possible that the noise imposed upon the actual function is primarily composed of a certain frequency. Removal of this noise frequency removes the noise from the function. Analysis of the function is easier at this point. PRIDE does not presently utilize Fourier analysis to control noise. Another situation in which Fourier analysis is applicable is when the frequency content of the function is known to be useful knowledge in and of itself. An example of this is when a given vehicle contains equipment which is sensitive to certain vibrations. For example, a space vehicle may have electronic equipment vital to its continued existence which could be damaged by certain vibrations. The vibrations that are presently in existence in the space vehicle are therefore of interest. Fourier

analysis is used by PRIDE to analyze the frequency composition of high energy events. One method of categorizing such high energy events is to use frequency composition to differentiate between these events.

2.4.1. Standard *Fft*

The raw acceleration data consists of 4-tuples associating a given mission-elapsed time with a_x, a_y, and a_z acceleration. These tuples are grouped into high energy events by vibration windowing. Fourier analysis is applied to the acceleration data associated with these high energy events. Since each acceleration series associated with a particular dimension is a function of time, there are three Fourier transforms for each high energy event. This frequency information is stored in the database and used for classification purposes.

2.4.2. *3dfft*

One of the unique aspects of PRIDE is the ***3dfft*** visualization algorithm, which is designed to combat some of the difficulties associated with using Fourier data. The ***3dfft*** algorithm allows the user to see the interrelations of any number of FFTs simultaneously. Since all information is plotted at one time, the user is not subjected to the harrowing process of shuffling many sheets of FFT plots in order to find similarities and dissimilarities.

The ***3dfft*** takes FFTs for a given acceleration window and produces a three dimensional representation of those FFTs. The original data consists of three functions of time; i.e. $a_x(t)$, $a_y(t)$, and $a_z(t)$. Thus, for any acceleration window there are 3 FFTs, each of the same frequency range and frequency delta. Each specific frequency has an associated 3-tuple consisting of the magnitudes from each function for that frequency. Each tuple is considered to be a point in three dimensional space. A sequence of connected line segments is drawn from one point to another, starting with the lowest frequency and ranging to the highest frequency for a given window. Figure 8 shows a depiction of this form of information display. This three dimensional graph contains all the information present with the three two-dimensional plots normally used to describe the FFT information associated with a given time window. When multiple windows are subjected to this process and plotted on the same screen, a visual representation of the frequency characteristics of all events is obtained. If the frequency information associated with events serves to differentiate the events into discrete classes, then this fact should be apparent on the composite screen.

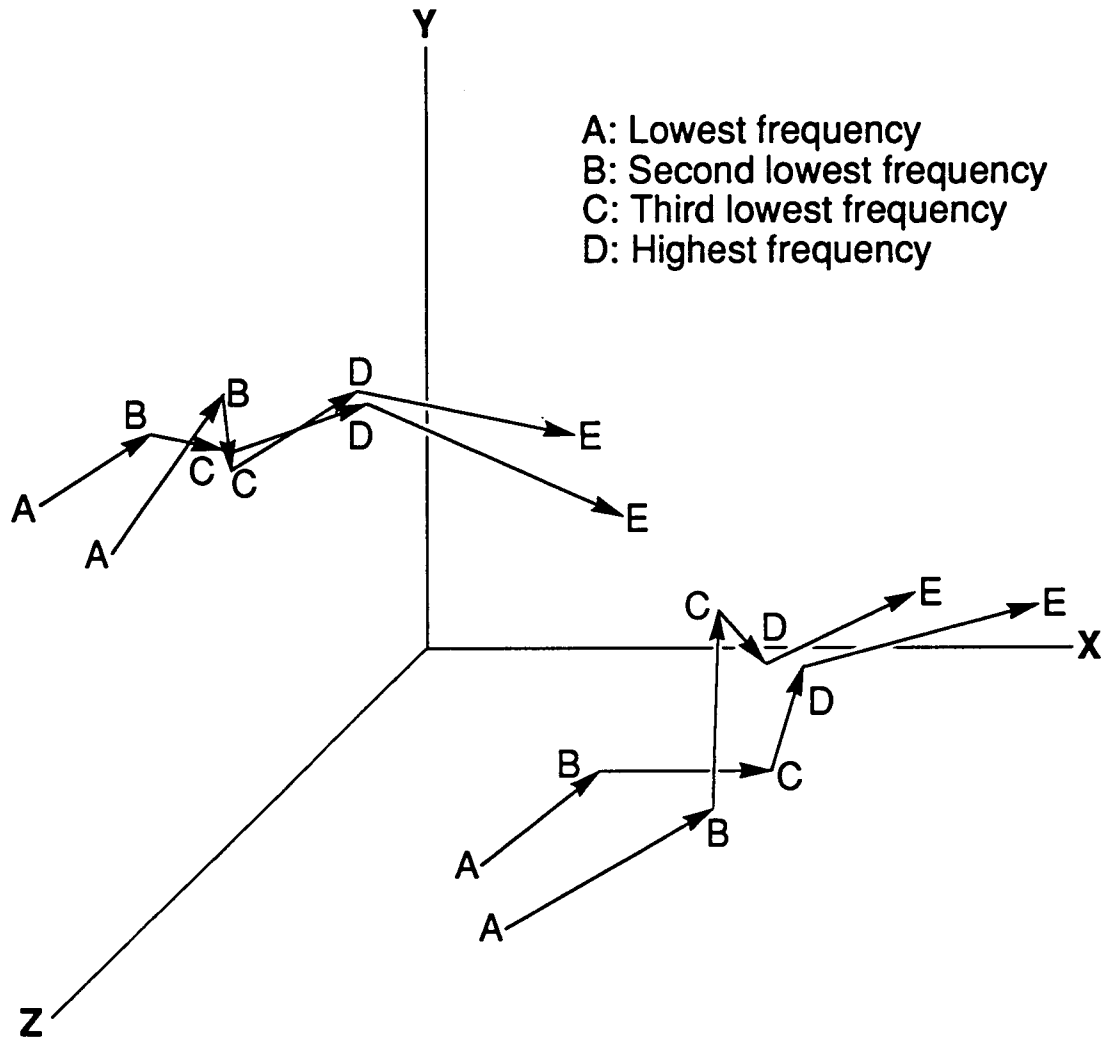

Figure 8. Example of 3dfft.

2.5. Expert Systems

Expert systems use knowledge and knowledge manipulation to acquire new knowledge [26]. Expert systems are usually crafted to be able to mimic the responses of a human expert. The range of disciplines that expert systems may be applied to is unlimited. Expert systems have been created to perform in fields ranging from prospecting to agriculture to pollution control to speech understanding. PRIDE presently uses the CLIPS expert system shell to imitate the activity of an expert in the use of the ISODATA program [27,28]

2.5.1. Controller of Unsupervised Pattern Recognition

PRIDE provides the ability to let an expert system control the function of the ISODATA program. This is an attractive capability due to the amount of time required to run the ISODATA program and the large amount of information produced by ISODATA. Both of these disadvantages make it difficult for the ISODATA algorithm to be used interactively despite the fact that ISODATA is designed for interactive use.

2.5.2. Discovery Mode

This is a method of applying expert system technology that would potentially be useful for acceleration databases. The idea here is to use the reasoning ability of the expert system in conjunction with knowledge concerning physics and the acceleration database [29]. It is possible that a suitably designed expert system will be able to independently produce useful knowledge concerning the database in general and acceleration window classification specifically. PRIDE does not presently provide such a capability, but such a capability should be investigated.

2.5.3. Future Experts

It can be expected that as time passes and experience with various types of orbital activity accumulates that human experts on orbital acceleration data will gradually begin to appear. Although such experts do not presently exist, PRIDE does provide the framework within which expert system shells based upon the knowledge of the yet-to-be experts could be effectively applied.

CHAPTER III
PHILOSOPHY OF EVENT DETECTION

There are two concepts which are central to the analysis produced by this research: physical acceleration events andabstract acceleration events. A physical acceleration event is defined to be a physical action sufficient to influence the accelerations recorded. An abstract acceleration event is a series of acceleration readings which have been selected by the windowing method. There is a many-to-one mapping from physical events to acceleration vectors and a many-to-many mapping from physical events to abstract acceleration events. These definitions arise from the nature of events for acceleration data.

The philosophy of the nature of events for acceleration data is somewhat different from the usual philosophy concerning events. In particular, in most of the literature, events are considered to be mutually exclusive in one sense or another. In one of the classical examples of the pattern recognition problem, the task is to separate a group of athletes into two classes. Since the group of athletes is composed of basketball players and horse jockeys, the two classes into which the athletes are to be partitioned are the class of basketball players and the class of horse jockeys. The two variables which describe the athletes are height and weight and thus the cluster for jockeys will consist of vectors of low weight and height while those of basketball players will consist of vectors of high weight and height. The data is mutually exclusive in the sense that each event/individual is described by exactly one vector. Figure 9a shows this clustering.

A recognition problem that illustrates another form of mutual exclusion is the problem of object recognition in an image containing a number of physical objects. In this case, the information which could be used to perform the recognition could be the varying intensity of the different objects. Figure 9b is an example of such an object. The existence of an object depends not upon one pixel value but upon many. Nevertheless, the information used to locate a given object is spatially mutually exclusive from the information used to locate a different object. The information used to characterize a physical acceleration event is neither physically nor temporally mutually exclusive from information used to distinguish another physical acceleration event.

Each recorded acceleration vector can be considered to be the summed effects upon the accelerometer recording head of the various physical events that managed to propagate to the head. None of these physical events occurred at the same time they were measured. Note that the physical events may very well be overlapping and that the

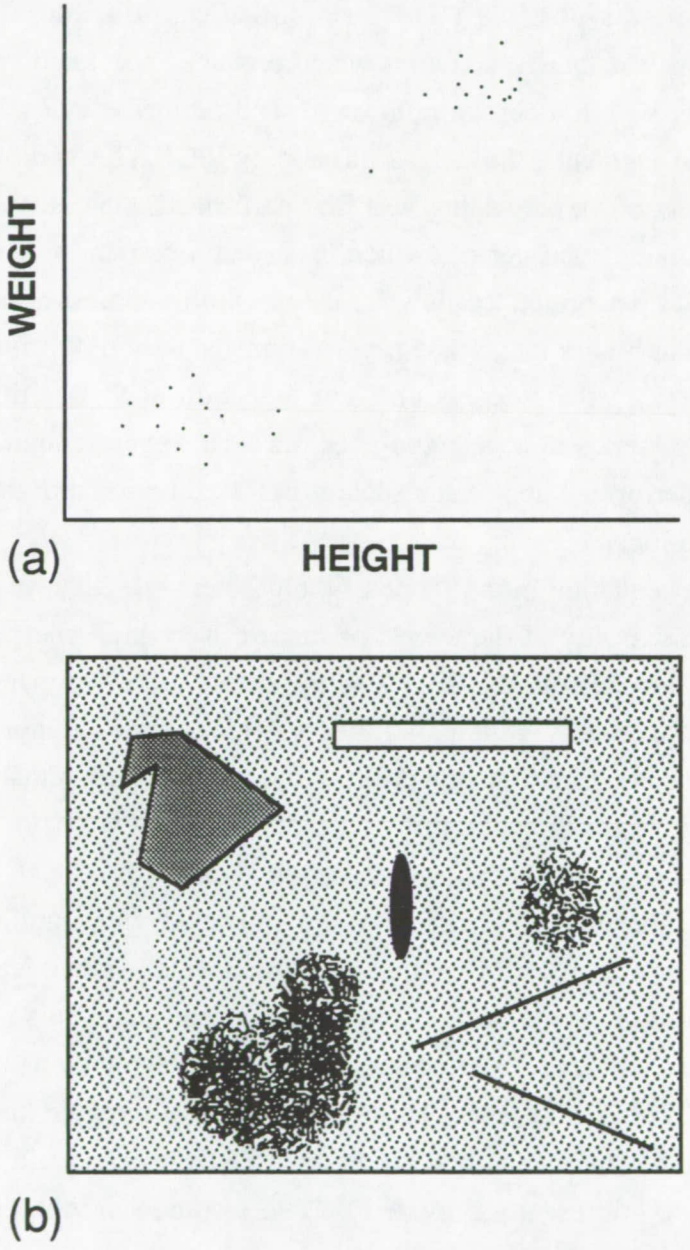

Figure 9. (a) Simple pattern recognition problem. (b) Simple visual pattern recognition problem.

recording head may detect the effects of the event at multiple time points after the time the event occurred. All these factors make the classification effort difficult. Figure 10 shows the relation between physical events and abstract events. Physical events and abstract events are connected by a many-to-many relation.

The earliest attack on the acceleration data problem was an attempt to determine whether it was possible to perform classification upon the individual vectors. The hypothesis was that all activities which produced acceleration readings produced vectors which fell within a certain number of well defined classes. Testing of this hypothesis upon time segments of the SL-3 mission by ISODATA and by visualization methods led to its rejection. This testing was first performed upon all vectors of the time segments and then later upon vectors which exceeded a certain threshold magnitude. The latter testing was performed to allow for the possibility that low magnitude accelerations were random but higher magnitude accelerations were not. All further work was based upon the conjecture that successful event detection and classification would depend upon analysis of series of acceleration vectors. However, it should be noted that this testing was not performed upon a statistically significant portion of the SL-3 data due to practical considerations.

A reduction in the scope of the problem was achieved when it was decided that, since the majority of the events of interest were high energy events, only this type of event would be sought. High energy events are of primary importance because they could conceivably ruin experiments which depend upon stable, low acceleration environments. Classification efforts were concentrated in this direction. Classification of events by vector direction or by specific frequency were not attempted. This restriction of analysis to a small portion of the original data was not only necessary due to pragmatic considerations but it was also helpful in only analyzing significant acceleration activity.

The classification of high magnitude windows will leave the problem of mapping these abstract events back to physical acceleration events and thus back to real world activities and situations, since any given high magnitude window could be the result of a number of physical events. This final mapping will require the availability of information concerning orbiter and crew activities to PRIDE. The ability to locate windows of high magnitude is presently provided by two techniques: vibration windowing and ergodic windowing.

3.1. Vibration Windowing

Vibration windowing uses the classical definition of a vibration in order to locate windows of high magnitude vectors [30]: vibration is oscillatory motion. Thus the

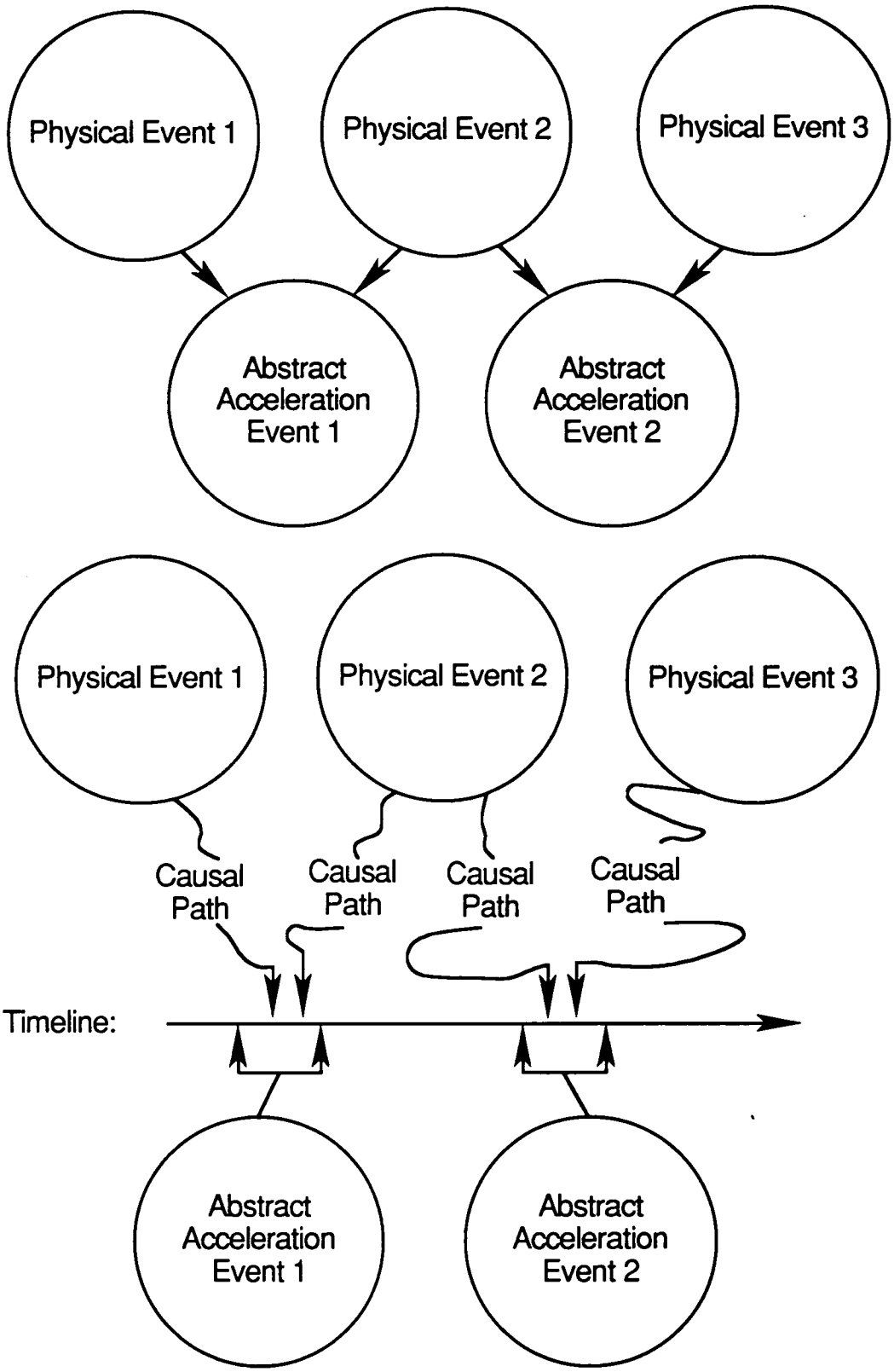

Figure 10. Relation of abstract and physical events.

mathematics describing vibration are concerned with position, velocity, and acceleration information about the vibrating object. One of the defining characteristics of vibratory motion is that the vibrating object centers its motion about an equilibrium position. Thus the position, velocity, and acceleration functions describing the vibratory motion are continuous and bounded. Since a vibration occurring in two or three dimensions may be broken down into the vibrations along each component dimensions, figure 11 shows a simple harmonic vibration. This harmonic vibration only exists in an idealized environment however. A system will tend to seek its lowest energy state and any real world vibration that is not being maintained by an influx of energy will damp out. Figure 12 illustrates the pattern of a damping vibration. That is, this vibration has been created by some undefined action and then receives no further energy with which to maintain its motion. Since the vibrating object interacts with its environment via friction, the vibration amplitude is damped. Figure 13 displays a vibration which is created by some undefined activity and then maintained and indeed modified by additional energy inputs. The sensor head of an accelerometer can be expected to sense vibrations which have a mix of the characteristics of damped and forced vibrations.

The vibration windowing technique capitalizes upon the behavior of these vibration types. The dual purpose of the technique is to find high energy events because those events are likely to affect microgravity experiments and to eliminate lower energy events from consideration because there simply isn't enough data storage and computation time available to analyze all vibration types. This reduction is achieved by arbitrarily setting a threshold for the magnitude of the acceleration vector. This magnitude is defined to be $\sqrt{a_x(t)+a_y(t)+a_z(t)}$. Once an acceleration vector is detected whose magnitude exceeds this threshold, the vibration windowing method defines the present vector and following vectors as potentially being part of a high energy vibration. Another arbitrarily set parameter A comes into play at this time. This parameter A controls the minimum length of detected high energy events. The parameter A forces vibrations detected to contain A more acceleration vectors with a magnitude greater than or equal to the threshold than it contains vectors below the threshold. The events detected by vibration windowing have a number of characteristics. One characteristic is that at least half of the magnitudes of the acceleration vectors exceed the threshold magnitude. Potentially, all of the magnitudes of the vectors exceed the threshold magnitude. The selected windows could conceivably contain long series of low acceleration vectors as long as the requirement concerning the ratio of high magnitude vectors to low magnitude vectors is not violated. Finally, the length of these windows is variable because it is dependent upon the character of the acceleration data.

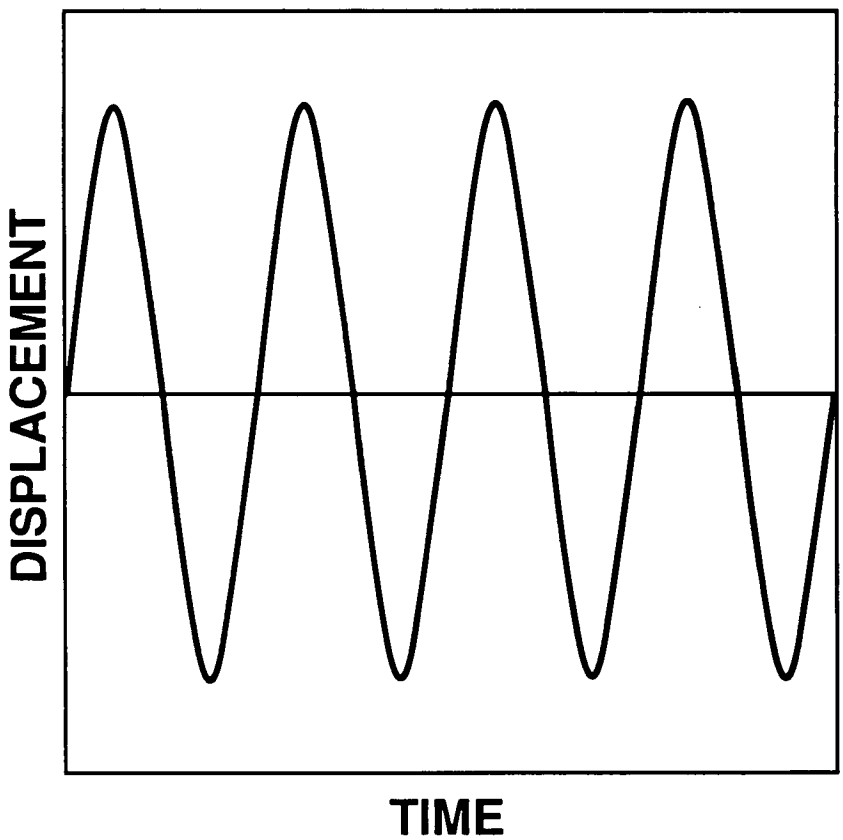

Figure 11. Harmonic vibration.

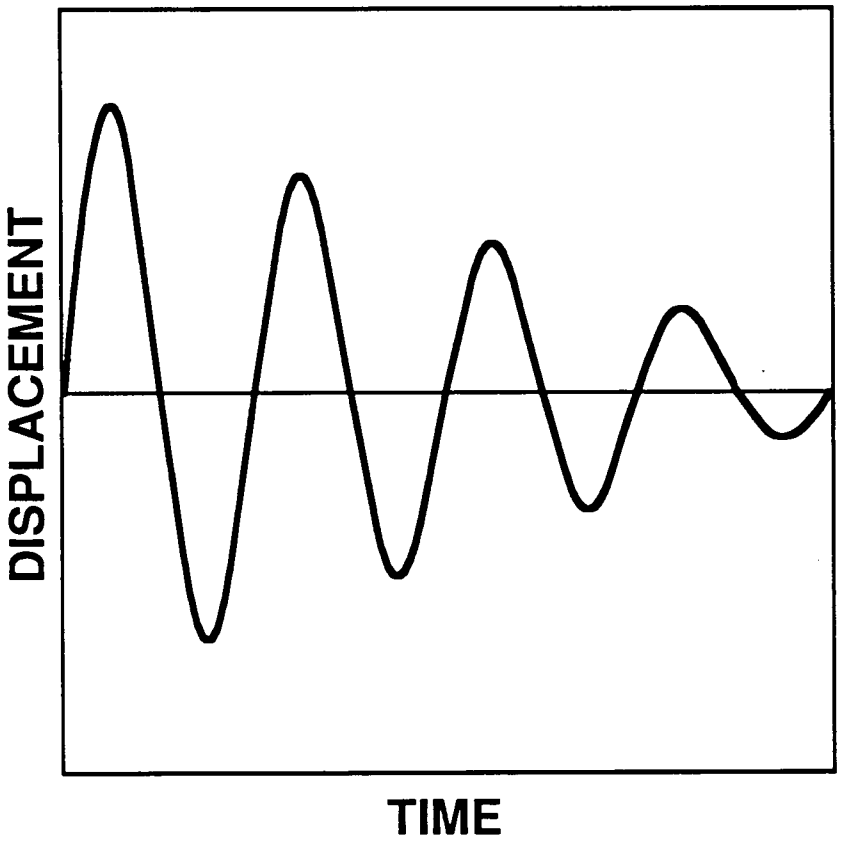

Figure 12. Damped vibration.

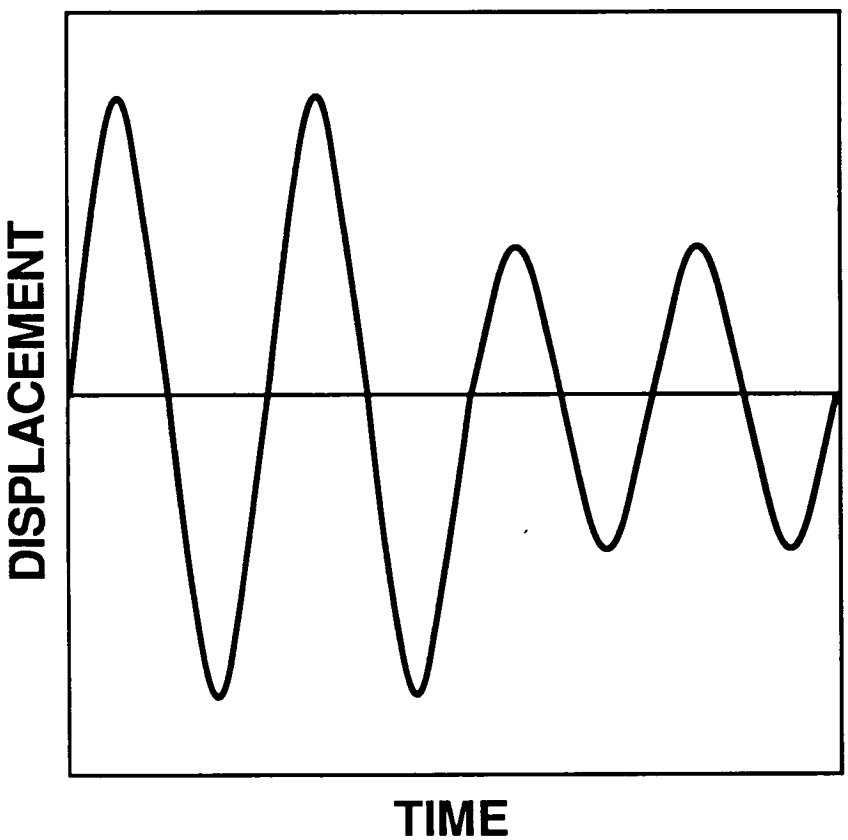

Figure 13. Forced vibration.

3.2. Ergodic Windowing

3.2.1 General Description

Ergodic windowing is intended to perform two basic services. The first service is to provide an alternate form of detecting high energy events. Since the vibration windowing method is highly dependent upon the arbitrarily selected threshold and count parameters, it is desirable to have another event detection method available and to use the two methods in conjunction to develop a consistent classification scheme. The second service that ergodic windowing provides is information concerning the distribution of the lengths of abstract acceleration events. One of the questions to be answered concerning acceleration databases is whether it is possible to consider the database to be composed of a series of constant size abstract acceleration events. In other words, is there such thing as an acceleration token? Is the structure of the accelerations composed of a series of such indivisible constant-sized tokens? Or is the structure composed of variable sized primitive elements? The former possibility is more appealing from the viewpoint of an analyst. If the acceleration database did consist of constant tokens and the size of these tokens could be determined, then analysis would be much easier and rapid.

Suppose that the abstract acceleration events in the database were composed of tokens and each abstract acceleration event only had one token(Figure 14). The desired result from the ergodic analysis program in this case would be to report that the best length for events is A. Suppose that figure 15 was the configuration of the acceleration information. Ergodic analysis should report that the best length is A and the second best length is 2A. Note that events in both of the these figures are assumed to be well separated. Knowing these preferred lengths will allow Fourier analysis routines to use the appropriate window size. In fact, knowing the correct window size allows a simple thresholding routine to select the high energy events.

The previous two examples were simplistic in that the magnitude of accelerations was assumed to be constant. This is not true in the real world. Figure 16 begins to be more realistic. Ergodic windowing should still report that length A is the best length. However, not all acceleration events are high energy. In this case, a threshold of magnitude B is the obvious value to select for thresholding. Figure 17 is the histogram for the "energy" associated with the windows in figure 16. Speaking precisely, this histogram is not based upon energy but rather upon a more easily computed value which is directly proportional to energy. This value is the summed magnitudes of the acceleration vectors associated with a window of length A starting at a given position.

At this point, the discussion of the ergodic technique focuses upon ordering histograms of the energy values based upon "goodness" of the window size. This

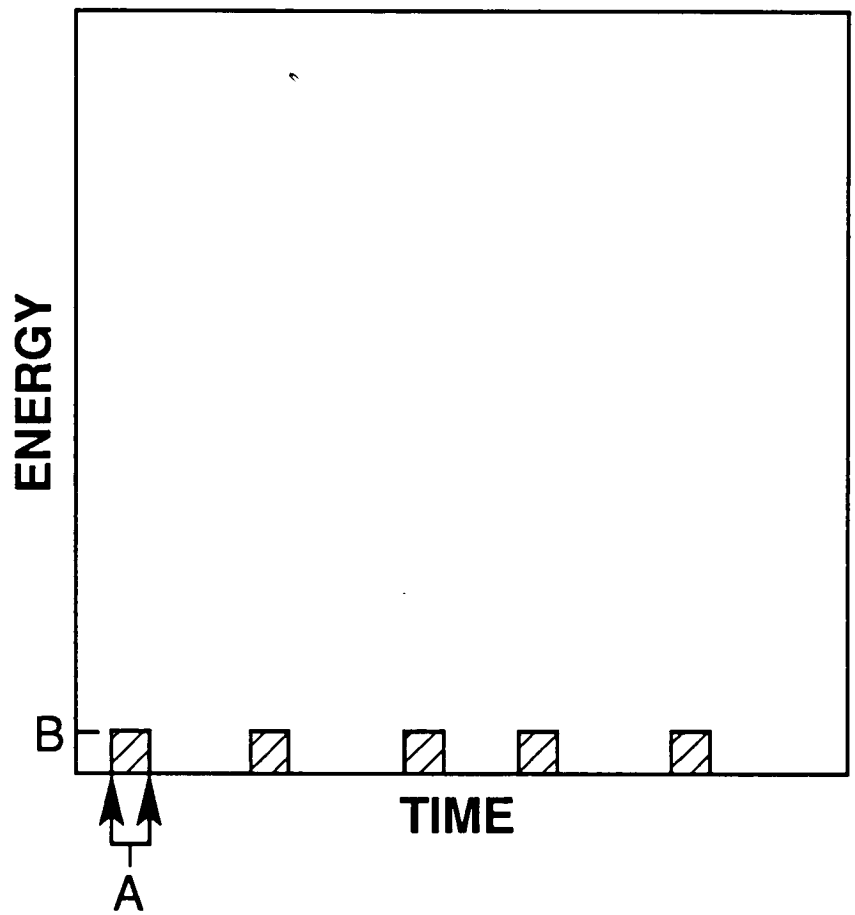

Figure 14. Constant magnitude, noncontiguous event.

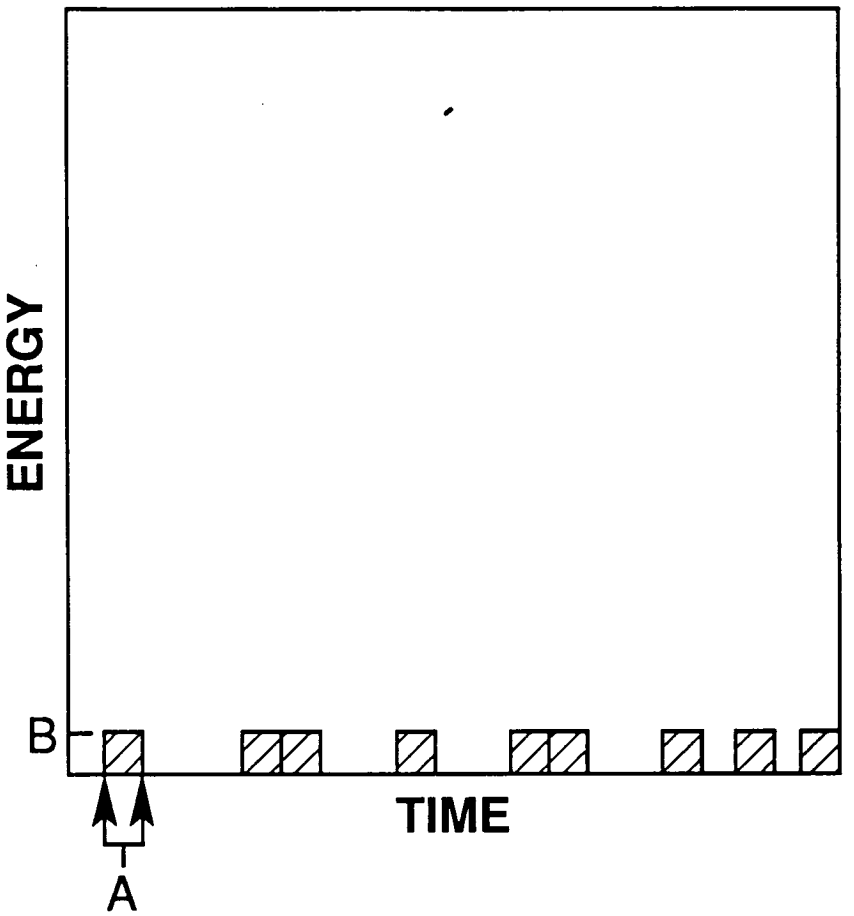

Figure 15. Constant magnitude, contiguous event.

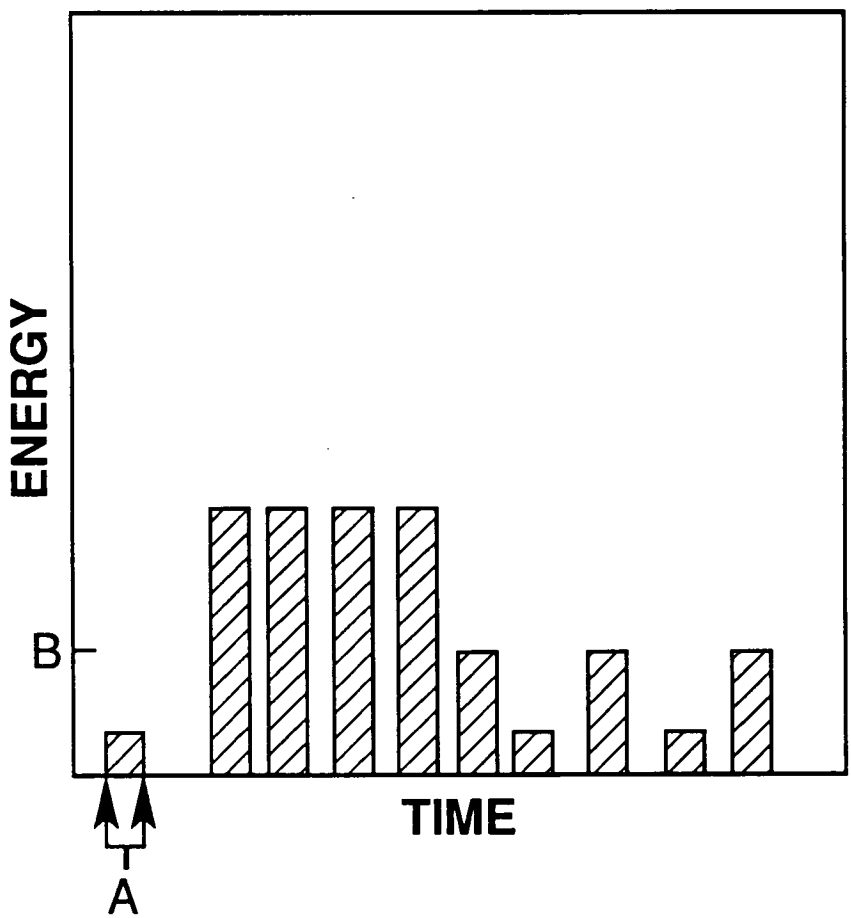

Figure 16. Variable magnitude, contiguous event.

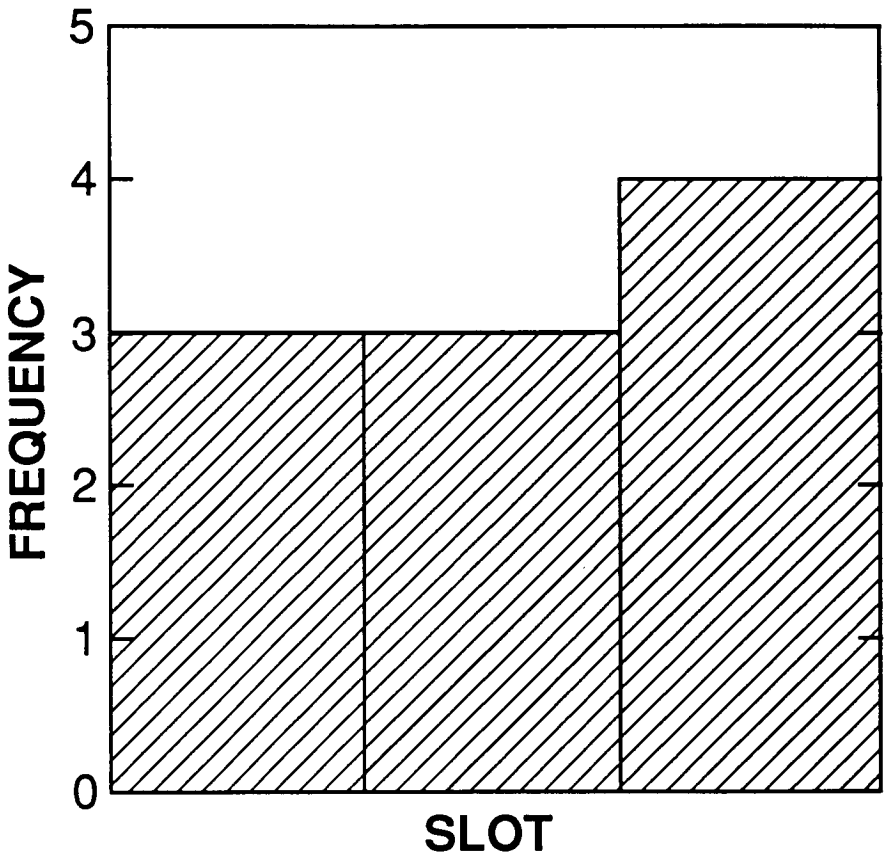

Figure 17. Histogram of variable magnitude, noncontiguous event.

ordering is accomplished by computing a weighted value indicating the desirability of the histogram of any given window size. This ordering is the result of three normalizations.

The first normalization is concerned with the fact that there is a given maximum acceleration that could be recorded by the SL-3 accelerometer. Figures 18 and 19 illustrate the situation. Figure 18 has one event which consists of a series of constant acceleration vectors which happen to be the highest possible recordable acceleration vectors. Figure 19 has one event which contains more points than the event in figure 18 but the magnitude of the vectors in figure 19 are below the maximum recordable magnitude. If everything else is the same then the length of the event in figure 18 should be preferred.

The second normalization is concerned with the fact that the window sizes are different. The amount of energy associated with histograms slots should be normalized to take this into consideration.

The third normalization is concerned with the skewdness of the histogram. Figures 20 and 21 illustrate this situation. If everything else is the same, figure 21 contains more higher energy events than does figure 20.

These three normalizations assign a goodness value to a window size. The best window size is the "natural" window size for events in the acceleration database. These histograms associated with specific window sizes may be used to detect events.

3.2.2 Detailed Description

The following is a detailed description of the ergodic process for determining the natural window size.

Let A be a sequence of acceleration readings:

$$A = \{(x_0, y_0, z_0),(x_1, y_1, z_1),\ldots(x_{n-1}, y_{n-1}, z_{n-1})\}$$

where n is the number of acceleration readings and define **B** to be the one dimensional array of sequences

$$\mathbf{B}=[\{b_{00},b_{01},\ldots,b_{0\,n-w_0}\},\{b_{10},b_{11},\ldots,b_{1\,n-w_1}\},\ldots,\{b_{M0},b_{M1},\ldots,b_{M\,n-w_M}\}]$$

Here w_i is the window length of the i^{th} window size, m is the number of window sizes, and

$$b_{ij}=\sum_{k=j}^{j+w_i-1}\sqrt{x_k^2+y_k^2+z_k^2},\ \text{for } 0<=i<=M, \text{ where } M=m-1 \text{ and } 0<=j<=(n-w_i)$$

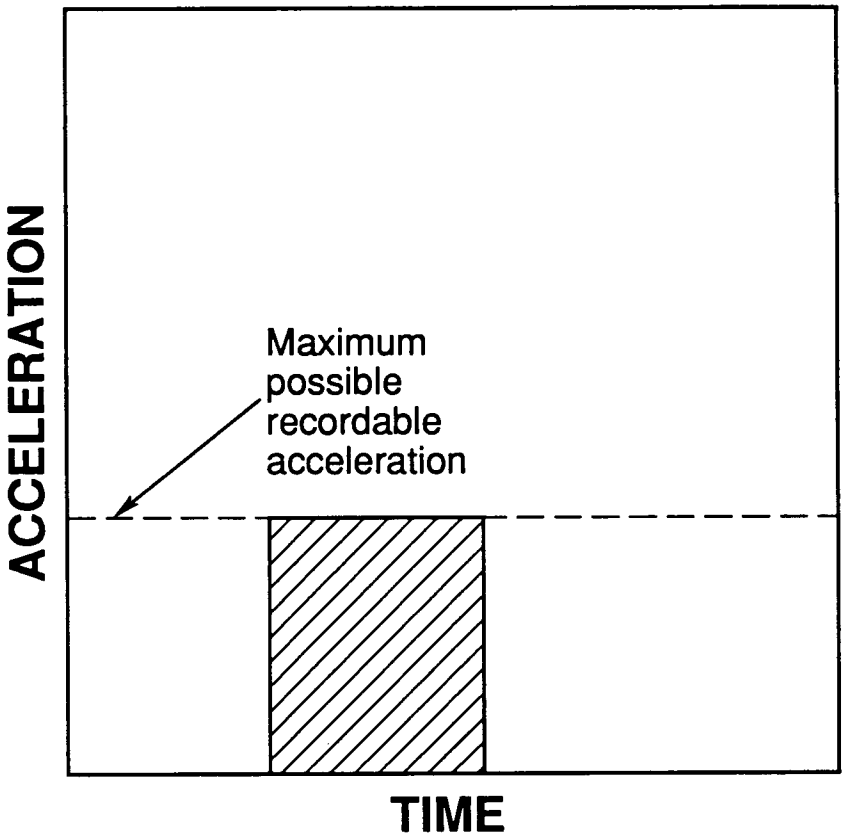

Figure 18. Maximum recordable acceleration.

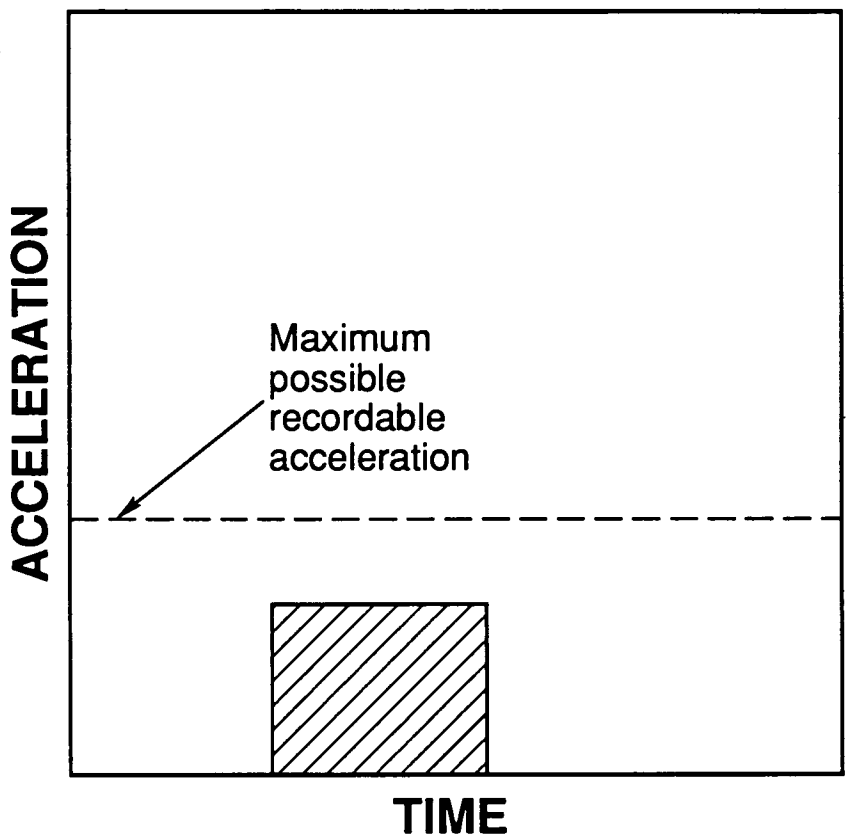

Figure 19. Less than maximum recordable acceleration.

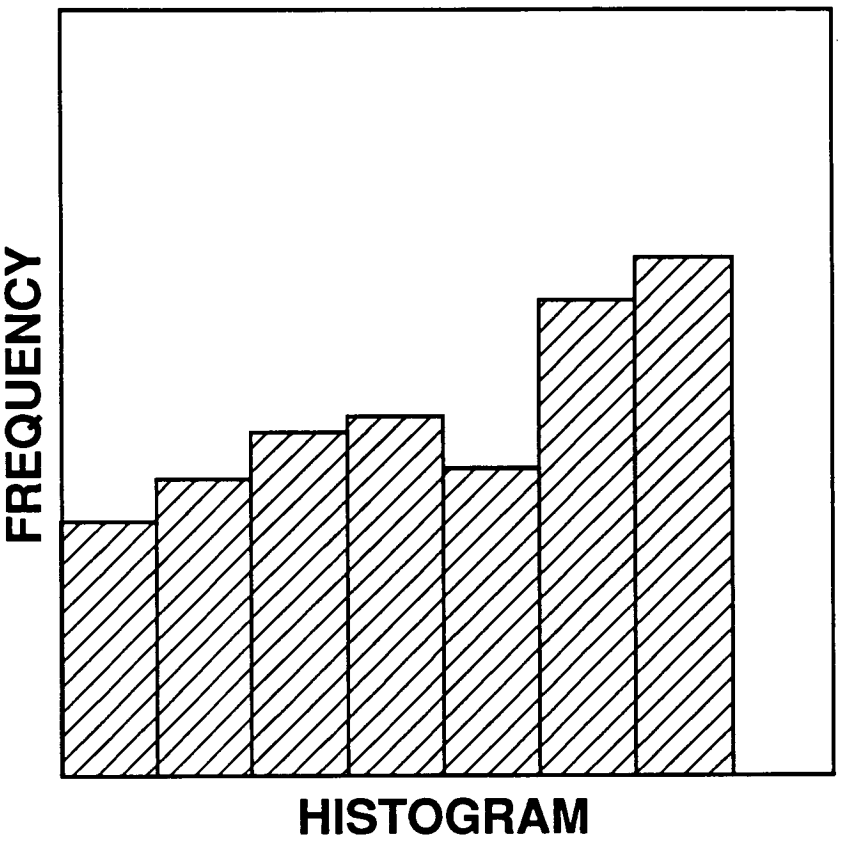

Figure 20. Skewed histogram.

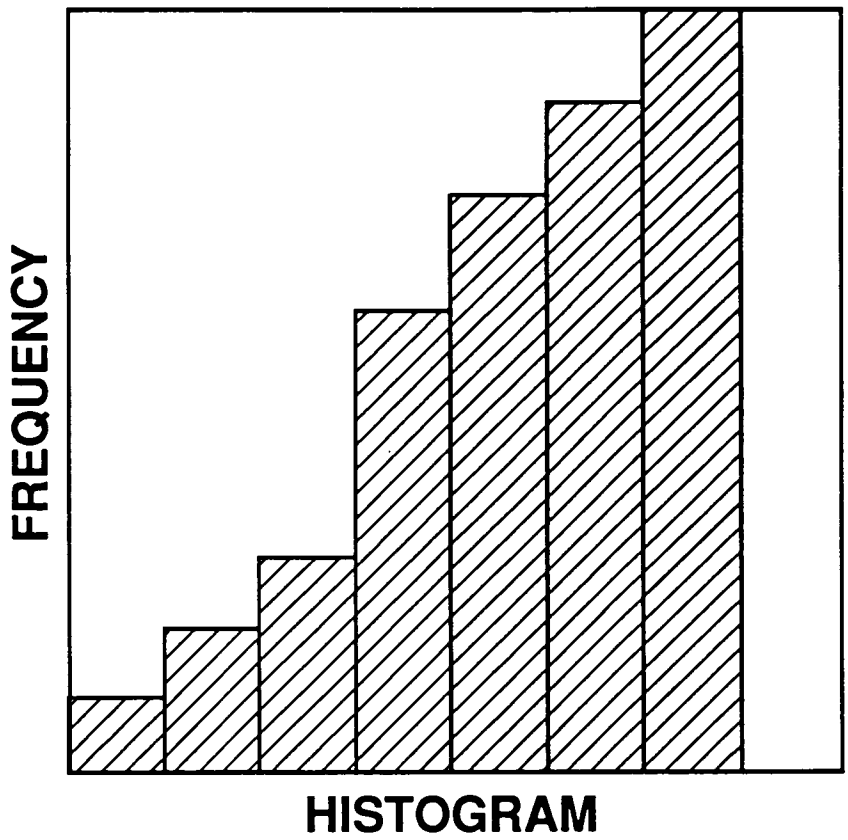

Figure 21. More skewed histogram.

Each b_{ij} represents the sum of the acceleration magnitudes for each window of size w_i starting at the time corresponding to the index j. Now a subset of B is defined which contains particular values of b_{ij}. That is:

$$\mathbf{D}=[\{b_{0e_{00}},b_{0e_{01}},\ldots,b_{0e_{0f_0}}\},\{b_{1e_{10}},b_{1e_{11}},\ldots,b_{1e_{1f_1}}\},\ldots\{b_{Me_{M0}},b_{Me_{M1}},\ldots,b_{Me_{Mf_M}}\}]$$

where the index e_{gh} is chosen such that it denotes the set of minimal size:

$$\sum_{g=0}^{f_i} b_{i e_{ig}} > 0.1 * \sum_{j=0}^{n-w_i} b_{ij}.$$

Let $\boldsymbol{H}=\{h_0,h_1,\ldots h_{M-1}\}$ be a sequence where

$$h_i=\max(b_{ij}),\ \text{for}\ 0<=i<=M \text{ and } 0<=j<=(n-w_i)$$

and let S be the norm of the maximum energy acceleration vector that can be recorded by the accelerometer. The natural window size can now be defined by the maximum of the array **U**. That is:

$$\max(\mathbf{U}),\ \text{where}\ \mathbf{U}=[u_0,u_1,\ldots,u_M] \text{ and } u_i=\sum_{v=1}^{f_i} e_{iv} * (\max(f_r)-(f_i-v))$$

where the t_{qr} are elements of the array **T** which normalizes the maxima of the magnitude sums b_{ij}. That is:

$$t_{qr}=p_{qr}\times\left(\frac{w_M}{w_q}\right)\text{: are elements of the array}$$
$$\mathbf{T}=[\{t_{0e_{00}},t_{0e_{01}},\ldots,t_{0e_{0f_0}}\},\{t_{1e_{10}},t_{1e_{11}},\ldots,t_{1e_{1f_1}}\},\ldots,\{t_{Me_{M0}},t_{Me_{M1}},\ldots,t_{Me_{Mf_M}}\}]$$

where the p_{qr} are elements of the array **P** which represents for a window of length w_q the value of the summed magnitude b_{qr} scaled by the maximum value of b_{qr} for $0<r<f_q$ divided by the maximum possible recordable value for the window size w_q.

$$p_{qr}=b_{qr}\times\left(\frac{h_q}{S\ w_q}\right)\text{: are elements of the array}$$
$$\mathbf{P}=[\{p_{0e_{00}},p_{0e_{01}},\ldots,p_{0e_{0f_0}}\},\{p_{1e_{10}},p_{1e_{11}},\ldots,p_{1e_{1f_1}}\},\ldots,\{p_{Me_{M0}},p_{Me_{M1}},\ldots,p_{Me_{Mf_M}}\}]$$

Both ergodic and vibration windowing provide a practical means to process entire large datasets.

CHAPTER IV
PRIDE CONFIGURATION

4.1. Software Configuration

4.1.1 System Level Software Configuration

PRIDE was designed to be portable and to take advantage of the capabilities provided by several standard software components. Its portability is derived from its use of the UNIX operating system [31], the X network graphics windowing system, the CDATA relational database, the DORE variant of the PHIGS hierarchical three-dimensional graphics standard, and the CLIPS expert system shell. With the exception of DORE, none of these packages require particular hardware. With the possible exception of DORE, all of these packages are written in the C language [32]. Thus compatibility is preserved at the source code language level. The base source code is available for all of the packages ,with the exception of DORE, and thus problems concerning interaction between the packages can be more readily analyzed. Availability of the source code for CDATA and CLIPS was instrumental to the development of PRIDE. Figure 22 displays the system software configuration for PRIDE.

4.1.2 PRIDE Software Components

The software components of PRIDE are UNIX processes. The only exception to this are the programs on the VAX which prepare and transmit the raw acceleration data. Usually these processes are linked to a particular X window. Some of these processes are designed so that multiple copies of the same process type may run simultaneously. Some processes are not able to support multiple instantiations of the same process type. Some processes will not "peacefully coexist" with certain other processes. Concurrent processes are problematic in PRIDE because the CDATA database management system does not provide for concurrent usage.

There are eleven PRIDE software components. These components are ***pride***, ***staticcloud***, ***timeseries***, ***fft***, ***query***, ***loadwindow***, ***classify***, ***isodata***, ***expertiso***, ***ergodic***, and ***3dfft***. The ***pride*** component is the X-based main program for PRIDE and allows the user to activate the various functions of PRIDE. The ***loadwindow*** component is an X window used to allow the user to select a given window. The ***staticcloud*** component shows a static drawing of the acceleration vectors of a given event. The ***timeseries*** component provides a dynamic presentation of the time dependent activity of the acceleration vectors

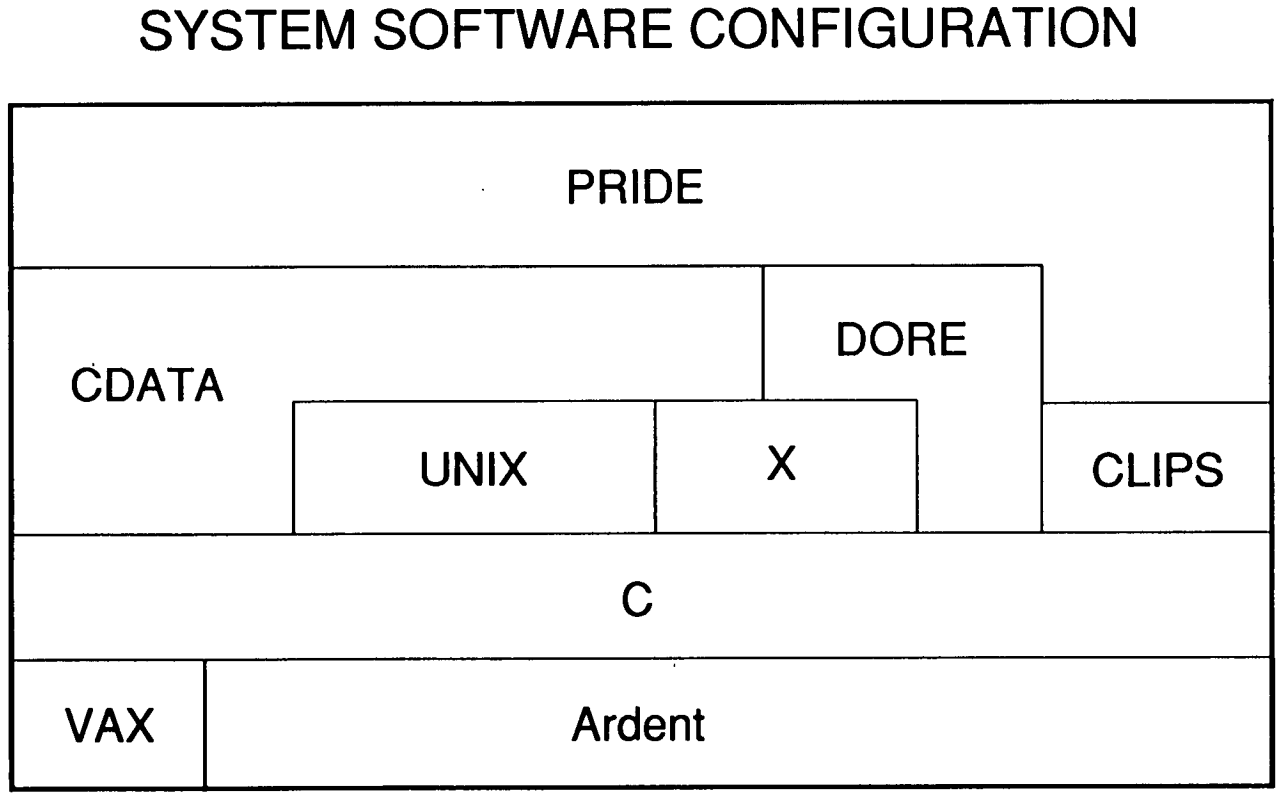

Figure 22. System software configuration.

of a given event. The ***fft*** component provides a two-dimensional display of various Fourier information concerning a given event. The ***3dfft*** component provides a three-dimensional representation of the Fourier information associated with either a single event or a group of events. The ***staticcloud***, ***timeseries***, ***fft***, and ***3dfft*** X-based components may have multiple copies of the same component type running simultaneously . In fact, these components may be freely mixed. None of these component types conflict with the other types or other self-copies.

The ***query*** component is the X-based main query facility for the PRIDE database. The ***query*** component is quite unfriendly in terms of its interaction with the database. No other component may run while ***query*** is running and ***query*** will not run while any other component is running. If by chance another component is activated while ***query*** is active, then the database is corrupted. Recovering from the corruption requires reindexing of the database. The time it takes to reindex is proportional to the size and number of abstract acceleration event windows. If the database contains the events for only a 30 minute period, reindexing takes approximately 10 minutes. A significant sample for the 144 hour SL-3 mission would be in the neighborhood of 30 percent of the data and thus be 42 hours. This is 84 half hour segments and thus 840 minutes of reindexing time in the event of database corruption. The test and development of PRIDE was performed with 30 minutes of data in the database.

The ***classify*** X-based component is based upon the ***query*** component and has a functionality that is simultaneously limited and expanded. The ***classify*** component is limited to modification of the CLASSIFY dataset within the database but it also is capable of X-based interaction with the ***staticcloud***, ***timeseries***, ***fft***, and ***3dfft*** components. The user views different representations of events and then by mouse activity gives commands to ***classify*** to create a classification.

The ***ergodic*** X-based component allows an analyst to analyze the effect of varying the window sizes used to calculate the energy distribution in the raw acceleration data. The ***ergodic*** component does not conflict with other components but it makes no sense to have multiple instantiations of the ***ergodic*** component.

The ***isodata*** non-X-based component provides the ISODATA algorithm for use on the Fourier information of events. The ***expertiso*** component provides a combination of expert systems and the ISODATA algorithm. The expert system performs many of the same activities that a human analyst would perform.

4.1.3 X Usage

PRIDE interacts with X on more than one level. PRIDE uses X protocol calls in order to perform basic X activity such as window creation and drawing. PRIDE uses the Xt Intrinsics Toolkit in order to build new widgets, which are in turn used to control user interaction. PRIDE uses two custom-built widgets. Dorex is the first such widget and is used as a child widget of a form widget. The availability of a Dorex widget allows the combination of DORE graphics with control widgets such as buttons in order to create useful new types of window. Fftx is the other new type of widget. Fftx is used to combine two-dimensional graphics with control widgets. Dorex is used in the ***staticcloud***, ***timeseries***, and ***3dfft*** components while fftx is used in the ***fft*** and ***ergodic*** components. PRIDE uses prebuilt Athena widgets wherever possible because this speeds code development, because they are free, and because they are standard. This availability of multiple levels of interaction has advantages and disadvantages. The advantage lies in versatility. There is more than one way to get from point A to point B. The disadvantage lies in the increase in complexity of creating the capability. X is noted for its complexity.

4.1.4 Database Configuration

The following is the definition of the PRIDE database:

```
#schema      ACCEL
#dictionary
             X_ACCELERATION,     F,    4
             Y_ACCELERATION,     F,    4
             Z_ACCELERATION,     F,    4
             START_TIME,         I,    4
             POINT_TIME,         I,    4
             CLASS,              I,    4
             CLASSIFICATION,     I,    4
             FREQUENCY,          F,    4
             MAGNITUDE,          F,    4
             DIMENSION,          I,    4
             WINDOW_LEN,         I,    4
             END_TIME,           I,    4
             TAPE_NAME,          A,    12
             FILE_NUMBER,        I,    4
             FILE_LEN,           I,    4
```

```
                TAPE_START,             I,      4
#end dictionary
#file ACCEL
                POINT_TIME
                START_TIME
                X_ACCELERATION
                Y_ACCELERATION
                Z_ACCELERATION
#end file
#file CLASSES
                CLASSIFICATION
                CLASS
                START_TIME
#end file
#file SPECTRA
        START_TIME
        DIMENSION
        FREQUENCY
        MAGNITUDE
#end file
#file WINDOWS
        START_TIME
        WINDOW_LEN
#end file
#file TAPEFILES
        TAPE_NAME
        FILE_NUMBER
        TAPE_START
        END_TIME
        FILE_LEN
#end file
#key    ACCEL           POINT_TIME
#key    ACCEL           START_TIME,     POINT_TIME
#key    CLASSES         CLASSIFICATION, CLASS,
START_TIME
```

```
#key   SPECTRA          START_TIME,     DIMENSION,
FREQUENCY
#key   WINDOWS          START_TIME
#key   TAPEFILES        TAPE_NAME,      FILE_NUMBER
#key   TAPEFILES        TAPE_START
#end schema ACCEL
```

This definition consists of three parts. The first part is the data dictionary which defines the glossary of types of information that make up the database. This is a feature common to many databases and is another example of non-redundant storage of information and of enforced data integrity. The second part is the definition of the relations of the database. The third part is the definition of the keys. Each relation may have one or more keys defined. The first such key defined for a relation is the primary key; all other keys are secondary. Primary keys must be unique, while duplicate secondary key values may legally exist.

The ACCEL relation in conjunction with the WINDOWS relation defines the high energy events. WINDOWS stores the start times and lengths of the high energy events while ACCEL stores the actual acceleration information for these events. Note that the raw acceleration does not have a defined relation. Nevertheless, this information is part of the database; it is stored offline. The TAPEFILES relation records which physical cassette tape holds which 30 minute segment of SL-3. The SPECTRA relation holds the spectral information associated with event data. The CLASSES relation is modified by either the ***query*** component or the ***classify*** component. It contains the present classifications that have been made of the stored high energy events. The ***classify*** component has specialized, convenient editing capabilities for working with the CLASSES relation.

The definition of the keys has a strong effect on the operation of the database. ACCEL stores unique acceleration values while WINDOWS stores unique window locations. SPECTRA is more complicated. For each frequency for each dimension for each event, SPECTRA stores the magnitude. CLASSES's key structure indicates that for a given classification, each class has a number of start times that must be unique. TAPEFILES key structure indicates that there are multiple cassette tapes which each have multiple files.

4.1.5 System Storage Requirements

In addition to the enormous storage requirements for the data, there are also the storage requirements for the PRIDE system to consider. PRIDE consists of approximately 22000 lines of C source code which requires 541Kbytes of disk storage. The executables for the PRIDE system require approximately 10Mbytes. The peak disk storage requirement for PRIDE activity is in the vicinity of 60Mbytes.

4.2. Hardware Configuration

The present hardware used by PRIDE is the Ardent graphics mini supercomputer and a VAX 11-785. The majority of the functionality of PRIDE resides on the Ardent. The VAX is used to reformat and transfer information from 6250 BPI tape to the Ardent.

The PRIDE Ardent 1500 is a MIMD machine with two processor boards each possessing a vector capability [33]. There is 32 Mbytes of RAM and approximately 500 Mbytes disk storage. This amount of disk is woefully inadequate with respect to the enormous data needs of PRIDE. There is also a graphics expansion board which provides a hardware buffered graphics capability. Figure 23 shows the hardware configuration of PRIDE.

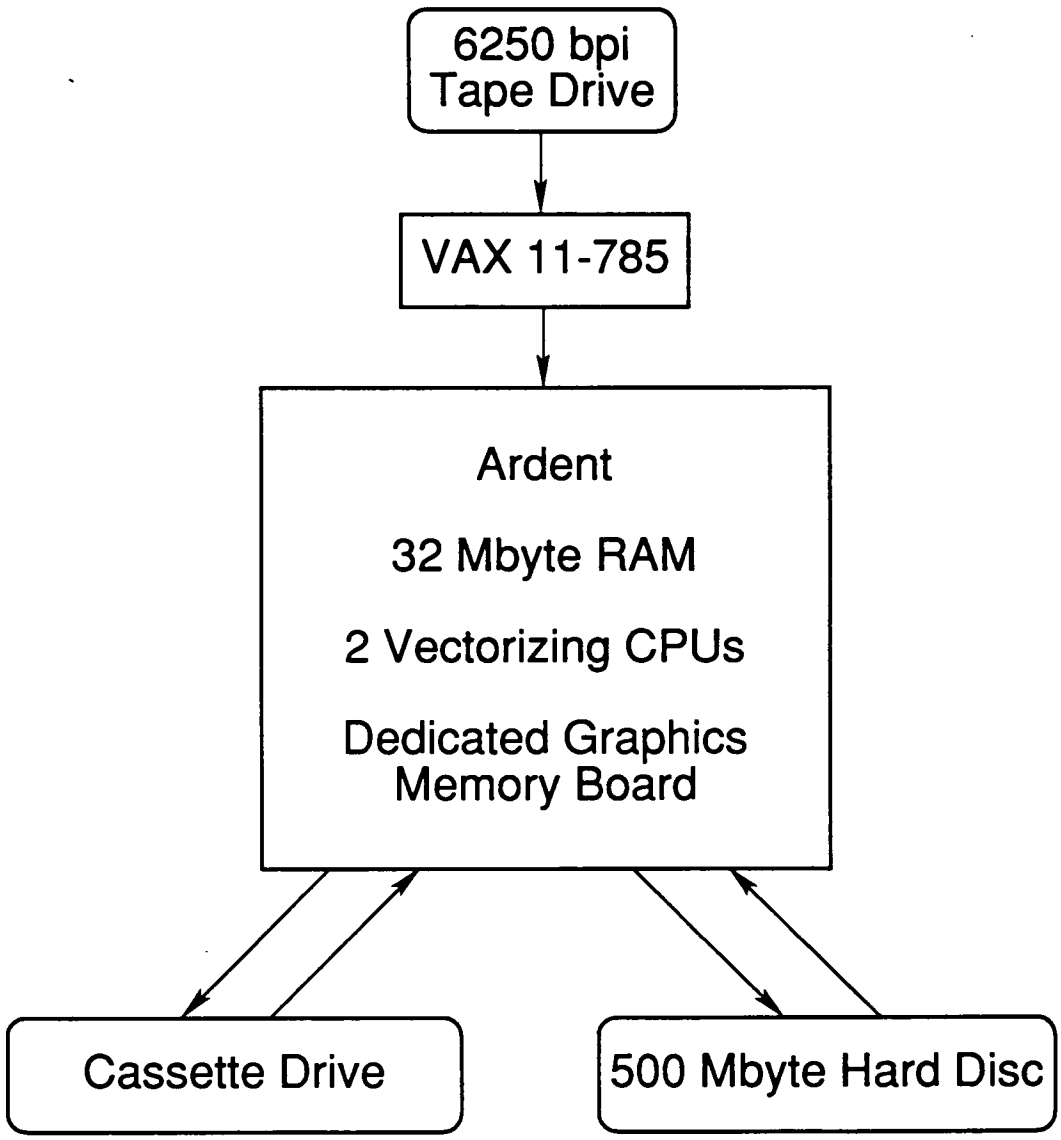

Figure 23. Hardware platform for PRIDE.

CHAPTER V
PRIDE USAGE

Assuming the user is signed on the system and that the X window system is up and running, the user starts PRIDE by typing "pride"<cret>. At this point, the main menu appears (see figure 24). To activate an option the user positions the pointer on the proper button and clicks.

5.1 *Staticcloud* Usage

Staticcloud provides a three dimensional color image of a given event. The acceleration vectors are individually displayed as spheres in three dimensional space. This presentation gives the user a better idea of the overall spatial locations of the accelerations which occurred during the abstract acceleration event. The user is divorced from the time-varying nature of individual acceleration events. Figure 25 shows such a display. Note the strong unidirectional clustering, close to the z-direction. Clicking on *loadwindow* brings up the *loadwindow* window (see figure 26). Once the *loadwindow* is visible, the user clicks on one of the start times and then clicks on the display area of ***staticcloud***. By doing this, the user is indicating that the selected window should be displayed in the selected component. Clicking on *octant* overlays a set of translucent bounding planes over the present display. Furthermore, the user can rotate the displayed acceleration vectors, can zoom in on the vectors, and can zoom out from the vectors. These three actions are created by proper use of the three-buttoned mouse. Rotating is controlled by the left button. Holding down the left mouse button while simultaneously moving the cursor in a certain direction induces a rotation along that direction. Zooming in is controlled by the middle button. Holding the middle mouse button down while simultaneously moving the cursor in any arbitrary direction causes the view to zoom in on the acceleration vectors. The direction that the cursor is moved is irrelevant - it is merely the distance the cursor is moved that controls the magnitude of the zoom. Zooming out is controlled by the right mouse button. Holding the right button down while dragging the cursor causes the view to zoom out from the object.

5.2 *Timeseries* Usage

Timeseries provides a three dimensional color animation of a given event. The acceleration vectors are individually displayed as spheres in three dimensional space. This presentation gives the user a better idea of the time-varying interrelation of the

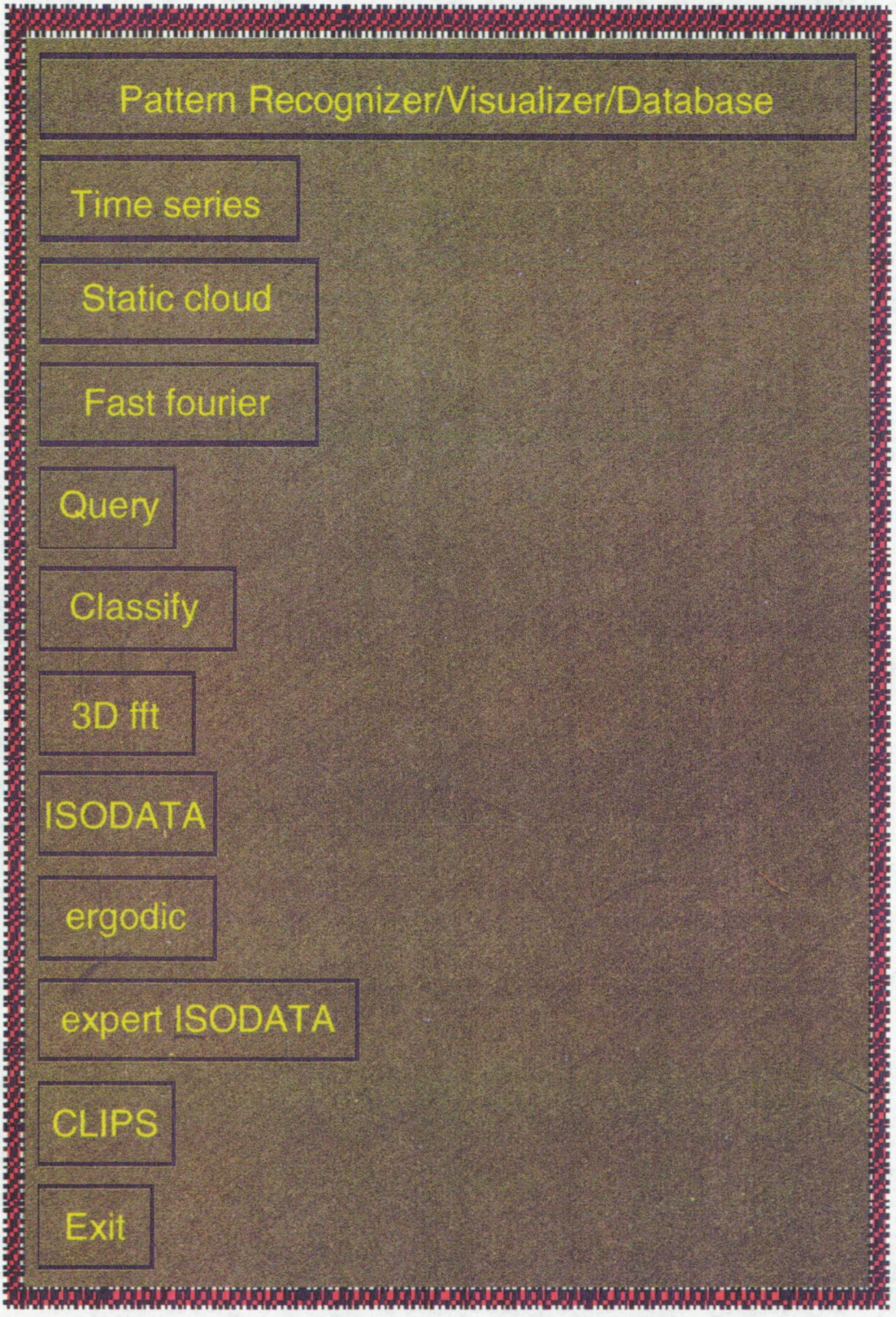

Figure 24. PRIDE Main Menu.

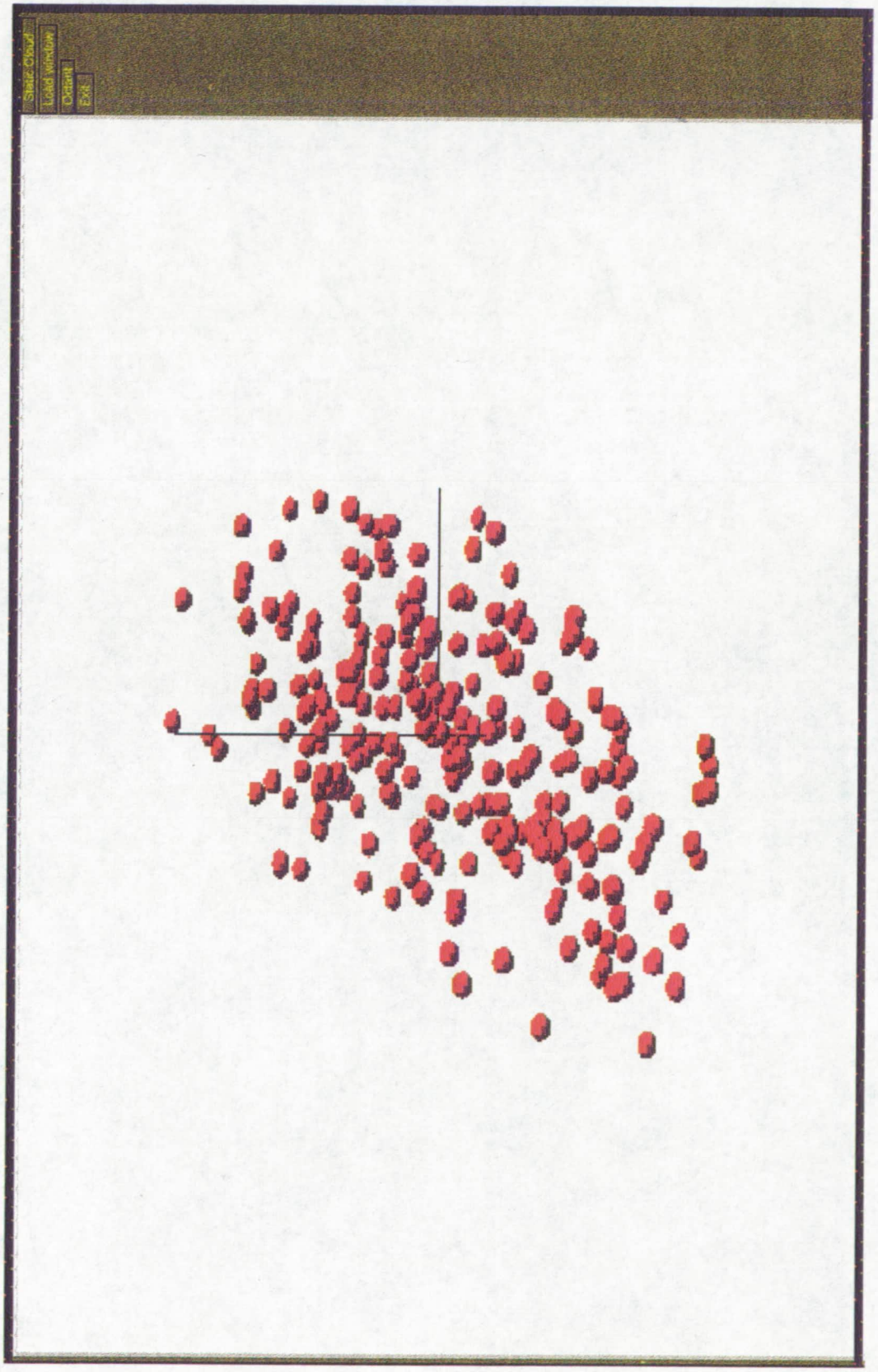

Figure 25. *Staticcloud.*

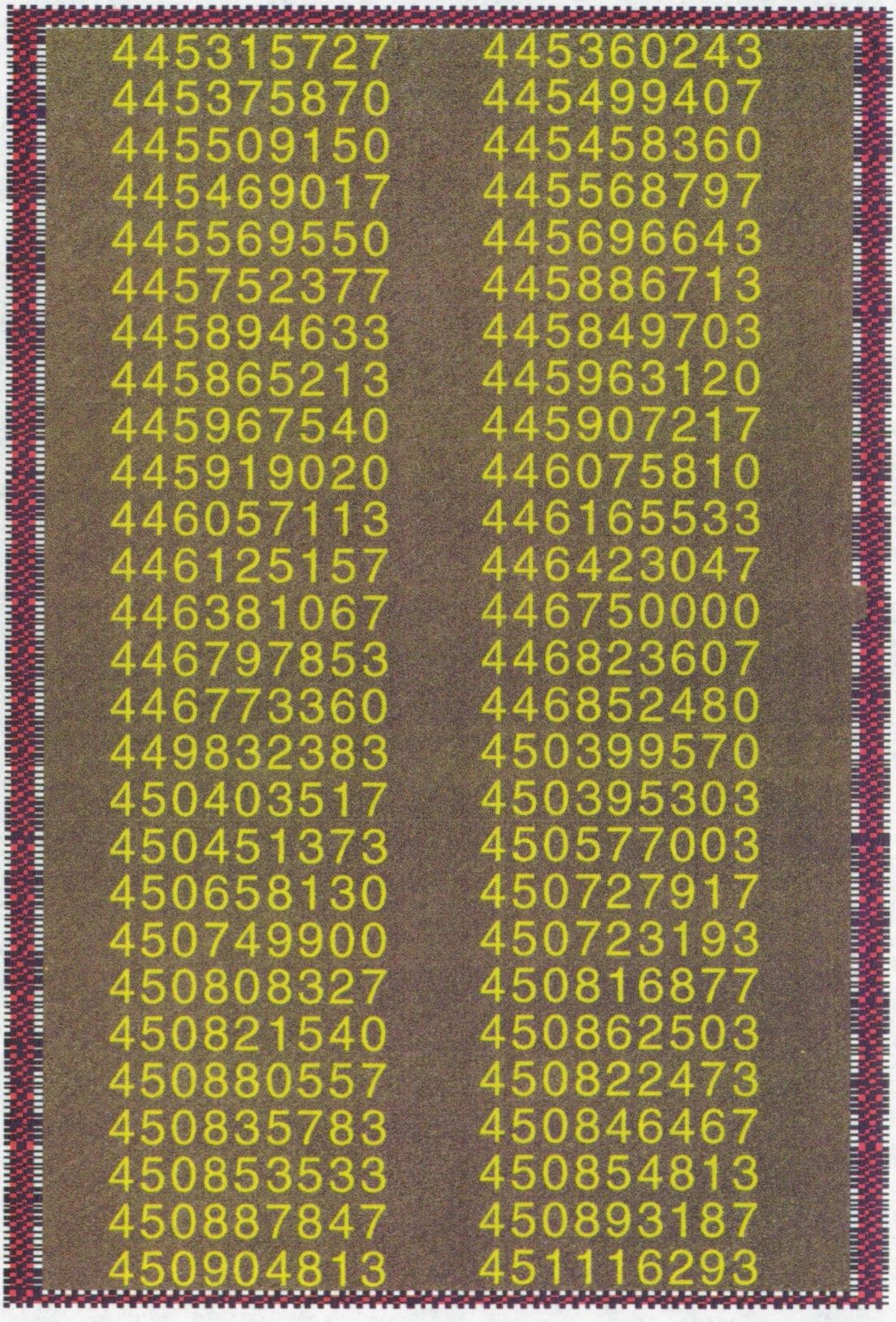

Figure 26. Loadwindow.

acceleration vectors of a given event. Figure 27 shows an example of this type of window. Note the well-defined elliptical pattern indicative of a high energy event varying between positive and negative axes. Once again, clicking *loadwindow* causes the *loadwindow* window to be shown. There is never any reason to have more than one *loadwindow* active at any time. The operations for causing an event to be loaded into the ***timeseries*** component is identical to the method used in ***staticcloud.*** Once an event has been loaded, ***timeseries*** displays the very first acceleration vector as a red sphere. At any time during the animation, the newest acceleration vector is colored red while all previous vectors are colored green. The default number of displayed acceleration vectors is 20. Clicking on the *animate* button causes the animation to begin. Clicking on the *animate* button while the animation is proceeding causes the animation to freeze. Note that this also implies that the oldest acceleration vector is dropped (assuming that 20 more vectors have already been plotted). *Octant* causes the same set of translucent bounding planes to be drawn that were drawn in ***staticcloud.*** *Reset* causes the present animation to start over from the beginning. *Connect* causes the acceleration spheres to be connected by green lines.

5.3 *Fft* Usage

The ***fft*** window provides a number of types of display of information concerning the Fourier transform of a given event. Since any acceleration vector is composed of three values, any event may be consider to consist of three functions of time, one for each acceleration recorder axis. Thus, there are separate displays for the x, y, and z Fourier transforms. Once *loadwindow* has been used to select an event, clicking on X causes a display of the x transform. Similarly clicking on Y and Z cause the y and z transforms to be shown.

There is also a display function to show the overlaid x, y, and z Fourier transforms. Clicking on *XYZ* causes this display. Finally, there is a display for the magnitude of the Fourier transform vectors. Clicking on *NORM* causes this display. Figure 28 shows an example of the Fourier information for just the x component of an event. Figure 29 provides an example of the Fourier information for x, y, and z overlaid on the same plot. Figure 30 shows an example of the norm of the magnitudes.

Clicking on *Pixmap-write* causes a copy of the ***fft*** window to be stored to disk. Clicking on *Pixmap-read* causes a copy of a previously stored ***fft*** window dump to be displayed. This is a vestigial capability at the moment.

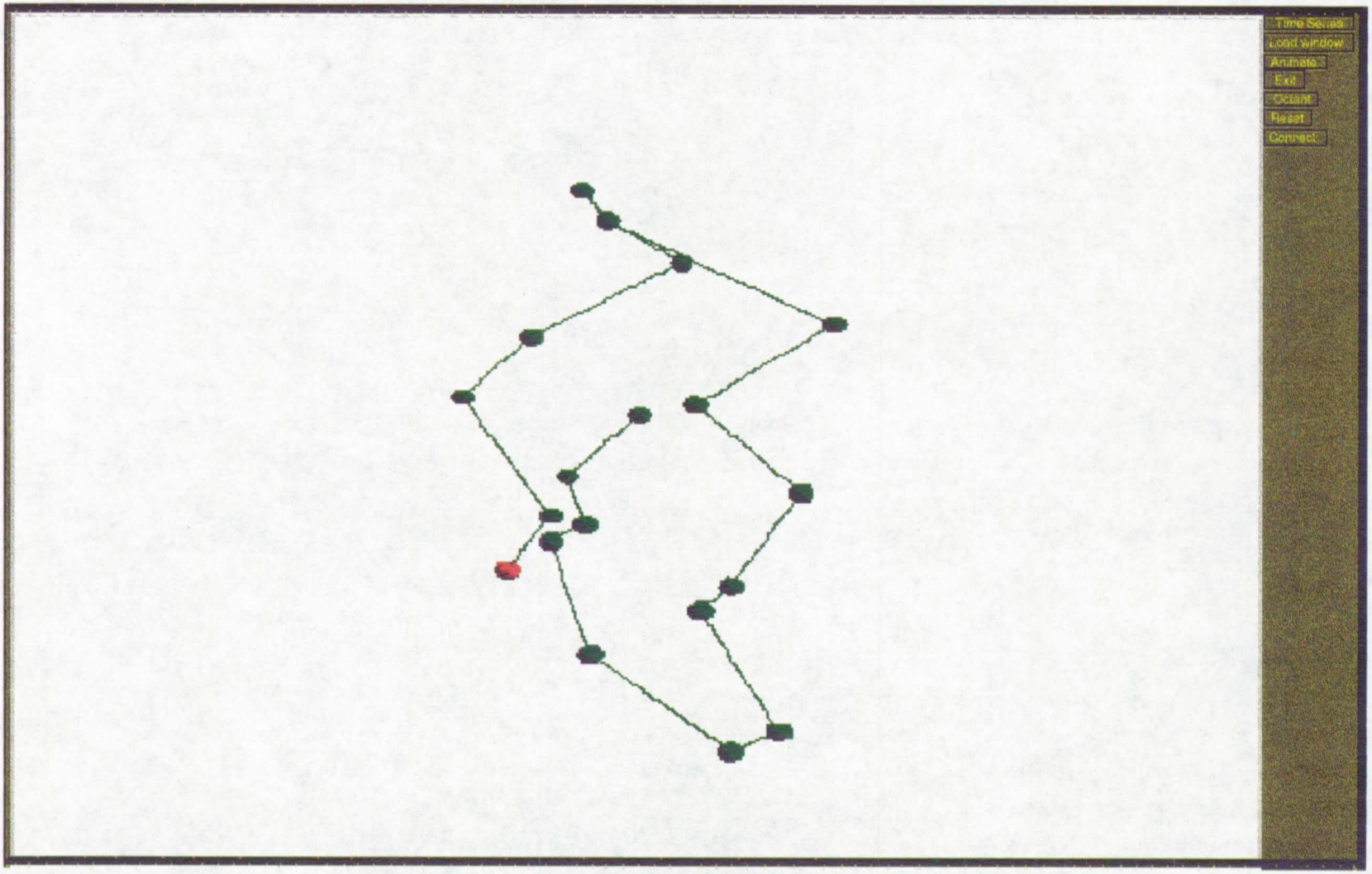

Figure 27. ***Timeseries.***

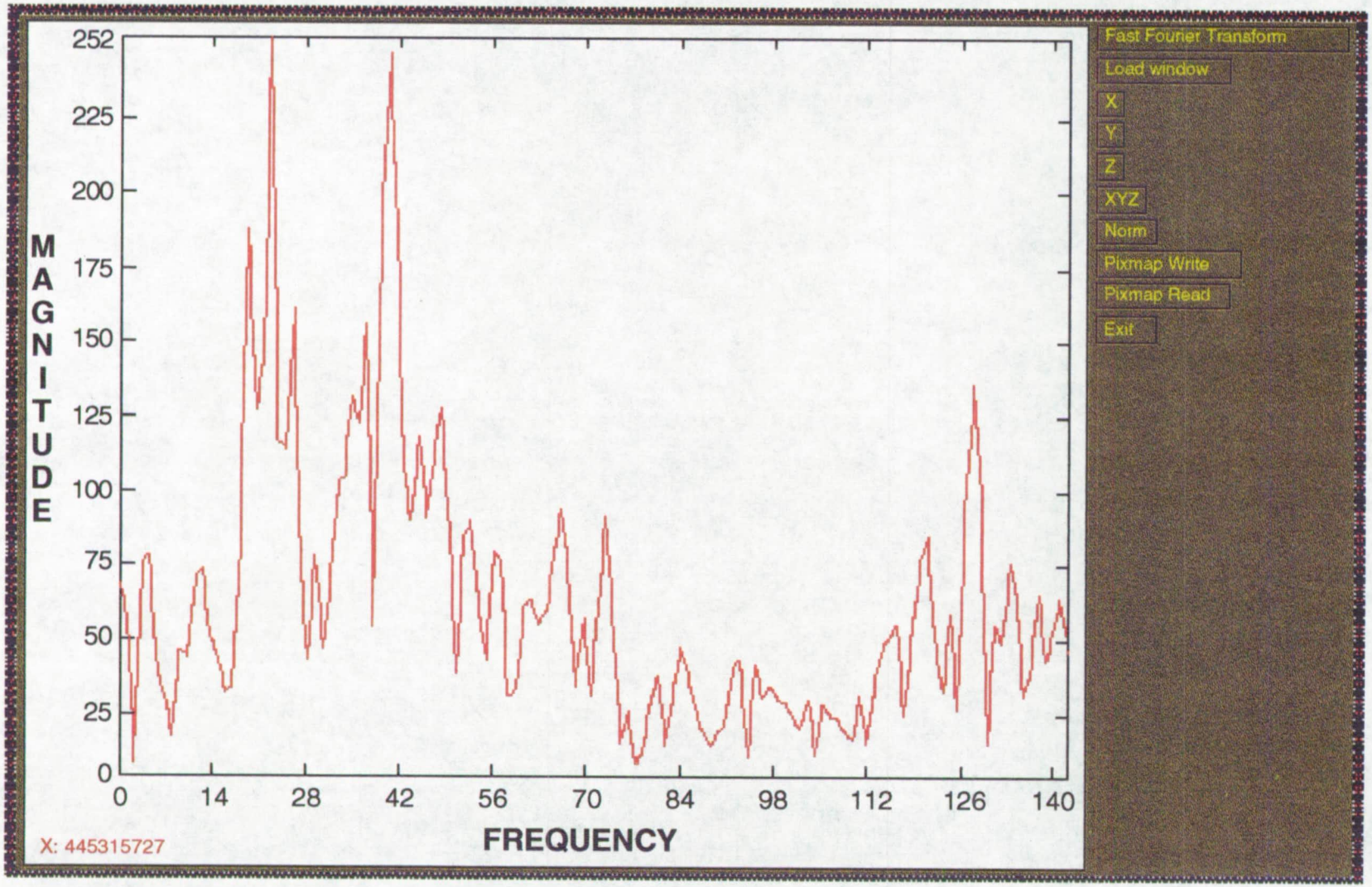

Figure 28. *Fft* X.

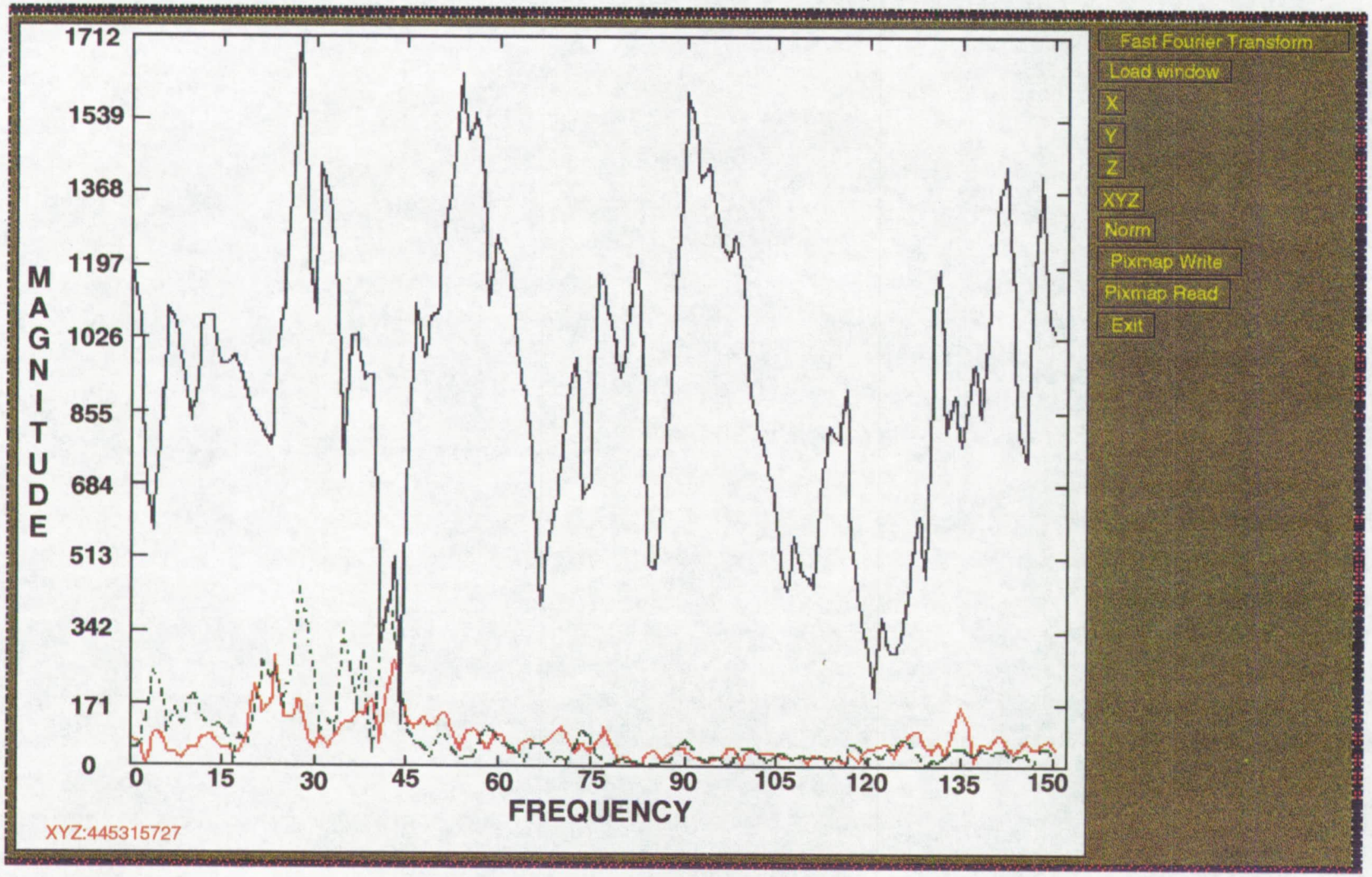

Figure 29. ***Fft*** XYZ.

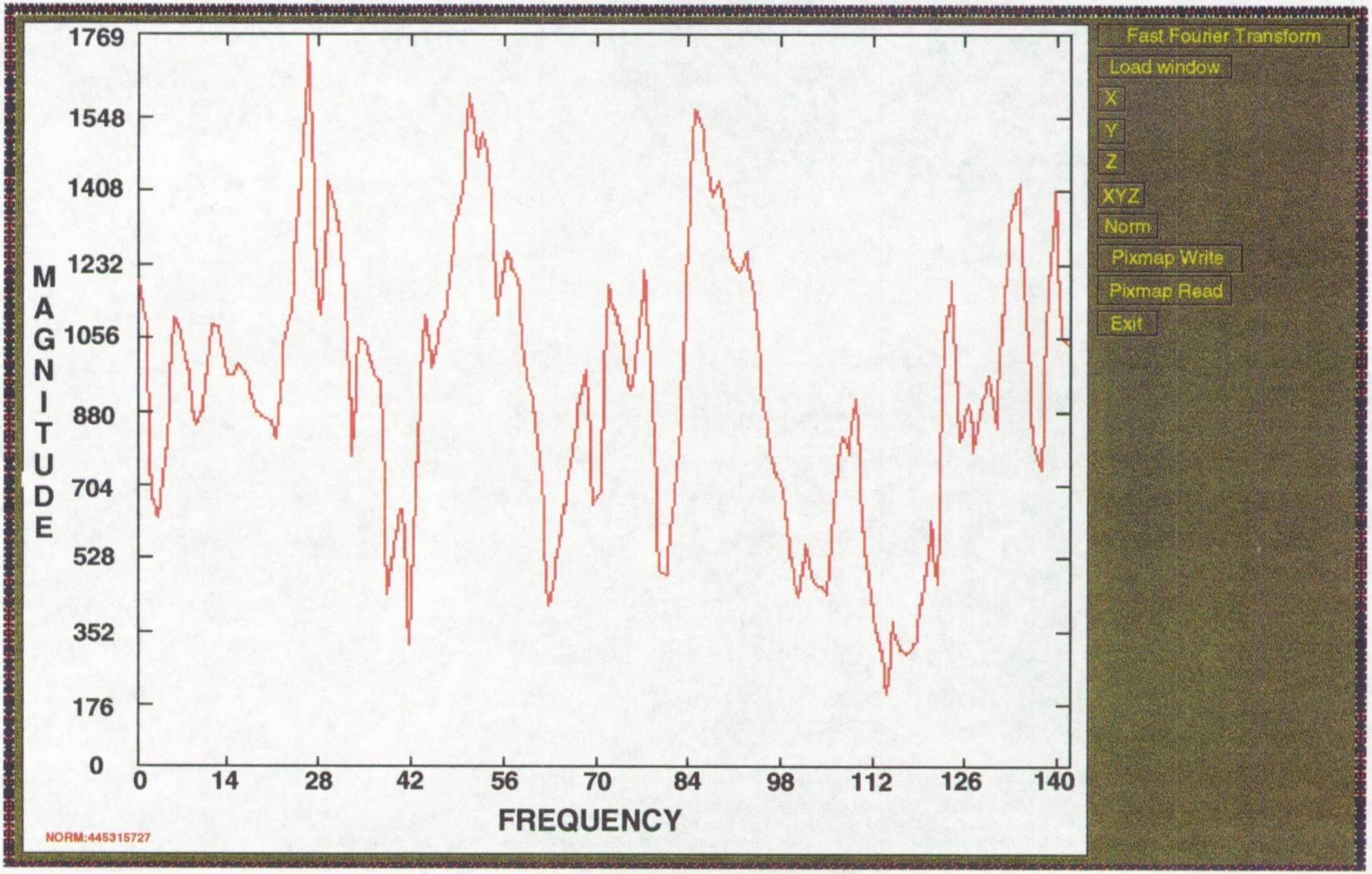

Figure 30. *Fft* NORM.

5.4 ***Query*** Usage

The ***query*** screen provides the query facility for the CDATA database. The ***query*** facility provides listing, editing, and searching capabilities. Selection of ***query*** from the main menu X window causes figure 31 to appear. At this point, the user must select the dataset on upon which he/she desires to operate. Once the user has selected the dataset, PRIDE displays a ***query*** window tailored to that dataset. Figure 32 shows the ***query*** window for the ACCEL dataset of PRIDE. Clicking on *next* causes the next record in the dataset to be displayed. Each dataset remembers which one of its records was last accessed. *Next* locates and displays the record which is located in the next position. Clicking on *prev* causes the previous sequential record to be located and displayed. *Clear* causes all fields in the window to be cleared. If the user enters a value in each slot of the primary key and then clicks on *search* then PRIDE will locate the record in the dataset which matches that primary key. If the user creates an entirely new entry or modifies an old entry and then clicks on *write*, then the present entry is written to the database. If the user clicks on *delete,* then the present entry is deleted from the database.

5.5 ***Classify*** Usage

The ***classify*** screen is a specialized query screen. This screen is used in order to enter the classification results of viewing the various visualization screens. Figure 33 shows this screen. The ***classify*** window works on the CLASSES dataset and no other dataset and thus its options are specialized. Recall that each dataset remembers its last accessed entry. This memory is retained on disk over different runs of the database programs. Clicking on *next-classification* causes ***classify*** to look up the present entry, note the classification value, search for the first entry further down the primary key trail that has a higher classification value, and display that entry. Clicking on *prev-classification* causes ***classify*** to look up the present entry, note the classification value, search for the first entry back up the primary key trail that has a lower classification value, and then display that entry. Clicking on *next-class* causes ***classify*** to look up the present entry, note the class value, search for the first entry further down the primary key trail that has a higher class value, and display that entry. Clicking on *prev-class* causes ***classify*** to look up the present entry, note the class value, search for the first entry back up the primary key trail that has a lower class value, and then display that entry. Clicking on *next-window* causes ***classify*** to look up the present entry, note the window start time, search for the first entry further down the primary key trail that has a later window start time, and display that entry. Clicking on *prev-window* causes ***classify*** to look up

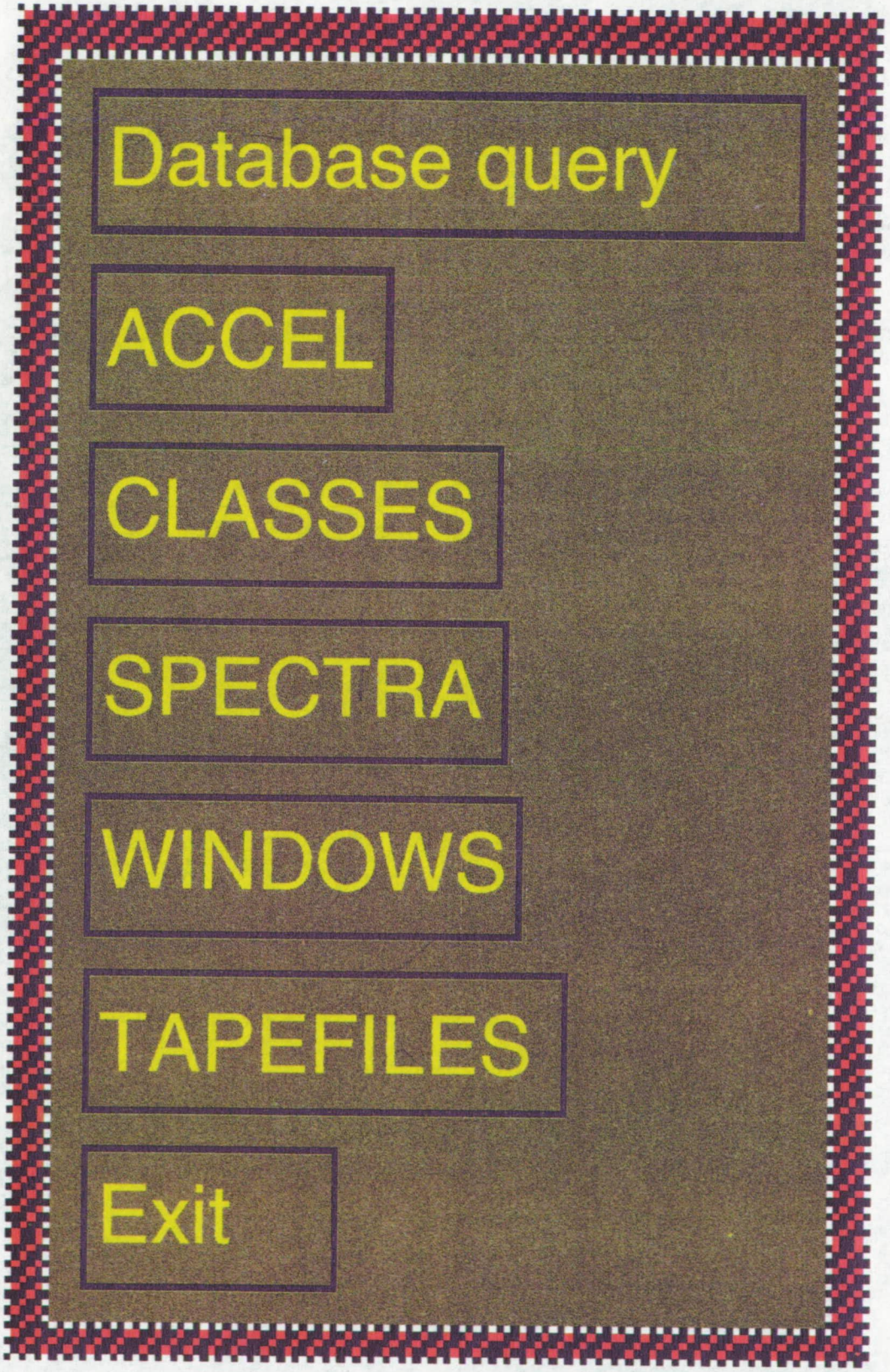

Figure 31. Dataset selector.

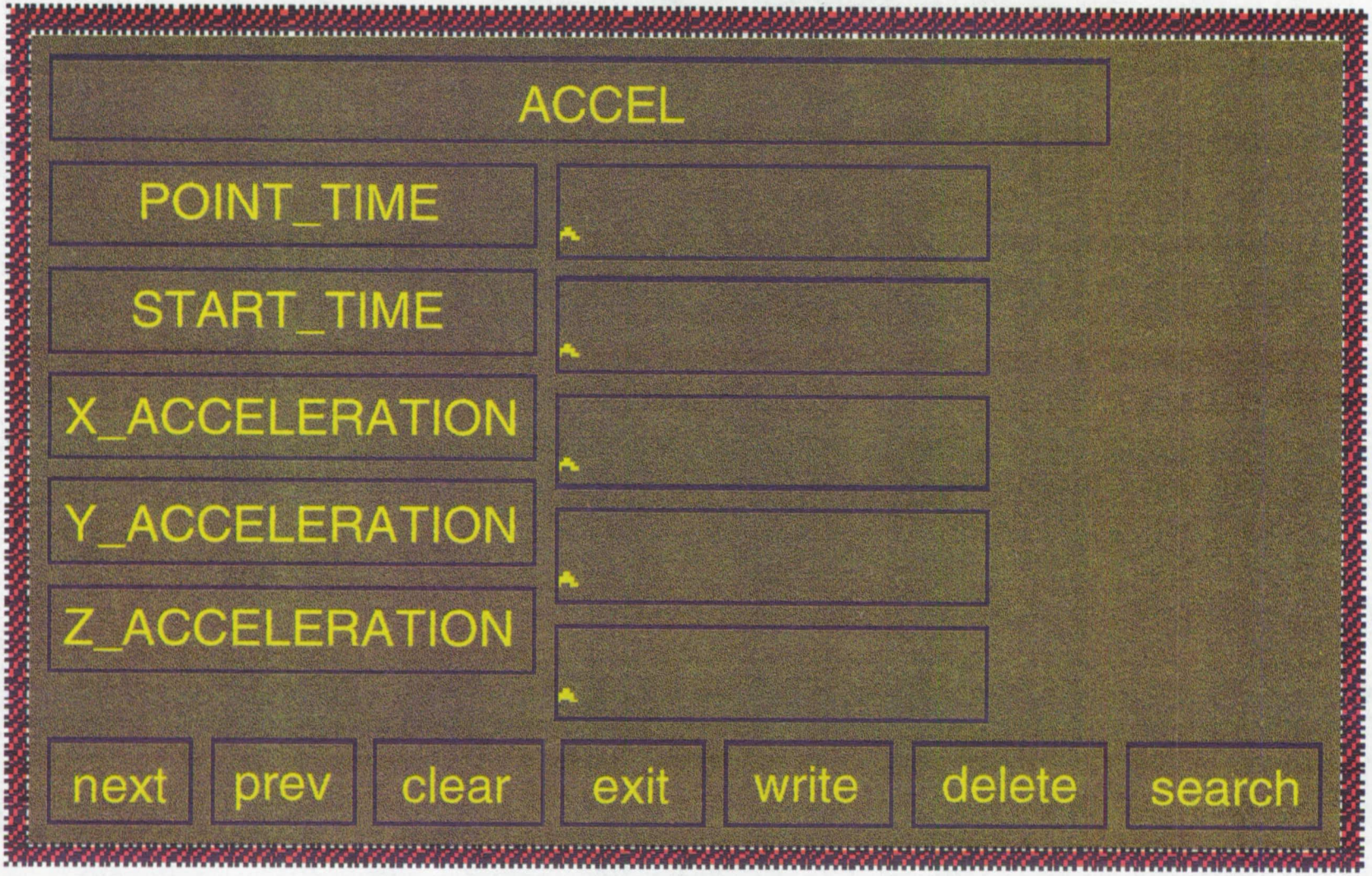

Figure 32. ACCEL *Query*

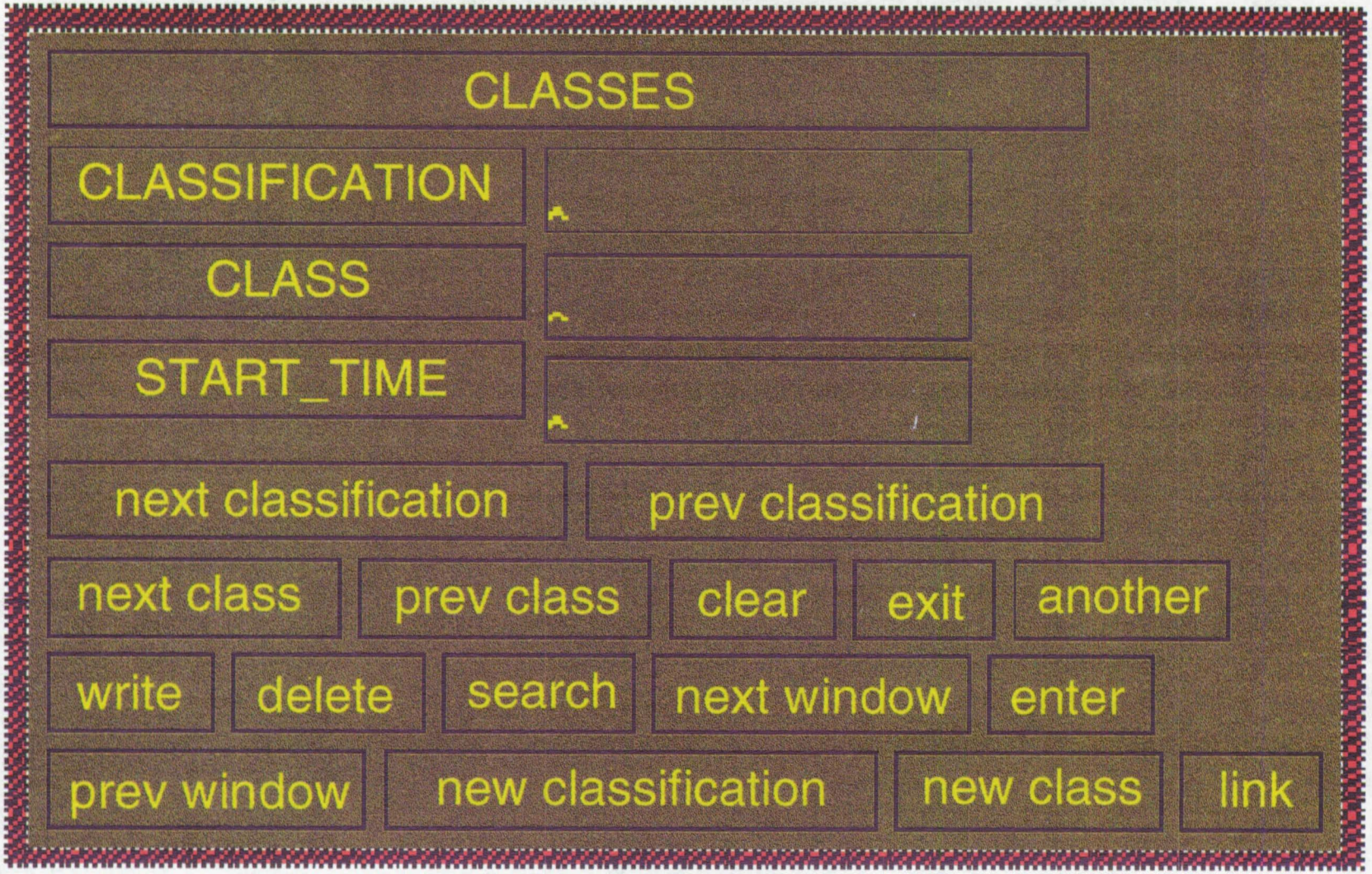

Figure 33. ***Classify.***

the present entry, note the window start time, search for the first entry back up the primary key trail that has an earlier start time, and then display that entry.

Clicking on *another* causes the window field to be cleared while retaining the present classification and class values. This is useful when the user knows the start time of a window that he/she wishes to enter into the present class of the present classification. The other way to enter a window into the present class and classification is to use the *link* and *enter* buttons in conjunction with one of the visualization screens. This method of placing an event into a class begins by bringing up one of the visualization screens and then clicking on *link*. At this point, the programs which control the visualizations are listening for a click event inside their windows. The user now clicks inside the drawing area of the visualization component which is presently displaying a graphic representation of the event that the user wishes to place in the present class. The program controlling the visualization notes this click and then enters the time of the event into a cut buffer. A cut buffer is a memory area provided by X into which an X program can use for interprogram communication. At this point, the user clicks on *enter* on the ***classify*** screen. The controlling program for ***classify*** looks in the cut buffer for the window start time and enters that into the window slot. The linkage is now complete. Note that the user never had to know the start time of the event to create this linkage.

Clicking on *new class* causes the window slot to be cleared, the class slot to be incremented by one, and the classification value to be retained. This is the way that a user stays within the present classification but creates a new, empty class. Clicking on *new classification* causes the window slot to be cleared, the class slot to be set to zero, and the classification slot to be set to the next available unused classification value.

In addition to these specialized functions, ***classify*** provides the *write*, *delete*, and *clear* functions described in the discussion of the ***query*** component.

5.6 *Isodata* Usage

The ***isodata*** option activates the ISODATA program to run upon the FFT information concerning the present set of located events. This option does not have an associated GUI. Rather, it is controlled by keyboard input from the xterm from which the PRIDE main menu GUI was activated. When activated, the ***isodata*** component requests the starting desired number of clusters and the maximum number of iterations. After this point, ***isodata*** iteratively clusters the data depending upon the present set of parameters. Appendix ISODATA contains a few pages from the ***isodata*** component. Some of the options such as removing a cluster from consideration are not fully implemented in the full-blown database version of PRIDE.

5.7 *Expertiso* Usage

The ***expertiso*** option triggers the ISODATA program to run upon the FFT information concerning the present set of located events. The difference is that a CLIPS expert system is controlling the operation of ISODATA, not a human operator. The ***expertiso*** component analyzes how varying the number of desired clusters affects the clustering. The information for each clustering is stored and is evaluated after a fixed number of clusterings has been generated. For each number of clusters, ***expertiso*** determines which clustering was optimal. An optimal clustering was defined to be a clustering in which the clusters were far apart and in which the points of each individual cluster were grouped close together. Appendix EXPERTISO is the output of such a program.

5.8 *3dfft* Usage

The ***3dfft*** component simultaneously shows the Fourier transform information of either individual events or of all defined events. The *loadwindow* button functions as previously described. The *sphere* button causes the Fourier information to be plotted as a set of unconnected spheres for a given event. The *line* button causes each event to have its Fourier information to be plotted as a set of connected line segments. The ***3dfft*** component is normally is line mode. Clicking on *loadall* causes the Fourier information for every event to be plotted simultaneously. The *remove* button is used to clean up the display after a single event has been displayed. The sequence of events is that a given event is plotted and then the user can either overlay the plot of another event or the user can click on the *remove* button, click on the *loadwindow* to indicate which event to remove, and finally click within the display area to indicate that the selected window should be removed from that component. Figure 34 provides an example of the plot of the FFT information for a single event.

5.9 *Ergodic* Usage

The ***ergodic*** component provides an analysis capability about the distribution of energy within the acceleration data. Clicking on *base* provides an two-dimensional animation of the energy distribution according to window size. The independent variable in this case is window size. Figure 35 provides an example of one such distribution. Clicking on *energy* normalizes with respect to the maximum recordable acceleration and displays an animation of these results. Clicking on *normalize* normalizes for the effect of different window sizes and thus different ranges of possible energy. Clicking on

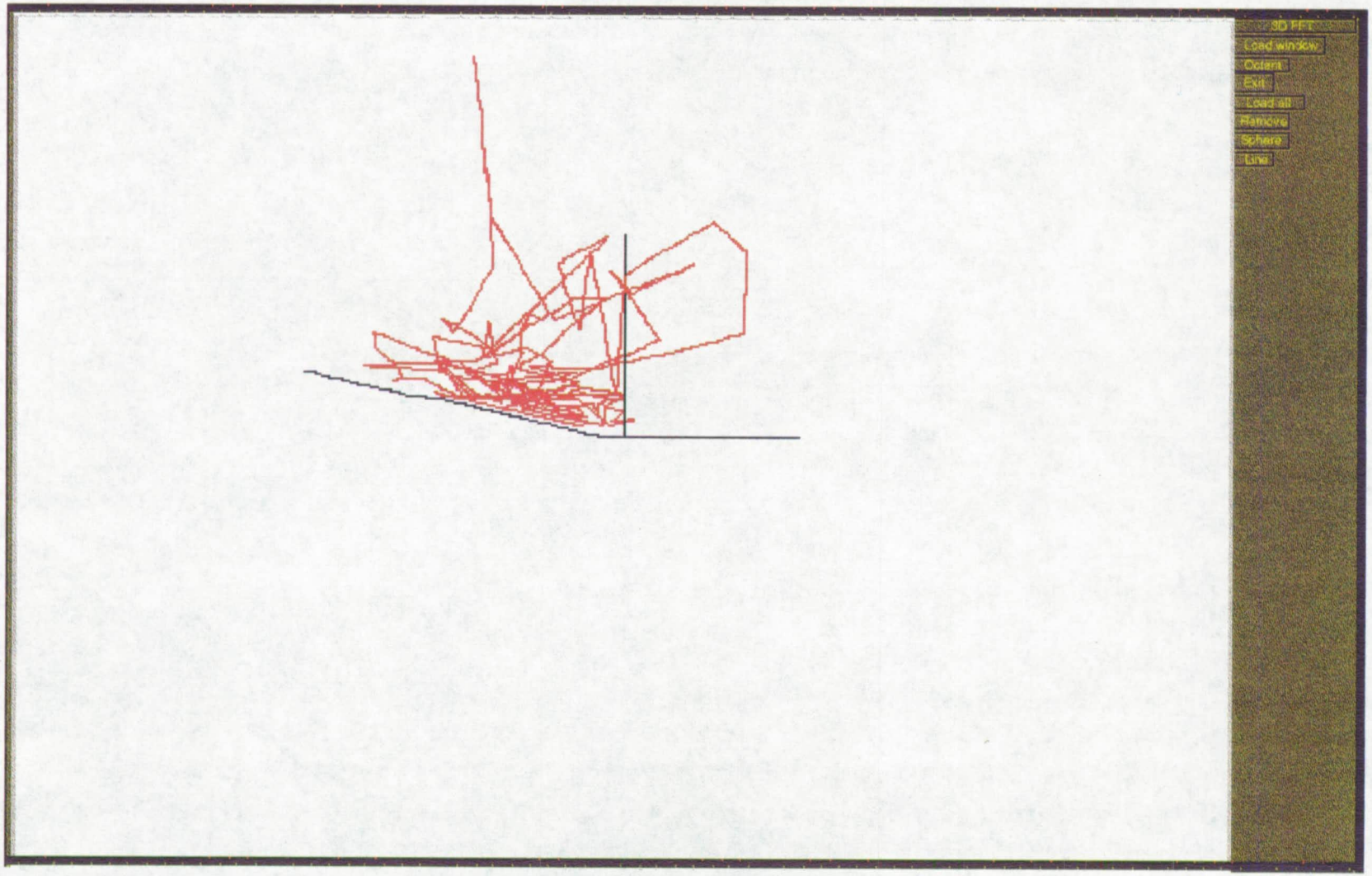

Figure 34. ***3dfft*** for a single event.

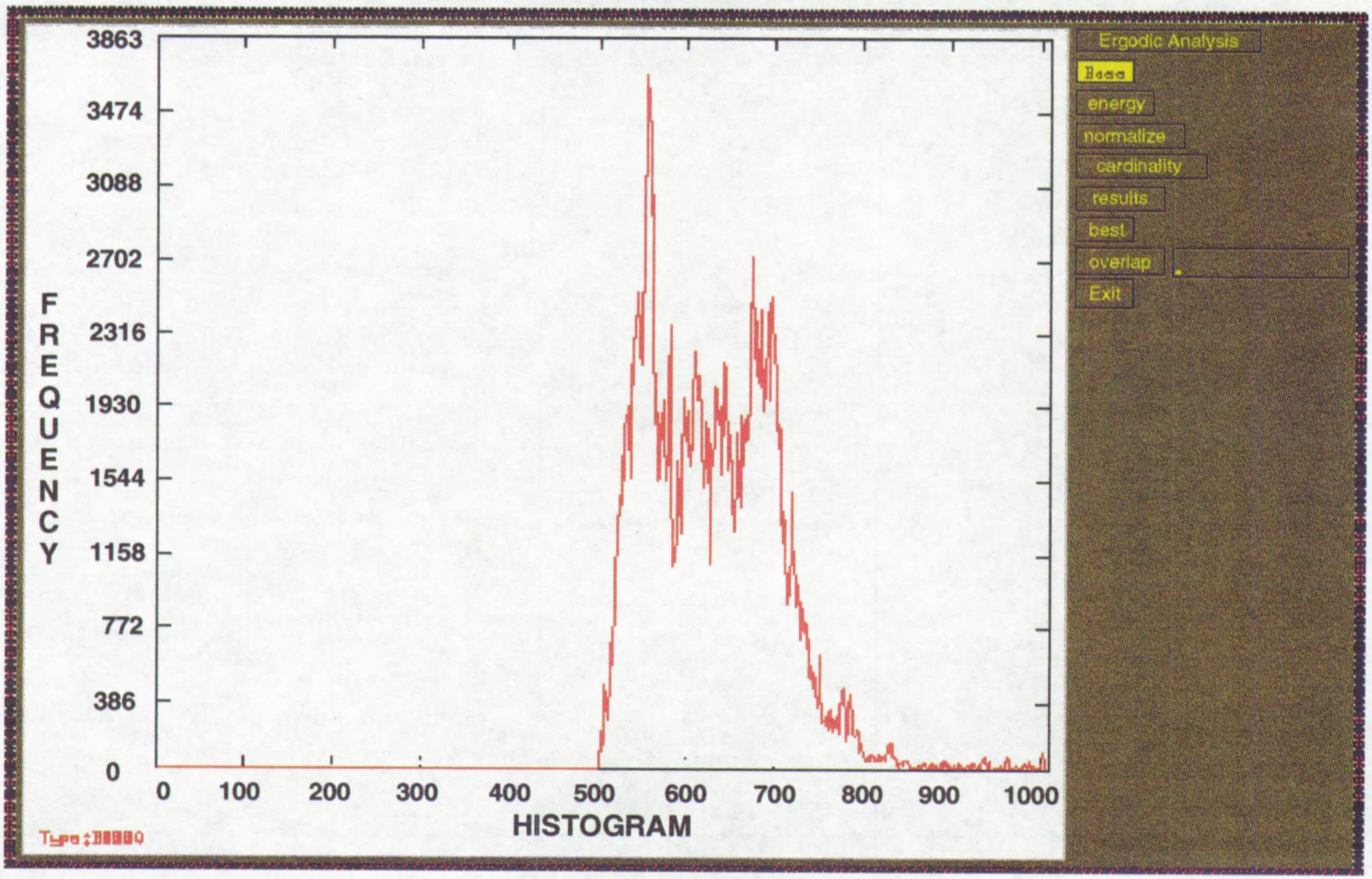

Figure 35. ***Ergodic*** base.

cardinality normalizes for the various skews of the windows. Clicking on *results* displays the goodness values for each window size. Figure 36 contains an example of this type of display. The independent variable is window size and the dependent value is goodness. Clicking on *best* displays the energy histogram for the window size associated with the highest goodness. If the user first clicks on *best*, then enters a number between 0 and 1000 in the text window next to the *overlay* button and then clicks the *overlay* button, then a display of where the high energy events are in the window is produced. Figure 37 shows this output for a given 30 minute window. The number that is entered indicates a histogram slot. Every event which has an energy value greater than or equal to the energy value associated with that slot is located in the raw acceleration data. Subsequently, every located event is displayed.

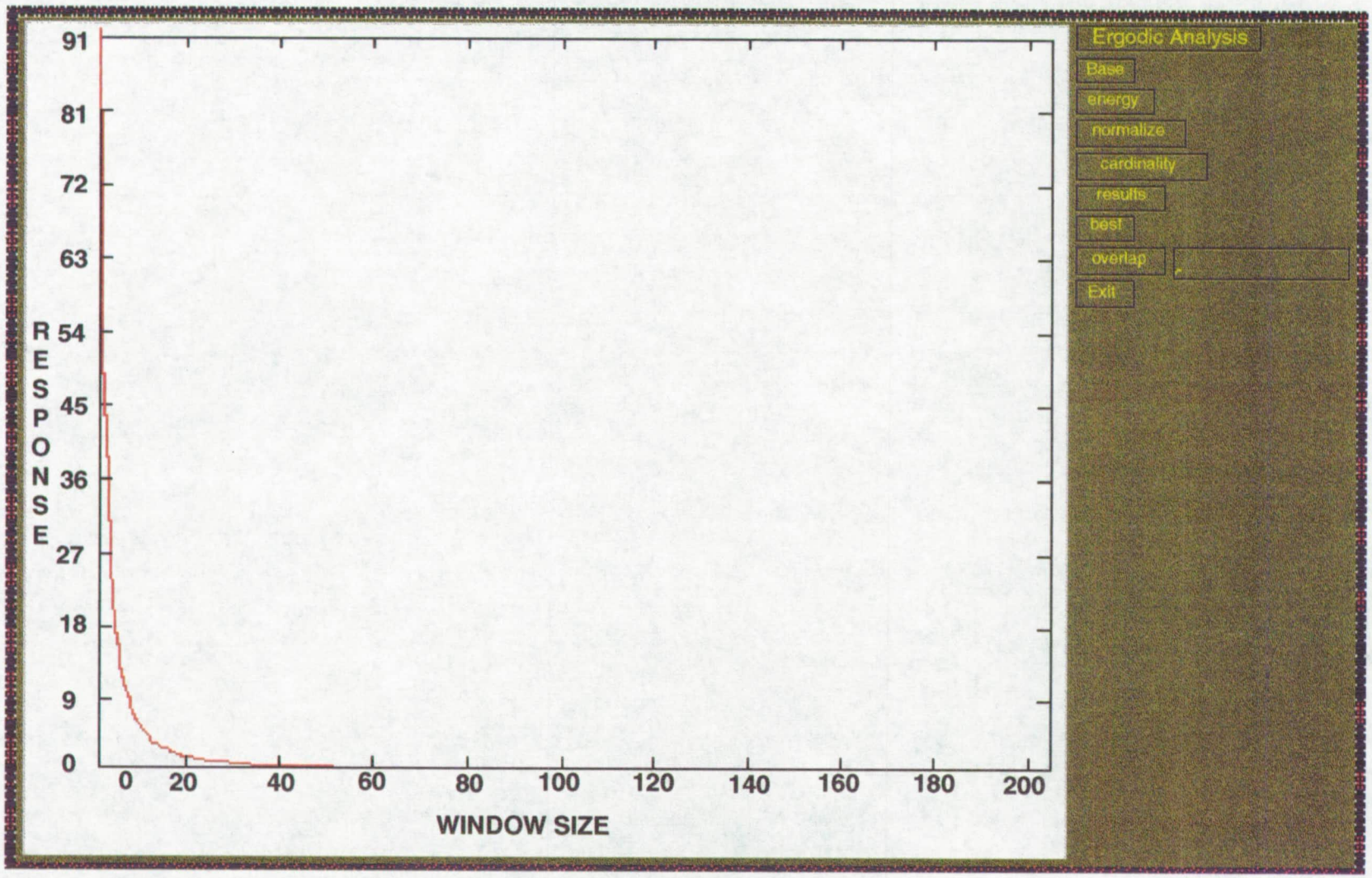

Figure 36. ***Ergodic*** Results.

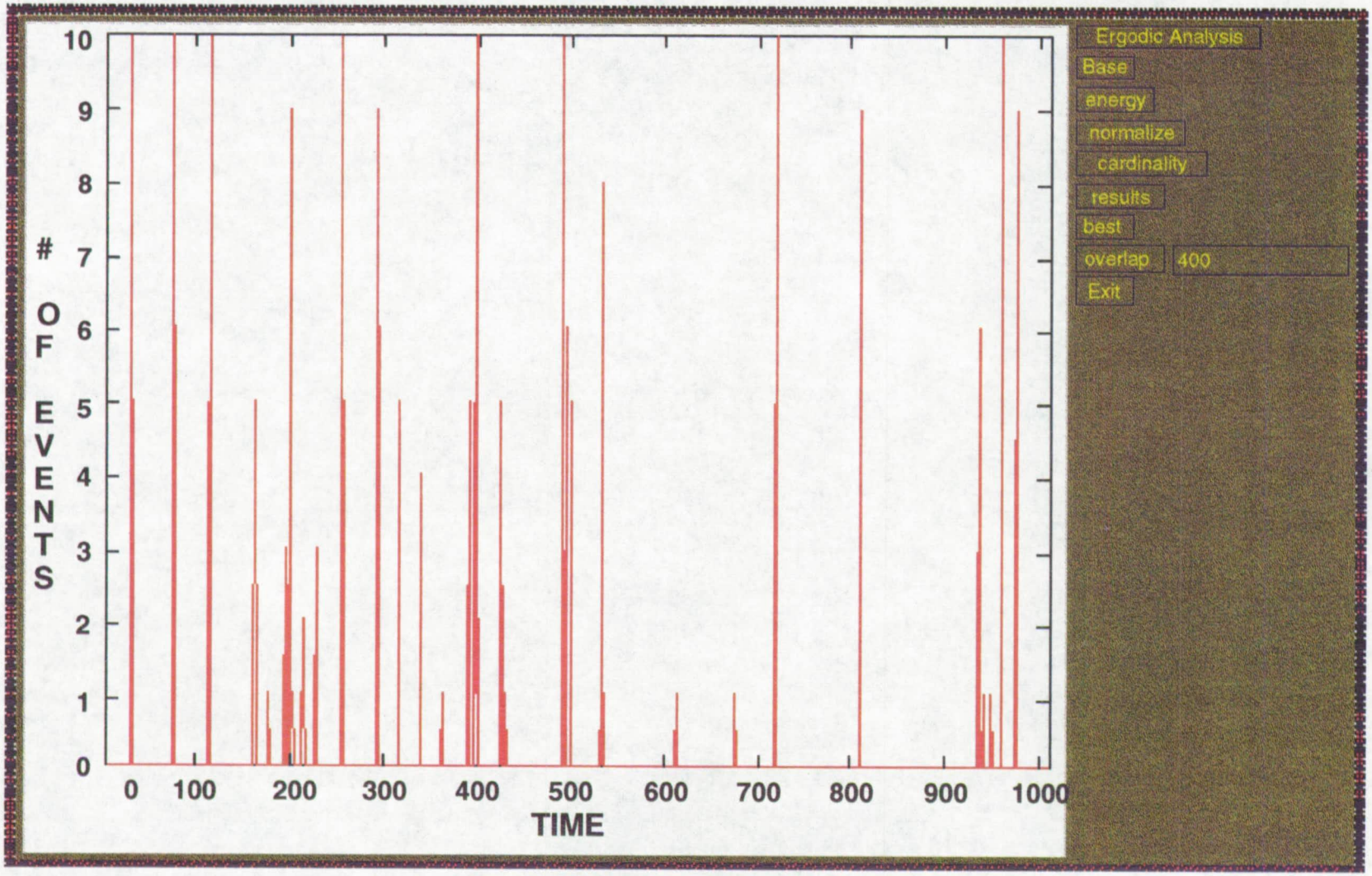

Figure 37. ***Ergodic*** Overlay

CHAPTER VI
CONCLUSIONS AND RECOMMENDATIONS FOR FOLLOW-ON RESEARCH

The benefits of PRIDE summarized here are a classification of the observed events, an evaluation of the validity of this classification, and an assessment of the PRIDE features.

6.1 Conclusions

6.1.1 Classification

6.1.1.1 Standalone *Timeseries*

The results of analyzing the abstract acceleration event windows produced by vibration windowing using ***timeseries*** are that most of the events display strong oscillatory tendencies. Visually this appears as a changing preference for certain curves in three dimensional space. In other words, the track of acceleration vectors like to go where they have gone before. Figure 38 shows an example of this behavior. These preferred curves change constantly and can assume several different configurations during a single event. From one event to another; to the human eye, there does not appear to be much correlation between the preferred space curves. There are a few shapes which appear more than once. These space curves are oval/elliptical curves , spiral curves, and a space curve which is reminiscent of a two-dimensional representation of a fish. Figures 27, 39, and 40 are respectively examples of elliptical curves, spirals, and fish. The existence of these space curves suggests that syntactic pattern recognition may be applied to the windows.

The events contain a few highly energetic windows while the majority of the events are of similar average magnitude. This suggests the possibility of using the average magnitude of the acceleration vectors as an attribute to be assigned to individual events.

The amount of time it takes to view the events can be burdensome. The average size of the windows is 100 acceleration vectors and the upper range is approximately 1000 acceleration vectors. At a display rate of 1 new vector per second, it takes 100 seconds to display the average abstract acceleration event. The amount of data utilized during this analysis was 1.5 hours of acceleration raw data and 53 abstract events. Thus, the time it took to view the 53 events was approximately 2 hours. In order to compare animation in general, the time is considerably larger. The order shifts from order n to order n^2 and the time shifts from 2 hours to 106 hours. This full inspection was not performed. This inspection time is strongly influenced by the parameter settings for the

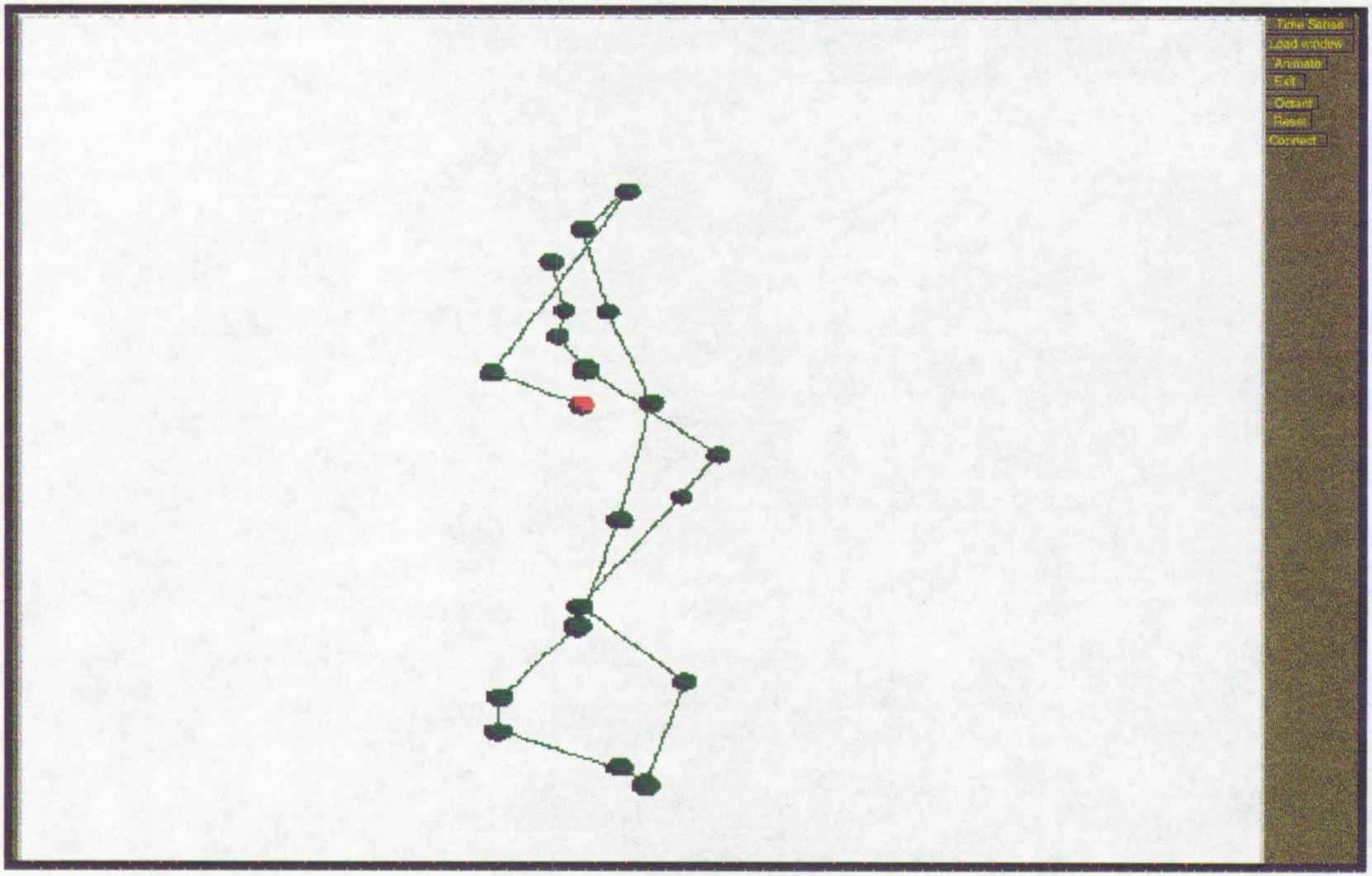

Figure 38. ***Timeseries*** Elliptical Curve

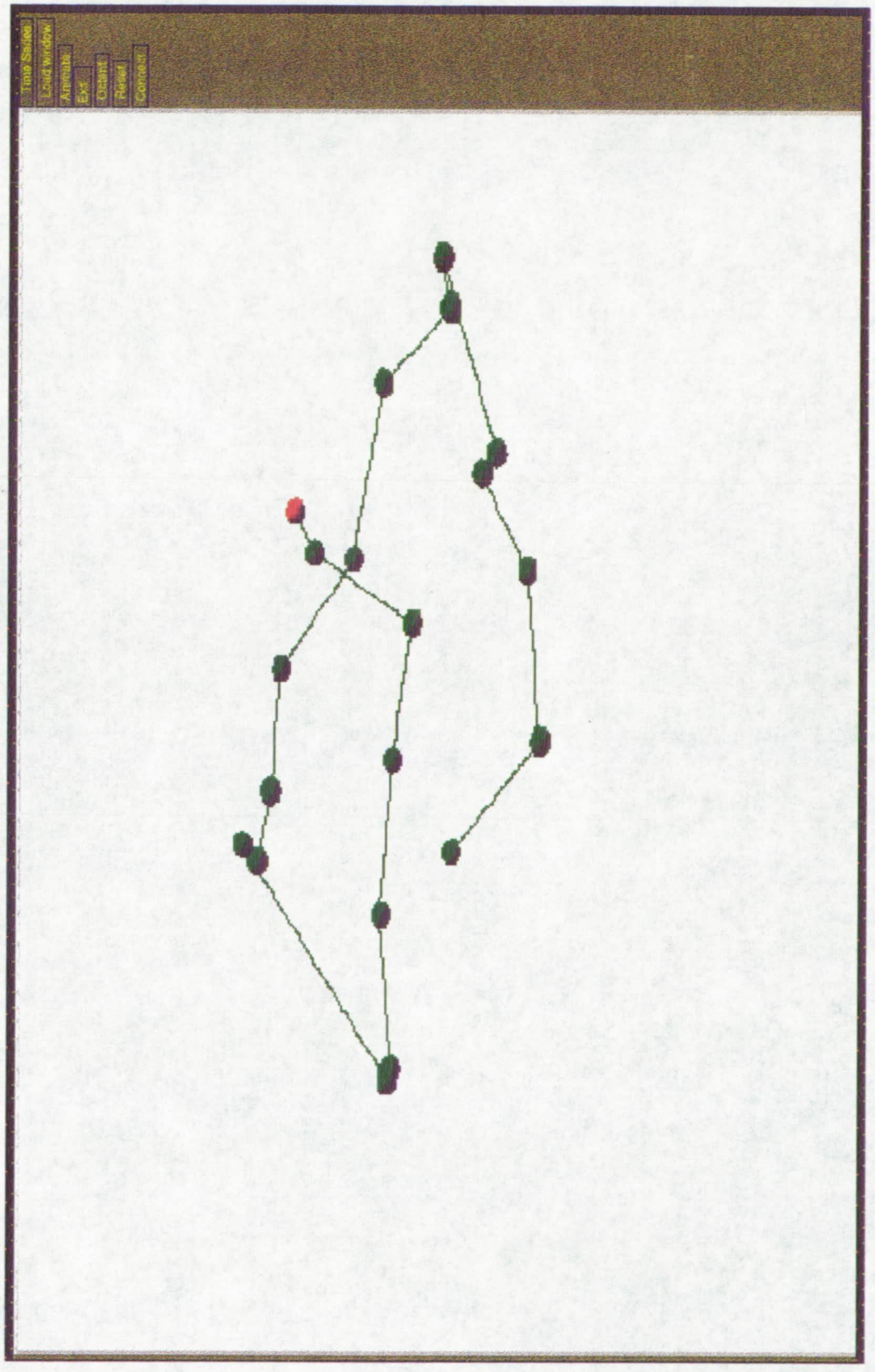

Figure 39. ***Timeseries*** Spiral

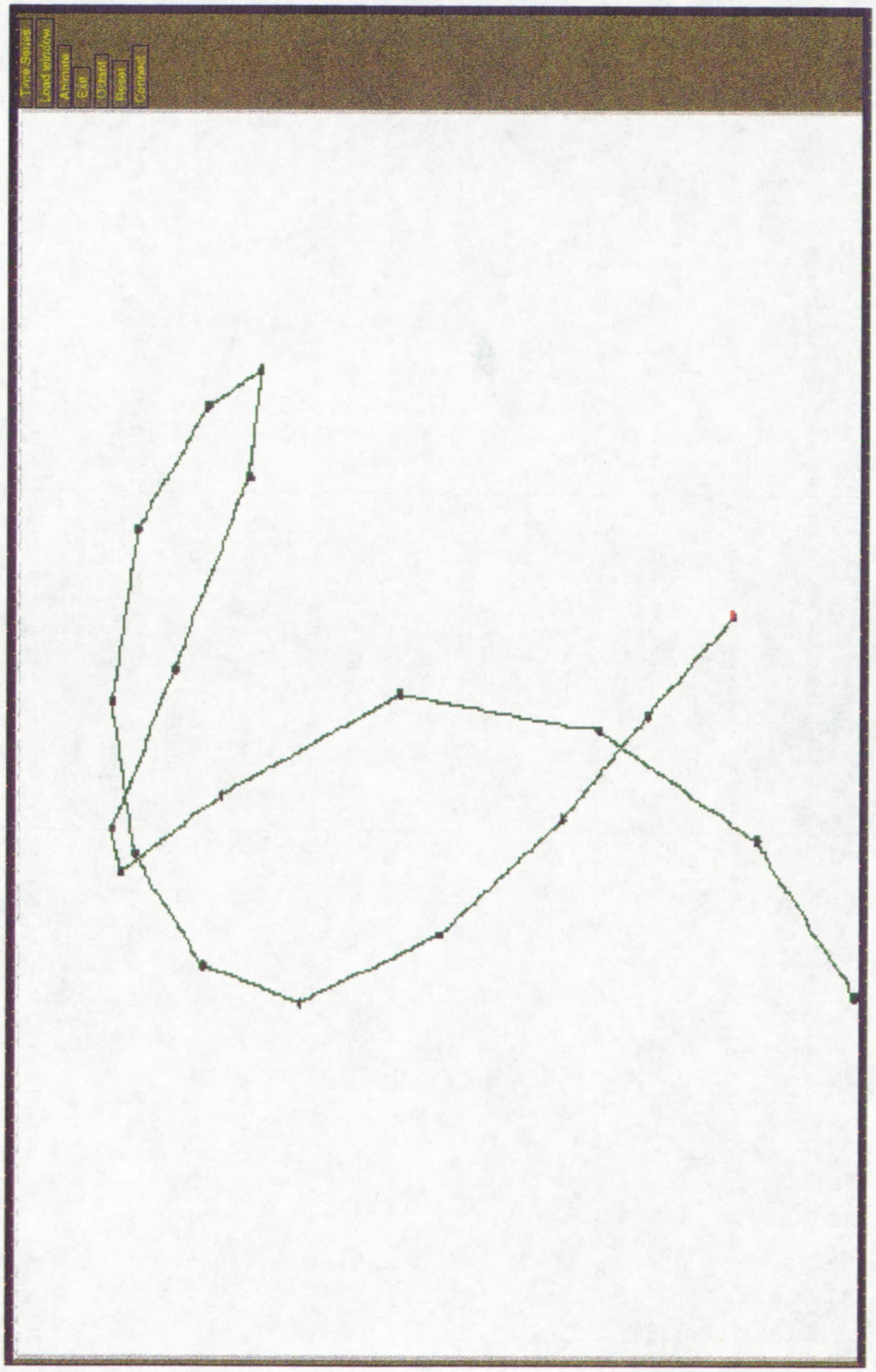

Figure 40. ***Timeseries*** Fish.

vibration windowing technique. The inspection time is completely determined the by parameter settings for the vibration windowing technique in conjunction with the configuration of the raw acceleration vectors.

6.1.1.2 Standalone ***Staticcloud***

The results of analyzing the abstract acceleration event windows produced by vibration windowing using ***staticcloud*** are that there exist a number of configurations which reappear in the data. Not all events are definitely one or the other but some event windows are clearly typical examples of a type of event. The four event types observed are fish, football, spheroid, and left-right ellipsoid. These events are named for the three-dimensional shape that they most resemble. The fish event is the most prevalent and contains the majority of high energy events. Figures 41 and 42 are examples of such ***staticclouds***. The primary characteristic of fish events are that they are aligned along the y axis. The secondary characteristic is that there are a number of acceleration events which are away from the y axis and are high magnitude. It is these events which form the shape of the fish in figure 40.

The second most common form of event is the football event. The accelerations in footballs tend to be of lower magnitude, to be evenly distributed within the interior of the football, and to completely fill the football. There appears to be two primary orientations of the football. Figure 25 is an example of a football.

The third event type is the spheroid event type. Figure 43 shows an example of this type of event.

The fourth event type is the left-right ellipsoid. Figure 44 provides an example of this type of event. This type of event is oriented along the x axis and thus runs from left to right on the screen. It is possible that left-right ellipsoids are merely variants of footballs but left-right footballs tend to be much more elongated than footballs and thus were assigned to a separate class.

These four classes may or may not be sufficient to partition the sample space. There are a number of events which do not clearly fall within these four classes.

The time is takes to use ***staticcloud*** is generally less than the time it takes to use ***timeseries***. The original draw of an event is fairly rapid. It is the repeated redraws triggered by rotation of the event in three-space that takes a considerable amount of time. Since the overall forms do tend to fall within certain classes the order of the classification process using only ***staticcloud*** is not n^2 but rather is closer to order n.

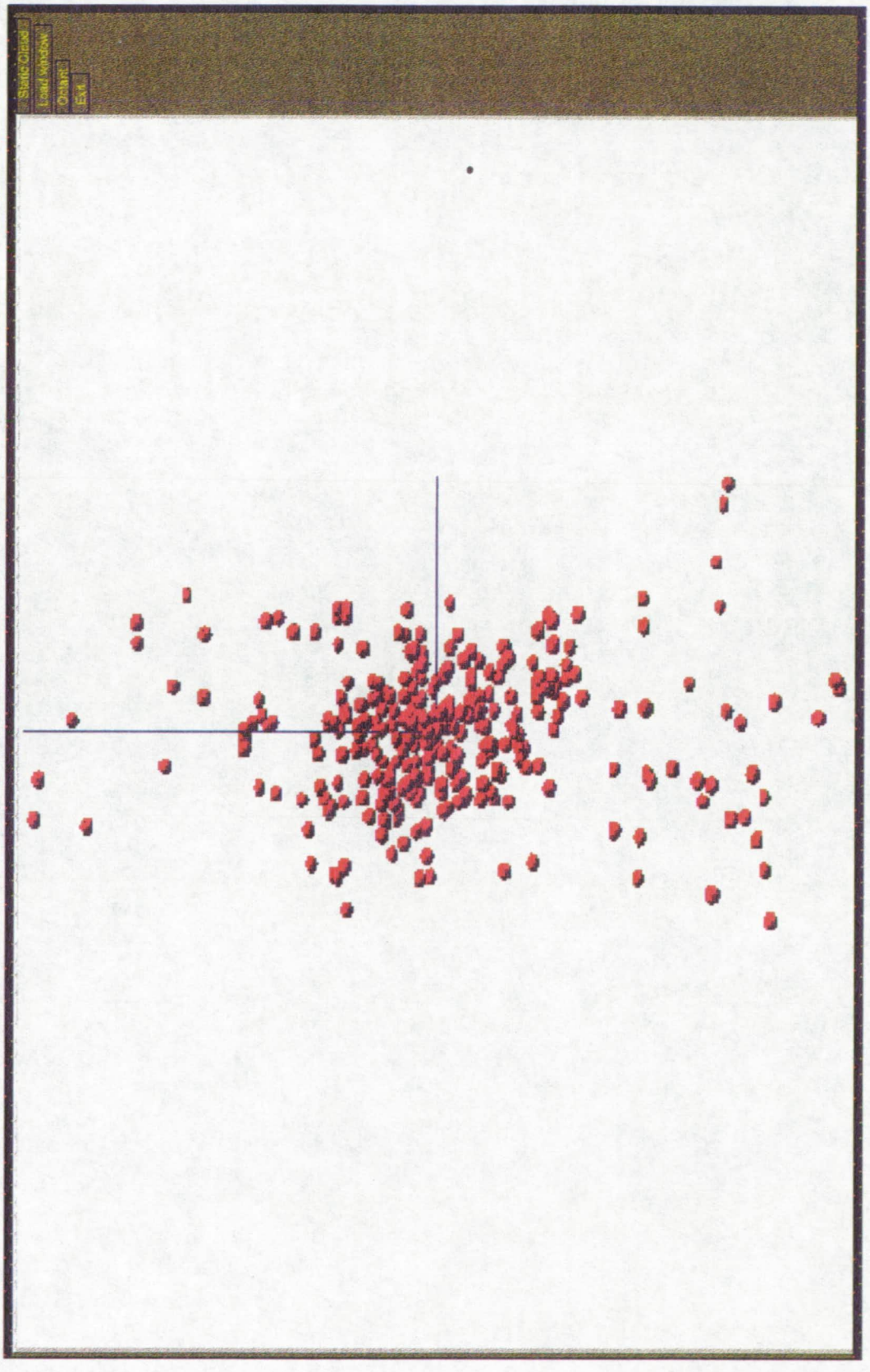

Figure 41. ***Staticcloud*** Fish.

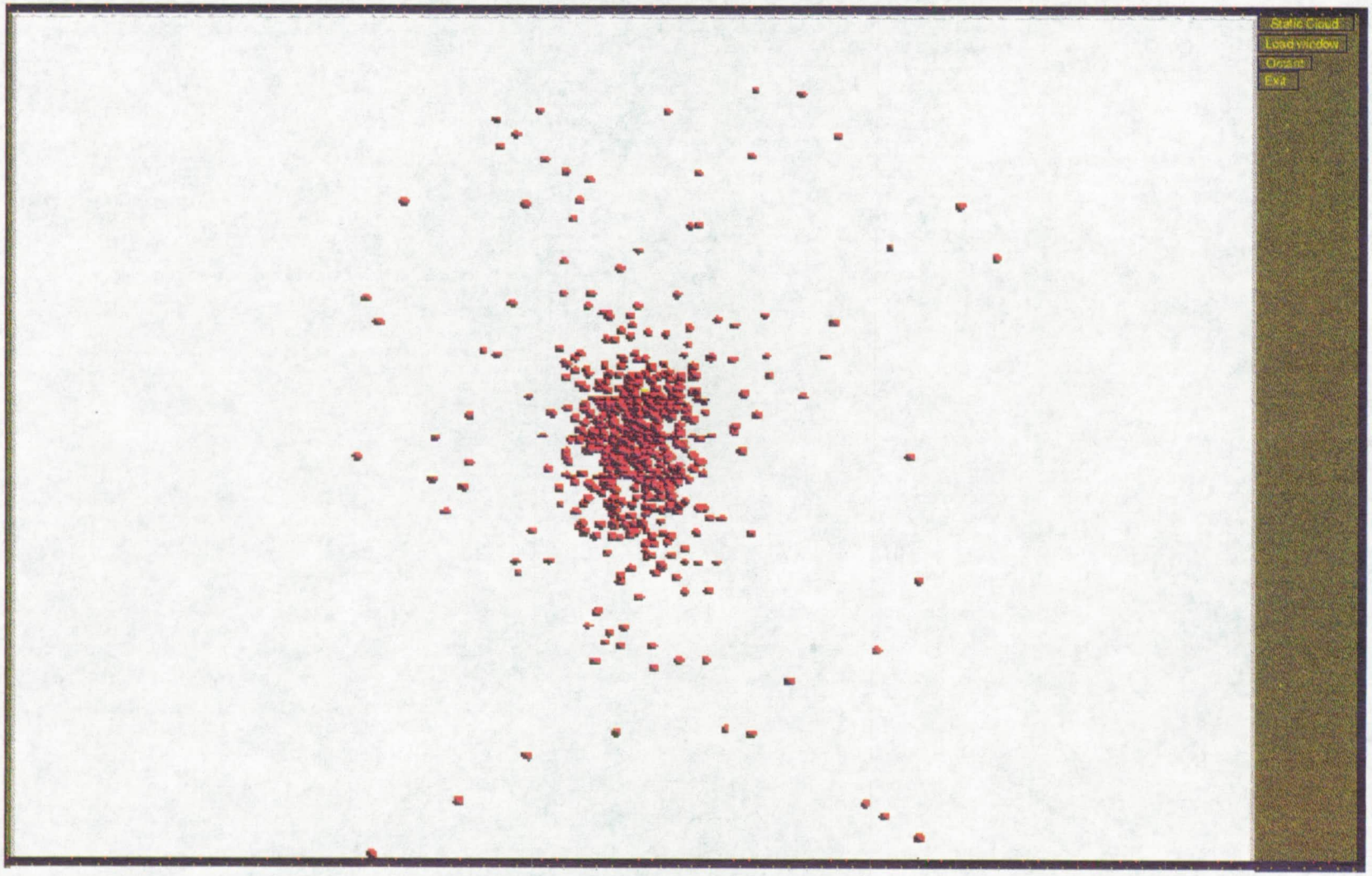

Figure 42. ***Staticcloud*** Fish.

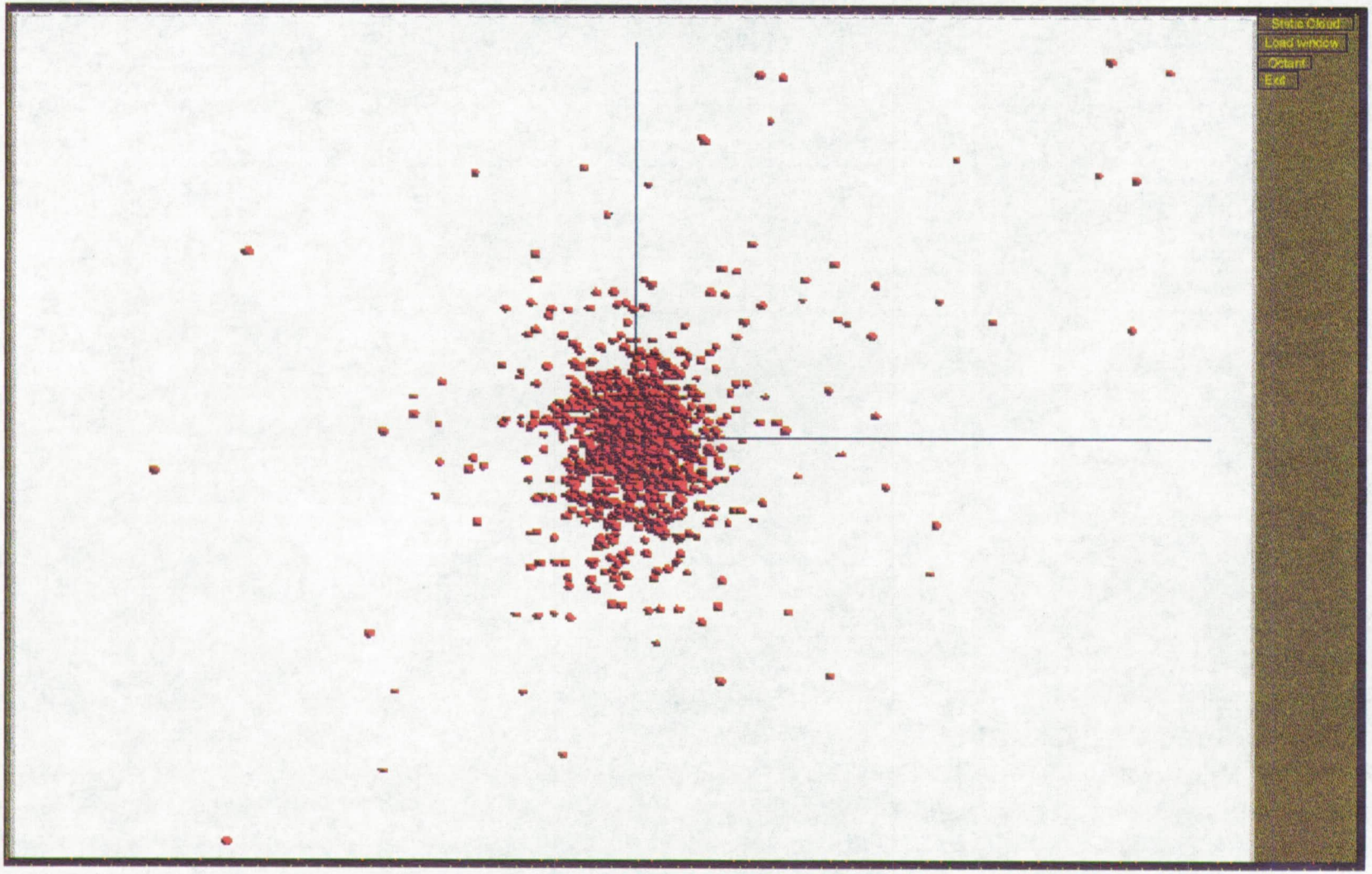

Figure 43. ***Staticcloud*** Spheroid

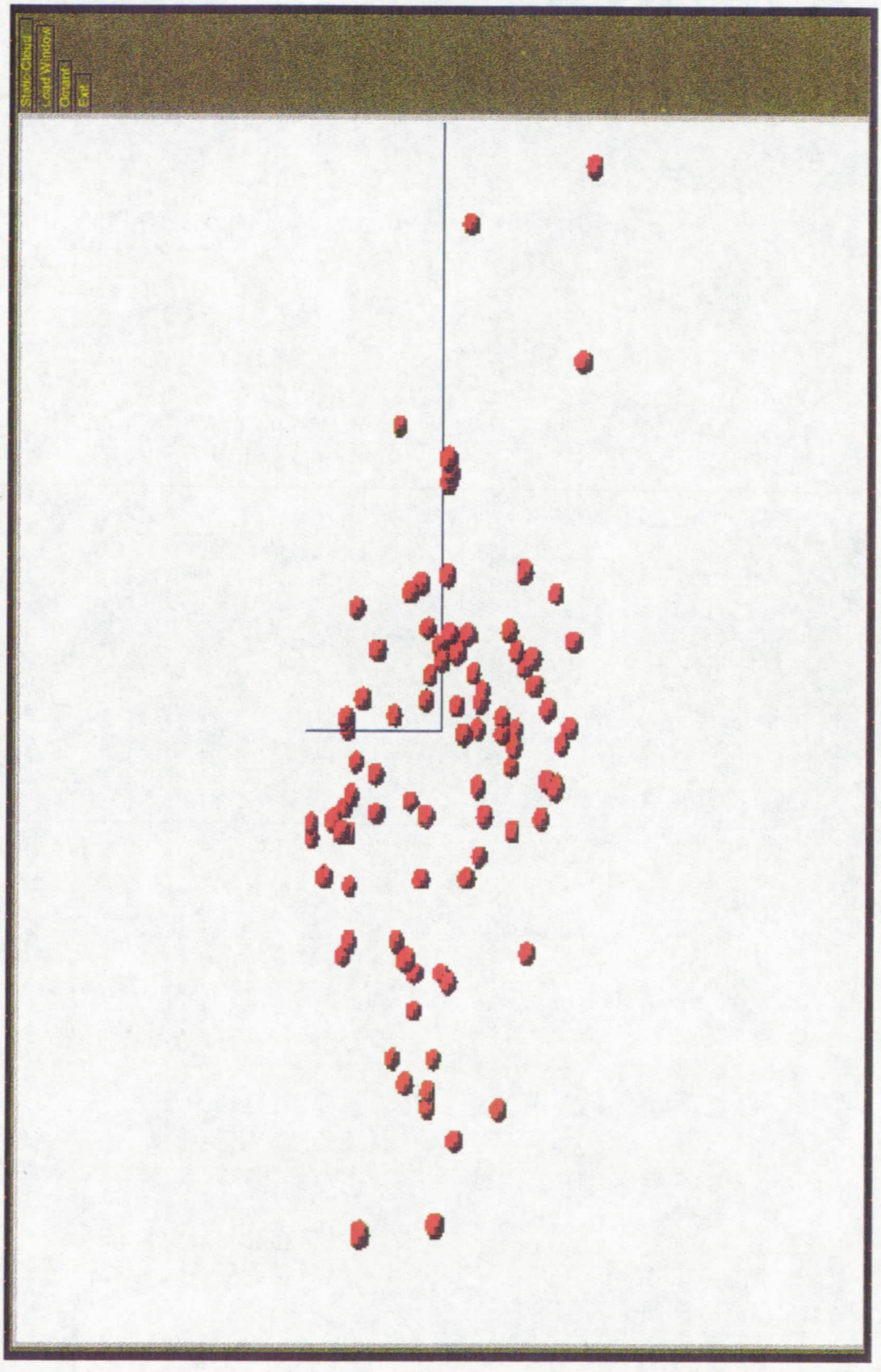

Figure 44. Staticcloud Left-right Ellipsoid.

6.1.1.3 Standalone ***FFT***

The results of analyzing the abstract acceleration event windows produced by vibration windowing using standard Fourier analysis are that the z component dominates the x and y components in every event and that the z magnitudes do not appear to follow any specific pattern. They appear to be nearly random. Since the z dominates x and y, the x and y options on the ***fft*** component are useless and the z and norm options are redundant.

Any given Fourier spectrum is rapidly drawn but since the spectra are so variable, any attempt to define classes will require an order n^2 operation. That is, each spectrum will have to be compared to every other spectrum in a pairwise fashion. Rough calculations indicate that approximately 50 hours would be required for this operation. This activity was not performed.

6.1.1.4 Standalone ***3dfft***

The results of analyzing the abstract acceleration event windows produced by vibration windowing using three-dimensional Fourier analysis are that the z component dominates the x and y components. This fact is made apparent by both the all-events-in-one plot and in each individual plot. These individual plots show extremely complex space curves and thus it is impossible to partition the data into classes using an order n method. If every individual event were compared to every other individual event then conceivably this would not be true. Since the time required for this activity is order n^2, the estimated required time is 50 hours. This was not done.

6.1.1.5 Standalone ***Expertiso***

The results of analyzing the abstract acceleration event windows produced by vibration windowing using a CLIPS expert system shell to control the operation of the ISODATA algorithm are that this technique will work but that there is a limit on the amount of data that may be processed. The ***expertiso*** component is unable to handle the 53 events with which the previous section dealt.

When run upon a single half hour data set, the ***expertiso*** component produces as its final result a description of the linkage from a given cluster size to a given time point within the run of the ***expertiso*** component. This linkage can be used to trace back to the exact description of the clustering. The linkage between clusters and events is not presently available from the program so the present utility of ***expertiso*** is limited.

6.1.1.6 Standalone ***Ergodic***

The results of analyzing the abstract acceleration event windows produced by vibration windowing are that the technique does produce useful data but that there is probably an error in the formulation of the selection method for the best window size. The initial histogram results of the technique indicate that the energy distribution begins as being close to a normal distribution but diverges from this distribution of the window size is increased. Figure 45 is the histogram for a window size of 10. Note the close resemblance to a normal distribution with a small standard deviation. Figure 35 shows the histogram for a larger window size. The distribution is clearly no longer normal and in fact is exhibiting strong modalities.

Figure 46 shows the "goodness" of various window sizes. This graph indicates that smaller window sizes are always better than larger sizes. Since the window size increment was 2000 in this case, then the best window size was window size 2000. There were 200 different window sizes used during the analysis. The largest window size was 400000 which is approximately 30 minutes of data. Figure 47 shows "goodness" for window sizes ranging from 10 to 2000. Note that this graph also indicates that smaller is better. Unfortunately, this seems counterintuitive. At this point, the most reasonable assumption is that there is problem in the normalization processes that produced these graphs.

Figure 37 shows the distribution of high energy events in the original raw data based upon the best window size The events that are defined to be high energy in relation to this graph are those windows whose energy value exceeds a user-selected energy threshold. This figure shows that these non-mutually exclusive events do indeed overlap in time. The present configuration of the program does not lend itself to comparing ergodically located events with vibration windowing located events.

6.1.1.7 ***Staticcloud/Fft*** Interaction

Viewing the standard ***fft*** information for each of the classes established by ***staticcloud*** does not impart any additional knowledge.

6.1.1.8 ***Staticcloud/Timeseries*** Interaction

The ***timeseries*** animation of fish type events show a preference for a certain axis which leads to an up and down activity along that axis. Spirals are also strongly featured. The interior of the fish is composed of damping vibrations.

The ***timeseries*** animation of football type events displays a behavior that is similar to fish events, i.e., there is a preference for a certain axis. However, the vectors appear to

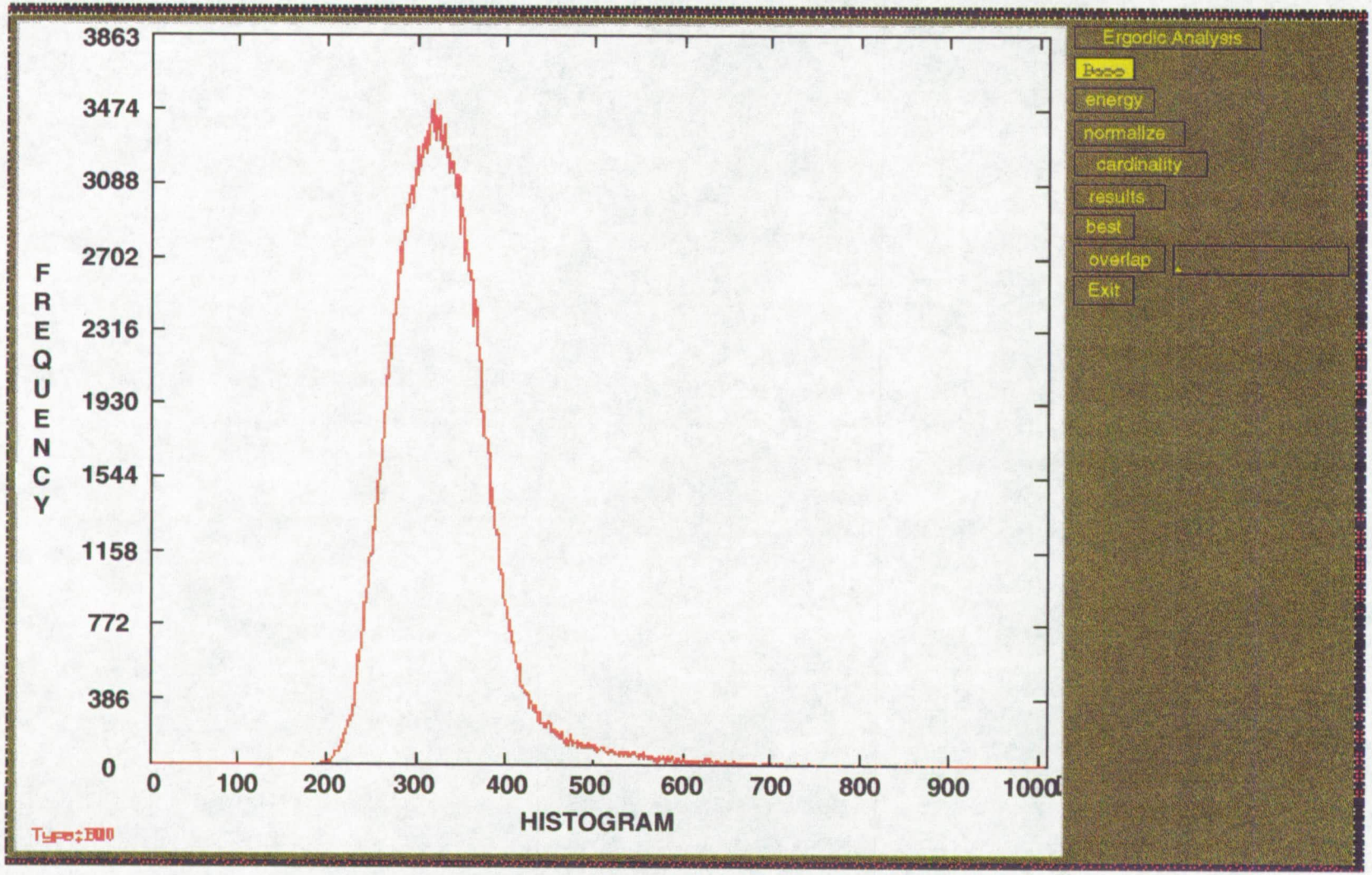

Figure 45. ***Ergodic*** Base Window Size 10.

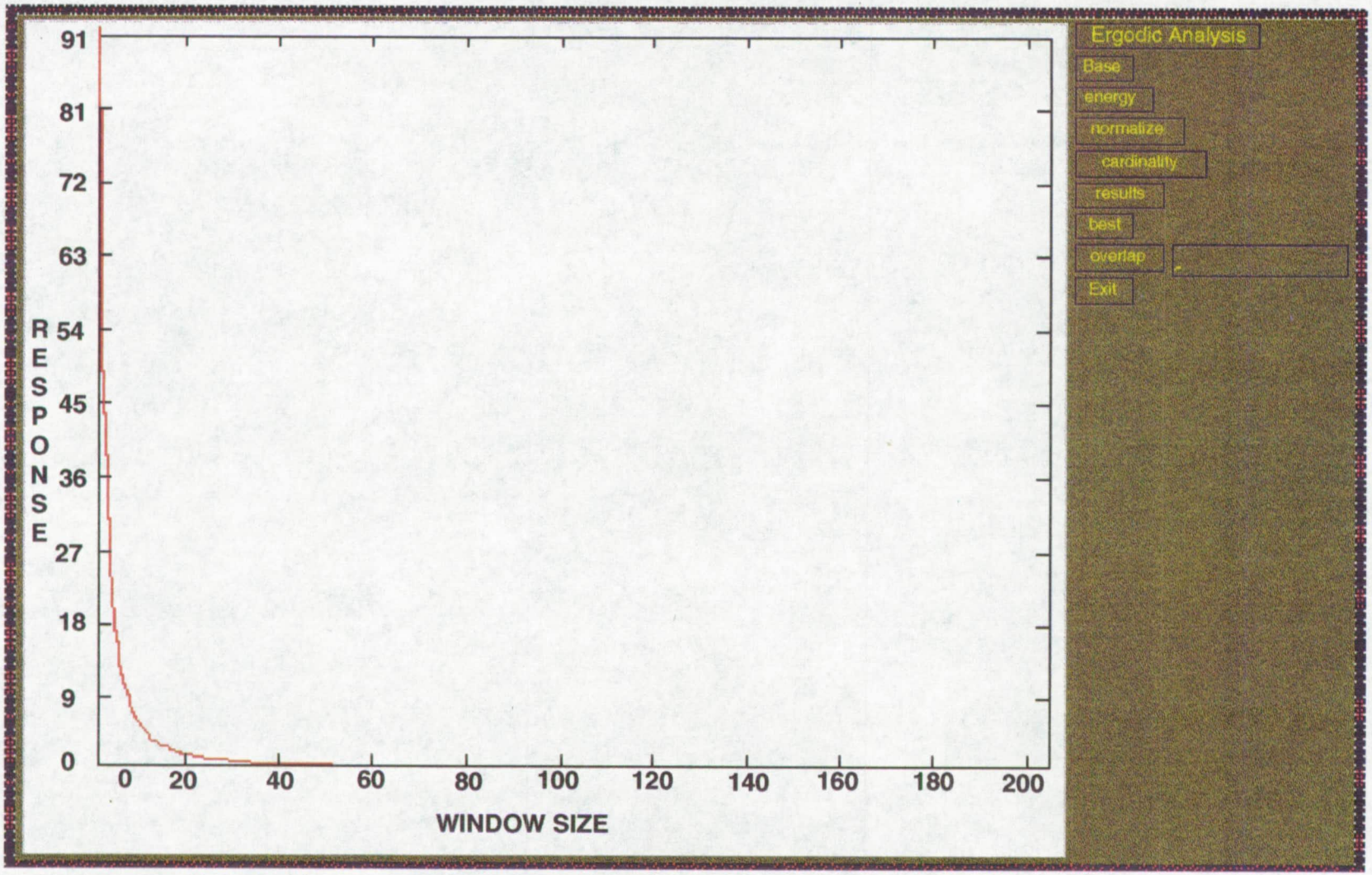

Figure 46. ***Ergodic*** Results Window Size 2000.

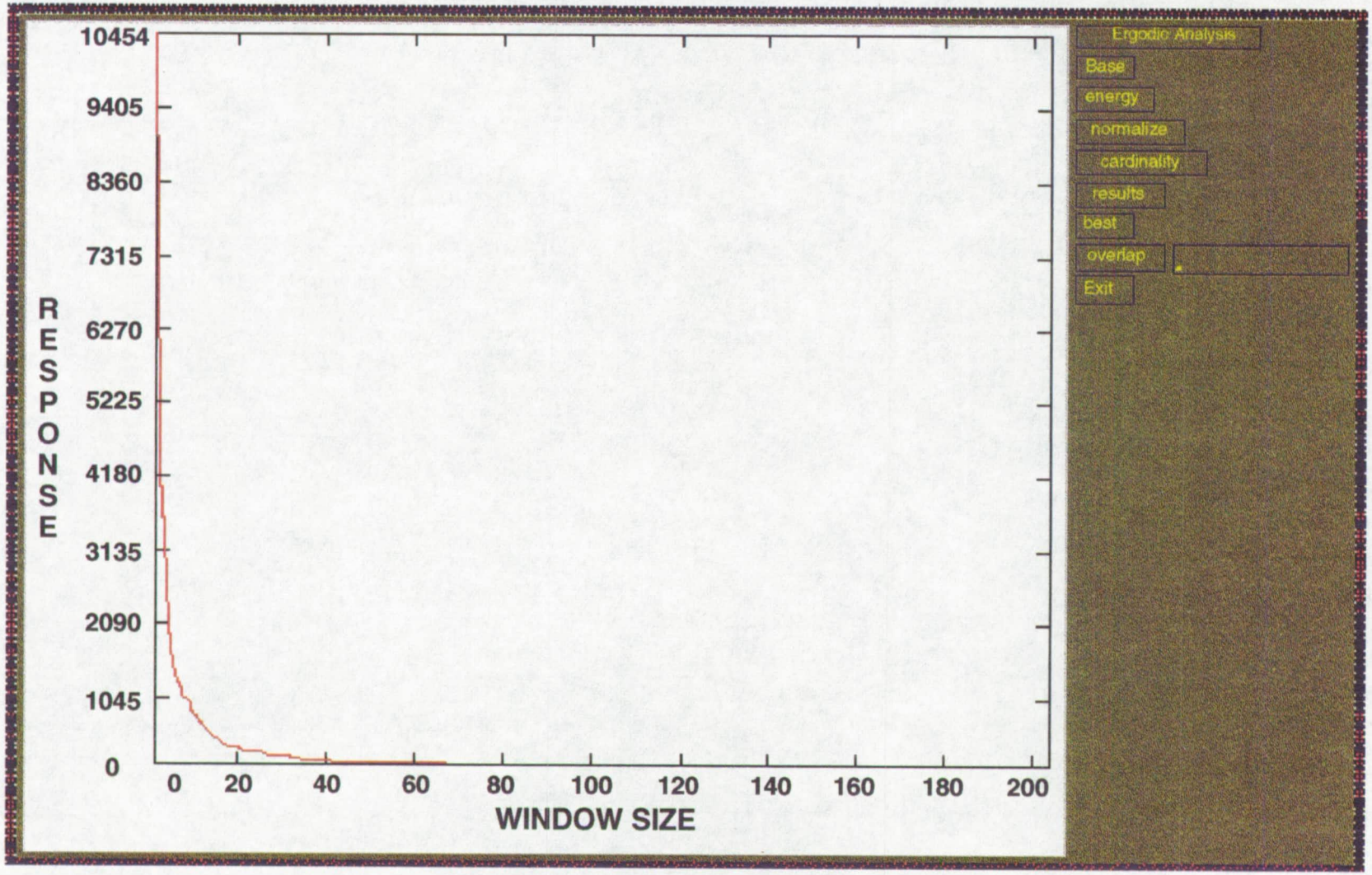

Figure 47. ***Ergodic*** Results Window Size 10

be more random and evenly distributed within the interior of the solid shape which bounds the acceleration data. It should be noted that within the acceleration vectors of both fish and football events, that occasionally there is acceleration change that is large and that reappears later. The marked line in figure 48 between the two vectors is an example of this behavior. This behavior is one of the reasons that syntactic pattern recognition may be useful.

The analysis of spheroid events indicates that these events have no preference for a specific axis. They appear to composed of spirals and randomized accelerations. They generally tend to be of lower energy than fish and football events but not always.

The analysis of left-right ellipsoids show that they are primarily characterized by preference for a given axis. They are of moderate energy.

6.1.1.9 ***Staticcloud/3dfft*** Interaction

The ***3dfft*** individual plots for fish events show definite similarities. There is a lobe in the high z, low x, and low y area (see figure 49). The ***3dfft*** individual plots for football and spheroid events appear to be very similar. There is an elongated lobe in the low x and low y which runs all along the z axis (see figure 50).

6.1.1.10 Unified Classification Results

The information provided by all analysis techniques indicate that the acceleration data from SL-3 is not random and does contain a number of high energy events that may be classified. The most useful classification method is ***staticcloud*** which is trailed in utility by ***timeseries*** and ***3dfft***. The standard Fourier information is of little use as is the present configuration of ***expertiso***. ***Expertiso*** can be modified so that its results may be patched back into the other analysis methods.

6.1.2 Classification Validity

Creating a classification and evaluating a classification for its validity are two separate activities. There are a number of validity testing techniques in the literature but none are implemented in PRIDE. The validity of the clustering produced by PRIDE is based upon the use of multiple, different techniques at each stage of the process. One of the original intentions in the development of ergodic windowing was to provide an independent method for selecting events. Despite the fact that there is a problem with ergodic windowing and thus the ergodic windowing technique cannot be used for such confirmation, perfection of ergodic windowing will provide improved validity of clustering at an early stage. The fact that the events are similarly differentiated by

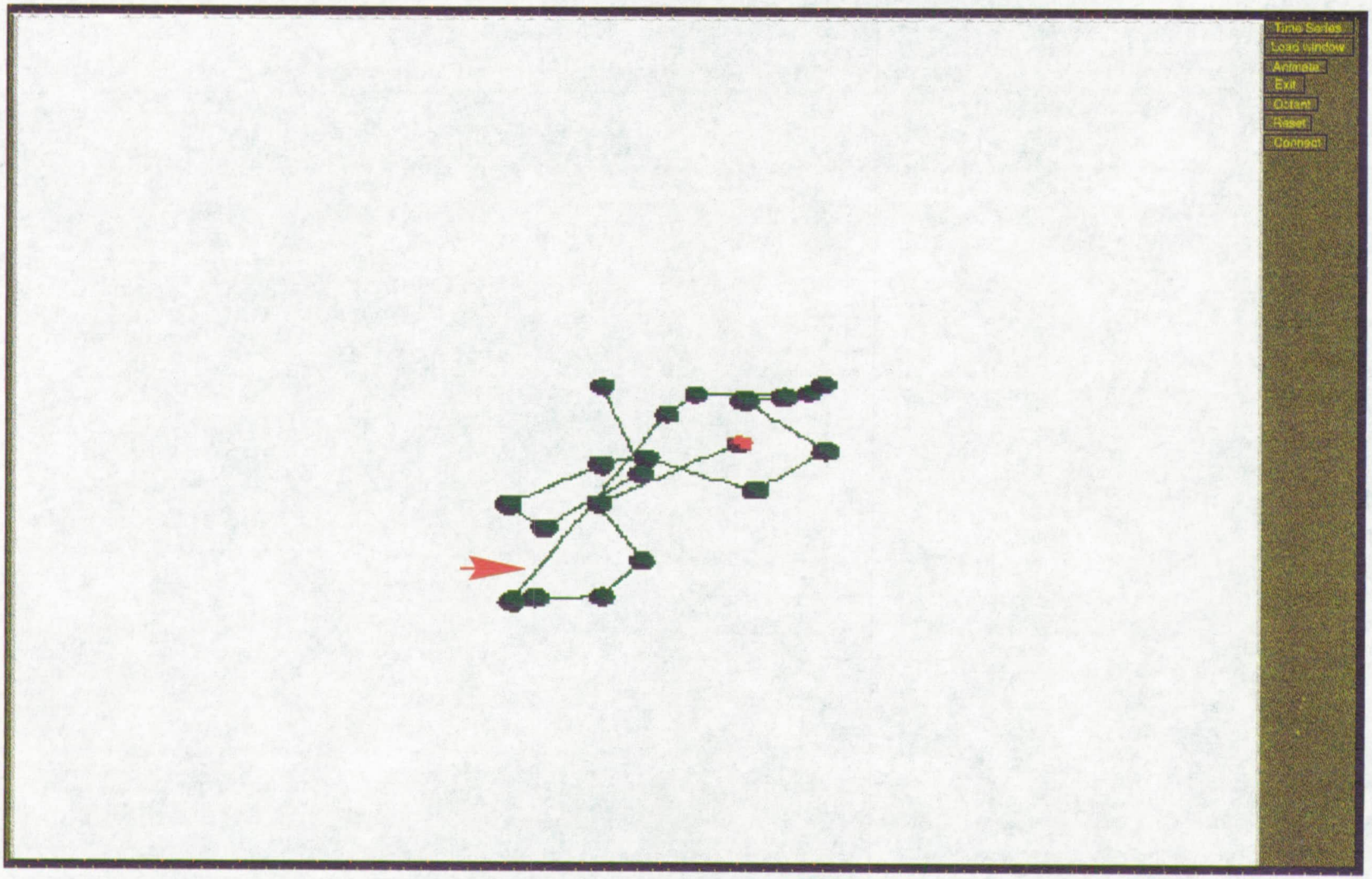

Figure 48. ***Timeseries*** Common Vector.

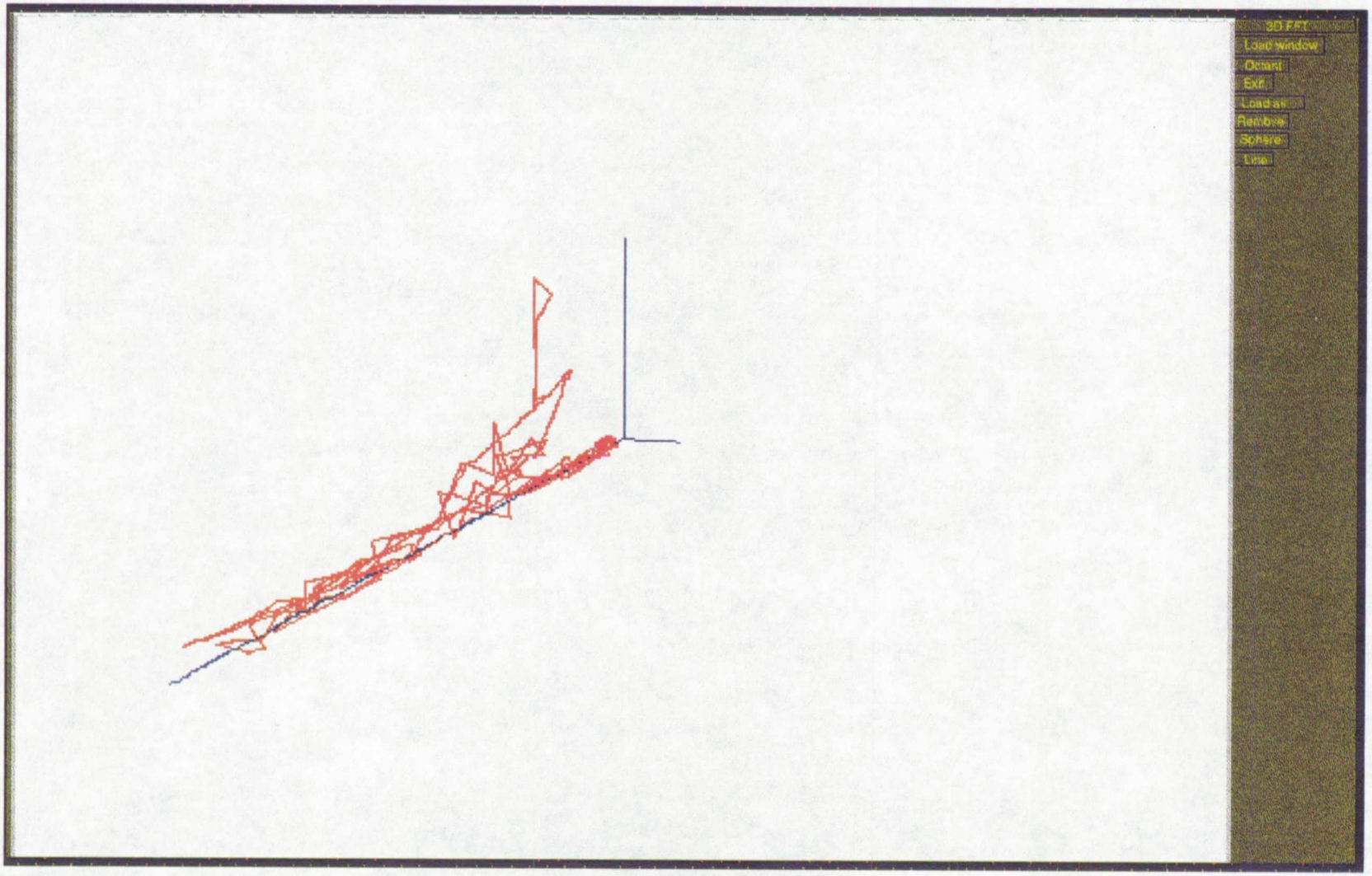

Figure 49. ***3dfft*** High Lobe.

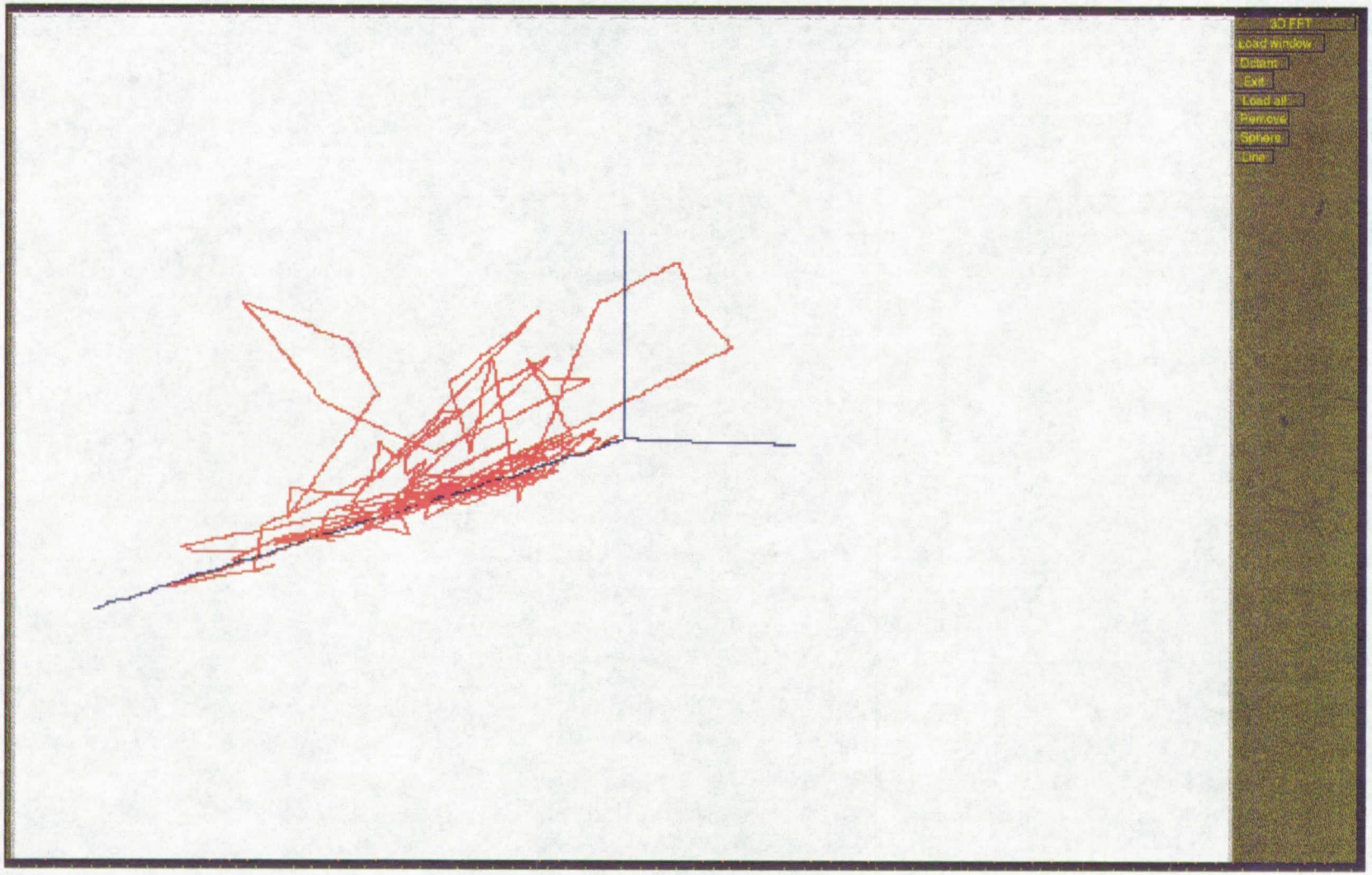

Figure 50. ***3dfft*** Elongated Lobe.

staticcloud, timeseries, and ***3dfft*** is an indication of validity. Validity is damaged by the fact that a significant data sample was not used for analysis.

6.1.3 Overall Assessment of Research Results

The useful results of this research effort are:

• The classification itself: The acceleration data has a strong vibrational character and it is possible to extract high energy events. These high energy events appear to be weakly clustered. Further analysis can be expected to clarify the nature of the classes.

• Confirmation that techniques from several disparate disciplines were needed to make the classification possible: Pattern recognition was selected because of the ill-understood nature of the data. Pattern recognition specializes in such phenomena. Data visualization was selected to provide a wedge to pry open some of the more intractable aspects of the problem so that other methods could be applied. Fourier analysis was selected because of the suspected vibrational characteristics of at least some of the acceleration data. Expert systems were selected because they provide for the inclusion of future expertise of human experts into PRIDE and because the discovery mode of expert systems offers a capability that is not represented in the other selected attack technologies. Database technology was selected because the flip side of the problem was the size of the data and databases specialize in handling large amounts of data.

• Creation of a technique for displaying hyper-dimensional data: This technique is particularly suited for displaying Fourier information that occurs in triple series and is a direct example of the advantage of multi-disciplinary approaches.

• Creation of a technique for using an expert system to control unsupervised pattern recognition: This is another example of the advantage of multi-disciplinary approaches

• Creation of a technique intended to identify the optimal token length for acceleration data: Unfortunately, this was unsuccessful. If it had been successful then syntactic pattern recognition techniques could have been applied to acceleration data.

6.2 Recommendations for Follow-On Research

The PRIDE system has a number of bugs which need to be fixed and a number of new capabilities that should be added. It may also be useful to make a few major changes in the configuration of PRIDE.

6.2.1 Known bugs

Timeseries is presently configured for printing and has white as the background color. The translucent planes added by the *octant* option are invisible and serve only to obscure the acceleration spheres.

Staticcloud suffers from the same problem that ***timeseries*** does. Use of *octant* causes the acceleration spheres to be obscured. A quick fix would be to change the background color back to black. A long term fix would be to make the setting for the translucent planes to be dependent upon the present background color.

The tick marks and labels for the independent variable are slightly off for standard ***fft***. The degree of error is not such that the correctness of the results is compromised but the error is visible and irritating.

There are two problems with the ***3dfft*** component. One problem is that the zoom and unzoom mouse functions do not work. The other problem is that there are small inaccuracies in the display of ***3dfft*** information when the *loadall* option is used. When the number of events being displayed is small, i.e. 27, then a small line segment which appears to be incorrect may be seen. The disposition of the overwhelming majority of the Fourier information is correct. When the data size is increased to 1.5 hours and the number of events subsequently rises to 53, then the error in the display is more prominent.

The only problem with ***expertiso*** is that it errors off when the number of events becomes too large. This problem appears to occur with the CLIPS source code and may not be correctable.

Ergodic suffers from misaligned tick marks in the same fashion as ***fft***. There is also a problem with the labeling of the entire graph. This should be easily correctable.

In terms of multi-component interaction bugs, the main problem is that ***query*** and ***classify*** will not peacefully coexist with other components. This is true because the CDATA DBMS is not a multi-user database and is not a concurrent access database. Additionally, if too many X windows are brought up at the same time then the system will crash. This is an unfortunate characteristic of the Ardent computer.

6.2.2 New Capabilities

There is still a great deal of work to be done in order to bring PRIDE to the degree of functionality that it is possible for it to achieve. There are improvements that should be made to every component and there are many new components that should be created.

6.2.2.1 *Timeseries*

Line segments along the three major axes should be added. An ability to click on an acceleration sphere and see the actual acceleration values should be available. An ability to create various threshold levels which are color coded should be available. There should be a way to replace the sphere and line representation with three-dimensional arrows. There should be a way to change the default number of acceleration points in the animation.

There should be a way to plot the thresholded acceleration change vectors. Take two acceleration readings which are contiguous in time. Presently, ***timeseries*** will draw a line between these spheres if ***timeseries*** is in connect mode. This line is an acceleration change vector. If a threshold is applied, then only change vectors which exceed the threshold will be plotted. Observation of the ***timeseries*** behavior of indicates that this would be a possible analysis method. This would be related to jerk windowing which will be described later.

It should be possible to activate the other components directly from the ***timeseries*** screen. The present arrangement would force the user to create a new component from the main menu and then click on the correct window in the *loadwindow*. Usually the window which was clicked to create the ***timeseries*** would still be highlighted but it is possible that some other window had been clicked and the user might not remember exactly which window created the present ***timeseries*** display.

For documentation purposes, each ***timeseries*** display should have a description of the presently selected window. It should be possible to change the dimensions of the screen. It should be possible to display the next event based on primary key.

6.2.2.2 *Staticcloud*

For documentation purposes, each ***staticcloud*** display should have a description of the presently selected window. Additionally, each sphere should be clickable to allow a display of the exact accelerations that define the sphere. There should be a capability to plot the centers of mass of all events as spheres. This display would provide a way to study the distribution of events with the three dimensions. Another version of this display should be able the display the major axes of the events simultaneously. A third version of

this display should combine the information from the first two displays. This display would consists of spheres indicating the center of events which are pierced by cylinders which indicate the direction of the major axis.

It should be possible to change the dimensions of the screen and to directly activate other components from the ***staticcloud*** component. It should be possible to display the next event based on primary key. There should be a display which drops one of the dimensions of the data. This screen would be two dimensional. This should be explored because a subspace of the three dimensional data may be more useful for classification than data with all three dimensions.

6.2.2.3 Standard ***Fft***

It should be possible to change the dimensions of the screen and to interactively change the limits on the independent and dependent variables. It should be possible to activate the other components directly from the ***fft*** screen and to display the next event based on primary key.

There should be a capability to perform three dimensional analyses of the Fourier information for specific dimensions. Figure 51 shows a mockup of this capability. This plot has two independent variables and one dependent variable. The first independent variable is frequency and the second independent variable is event number. The dependent variable is magnitude. One of this type of plot should be available for the x, y, and z dimensions.

There should be a capability for a two-dimensional gray-scale overlay of all events. Figure 52 is an example of this screen. The idea behind this screen is very similar to ***3dfft*** except that there will be three of these screens, one for each dimension. For example, the x dimension version of this screen would plot every x FFT simultaneously on the two-dimensional screen. The more times that a particular pixel is overwritten by different x FFTs, the darker the point is shaded. Therefore, magnitude/frequency pairs which occur repeatedly will appear dark while less common magnitude/frequency pairs will be lightly colored and will stand out less from the background.

There should be a capability to threshold magnitudes and to directly specify desired frequencies. This will provide data reduction capabilities to the ***fft*** analysis.

6.2..2.4 ***Query*** and ***Classify***

The improvement needed for ***query*** and ***classify*** depend upon whether CDATA is retained as the database associated with PRIDE. A database management system could

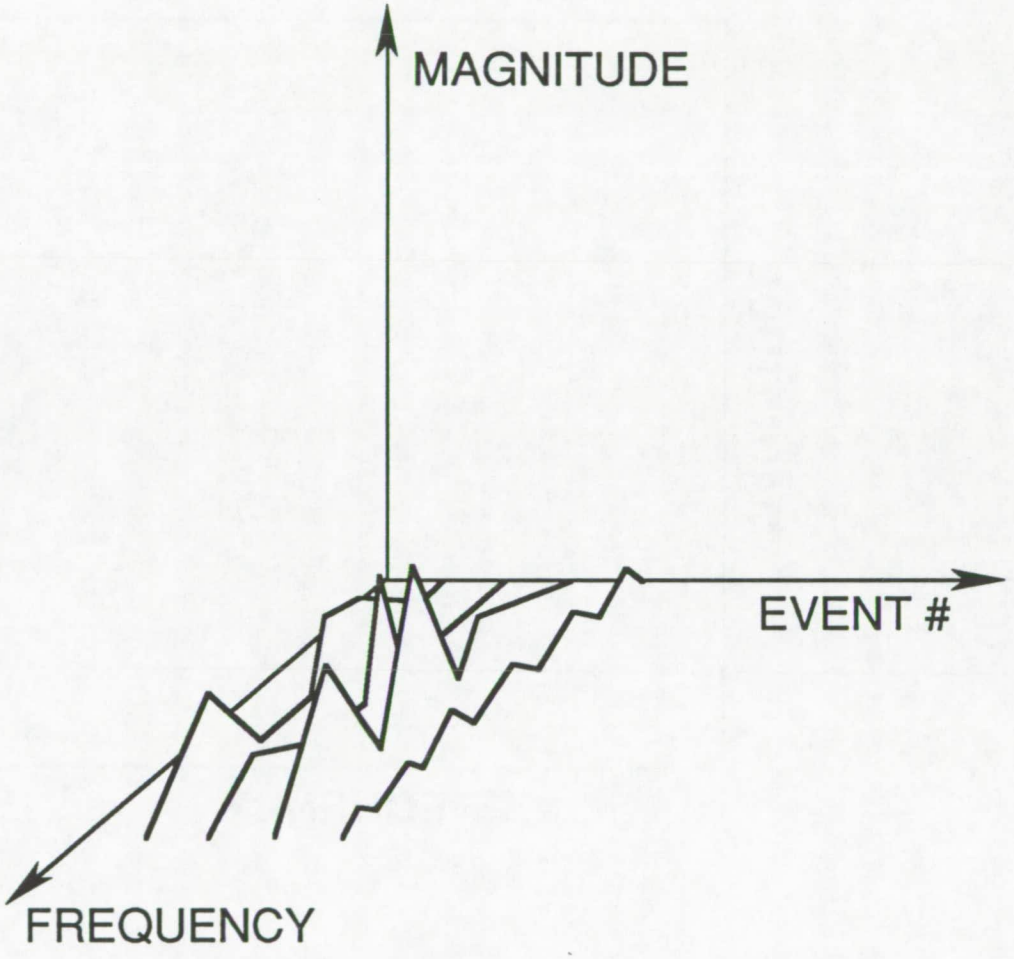

Figure 51. Three dimensional version of ***Fft.***

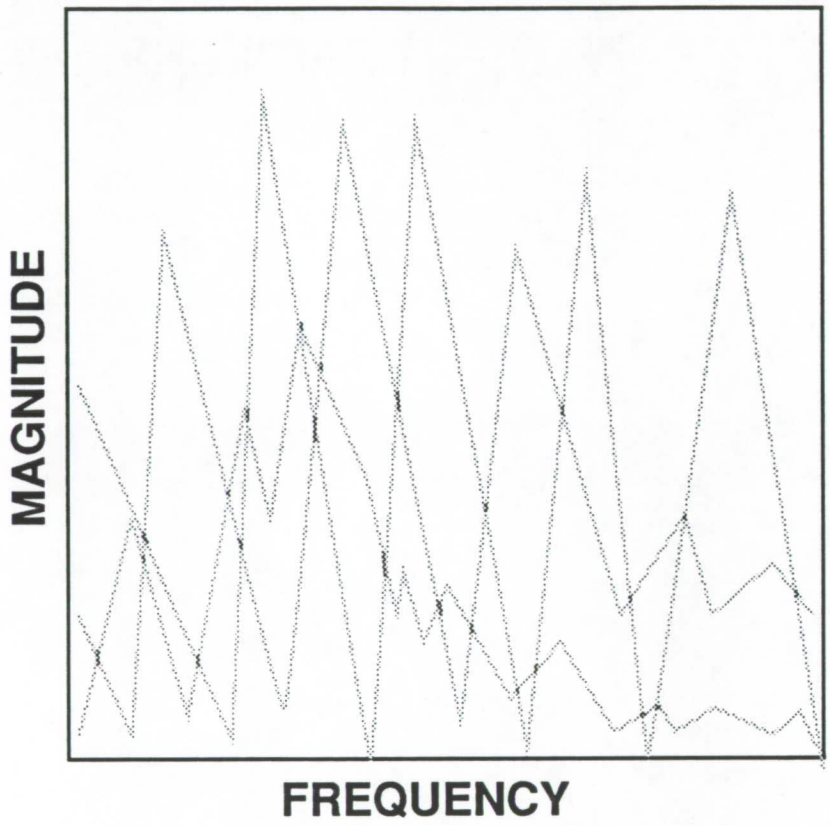

Figure 52. Intensity level variation of ***Fft.***

be built from scratch, or a more sophisticated database system could be purchased, or CDATA could be drastically upgraded to solve the present database problems. The primary problem that needs to be solved is the problem with concurrent access to database information. The second most important problem is the problem of recovery from database corruption. The third problem is the fact that CDATA does not provide a full set of relational operators. Solution of these problems would go a long way toward improving the usefulness of PRIDE.

Other issues that could conceivably be addressed is the use of database techniques to store graphic image data. The PRIDE system can rapidly produce a great deal of this type of data. The available disk storage cannot handle this load but the use of tape storage offers a potential solution. It would be nice to be able to generate graphics, save the graphics to tape, and then to be able to retrieve such graphics upon demand. The database would store the information needed to efficiently retrieve this information.

6.2.2.5 Manual ISODATA

The present implementation of the human operated ISODATA algorithm is not X based. This could be corrected. The main problem involved with this endeavor would be the fact that ISODATA can produce voluminous text data which would require variable size screens. Initial study of this problem seems to indicate that the solution would be quite difficult.

The data output by the ISODATA algorithm is such that a number of graphic displays could be used to better describe the present classification being presented by ISODATA. One such display would be a two-dimensional display of the standard deviations for a given event. A similar display would be a two-dimensional display of the average standard deviations for all events. Another display would be a three-dimensional animation which would use data consisting of projections from n dimensions to four dimensions. This display will be an exercise in displaying hyperspace data just as ***3dfft*** is such an exercise. It should be possible to change the dimensions of the screen.

6.2.2.6 ***Expertiso***

An attempt must be made to increase the efficiency of storage utilization in order to allow ***expertiso*** to handle larger numbers of events. Additionally, the operation of ***expertiso*** must be made so that the events within a given class within a given classification are retrievable. This will allow the results of ***expertiso*** to be utilized in conjunction with the other components of PRIDE. The operation of ***expertiso*** must be extended. The ***expertiso*** component does not perform every operation that a human

operator could perform. A human operator would never have the time or memory to be able to perform all these operations in any case.

The suggested graphics improvements for manual ISODATA also apply to the ***expertiso*** component. It should be possible to change the dimensions of the screen.

6.2.2.7 *Ergodic*

The most important improvement for the ***ergodic*** component is a capability to generate synthetic data. Once such a generating component has been created, the ergodic analysis may be completed. Another capability that should be added is a two dimensional display which shows the desirability of vectors for inclusion in events. The basic idea is that analyzing the energy of windows for a given size causes any given vector to fall within a fixed number of windows. These windows have varying energy. A vector which falls within consistently low energy windows is less likely to be part of a high energy event than is a vector which consistently falls within high energy windows for a given window size. Extending this high energy versus low energy classification for a vector across all window sizes causes each vector to have an associated value which indicates the amount of energy in the windows into which that vector fell. Once this function has been determined, a variant of vibration windowing could be run upon the function and high energy events should be detected.

Validity of classification would be improved if a way to display overlaps between windows selected by vibration windowing and windows selected by ergodic windowing were available. It should be possible to change the dimensions of the screen.

6.2.2.8 *3dfft*

The greatest improvement in ***3dfft*** would be for a capability to selectively drop and add dimensions to be added. Another improvement would be if the ***3dfft*** lines were clickable so that a user who was interested in a particular point on a line could determine the associated frequency. It should be possible to change the dimensions of the screen. It should be possible to display the next event based on primary key. It should be able to show ***3dfft***s by selecting a class from a classification.

6.2.3 Changes

It may be desirable to shift from C to C++ so that object-oriented development may be achieved. It may be desirable to add an animation language capability. It may be desirable to add a user interface generation/management capability. It would be desirable to shift the system to a computer which implements X11R4 and not just X11R3. The X

interface for CLIPS would be available if this were true. The system needs to be upgraded so that network use is possible. Syntactic pattern recognition should be investigated.

The availability of examples of known acceleration events would aid the functionality of PRIDE immensely. The availability of orbiter and crew activity timelines and information concerning the validity of such timelines would also aid the functionality of PRIDE. Statistical techniques could be applied to this timeline data in conjunction with raw acceleration data. Early in the project, statistical analysis was applied to a small amount of raw acceleration data using the IMSL library available on the VAX but since no immediate benefit was noted and IMSL was not available for the Ardent, statistical analysis was not pursued in the later development stages of PRIDE [34].

It would be useful to have a capability to display raw acceleration data, either three dimensionally or two dimensionally. It would be useful to have an immediate data reduction capability. Originally, this was avoided in an attempt to stay as close to the real data as possible.

NASA

Report Documentation Page

1. Report No.	2. Government Accession No.	3. Recipient's Catalog No.
NASA TM-103507		

4. Title and Subtitle	5. Report Date
Analysis Techniques for Residual Acceleration Data	July 1990
	6. Performing Organization Code: ES76

7. Author(s)	8. Performing Organization Report No.
Melissa J.B. Rogers,* J. Iwan D. Alexander,* and Robert S. Snyder	10. Work Unit No.

9. Performing Organization Name and Address	11. Contract or Grant No.
George C. Marshall Space Flight Center Marshall Space Flight Center, Alabama 35812	13. Type of Report and Period Covered: Technical Memorandum

12. Sponsoring Agency Name and Address	14. Sponsoring Agency Code
National Aeronautics and Space Administration Washington, DC 20546	

15. Supplementary Notes

Prepared by Space Science Laboratory, Science and Engineering Directorate.

*Center for Microgravity and Materials Research, University of Alabama in Huntsville, Huntsville, Alabama 35899

16. Abstract

Various aspects of residual acceleration data are of interest to low-gravity experimenters. Maximum and mean values and various other statistics can be obtained from data as collected in the time domain. Additional information may be obtained through manipulation of the data. Fourier analysis is discussed as a means of obtaining information about dominant frequency components of a given data window. Transformation of data into different coordinate axes is useful in the analysis of experiments with different orientations and can be achieved by the use of a transformation matrix. Application of such analysis techniques to residual acceleration data provides additional information than what is provided in a time history and increases the effectiveness of post-flight analysis of low-gravity experiments.

17. Key Words (Suggested by Author(s))	18. Distribution Statement
Microgravity, Residual Acceleration, Fourier Analysis, Time Series Analysis, Axes Transformation	Unclassified----Unlimited

19. Security Classif. (of this report)	20. Security Classif. (of this page)	21. No. of pages	22. Price
Unclassified	Unclassified	28	NTIS

NASA FORM 1626 OCT 86

For sale by the National Technical Information Service, Springfield, VA 22161-2171